STRUCTURAL AND SIGNALING MECHANISMS OF ICMT-MEDIATED KRAS4B METHYLATION

by

Ariana L. Cardillo

A Dissertation

Submitted to the Faculty of Purdue University

In Partial Fulfillment of the Requirements for the degree of

Doctor of Philosophy

Department of Chemistry

West Lafayette, Indiana

May 2022

THE PURDUE UNIVERSITY GRADUATE SCHOOL
STATEMENT OF COMMITTEE APPROVAL

Dr. Christine A. Hrycyna, Chair
Department of Chemistry

Dr. Shalini T. Low-Nam
Department of Chemistry

Dr. Chittaranjan Das
Department of Chemistry

Dr. Andrew D. Mesecar
Department of Biochemistry

Approved by:
Dr. Christine A. Hrycyna

For my family

ACKNOWLEDGMENTS

My journey and pursuit of this degree was not without the support of many people. I am firstly, eternally grateful to my family for their belief in me and their understanding, especially over these past six years. As a middle child, it would be mild to say that I was introverted while growing up. I credit my parents for encouraging me to work outside of my comfort zone and for instilling in me a drive to work hard – the best qualities of myself come from you. To my sisters, thank you for showing me true love, friendship, and honesty while always making me laugh through the hardest of times. To my grandparents and extended family, thank you for your continual encouragement and presence in my life, even with the hundreds of miles between us. Especially to my Grammy, Catherine Cardillo. Thank you for teaching me to have grit – your fiery spirit will live on within myself and all of your grandchildren. I'm grateful to my Zuri, who would always greet me after work by peeking through the blinds with a goofy smile. You are my source of happiness. And to Joe Cacciatore, thank you for being my confidant and source of strength. Your voice of reason has guided me through frustration but also shown me when to advocate for myself and to know my worth. I'm grateful and excited for our life together with Zuri.

I would like to thank my advisor, Dr. Christine Hrycyna for your mentorship and guidance throughout my research. I am grateful for the opportunity you entrusted in me to launch a new project based on one of my curiosities. You have challenged me to become a confident scientist while reminding me to enjoy other important parts of life, like love of family and dogs. I am also grateful for my undergraduate mentor, Dr. R. Bryan Sears, who sparked my love for Chemistry and research. Your lively class my first semester of college and close guidance changed the course of my life. I would also like to thank my thesis committee members, Drs. Chittaranjan Das, Andrew D. Mesecar and Shalini T. Low-Nam for your support in my thesis work.

I would like to acknowledge the Low-Nam Lab, especially Kevin L. Scrudders, Vinay Menon, all of the Low-Nam Lab undergraduates, and especially MaryClaire Cooke, for taking on this project with us and making it such a fun experience. To Mary, I can't wait for you to break out and start your graduate journey – the future is so bright for you. I would especially like to thank Shal, for encouraging my ideas (and failures) as a collaborator, for pursing our joint project with the utmost rigor, and for being a selfless friend.

I would like to thank Dr. Mark D. Distefano and his laboratory members at the University of Minnesota, especially Taysir Bader, for creating a multitude of probes that helped not only my projects, but will continue to aid future projects in the Hrycyna Lab.

I am grateful to the members of the Hrycyna Lab, past and present, who have guided me. You all kept me accountable and sane during times when, thanks to COVID-19, the world didn't know what normalcy was. Amy Funk, thank you for providing the base for my project and mentoring me while trying to wrap up your own degree. I appreciate the help of Chelsea St. Germain and Jason Goebel in the various projects we had to tackle together. Thank you to the undergraduates of the Hrycyna Lab that I have been fortunate to work with, especially Gabrielle Snisky, for helping clone some of the mutants mentioned in this work. Thank you to honorary Hrycyna Lab member Elisabeth Garland-Kuntz, for infusing the lab with organization and structure and being a sounding board for many experiments. I am grateful to call someone as brilliant and thoughtful as you, a friend. To the second honorary lab member, Laura Mendoza, thank you for sharing your infectious laughter and being a confidant to me and so many other lab members, especially at the end of long days. To Elias Beretta, thank you for consulting on various experiments, being a listening ear, and for letting me laugh at your Minnesotan accent. You helped the tough final months of my degree be a little easier and I wouldn't have wanted to join the lab with anyone else. To Anna Ratliff, I will never understand how someone can be productive 95% of the time, especially after running 10-plus miles every morning. Since my first day of graduate school, you exemplified a diligent scientist with an unmatched kindness. Thank you for your friendship, for continuing to mentor me and for always having time on your walks with Maisie for a phone call. To all the Hrycyna Lab members that are continuing in their pursuit of a doctoral degree, I know you will be successful in whatever avenues life takes you, after all, you have already survived a pandemic while in graduate school.

I have been fortunate enough to have a great support system while at Purdue. Thank you to the Purdue faculty and staff, especially those behind the scenes, that helped me to be a successful teaching assistant and scientist. And thank you to my friends who truly understood the burdens of undertaking a graduate degree. To Casey Wright, John Andjaba, Erica Wleklinski, Michelle Van Camp, Shannon Daily, Hannah Konicki, Jessica daSilva, Anastasia Yogas, and Alandra Lopez, I cannot express how grateful I am to each of you for your lifelong friendships. And to those I have forgotten to mention but am still grateful for, thank you for joining me on this journey.

TABLE OF CONTENTS

LIST OF TABLES

LIST OF FIGURES

LIST OF ABBREVIATIONS

5-FAM	Fluorescein isothiocyanate
ABC	Ammonium bicarbonate
AEBSF	4-(2-Aminoethyl)benzenesulfonyl fluoride hydrochloride
AFC	*N*-acetyl-*S*-farnesyl-L-cysteine
AGGC	*N*-acetyl-*S*-geranylgeranyl-L-cysteine
Ag-Icmt	*Anopheles gambiae* (mosquito) isoprenylcysteine carboxyl methyltransferase
Akt	Protein kinase B
AML	Acute myeloid leukemia
ATP	Adenosine triphosphate
BSA	Bovine serum albumin
ddH_2O	Deionized, distilled water
DDM	*N*-Dodecyl-β-D-maltopyranoside
DGS-NTI(Ni)	1,2-Dioleoyl-sn-glycero-3-[(N-5-amino-1-carboxypentyl)iminodiacetic acid)succinyl] (nickel salt)
DMEM	Dulbecco's modified eagle media
DOPC	Dipalmitoylphosphatidylcholine
DTT	Dithiothreitol
ECL	Enhanced chemiluminescence
EDTA	Ethylenediamine tetraacetic acid
EGF	Human epidermal growth factor
EGTA	Ethylene glycol-bis(βaminoethyl ether)-N,N,N',N'-tetraacetic acid

ER	Endoplasmic reticulum
ERK	Extracellular signal-regulated kinase
FBS	Fetal bovine serum
FDA	Food and Drug Administration
FGTI	Farnesyltransferase and geranylgeranyltransferase inhibitor
FITC	Fluorescein isothiocyanate
FPLC	Fast protein liquid chromatography
FTase	Farnesyltransferase
FTIs	Farnesyltransferase inhibitors
GAP	GTPase-accelerating protein
GDP	Guanosine diphosphate
GEF	Guanine nucleotide exchange factor
GGTase	Geranylgeranyltransferase
GTP	Guanoside triphosphate
HEPES	4-(2-Hydroxyethyl)-1-piperazineethanesulfonic acid
hIcmt	Human isoprenylcysteine carboxyl methyltransferase
His-Ste14p	$His_{10}myc_3N$-Ste14p
HRas	Harvey rat sarcoma viral oncogene homolog
HRP	Horseradish peroxidase
HVR	Hypervariable region
Icmt	Isoprenylcysteine carboxyl methyltransferase
IEtOH	2-Iodoethanol
IF	Immunofluorescence

K_D	Dissociation constant
kDa	Kilodalton
K_m	Substrate concentration at half the maximum velocity
KRas	Kristen rat sarcoma viral oncogene homolog
LC-MS/MS	Liquid chromatography coupled tandem mass spectrometry
Ma-MTase	*Methanosarcina acetivorans* (prokaryotic) methyltransferase
MALDI-TOF/TOF	Matrix-assisted laser desorption/ionization – time of flight/time of flight
MAPK	Mitogen-activated protein kinase
MEF	Mouse embryonic fibroblast
MOPS	3-(*N*-Morpholino)propanesulfonic acid
MOPS-Tris-SDS	3- morpholinopropane-1-sulfonic acid-Tris-sodium dodecyl sulfate
MS/MS	Tandem mass spectrometry
MTOR	Mammalian target of rapamycin
MW	Molecular weight
NCI	National Cancer Institute
NRas	Neuroblastoma rat sarcoma viral oncogene homolog
NSCLC	Non-small cell lung cancer
NTCB	2-Nitro-5-thiocyanobenzoic acid
PBR	Polybasic region
PBS	Phosphate-buffered saline
PBST	Phosphate-buffered saline with 0.05% Tween
PDE	Phosphodiesterase-δ
PE	Phosphatidylethanolamine

PFA	Paraformaldehyde
PG	Phosphatidylglycerol
PI3K	Phosphatidylinosiol-3-kinase
PM	Plasma membrane
PTM	Post-translational modification
Raf	Rapidly accelerated fibrosarcoma protein
RBD	Ras binding domain
Rce1	Ras converting enzyme 1
RIPA	Radioimmunoprecipitation assay
RNA	Ribonucleic acid
SAH	*S*-adenosyl-L-homocysteine
SAM	*S*-adenosyl-L-methionine
[^{14}C]-SAM	*S*-adenosyl-L-[methyl-^{14}C] methionine
Sc-Icmt	Ste14 or *Saccharomyces cerevisiae* (yeast) isoprenylcysteine carboxyl methyltransferase
SC-URA	Synthetic complete medium without uracil
SDS	Sodium dodecyl sulfate
SDS-PAGE	Sodium dodecyl sulfrate-polyacrylamide gel electrophoresis
SEC	Size exclusion chromatography
siRNA	small interfering ribonucleic acid
TA-Ste14	Triple alanine or cysteine-less Ste14
Tc-Icmt	*Tribolium castaneum* (Beetle) isoprenylcysteine carboxyl methyltransferase

TEP	Triethylphosphine
TGS	Tris-glycine-SDS
TM	Transmembrane
UV	Ultraviolet
V_{max}	The maximum rate at which the enzyme can perform
WT	Wild-type
YPD	Yeast peptone dextrose medium
ZMPSTE24	Human zinc metalloprotease STE24

ABSTRACT

Mutated Ras proteins are implicated in ~20% of all human cancer cases. Of these cancer-causing Ras mutations, 80% of missense mutations are in the isoform KRas4B. In the decades since the discovery of KRas4B, extensive research of its signaling pathways, from protein translation to cellular outputs, have helped characterize the routes of oncogenesis. Until 2021, KRas4B had been thought to be "undruggable," as no specific inhibitors had been approved by the Food and Drug Administration (FDA) as effective treatments. This fueled researchers to design treatments that targeted the signaling pathways up- and downstream of KRas4B association to the plasma membrane; of which multiple downstream targeting drugs are currently in various stages of clinical trials. However, these downstream effectors are implicated in multiple cellular pathways and, thus, are nonspecific. Some researchers have since focused their studies on targeting the specific upstream modifications necessary for proper KRas4B cellular localization and function.

KRas4B is classified as a CAAX protein, where its four C-terminal residues consist of a cysteine ("C"), two aliphatic residues ("AA") and a residue of various identities ("X"). CAAX proteins undergo three post-translational modification (PTMs). First, dependent on the identity of the "X" residue, an isoprenoid group of either 15 or 20 carbons is added to the C-terminal cysteine by farnesyltransferase (FTase) or geranylgeranyltransferase (GGTase) respectively. KRas4B is farnesylated since its sequence terminates with a leucine. After prenylation, the three C-terminal residues ("AAX") are removed by the protease Ras converting enzyme-1 (Rce1). Finally, the free carboxylate of the terminal cysteine is methylated by isoprenylcysteine carboxyl methyltransferase (Icmt). Following methylation, KRas4B is translocated to the plasma membrane where it associates in a functional protein complex. Interestingly, of these three required PTMs, methylation is the only reversible step, suggesting a possible point of regulation of many CAAX proteins and their signaling pathways, including that of KRas4B. The regulatory function of methylation has long been speculated, but never fully characterized. The research described herein worked to characterize the mechanism of methylation by Icmt and to better understand KRas4B signaling as a function of methylation, with the ultimate goal of elucidating the large implications methylation may have on the regulation of KRas4B.

To understand the mechanism of methylation, we first sought to identify the substrate binding site of Icmt. Icmt is an integral membrane protein localized within the outer membrane of the endoplasmic reticulum (ER) and is currently the sole methyltransferase known to act on CAAX proteins, thus providing a specific target for future chemotherapeutics. Using biochemical tools, we interrogated the ability of a model Icmt from *Saccharomyces cerevisiae*, Ste14, to accommodate both a hydrophilic cofactor, *S*-adenosyl-L-methionine (SAM), and a lipophilic isoprenylated substrate, which can have one of two different isoprenoid groups. Through alanine-scanning mutagenesis in combination with enzymatic activity assays using substrate mimetics of farnesylated or geranylgeranylated peptides, we identified several residues in the N-terminal half of Ste14 that appear to decrease recognition of *N*-acetyl-*S*-farnesyl-L-cysteine (AFC) but not *N*-acetyl-*S*-geranylgeranyl-L-cysteine (AGGC). When mutated to alanine, residue Leu56, which sits in the middle of transmembrane helix 2 (TM2), preferentially methylated AGGC over AFC by a factor of over 100. In agreement with a recently resolved eukaryotic crystal structure of Icmt, we hypothesized that this N-terminal region facilitates substrate binding to Icmt. To further localize and confirm TM2 as an important region for substrate binding, we performed a multistep workflow combining photoreactive AFC-based substrate analogs, cysteine-specific cleavage reagent 2-nitro-5-thiocyanobenzoic acid (NTCB), and a library of purified Ste14 cysteine mutants. Our data confirmed that the photoreactive substrate labels Ste14 between residues 44 and 77, which spans TM2 and part of Loop 2.

This new information regarding substrate binding allows for more rationale design of small molecule Icmt inhibitors as chemotherapeutics. More so, it allows for enhanced targeting of Icmt to better understand its possible role in regulating CAAX proteins such as KRas4B. To date, there are very few comprehensive studies that examine the effects of methylation on broader cellular output levels, spanning orders of magnitude in space and time, specifically at the single-cell level. Most research has focused on interrogating the connection of methylation and KRas4B localization and function through systems that overexpress KRas4B. However, these results may not best represent the natural state of KRas4B and the signaling outputs being measured. Herein, we propose to employ of more modern techniques including, single-cell studies, endogenous KRas4B monitoring within an isogenic background, and single-molecule tracking to better understand KRas4B mechanisms as a function of methylation. With the knowledge that KRas4B mutants have different oncogenic mechanisms and the new FDA approval of sotorasib, which preferentially

inhibits G12C mutated KRas4B, we also seek to explore how methylation may have differing regulatory effects on the KRas4B oncogenic variants which contributes to their divergent oncogenic mechanisms. Herein, we describe the methodology used to test our hypotheses such as quantifying the recruitment of a Ras-GTP fluorescent sensor templated on the Ras-binding domain (RBD) and measuring signal propagation based on ERK dynamics using a kinase translocation reporter (KTR) all at the single-cell level with endogenous expression of KRas4B. We will also present preliminary data that suggests the KRas4B oncogenic mutants have differing cell crawling rates. Together, the structural investigation of the substrate binding site and cell-to-cell signaling of endogenous, mutant specific KRas4B will provide a structural basis for designing Icmt inhibitors not only for chemotherapy treatment, but also to better interrogate the role of methylation in regulating KRas4B and other CAAX proteins involved in various disease states.

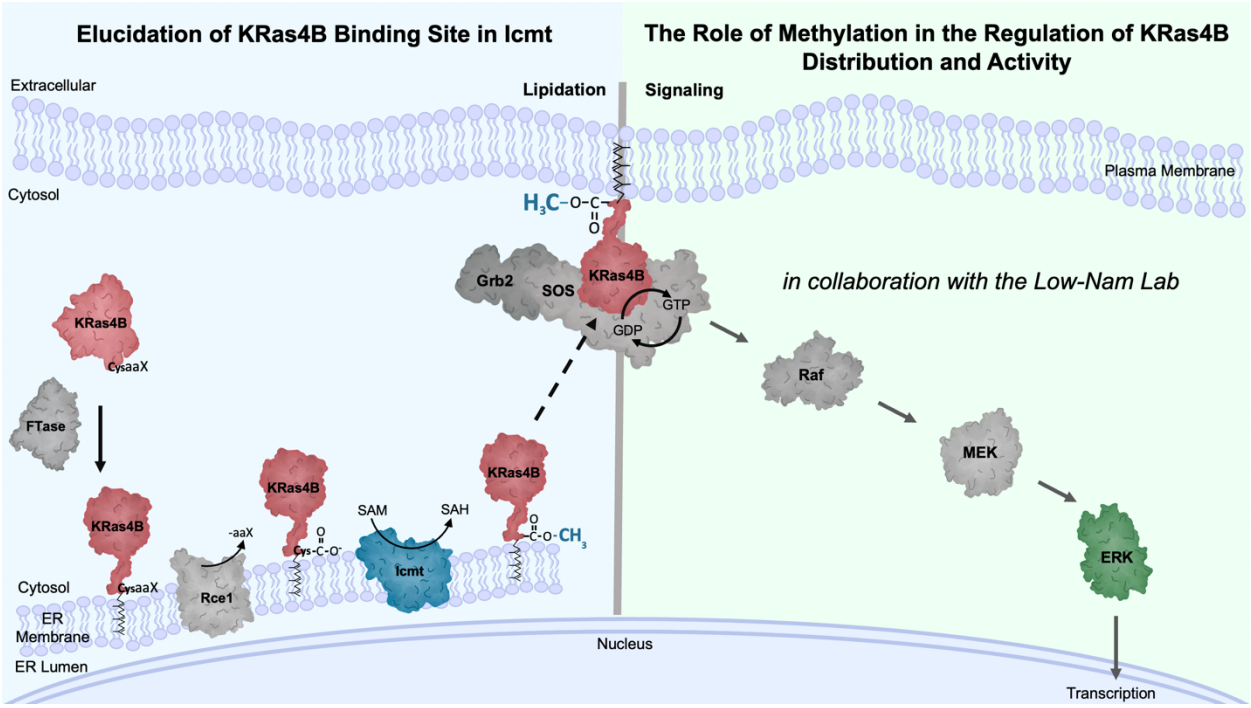

Figure A.1 Chapter outline for dissertation.

"Elucidation of the KRas4B Binding site in Icmt" is the third chapter while the "The Role of Methylation in the Regulation of KRas4B Distribution and Activity" is the fourth chapter. The methodologies designed and optimized to serve both projects are described in chapter two. The PDB structures of which each protein is based are, Ras: 4OBE & 4DSO, FTase: 1S63, Rce1: 4CAD, Icmt: 5VG9, Grb2: 1JYU, SOS: 3KSY, Raf: 3C4C, MEK: 4MNE, ERK: 4GT3,

CHAPTER 1. INTRODUCTION

1.1 Ras protein significance and function

Nineteen percent of all human cancers contain mutations within Ras proteins, making them the most frequently mutated gene family contributing to oncogenesis.[1, 2] Over 80% of the cancerous Ras missense mutations are in the KRas4B isoform.[2] This percentage increases further for specific cancers such as pancreatic cancer, which has a 90% mutation rate in KRas.[1] Therefore, these small GTPases, especially KRas4B, have been the topic of extensive research with the primary goal of designing potent, targeted small molecule inhibitors.

There are three *RAS* genes, *NRAS*, *HRAS* and *KRAS* which contribute to four different Ras isoforms: NRas, HRas, KRas4A and KRas4B. The two KRas isoforms are splice variants of the *KRAS* gene, with KRas4B being the predominant variant that is widely expressed across various tissue types.[3] All isoforms share 100% sequence identity within the N-terminal, catalytic G domain, otherwise known as the effector lobe and 82% sequence similarity within the allosteric lobe.[4] The lowest homology is in the C-terminal hypervariable region (HVR). The effector lobe contains the sites of protein-protein interaction between the Ras protein and its effectors. These sites include the active site components (switch I, switch II and the P-loop) and the majority of the nucleotide binding pocket (Figure 1.1).[5] The second lobe, the allosteric lobe, contains the membrane-interacting domains as well as the allosteric switch (helix 3/loop 7).[5] The Ras isoforms are thus distinguished by the variation in the 25 C-terminal residues that make up the HVR and as a result are also classified by their differing post-translational modification (PTMs) that occur within the HVR.[6] These post translational modifications will be further discussed throughout this dissertation.

Ras proteins are small GTPases whose nucleotide-bound states confer specific conformations that modulate activity.[7] Active Ras proteins localized to the plasma membrane (PM) are characterized by their GTP-bound states (Ras-GTP), while the inactive state is bound to GDP (Ras-GDP). Upon PM localization and stimulation by extracellular signal integration, inactive Ras-GDP will exchange its nucleotide for GTP, as GTP is at 10-fold higher cellular concentrations than its less active counterpart.[8] Ras will then hydrolyze GTP to GDP to return Ras to its inactive state. Ras proteins possess intrinsically low rates for both GTP hydrolysis and GDP dissociation

and therefore use two different proteins to help speed up these processes. GTPase activating proteins (GAPs) help to accelerate the hydrolysis of GTP to GDP.[9, 10] To aid in GDP dissociation, guanine exchange factors (GEFs) will associate with Ras in a way that alters is nucleotide preference for binding GDP, allowing it to bind the more bioavailable GTP form.

Active, GTP-bound Ras localized to the PM will associate with and activate other proteins, called effectors, to regulate the relay of extracellular, mitogenic signals to downstream signal propagation, cell growth and differentiation (Figure 1.2).[11-13] These pathways have been well studied and include the mitogen-activated protein kinase (MAPK) pathway and the phosphatidylinositol-3-kinase (PI3K) pathway.[14-18]

1.2 Post-translational modifications of Ras and its association to the plasma membrane

The four Ras isoforms are distinguishable by their HVR, as stated above. These regions contain residues that are further modified post-translationally to ensure association with the PM. It is a well-established model that Ras must be localized to the PM for proper function, highlighting the importance of this C-terminal region.[6, 19-22] Within this region, each Ras isoform terminates its sequence with a CAAX motif. The four most C-terminal residues are composed of a cysteine ("C"), two aliphatic residues ("AA") and a residue of varying identities ("X"). Each isoform has their own specific CAAX sequence which signals PTMs within this area that are required for its proper localization to the PM. It has previously been shown that mutations of the CAAX residues will render Ras inactive, emphasizing the role of CAAX processing in proper Ras function.[19]

Many CAAX proteins, including Ras, undergo three required PTMs (Figure 1.3).[23-25] First, the CAAX proteins are prenylated on their C-terminal cysteine residue by either farnesyltransferase (FTase) or geranylgeranyltransferase (GGTase). The addition of either a 15-carbon farnesyl or 20-carbon geranylgeranyl group is determined by the identity of the X residue. FTase will farnesylate proteins that terminate in Ser, Met, Ala, or Gln, while GGTase will geranylgeranylate proteins terminating in Leu.[26] All Ras isoforms are farnesylated by FTase since all except HRas (Ser) terminate in Met.[27] Following prenylation and translocation to the endoplasmic reticulum (ER), CAAX proteins will undergo proteolysis of the -AAX residues by Ras converting enzyme 1 (Rce1). Lastly, the carboxylate of the C-terminal cysteine will be methylated by isoprenylcysteine carboxyl methyltransferase (Icmt), a membrane protein in ER.[23]

These modifications add hydrophobic groups to the otherwise soluble, hydrophilic Ras proteins that further allow the proteins to associate and anchor to membranes.[28, 29]

After CAAX processing, some Ras proteins are further modified based on their isoform identity. HRas and NRas will move from the ER directly to the Golgi, where they are palmitoylated and will eventually reach the PM by vesicular transport.[6, 28] However, KRas4B takes a different path to reach the PM. It contains a polybasic region (PBR) within its HVR. This PBR allows KRas4B to be trafficked from the ER directly to the PM. The mechanisms by which KRas4B translocates to the PM were previously unknown but speculated to include unidentified chaperone proteins that shield the newly added hydrophobic groups from the cytosol.[6, 28, 30, 31] One such chaperone is phosphodiesterase-δ (PDEδ), which aids in the correct localization of farnesylated KRas4B by facilitating its diffusion into the cytoplasm.[32, 33] However, chaperones like PDEδ may not be involved in trafficking KRas4B to the PM but more so in KRas4B recycling after membrane dissociation.[22]

1.3 Ras mutations and oncogenesis

The majority of oncogenic mutations are gain-of-function mutations within three codons or "hotspots," Gly12, Gly13 or Gln61 (Figure 1.1).[3] This increased function causes the hallmark oncogenic phenotypes of uncontrollable cell proliferation, differentiation and cell death. However, point mutations vary among cancer type, tissue samples and even Ras isoforms. For example, Gly12 is typically mutated in KRas whereas Gln61 mutations are more prevalent in HRas.[1, 34] Of the Gly12 mutations in KRas, the majority were substituted with aspartic acid, followed by valine and cysteine respectively.[34]

These mutations also have different mechanisms of action in oncogenesis. In a study performed by Smith *et al.* (2013) mutants G12V and Q61L both show lower GTP hydrolysis rates whereas G13D has very rapid nucleotide exchange of GDP for GTP. With the addition of GAPs, WT protein had the fastest rate of GTP hydrolysis compared to the three mutants. In the presence of the GEF SOS, G13D had the fastest nucleotide exchange rate, however Q61L showed the largest increase in exchange rate compared to basal rates.[35] This suggests that G13V and Q61L may be hypersensitive to GEF activation. These mutations have also been shown to have differing GTP-binding affinities, intrinsic and GAP-mediated GTP hydrolysis rates, and effector binding affinities.[36]

1.4 Ras, the "undruggable" oncogenic target

Most initial small molecules were designed to be direct, competitive inhibitors that bind Ras within its active site and nucleotide binding domain. Previously, adenosine triphosphate (ATP) mimetic compounds were found to be successful competitive inhibitors within protein kinases.[37] However, the affinity of Ras for its respective nucleotide, GTP, is about 1000-fold greater than that of a kinase with ATP. The picomolar binding affinity of Ras for GTP requires a sub-picomolar inhibitor in order to outcompete its normal nucleotide substate, rendering most GTP-mimetic inhibitors insufficiently enough.[37]

An extensive review of Ras-inhibitory molecules spanning three decades of work was published by Cox *et al.* (2014). They summarized the molecules designed to inhibit Ras through means other than competitive inhibition within the nucleotide binding site. Some molecules worked to disrupt the protein-protein interaction between Ras and its effector and/or regulator proteins through direct contacts with Ras. For example, sulindac sulphide analogs bind Ras within its Raf-binding site and have shown decreased activation of proteins downstream of Ras signaling and also decreased cell proliferation.[38] However, these analogs do not have a high enough potency for use as treatments and do not contain studies on their possible off-target effects. Other molecules worked to disrupt interaction of Ras with its positive regulators, GEFs. The compound DCAI, for example, was shown to bind KRas4B and block its interaction with the GEF, SOS, thus, decreasing Ras activation in cells.[38] However, DCAI and its newer analogs have weak KRas affinity and low potency. The review concluded, as many other have, that current compounds that bind Ras need significant improvements to be even modest therapeutics for the clinic.

It is important to note, that under the current understanding, mutant Ras is what drives oncogenic signaling. Therefore, pan-Ras inhibitors, which target the common features of all isoforms of Ras proteins as well as characteristics maintained between the oncogenic mutants of Ras, are likely to have cellular toxicity, as Ras is essential for normal cell signaling and survival.[39] This has made classes of direct, allosteric inhibitors of Ras unsuccessful, as they are unable to differentiate and treat the oncogenic mutants of the specific Ras isoforms selectively. [40]

The lack of suitable binding pockets, as well as lack of specificity for Ras isoforms, caused research to turn to more indirect approaches by targeting the signaling cascade, up and downstream of Ras localization to the plasma membrane.

1.5 Indirect targeting of Ras

The signaling pathways of Ras are very well characterized and thus have allowed for targeting the processes up and downstream of Ras localization to the plasma membrane. These include its post-translational modifications, localization to the plasma membrane, nucleotide exchange process, and effector binding.

Most indirect inhibitors of the oncogenic pathway of Ras to be approved for treatment, target proteins downstream of Ras localization to the plasma membrane. Some inhibitors, such as sorafenib, have targeted the Ras effector Raf within the MAPK however within specific KRas mutated cell lines these inhibitors have caused an upregulation of ERK signaling through Raf's other isoform, C-Raf.[41, 42]

One-step downstream of Raf is MEK within the MAPK pathway. Unfortunately, MEK specific inhibitors alone have not shown much success within tumors across various phases of clinical trials. There are a few MEK inhibitors approved for treatment, but only in combination with inhibitors of other downstream proteins like B-Raf and EGFR.[43] The final protein of the MAPK pathway, ERK, does show some promise as an indirect inhibitor of Ras signaling, as there are a few different small molecule inhibitors in early stages of clinical trials.[43]

Other downstream targets include SHP2, which promotes MAPK signaling and has shown some progress as a chemotherapeutic target in decreasing the size of KRas mutant tumors.[44, 45] SOS, a Ras stimulating GEF, has also been a point of interest. Some small molecules have been designed to disrupt the SOS-Ras interactions (as described in Section 1.4) while others have attempted to disrupt the intrinsic GEF activity within SOS itself.[46] In addition to targeting proteins of the MAPK pathway, combination treatments with targets of the PI3K pathway have proven to be effective in multiple Ras mutant cancers.[47] Unfortunately, the MAPK pathway and the PI3K pathway are implicated in multiple cellular functions and are activated through various protein cascades. Thus, treatments that are not localized to the cancerous area will have toxic side-effects on many healthy cells.

Some researchers have targeted the proteins that process Ras before it reaches the plasma membrane. FTase has two notable inhibitors (FTIs), tipifarnib and lonafarnib. Although both were promising in treating mice and had advanced to Phase III clinical trials, human clinical trials did not show the same success. They were reported to not improve the outcome for advanced pancreatic cancer, advanced non-small cell lung cancer (NSCLC) or acute myeloid leukemia

(AML), even in combination with other chemotherapeutics.[48] Interestingly, upon FTase inhibition, Ras can be alternatively prenylated by GGTase-I and continue on with proper processing and signaling function (Figure 1.3).[49-51] To create better inhibitors of CAAX protein prenylation, dual FTI and geranylgeranyltransferase inhibitors (FGTIs) have been employed. Recently, FGTI-2734 based on the C-terminus of Ras, was able to prohibit KRas4B from localizing to the PM in pancreatic, lung and colon human cancer cells.[52] *In vivo* this inhibitor was also able to suppress Akt and mTOR mediated pathways and induced apoptosis in patient-derived xenografts.[52] Interestingly, along the lines of prenylation, statins have been considered to have suppressive effects on tumorigenesis. Recently, it has been thought that this is true based on statins' role in inhibiting the production of mevalonate, the precursor for farnesyl and geranylgeranyl pyrophosphates.[53, 54]

Small molecule inhibitors of Rce1 have been shown to induce mislocalization of Ras from the PM in human colon cancer cells, and mouse models. Rce1 NSC1011 is widely considered the best inhibitor of the protease.[55-57] However, genetic deletion of *Rce1* in mice led to the development of lethal cardiomyopathy and exacerbated the development of KRas-induced myeloproliferative disease.[58] It is also important to note that another protease, zinc metalloprotease STE24 (ZMPSTE24) has functional redundance with Rce1, as it can also cleave the C-terminal -AAX residues of certain CAAX proteins.[59, 60] However, ZMPSTE24 has two roles within the processing of specific CAAX proteins, such as nuclear scaffold protein lamin A or the mating pheromone **a**-factor in yeast.[61-63] Its primary role is to cleave upstream of the CAAX motif to produce mature lamin A. Upon further study, it was determined that Rce1 is the primary protease that performs the -AAX cleavage, as the Ras proteins within *RCE1* deficient cells were not methylated and also severely mislocalized from the PM without rescue by endogenous ZMPSTE24, suggesting that the uncleaved C-terminal residues restricted the protein form being methylated.[64] It is suggested that ZMPSTE24 may be able to perform the C-terminal -AAX cleavage only on certain CAAX proteins, as it has subtle substrate specific differences to substrates of Rce1. Therefore, all isoforms of Ras may not be substrates of ZMPSTE24.[60, 65, 66]

The final step of CAAX processing, methylation by Icmt, has also been targeted for inhibition of the oncogenic Ras pathway. As it is the sole methyltransferase known to act on CAAX proteins, it provides a very selective inhibitor target.[67, 68] Because it must accommodate both the prenylated-protein substrate and the methyl-donor cofactor, inhibitors could take on

features of both structures. Since the *S*-adenosyl-L-methionine (SAM) cofactor binding site is more well characterized amongst different Icmt species, SAM or *S*-adenosyl-L-homocysteine (SAH) mimetic inhibitors were designed.[23] However, SAM is the second most utilized cofactor within a cell, behind ATP, and therefore SAM or SAH mimetic inhibitors also non-selectively target other SAM-dependent methyltransferases.[69-71] For this reason, methotrexate, a very successful cancer drug that is known to decrease nucleotide biosynthesis and increase concentrations of homocysteine, was found to decrease Ras methylation, mislocalize Ras into the cytosol, and decrease the activation of downstream Ras effector, Akt.[72] Most Icmt inhibitors are now being designed with dual, substrate and cofactor properties in the hopes of creating a competitive inhibitor that strongly binds the active site of Icmt. To date, cysmethynil is the most potent and well-studied Icmt inhibitor.[54, 73] As with many integral-membrane protein targets, inhibitors struggle to maintain solubility, bioavailability, and other pharmacokinetic properties, making them unsuitable for clinical use. Newer classes of Icmt inhibitors have been developed, since the inception of cysmethynil, including by the Hrycyna Lab,[74-80] however they still have been unable to overcome poor solubility properties.

Other promising strategies that target pre-membrane associated of Ras include disrupting the binding of PDEδ with KRas4B. One such molecule, termed deltarasin, showed nanomolar affinity towards the prenyl-binding pocket of PDEδ.[32] It was able to decrease KRas4B signaling as well as suppress cell proliferation of pancreatic ductal adenocarcinoma cells that retain oncogenic KRas4B mutations *in vitro* and *in vivo.*[32] Utilizing the crystal structures from this study as well as from another (Dharmaiah *et al.*, 2016), structure-based drug design can be performed for newer, more specific inhibitors.

Many of these inhibitors, whether up or downstream of Ras signaling, have been approved for the treatment of cancers, however they largely lack potency and specificity, reinforcing the need for better Ras oncogenic pathway inhibitors.[43] Inhibitors of the enzymes responsible for the PTMs of Ras battle low cellular permeability and solubility.[81] This is due to the hydrophobic nature of the modifications that they are targeting. The strongest inhibitors of these enzymes generally contain characteristics of the isoprenoid chain, as this moiety sits near the reactive C-terminal cysteine and thus must be accommodated within portions of the modifying enzyme's active sites. The addition of these hydrophobic groups causes the solubility of these compounds to decrease as well as the permeability, since the endogenous role of the isoprenoid group is to

anchor the protein to its target membrane. Solubility and permeability decrease further for small molecule inhibitors of both Rce1 and Icmt. Since they are both integral membrane proteins, the majority of their amino acid sequence is hydrophobic in nature, thus requiring more hydrophobic binding partners.

1.6 Sotorasib, the first FDA approved KRas4B direct inhibitor

In May of 2021, the Food and Drug Administration (FDA) accelerated the approval of the first direct KRas4B inhibitor, sotorasib. This small molecule agent exploits the proximity of the cysteine residue of G12C mutated KRas4B to an adjacent pocket (termed P2) within the switch II region of the protein. Due to the previous identification of a class of inhibitors that can target P2 of KRas4B, future iterations of inhibitors were developed that not only utilize P2, but also target an unexploited surface groove of mutant KRas4B^{G12C} to enhance potency and selectivity.[82] The resulting compound, AMG 510 (now known as sotorasib), showed great promise as not only a combinatory therapy but alone as a monotherapy. In initial clinical trials of patients with non-small cell lung cancer (NSCLC), treatment with sotorasib resulted in a either a halt or regression of their cancer in about 30% of the 73 patients, and an 88.1% showed a halt in progression of their cancer [83]

The structure of KRas^{G12C} co-crystalized with sotorasib showed the inhibitor within the P2 pocket of KRas4B and also the His95 groove.[82] The increased potency of sotorasib is due to the extensive contacts of the drug within the His95 groove (25 van der Waals contacts). Sotorasib does not inhibit nonmutated, wild-type (WT) KRas4B. Therefore, this drug is a treatment for people with solid tumors that have KRas4B^{G12C} mutations in NSCLC. Treatment results revealed that the disease state of patients did not worsen for a period of 7 months, after which the cancer began to intensify.[84] This is not a staggering number compared to other cancer therapies, and therefore, while still continuing its use as a treatment, more research is needed to understand the best use of sotorasib at different stages of treatment and disease progression itself.

Nonetheless, the discovery and approval of sotorasib are important to consider as new therapeutics move towards directly targeting specific mutations of the Ras isoforms. This will afford fewer off-target effects of the drugs, especially to other isoforms of Ras that are not implicated in oncogenic pathways for those patients. It is also possible that sotorasib has

contributed to the increase in survival rate for lung cancer patients, which still continues to be the leading cause of cancer death.[85]

1.7 Reversible methylation as a point of regulation for CAAX protein signaling

In understanding how to create better inhibitors for mutated Ras and its oncogenic signaling pathway, it is also important to look at endogenous points of regulation within that pathway. Most common cellular regulation comes from feedback loops. Within Ras signaling pathways it has been found that, possibly as a result of evolved tumor suppression, oncogenic and activated Ras is regulated by negative feedback. This diminishes Ras signaling and thus decreases ERK and PI3K signaling, ultimately causing cellular growth arrest.[86] Other regulators of wild-type Ras pathways include GAPs which accelerate the hydrolysis of GTP to GDP and produce inactive, GDP-bound Ras. Other proteins translated in response to ERK activation also serve as feedback inhibitors of molecules along the MAPK pathway.[87]

Interestingly, along the CAAX PTM processing pathway, methylation is the only reversible step.[88, 89] Reversibility may allude a point of protein and signaling regulation. The subsequent parts of this section will provide information on the importance of methylation and taken together, emphasizes the possible role of methylation as a point of regulation for CAAX proteins, including KRas4B. Thus, further study on the role of methylation is an imminent need.

1.7.1 Methylesterase

There is a lack of evidence confirming a role for a methylesterase that specifically acts on this pathway, recent research continues to speculate about its existence. Methylesterases (also known as carboxylesterases) that are capable of acting on prenylated proteins have been identified in plants as well as in the liver tissue of rat, rabbit, bovine and porcine samples.[90-96] In parallel, human carboxylesterase 1 (hCES1) has been identified and crystallized.[97, 98] This esterase has 79% identity and 88% similarity with porcine liver methylesterase also known as polyisoprenylated methylated protein methyl esterase (PMPMEase).[99] Although it is known to have many different substrates, hCES1 has a large, hydrophobic and flexible active site that can accommodate polyisoprenylated groups, leading researchers to believe that hCES1 acts on isoprenylated proteins in addition to its other substrates.[97, 100]

As CAAX proteins are highly implicated in oncogenesis, hCES1 has also been studied for its possible role within cancer. It has been found to have heightened levels of expression in breast,[100] lung adenocarcinoma and NSCLC cell lines,[101] as well as in patient tissue samples of colorectal,[102] prostate,[103] and pancreatic[104] cancers. In 2013, Cushman *et al.* reported one of the first and only comprehensive studies of methylesterase activity on a CAAX protein, RhoA. They revealed that in thrombin stimulated breast cancer cells, which causes RhoA activation, unmethylated RhoA levels decreased by about 30%. When cells were treated with a CES1 specific siRNA, it enhanced methylated and reduced unmethylated levels of RhoA. This suggests a direct role of CES1 in the demethylation of RhoA. In the absence of CES1, but also under starvation conditions, cells displayed an increase in RhoA activity, which suggests that methylation does not indicate activation state of RhoA. These findings will need to be corroborated, as many previous studies, including those performed by Cushman and Casey, demonstrated that methylation has a direct impact on Rho activity.[105-107]

1.7.2 KRas methylation levels differ in colorectal cancer cells and tumor samples

In a recent study performed by Ntai *et al* in 2018, a proteomics approach was taken to better understand the different proteoforms of KRas4B within different colorectal tumor samples with known KRas4B mutations. Interestingly they found that some tumor samples, characterized for their known KRas4B mutation, only expressed a small fraction of mutated KRas4B compared to the total KRas4B expressed overall. When analyzing the structure of KRas4B within these samples, the methylation state varied between sample and cancer stage severity. Furthermore, within individual samples that contained both WT and mutated KRas4B, the mutant and WT protein contained differing methylation states.[108] Not only does methylation state of KRas4B vary between tumor sample, it also varies between mutated and nonmutated proteins within the same sample. This suggests that methylation may help to regulate tumorigenic Ras activity especially at different levels between the different oncogenic mutants of Ras.

1.7.3 SAM-dependent methylation is energetically costly to the cell

Methylation requires SAM as the methyl-donating cofactor. As the synthesis of a molecule of SAM requires a molecule of ATP, methylation of prenylated proteins is an energetically costly

for a cell.[109] Because SAM-dependent methylation is expensive to a cell, its product, SAH, constitutes a feedback loop that can negatively regulate the activity of Icmt.[54, 110] This further supports the need to uncover if methylation servs as a point of regulation for CAAX proteins, as this step is so energetically costly.

1.8 Isoprenylcysteine carboxyl methyltransferase (Icmt)

Methylated, isoprenylated proteins were first identified within the mating factors from jelly fungi *Tremella mesenterica* and *Tremella brasiliensis*.[111, 112] Shortly after, the yeast *Saccharomyces cerevisiae* mating hormone, **a**-factor was shown to also contain a prenylated and methylated C-terminus.[113] In parallel, Ras proteins, γ subunits of G proteins, α subunit of cGMP phosphodiesterase, and nuclear lamin B were also identified to contain prenylated and methylated C-termini.[114-117] These proteins would soon be classified by their shared C-terminal CAAX motif (see section 1.2 above). Their identification suggested a new class of methyltransferase, as no known methyltransferase could act on isoprenylated proteins.[114] During the first decade or so of identifying the various CAAX proteins and how these PTMs may implicate their respective functions, their specific methyltransferase was detected within mammalian membranes.[118-120] This methyltransferase would soon be termed isoprenylcysteine carboxyl methyltransferase (Icmt). Proximal to Icmt discovery, *Saccharomyces cerevisiae* mating cells were found to be sterile with the deletion of the gene *STE14* (aptly pronounced, sterile-14) (Blair PhD Dissertation, University of Oregon, Eugene, 1979). Just over 10 years later, Hrycyna and Clarke (1991) determined that Ste14 of yeast was the methyltransferase for isoprenylated proteins, specifically **a**-factor.[121, 122] The sterility of *ΔSTE14* yeast mating cells was thus connected to the lack of Icmt causing unmethylated **a**-factor mating pheromone to not be exported and thus not recognized by the cell's mating partner. The lack of export was specifically connected to unmethylated **a**-factor being unable to interact with its export protein, Ste6, and subsequently its failed recognition by receptor Ste3 on its mating partner cells.[123-126]

Icmt is an integral membrane protein of the ER.[120, 127] Until the discovery of Icmt, there were five classes of SAM-dependent methyltransferases characterized by their structural features.[128-130] Icmt was the founding member of a new class of integral membrane methyltransferases. Icmt has remained the sole member of its founding class and thus could provide a specific target for the indirect inhibition of the various disease pathways of CAAX proteins. Over the past three decades,

the structure, mechanism, and characteristics of Icmt have been extensively studied. Four species of Icmt have contributed to the majority of research including *Homo sapiens* (*Hs*-Icmt), *Saccharomyces cerevisiae (Sc*-Icmt or Ste14), *Tribolium castaneum* (*Tc*-Icmt), and *Anopheles gambiae* (*Ag*-Icmt). Human Icmt has yet to be functionally purified and as such the enzyme from other species are used as models. It is important to note that a prokaryotic model of Icmt was established and crystallized in 2011 (Yang *et al.)* termed *Methanosarcina acetivorans* Icmt (*Ma*-Icmt), however prokaryotes do not have any known prenylated proteins.[24, 128] It has since been renamed *Ma*-MTase but is no longer a suitable model for Icmt, as will be discussed in Section 1.8.1. The research of this dissertation will utilize Ste14 as a model for human Icmt, as robust methods are in place to functionally express and purify it.[131]

1.8.1 Ste14 as a model for human Icmt

Ste14 is a 28 kDa protein with 239 residues and multiple membrane spanning regions.[123] It shares 30% sequence identity and 46% sequence similarity with its human homolog (Table 1.1). These percentages increase when comparing the C-terminal catalytic regions of the protein; 44.7% sequence identity and 62.9% similarity. The sequence diverges for Icmt species within the N-terminal region of the protein. Specifically, between human and Ste14, this divergence is due to the two additional N-terminal helices of human Icmt. These two helices have contacts with other portions of the protein and are speculated to be involved in stabilizing protein structure, stability within the ER membrane and possibly in helping to create a depression within the membrane to accommodate the upstream portions of CAAX proteins as they are being methylated.[24] It is also postulated that the N-terminal extension may have a regulatory function.[23, 132] Nonetheless, human Icmt and Ste14 have functional redundancy as seen when mating resumed between *Saccharomyces cerevisiae* mating partners within human Icmt transformed strains of *ΔSTE14* cells.[120]

Court *et al*. (2011) aligned Icmts from 15 different species and depicted the results on the topology of Ste14 (Ste14 structure discussed in the following section) (Figure 1.4A). This representation clearly shows the homologous residues that are retained in the majority of the C-terminal portions of the protein. However, with extensive studies on the four species listed above, a better characterized homology diagram between the species is shown in Figure 1.4B.

Topology and Structure

Ste14 is composed of 6 transmembrane helices that span the ER membrane.[120, 127, 132, 133] Both the N- and C-termini are on the cytosolic face and along with the cytosolic loops between helices, contain residues that are important for catalytic activity.[132, 133] The last two helices are structured in a helix-turn-helix motif and obtain highly conserved aspartate (Asp191) and proline (Pro192) residues to aid in the structure of this motif (Figure 1.4B).[132, 133] Within the more homologous C-terminal half of Ste14, it is considered that, roughly, residues 115 to 239 compose the catalytic site of the protein.[133] The sequence of this region was compared to other SAM-dependent methyltransferases that lacked tripartite consensus sequences as well as a screening of other yeast proteins. It revealed a consensus motif RHPxY-hyd-EE consisting of two conserved parts flanking a hydrophobic stretch of amino acids.[133] This motif was further characterized and extended into two recognizable motifs (motif A and B), LVxxGxYxxxRHPxYxG and xRxxxEExxLxxxFGxxxxEYxxxVxxxxP respectively.[23] Many residues within this area were deemed to be important as Ste14 lost function upon their mutation. [23] Ste14 also contains a GxxxG motif that is proposed to be involved in homodimerization of the molecule (see dimerization section below).

To date, there is no three-dimensional structure of Ste14, but crystal structures have been solved for two other Icmt species, *Ma*-MTase and *Tc*-Icmt. The prokaryotic structure from *Ma*-MTase was published first and revealed a distinct cofactor binding pocket and a hydrophobic tunnel that would allow the reactive cysteine of the prenylated protein to orient itself in close proximity with SAM.[128] It also only has 5 transmembrane helices, compared to the 6 of Ste14 and 8 of human Icmt, giving the lowest homology with human Icmt of the other 4 most studied species (Table 1.1). Unfortunately, there are no known substrates endogenous to *Ma*-MTase as prokaryotes do not prenylate proteins.[24] This may not make *Ma*-MTase a suitable model for prenylated protein binding, but it does provide insights into SAM binding to an integral membrane methyltransferase. The second structure is the first eukaryotic Icmt solved (*Tc*-Icmt).[24] Of the four well studied species, it shares the highest homology with human Icmt (Table 1.1). This structure also revealed a well-defined SAM binding pocket as well as a hydrophobic substrate tunnel (Figure 1.5A). In addition, it identified many residues with proposed contact with both SAM and prenylated substrate (see cofactor and substrate binding section).

Ste14 functions as a homodimer

Sequence analysis with other Icmt species revealed a conserved GxxxGxxxG motif along transmembrane helix 1 (TM1) of Ste14. These motifs are well characterized for stabilizing interprotein interactions and structure, protein-membrane interactions, and protein-protein interactions of membrane proteins.[134] To probe the function of this motif, Griggs *et al.* (2010) performed crosslinking experiments within Ste14. The bis-sulfosuccinimidyl substrate homobifunctional crosslinking agent was able to crosslink Ste14 in both crude membrane and pure protein preparations revealing not only dimers, but also higher order homooligomers. To further confirm the presence of dimerization, crude membrane preparations expressing either His-tagged Ste14 or WT, untagged Ste14 were tested for coimmunoprecipitation. SDS-PAGE analysis revealed that untagged Ste14 was able to associate with His-tagged Ste14 and upon His-tagged Ste14 immunoprecipitation, untagged Ste14 was visible.

A recent crystal structure of a eukaryotic Icmt (*Tc*-Icmt) proposed a different role of the GxxxG motif for Icmts, confirming more than six TMs.[24] *Tc*-Icmt, like human Icmt, contains an extended N-terminal region with two more transmembrane helices than Ste14. TM3 of *Tc*-Icmt contains the GxxxG motif, which is homologous to TM1 of Ste14. Whereas the motif in Ste14 is proposed for homodimerization, the GxxxG motif in *Tc*-Icmt is proposed to stabilize helical association within the protein for structure stability.[24] This was proven by reassociation and coimmunoprecipitation of TM1 and TM3 of *Tc*-Icmt after proteolytic cleavage of the amino acid backbone between TM2 and TM3.

To more directly deduce the oligomeric state and function of Ste14, Dr. Anna C. Ratliff performed an extensive mutational and chemical crosslinking analyses of the N-terminal domain of Ste14. This revealed residues Met25, Thr26, Ser27, Tyr28, Leu30, Gly31, Gly35, Gly39, Phe41, Pro42, and Gln43 were essential for not only protein stability but activity.[135] In addition, biophysical data from size exclusion chromatography, multi-angle light scattering and small angle X-ray scattering (SEC-MALS-SAXS) revealed purified Ste14 existing mostly in dimeric form.

Ste14 is a zinc-dependent metalloenzyme

Icmt from rat liver samples was first found to require metal ions for activity and stabilization.[136] The membrane samples as well as recombinant protein reduced methylation of G

proteins by 1,10-phenanthroline specifically but not by EDTA nor EGTA. Anderson *et al.* (2005) expanded the profile of metal chelators tested on Ste14 and discovered that Ste14 is also sensitive to 4-(2-pyridylazo)resorcinol and 2-carboxy-2'-hydroxy-5'-sulfoformazyl-benzene (Zincon) in addition to 1,10-phenanthroline.[131] EDTA was also found not to inhibit Ste14 activity however this information with the addition of the increasing sensitivity from 4-(2-pyridylazo)resorcinol to Zincon suggests that more hydrophobic metal chelators are more effective and thus the metal Zn^{2+} ion of Ste14 must be buried deep within a hydrophobic portion of the protein. A similar study tested the effectiveness of cholesterol-based metal chelators against Ste14 for this reason.[137] This new panel of chelators proved to be useful as a tool to identify other intrinsically hydrophobic proteins, such as membrane proteins, that may be unidentified metalloenzymes.

Hodges, *et al.* also initially proposed that the three endogenous cysteine residues of Ste14 may interact with the metal ion. When all three cysteine residues were mutated to serine, there was no difference in protein expression or activity, suggesting that other residues must interact with the metal ion.

Kinetic mechanism of Ste14

Proteins with two substrates can have various kinetic mechanisms. Most SAM-dependent DNA methyltransferases have one of several bi bi mechanisms.[138] Substate binding and product release can happen in an ordered or random fashion. Other mechanisms include a double-displacement reaction otherwise called a Ping Pong mechanism. In rod outer segment membrane preparations, Icmt was determined to have an ordered bi bi mechanism with SAM binding first and SAH being released last.[110] The prenylated substrate will bind after SAM and once methylated, will be the first product released. Therefore, characteristics of the structure of SAM should be incorporated into inhibitor design processes to increase small molecule binding efficiencies. More than a decade later, kinetic mechanism studies were performed on recombinant human Icmt that agreed with the previous data.[139] Using different minimal substrates, they confirmed that Icmt acts in an ordered, sequential bi bi mechanism with SAM binding first.

The two crystal structures of Icmt were co-crystallized with SAH but only *Tc*-Icmt contained a minimal isoprenylated protein substrate as well.[24, 128] In both structures, the density of the SAH molecule was well resolved. In the *Tc*-Icmt structure, the density within the hydrophobic substrate

binding tunnel could not be resolved to the geranylgeranylated molecule that it was co-crystallized in the presence of. Looking at the kinetic mechanism studies, it is not surprising that the unmethylated substate was not co-crystallized with Icmt. The ordered bi bi mechanism proposes that SAH is a competitive inhibitor of SAM however the methylated substrate product is not a competitive inhibitor for the unmethylated substrate, suggesting that there is a conformation change after methylation occurs and the methylated product is now bound in an allosteric site with lower affinity.[110, 139] Therefore, SAH and unmethylated substrate would most likely not be crystallized together. The best pairs for crystallization would include methylated product with SAH, as unmethylated substrate with SAM would most likely react in the presence of Icmt.

Cofactor and substrate binding

The SAM binding site pocket and active site of Icmt is much better characterized than the substrate binding site. This is most likely due to the higher number of conserved residues within the C-terminal portions of the protein, which is proposed to house most of the residues important for SAM binding (Figure 1.4). As previously stated, the C-terminus of Ste14 contains motifs A and B (LVxxGxYxxxRHPxYxG and xRxxxEExxLxxxFGxxxxEYxxxVxxxxP respectively) that are conserved amongst not only different Icmt species but also methyltransferases of different classes.[23, 133] Upon mutation, this region revealed 31 loss-of-function mutants (<5% WT activity).[23] Of those residues, the cytosolic residues Glu213 and Glu214 are significantly critical for function, as when they are mutated to similarly charged residues they do not regain WT enzyme activity.[133] These residues were speculated to be part of a SAM binding site, however mutational analyses and subsequent activity assays alone are not enough to determine if a change in activity is due to SAM binding. It is possible these mutations could destabilize the enzyme structure, affect prenylated substrate binding, or be important for the catalytic mechanism of the enzyme.

The crystal structures both have highly resolved SAM binding pockets, co-crystallized with the reaction product, SAH.[24, 140] As previously mentioned, although prokaryotic *Ma*-MTase does not have any identified endogenous substrates, it undoubtedly binds SAM and is a methyltransferase. Therefore, it can still provide information about the SAM binding site of integral membrane methyltransferases. Similar to the structure for eukaryotic *Tc*-Icmt, the SAM binding pocket is at the top of the cytosolic side of Icmt. The pocket is composed of TM6 – TM7

connector of *Tc*-Icmt (Loop 4 of Ste14), the cytosolic extension of TM8 (TM6 of Ste14) and the cap helix (Figure 1.5). These components keep SAM shielded from the cytosol and membrane environments. The TM6 – TM7 connector (Loop 4 of Ste14) contains many conserved residues (Figure 1.4) and is speculated to perform one of the largest conformational displacements upon enzymatic catalysis. Residues Phe184, Tyr204 and Glu250 (Ste14: Phe147, Tyr167 and Glu213) of *Tc*-Icmt provide direct contacts to SAH which is mostly in agreement with *Ma*-MTase.

An extensive alanine scanning mutagenesis study was performed of the 76 conserved residues of the 15-Icmt species sequence alignment.[141] Of the conserved residues mutated to alanine (or in the case of an endogenous alanine residue, it was mutated to glycine), 40 were loss-of-function mutations (<10% WT activity) when tested with a minimal-farnesylated substrate (see Chapter 3 for more information). Of the 41 cytosolic or ER lumen exposed residues, 28 mutants were enzymatically inactive. This study is in agreement with other mutational analyses performed on Ste14 as well as on *Ag*-Icmt.[133, 140, 142] Inactive residues upon mutation are important for enzyme function, however the activity assays performed do not determine if the decrease in activity is due to a structural, substrate binding, or catalytic change. Therefore newer, more quantitative methods are needed to determine the function of each inactive residue.

The N-terminal half of the protein does not have nearly as many conserved residues as the proposed catalytic areas of Icmt (Figure1.4). Also as previously stated, the *Tc*-Icmt structure did not resolve the prenylated protein substrate.[24] It is well known that in order for methylation to occur, the CAAX protein must have already undergone the two preceding steps of its required PTM processing, prenylation and proteolysis,[118] In designing inhibitors it is important to understand how Icmt accommodates both SAM and the bulky hydrophobic prenyl group of the substate within close enough proximity to transfer a small methyl group from one to the other. The *Tc*-Icmt structure reveals a hydrophobic substrate cavity that is lined with hydrophobic and aromatic residues: Tyr95, Met99, Phe102, Val124, Asn126, Tyr131, Trp215, Trp218, Tyr235, Phe242, and Phe243 (Ste14: Phe52, Leu56, Phe59, Leu81, Asn83, Tyr88, Phe178, Trp181, Phe198, Phe205, and Phe206) (Figure 1.5). All residues are conserved between the four most studied Icmt species (Figure 1.4). The following are the comparisons of data between Ste14, *Tc*-Icmt and *Ag*-Icmt:[24, 140, 141]

- Phe52 of Ste14 (*Tc*-Icmt: Tyr95) decreases activity about 40% when mutated to alanine, but the similarly aromatic tyrosine mutation rescues WT activity. It was not tested in *Ag*-Icmt
- Leu56 of Ste14 (*Tc*-Icmt: Met99) is inactive when mutated to alanine, but regained some activity when mutated to similar or aromatic residues. It was not tested in *Ag*-Icmt.
- Phe59 of Ste14 (*Tc*-Icmt: Phe102) shows minimal activity when mutated to alanine (agrees with *Ag*-Icmt studies) and was rescued when mutated to tyrosine.
- Leu81 of Ste14 (*Tc*-Icmt: Val124) was inactive when mutated to alanine and was not rescued when mutated to an aromatic residue. This residue showed minimal activity when mutated in *Ag*-Icmt.
- Asn83 of Ste14 (*Tc*-Icmt: Asn126) is active when mutated to alanine in both Ste14 and *Ag*-Icmt. This residue is proposed to give the M4 – M5 connector (Loop 2) amphipathic character to better accommodate the amphipathic character of the reactive cysteine.
- Tyr88 of Ste14 (*Tc*-Icmt: Tyr131) is minimally active when mutated to alanine or another aromatic residue. This residue was not tested in *Ag*-Icmt but is proposed to be exposed to the cytosol in Ste14 or hydrogen bonded to the Ser128 within *Tc*-Icmt.
- Phe178 and Phe206 of Ste14 (*Tc*-Icmt: Trp215 and Phe243) were inactive when mutated to alanine in Ste14 and *Ag*-Icmt. They are both proposed to be within can der Waals distance of the isoprenoid group of the substrate.
- Trp181 of Ste14 (*Tc*-Icmt: Trp218) was not mutated however its counterpart in *Ag*-Icmt is inactive.
- Phe198 of Ste14 (*Tc*-Icmt: Tyr235) is inactive when mutated but was not tested in *Ag*-Icmt.
- Phe205 of Ste14 (*Tc*-Icmt: Phe242) was inactive when mutated to alanine and agree with the data from *Ag*-Icmt. When mutated to other aromatic residues within *Ag*-Icmt, activity was rescued.

In the enzymatic mechanism experiments, it was determined that Icmt acts in a sequential ordered bi bi mechanism (see mechanism section above).[110, 139] In both experiments, the SAH product was a competitive inhibitor for SAM. However, the methylated isoprenylated protein

product was not a competitive inhibitor for the unmethylated substrate. This indicates that the methylated product is located allosterically to the active site and has a lower affinity for the enzyme. It further suggests that a conformational change occurs to move the methylated product to the allosteric site without changing the SAM/SAH binding site. This may be possible, through the movement of Loop 2 (TM4 – TM5 connector) (Figure 1.5). As stated above, this region is speculated to create a depression in the lipid bilayer to accommodate the upstream portions of the prenylated protein in close proximity to the Icmt enzyme.[24] If the methylation reaction causes a conformational change that makes the unmethylated product have a lower affinity to Icmt, it is possible that the conformational change is within Loop 2 and causes the proximal portions of the protein to no longer be stable in such close proximity to Icmt. Another proposed theory is through the movement of Loop 4 (TM6 – TM7 in *Ts*-Icmt).

Although there is a lot of information about SAM binding of Icmt, more information is needed to characterize the isoprenylated protein binding site. This will allow better inhibitor design for increased affinity towards the active site, which must accommodate both the isoprenylated substrate and SAM cofactor. Chapter 3 will discuss methods and experiments that have localized isoprenylated protein binding to TM2 of Ste14.

1.9 Previous methods for studying Ras cellular distribution, methylation, and active states

Ras pathways, especially in oncogenic contexts, have been well characterized over the past few decades. Activity states and cellular distribution of Ras are common practice for new indirect inhibitors that target the processes upstream of Ras. However, for the advances made in understanding Ras signaling over the past decades, there are equal advances in experimental methods that can and should be applied to Ras. Here are the current questions that still remain in the field of Ras signaling and methylation. The new methods that can be used to answer these questions will be described in detail in Chapter 4.

1.9.1 Can KRas4B be at the plasma membrane when unmethylated?

The canonical methylation and Ras localization studies were performed by Bergo *et al.* (2000). They found that in Icmt $^{-/-}$ mouse embryonic stem cells transfected with a GFP-KRas4B fusion plasmid, KRas4B was mislocalized to the cytosol.[143] Although there is a significant amount

of KRas4B mislocalized from the PM, there is still a distinguishable amount at the PM (Figure 1.6) . When roughly quantified, about one half of the protein remains at the plasma membrane in the absence of Icmt (Figure 1.6). To support the immunofluorescence (IF) data, they performed cell fractionation to isolate KRas4B in the membrane and cytosolic fractions of Icmt $^{+/+}$ and Icmt $^{-/-}$ cells. These results displayed the majority of KRas4B within the cytosolic fraction, with lower levels at the plasma membrane, although the results look more similar to the quantifications performed in Figure 1.6. The question remains; is the KRas4B that remains at the plasma membrane in the absence of Icmt, methylated? In this study, radiolabeled ^{14}C-SAM was used to monitor a decrease in methylation of isoprenylated protein mimetic substrates in cell lysate samples of Icmt $^{-/-}$ and Icmt $^{+/-}$. Although there was no Icmt activity, there was no direct measurement of Ras methylation state. This is an important piece of information. This question is not to dispute that there is more than one methyltransferase that can act on Icmt. It serves to better understand if unmethylated Ras can still traffic to the membrane and furthermore, if it can still perform signaling at any level. We do know that there are some levels of unmethylated KRas4B within colorectal cancer samples, even as high as 90%, indicating that there may be some function of unmethylated KRas4B or a function for methylation itself as a regulatory step.[108]

Other studies have employed similar methods, especially with the purpose of proving new classes of Icmt inhibitors which cause mislocalization of KRas4B, or other CAAX proteins from reaching the PM or other endomembrane systems.[72-76, 144] Some newer methods have utilized probing expression levels of progerin within cells.[74] Progein is a permanently farnesylated and methylated form of prelamin A that cannot undergo a fourth PTM in proteolytic N-terminal cleavage by ZMPSTE24.[145] Progerin can build up and can cause disfigured nuclei and ultimately leads to Progeroid disease. Although these studies can distinguish progeria from prelamin A and fully mature lamin A protein, the information on the antibody used does not specify if the recognition by the antibody is to the methylated portion of the protein. If not, it is possible that they are measuring both methylated and nonmethylated prelamin A.

Even so, levels of unmethylated protein at or mislocalized from the plasma membrane have not been quantified through fluorescence imaging. Quantification requires employment of the proper controls, including positive control markers to designate the cell membrane and even the nucleus. This will be useful in understanding relative levels of mislocalized KRas4B in the presence of Icmt inhibition.

1.9.2 Can unmethylated KRas4B propagate a signal?

Since the first studies of the effects of Icmt on Ras and oncogenesis, immunoblotting of downstream Ras effectors has been used as a measure of Ras signaling. This commonly takes form in measuring phosphorylation of MEK, ERK or Akt, as that is a sign of their respective activation as a means of upstream Ras signaling. The MAPK pathway is more prominently probed as Ras is one of, if not the predominant protein that activates this pathway. However, the PI3K/Akt pathway is also probed but to a lesser extent as many other proteins aside from Ras activate and have influences within this pathway.[146]

Immunoblotting for many promising Icmt inhibitors has shown a decrease in Ras signaling by probing one of the above-mentioned proteins.[73, 75, 77, 147] However there is never a complete abrogation of expression. Another, more recent method is employed that incubated cell lysate with the Ras binding domain (RBD) of Raf-1 that is conjugated to a glutathione agarose resin. Once the RBD is bound to the GTP-bound (active) Ras within the cell lysate, a pull-down of the agarose beads will pull out the GTP-bound Ras.[75] It can then be visualized via western blot. Again, this is still an average of the activated state between thousands of cells and may be missing key cell-to-cell information.

This leads to the following questions:1) is the phosphorylation of proteins downstream of Ras occurring through pathways outside of Ras signaling? 2) is some Ras still methylated and still able to provide enough signal for detectable phosphorylation of downstream effectors? or 3) Is unmethylated Ras still able to propagate a signal at any level?

1.9.3 Are all cells responding uniformly to Icmt inhibition?

In most Icmt inhibition and subsequent Ras localization studies, immunofluorescence and confocal microscopy studies show a single field of view of a select few cells. These cells are a representative image of multiple fields of view, which are often not shown in supplementary information. Representative fields of view could be compared to western blotting, where hundreds of thousands of cells are contributing to the averaged result. However, it is more biased in the particular field of view selected by the author.

Displaying multiple fields of view, or quantifying results of multiple cells at the single cell level, will provide a cell-to-cell distribution of KRas4B signaling across many cells in a way that

is more descriptive and accurate than western blotting fractionation studies.[148-151] It is possible that some cells show hyperactivation of KRas4B and some do not, even under WT conditions.

1.9.4 What are the effects of methylation on endogenous KRas4B

Most central to these questions and future studies is the use of endogenous levels of KRas4B. All previous experiments listed for KRas4B localization studies whether under Icmt, Rce1 or FTase inhibition, utilized transformed KRas4B in an overexpression system in at least one if not all of their localization studies.[52, 72, 73, 75-77, 143, 147] Overexpression systems are useful to enhance signal for otherwise low expressing proteins at the endogenous levels. However, there is importance in studying cells in their most native forms. Disadvantages to overexpressing proteins include exhausting the resources of the cell, overloading signaling pathways, disrupting regulation, and more.[152]

Endogenous Ras has previously been reported to be difficult to detect through IF or visualize through immunoblotting. One comprehensive study of Ras antibodies validity, clearly stated that "Ras antibodies are unsuitable for IF of endogenous Ras proteins" and even western blotting.[153] However with continuous advances to immunofluorescence imaging technology, it's possible that this may be overcome sooner and is still important to pursue in creating the most native experiments possible.

1.10 Central hypothesis

Our central hypothesis is that methylation of Ras is a point of regulation in membrane localization and signaling of Ras through the MAPK and PI3K pathways. We further hypothesize that methylation, performed by the enzyme Icmt, binds to its Ras substrate predominantly through its N-terminally conserved residues. Through this research, we expect to generate actionable insights for small molecule development of novel therapeutics.

1.11 Tables

*

Table 1.1 Sequence homology of the four Icmt species, *Hs-, Sc-, Ag-,* and *Tc-* Icmt as well as the prokaryotic methyltransferase, *Ma*-MTase Sequences are aligned for the full-length protein as well as within the proposed C-terminal catalytic region.

	Sc-Icmt (Yeast)	*Hs*-Icmt (Human)	*Ma*-MTase (Prokaryote)	*Ag*-Icmt (Mosquito)	*Tc*-Icmt (Beetle)
Size	**28 kDa**	**32 kDa**	**~23 kDa**	**~31 kDa**	**~33 kDa**
Transmembrane Helices	**6**	**8**	**5**	**8**	**8**
Cytosolic Loops	**4**	**6**	**4**	**7**	**7**
Percent Identity with hIcmt (%)	**41%**	**-**	**32%**	**49%**	**59.0%**
Percent Similarity with hIcmt (%)	**62%**	**-**	**50%**	**67%**	**76%**

*analysis performed using EBMOSS Needle EMBL-EBI.

1.12 Figures

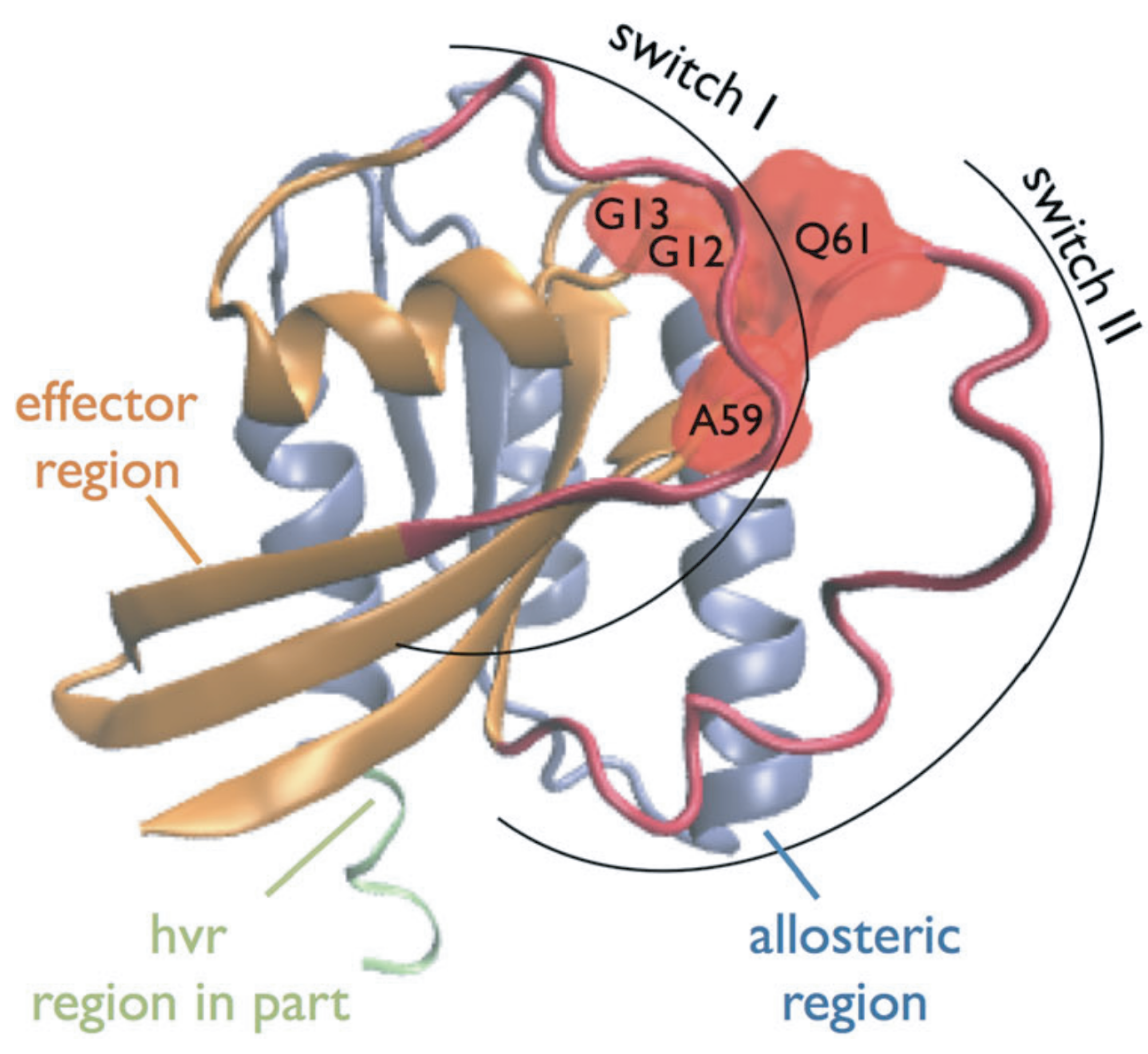

Figure 1.1 Ras general structure, C-terminal sequences of all isoforms, and mutational hotspot GEF/GAP rates

Crystal structure of HRas (PDB: 6Q21:A) with areas of importance highlighted. Residues that form mutational hotspots are globular and colored in red. From: Engin, H. B.; Carlin, D.; Pratt, D.; Carter, H., Modeling of RAS complexes supports roles in cancer for less studied partners. *BMC Biophysics* **2017,** *10* (1), 5.

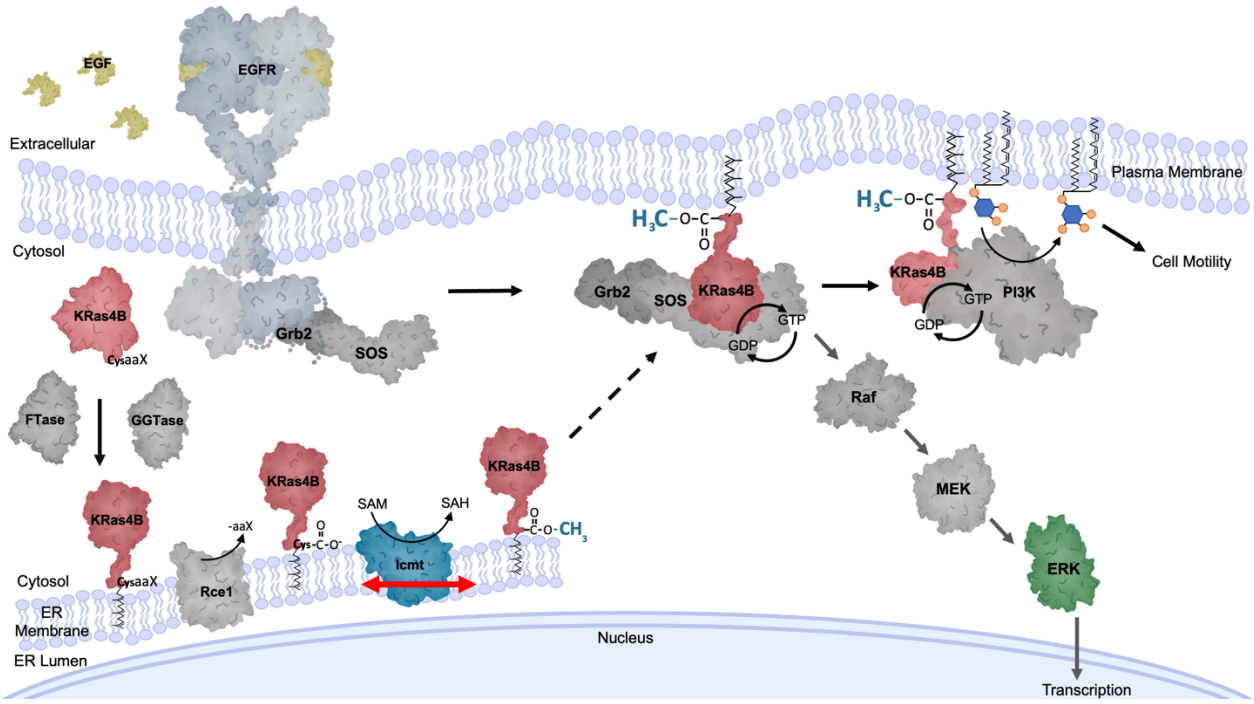

Figure 1.2 KRas4B post-translational modifications and signaling cascade.

Canonical KRas4B signaling begins with extracellular EGF binding to EGFR. This causes dimerization and recruits Grb2-SOS to the plasma membrane. Once at the PM, Grb2-SOS can bind fully processed KRas4B. Before its localization to the PM, KRas4B undergoes three required post-translational modifications on its most C-terminal cysteine residue of its CAAX motif: farnesylation, proteolysis, and methylation. Of those three steps, methylation is the only reversible process making it a possible point of regulation for KRas4B and other CAAX proteins. KRas4B then translocates to the PM possibly with the help of PDEδ and other unidentified chaperones. Once at the PM KRas4B can associate and bind SOS which helps it to stay in the GTP-bound (active) state. GTP-bound Ras can bind and activate effectors such as Raf of the MAPK pathway or PI3K which produces a secondary messenger involved in many processes including Akt and mTOR signaling. The PDB structures of which each protein is based are, Ras: 4OBE & 4DSO, FTase: 1S63, GGTase-I: 3GFT, Rce1: 4CAD, Icmt: 5VG9, Grb2: 1JYU, SOS: 3KSY, Raf: 3C4C, MEK: 4MNE, ERK: 4GT3, PI3K: 4OVV, EGFR: 1NQL, 1IVO, 2JWA, 1M17 and 2GS6.

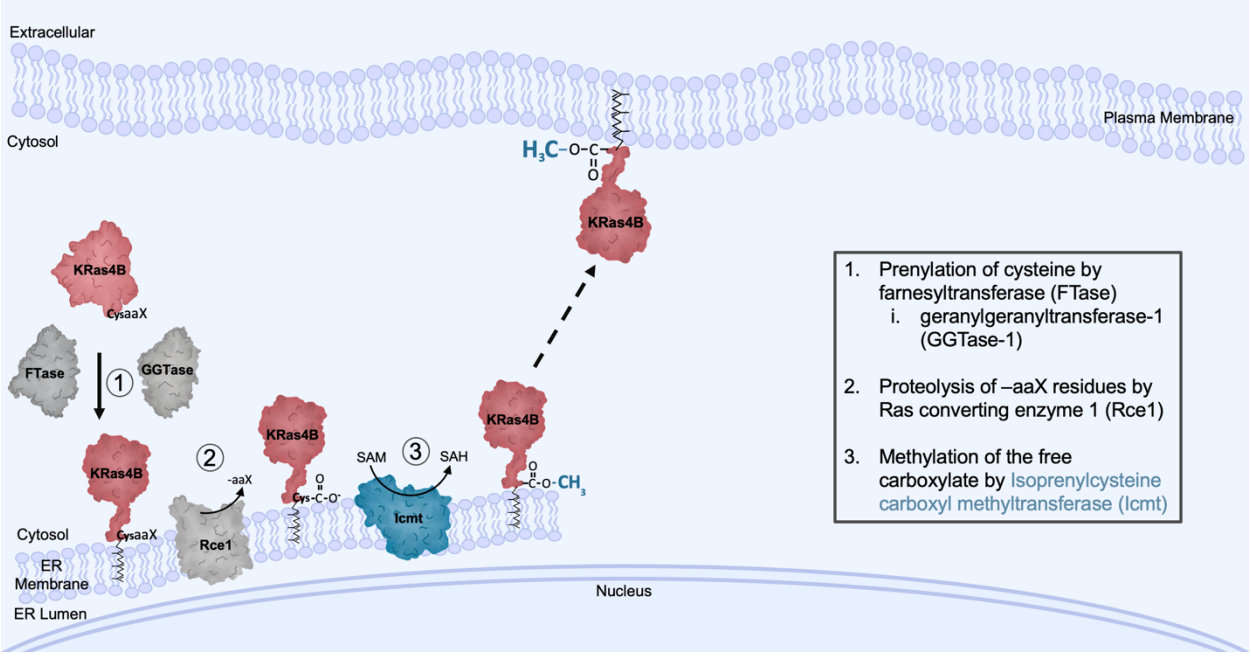

Figure 1.3 Post translational modifications of KRas4B.

KRas4B must undergo three post-translational modifications for proper plasma membrane localization and function. As a CAAX protein, its most C-terminal cysteine residue gets irreversibly farnesylated and proteolyzed by FTase and Rce1 respectively. Alternatively in the absence or inhibition of FTase, GGTase can geranylgeranylate KRas4B for its continuation and activation along this pathway. Finally, the free carboxylate of the C-terminus is methylated by Icmt. Once methylated, KRas4B can translocate to the plasma membrane possibly with the help of PDEδ and other unidentified chaperones, and perform its activation for signaling The PDB structures of which each protein is based are, Ras: 4OBE & 4DSO, FTase: 1S63, GGTase-I: 3GFT, Rce1: 4CAD, Icmt: 5VG9.

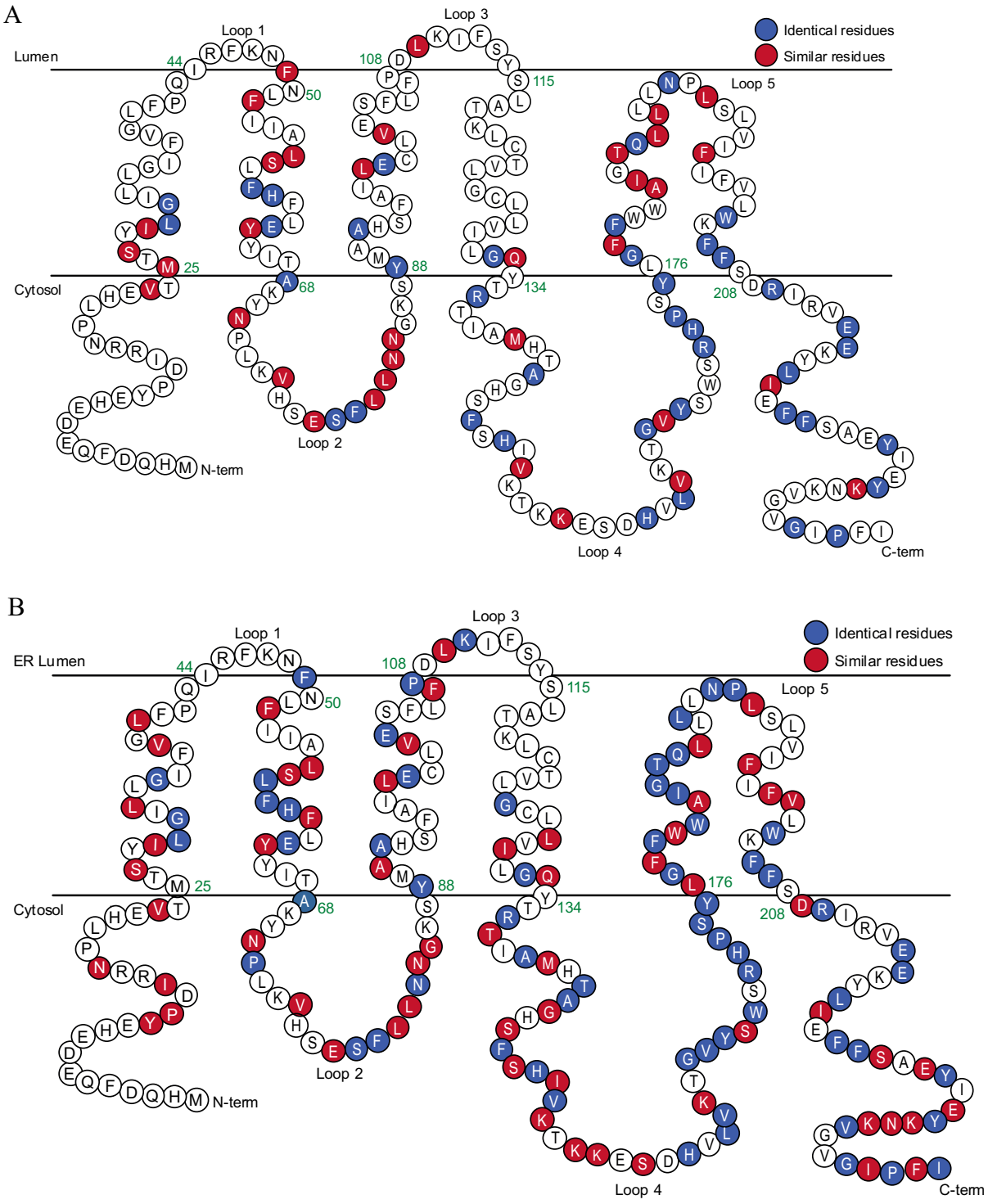

Figure 1.4 2D topology of Ste14 representing homology between multiple Icmt species.

Blue residues represent identical and red identify similar residues. (A) Sequence alignment of 15 Icmt species adapted from Court, H.; Hahne, K.; Philips, M. R.; Hrycyna, C. A., Biochemical and Biological Functions of I Isoprenylcysteine Carboxyl Methyltransferase. *The Enzymes* **2011,** *30*, 71-90. (B) Sequence alignment of the four most studied Icmt species *Hs*-, *Tc*-, *Ag*-, and *Sc*-Icmt.

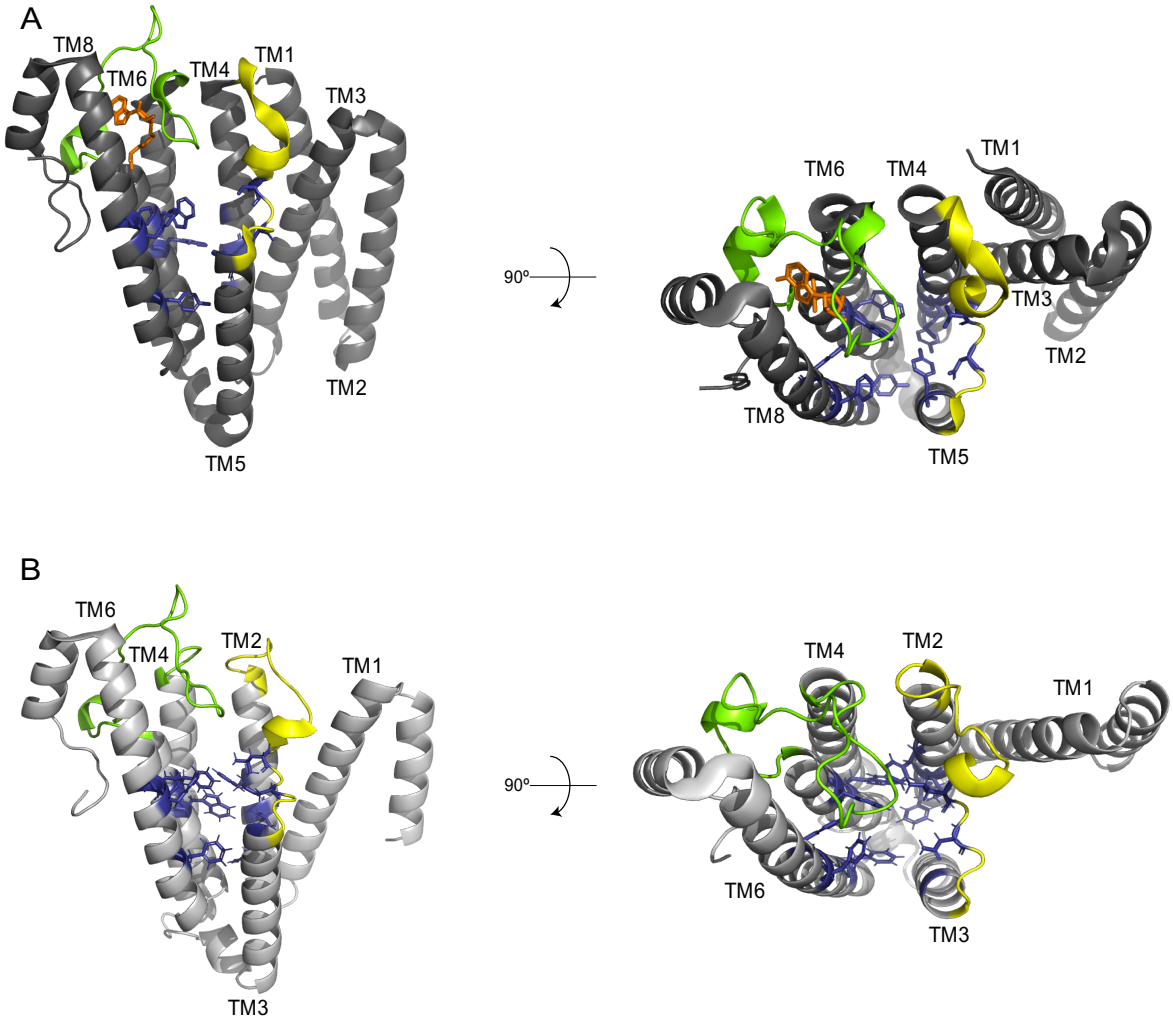

Figure 1.5 Structures of Icmt

PyMOL structures of (A) *Tc*-Icmt and (B) Ste14, which is mapped onto the structure of *Tc*-Icmt. The aromatic residues lining the proposed substrate binding tunnel are highlighted in blue. Loop 4 (TM6 – TM7 connector) is highlighted in green. Loop 2 (TM4 – TM5 connector) is highlighted in yellow. Methyl donating cofactor, SAM, is highlight in orange only in *Tc*-Icmt. The molecule is then rotated 90 degrees to look down into the substrate binding tunnel. (*Tc*-Icmt PDB: 5V7P).

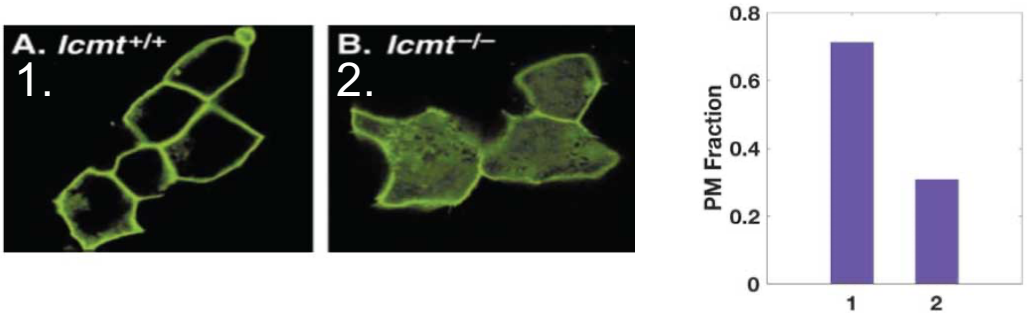

Figure 1.6 Mislocalization of GFP-KRas4B in Icmt $^{-/-}$ cells.

Left) Mouse embryonic fibroblasts transfected with GFP-KRas4B fusion protein in (1) Icmt $^{+/+}$ and (2) generated Icmt $^{-/-}$ cells. Right) Quantification of mislocalized GFP-KRas4B from the plasma membrane into the cytosol. Generated by Dr. Shalini T. Low-Nam. From: Bergo, M. O.; Leung, G. K.; Ambroziak, P.; Otto, J. C.; Casey, P. J.; Young, S. G., Targeted inactivation of the isoprenylcysteine carboxyl methyltransferase gene causes mislocalization of K-Ras in mammalian cells. *Journal of Biological Chemistry* **2000,** *275* (23), 17605-17610.

1.13 References

1. Prior, I. A.; Hood, F. E.; Hartley, J. L., The frequency of Ras mutations in cancer. *Cancer research* **2020,** *80* (14), 2969-2974.

2. Waters, A. M.; Der, C. J., KRAS: the critical driver and therapeutic target for pancreatic cancer. *Cold Spring Harbor perspectives in medicine* **2018,** *8* (9), a031435.

3. Hobbs, G. A.; Der, C. J.; Rossman, K. L., RAS isoforms and mutations in cancer at a glance. *J Cell Sci* **2016,** *129* (7), 1287-92.

4. Gorfe, A. A.; Grant, B. J.; McCammon, J. A., Mapping the nucleotide and isoform-dependent structural and dynamical features of Ras proteins. *Structure* **2008,** *16* (6), 885-896.

5. Buhrman, G.; O'Connor, C.; Zerbe, B.; Kearney, B. M.; Napoleon, R.; Kovrigina, E. A.; Vajda, S.; Kozakov, D.; Kovrigin, E. L.; Mattos, C., Analysis of Binding Site Hot Spots on the Surface of Ras GTPase. *Journal of Molecular Biology* **2011,** *413* (4), 773-789.

6. Hancock, J. F., Ras proteins: different signals from different locations. *Nature reviews Molecular cell biology* **2003,** *4* (5), 373-385.

7. Reuter, C. W.; Morgan, M. A.; Bergmann, L., Targeting the Ras signaling pathway: a rational, mechanism-based treatment for hematologic malignancies? *Blood, The Journal of the American Society of Hematology* **2000,** *96* (5), 1655-1669.

8. Mondal, S.; Hsiao, K.; Goueli, S. A., A Homogenous Bioluminescent System for Measuring GTPase, GTPase Activating Protein, and Guanine Nucleotide Exchange Factor Activities. *Assay Drug Dev Technol* **2015,** *13* (8), 444-455.

9. Cherfils, J.; Zeghouf, M., Regulation of small gtpases by gefs, gaps, and gdis. *Physiological reviews* **2013,** *93* (1), 269-309.

10. Bos, J. L.; Rehmann, H.; Wittinghofer, A., GEFs and GAPs: critical elements in the control of small G proteins. *Cell* **2007,** *129* (5), 865-877.

11. Hurley, J. B.; Simon, M. I.; Teplow, D. B.; Robishaw, J. D.; Gilman, A. G., Homologies between signal transducing G proteins and ras gene products. *Science* **1984,** *226* (4676), 860-862.

12. McGrath, J. P.; Capon, D. J.; Goeddel, D. V.; Levinson, A. D., Comparative biochemical properties of normal and activated human ras p21 protein. *Nature* **1984,** *310* (5979), 644-649.

13. Smith, M. R.; DeGudicibus, S. J.; Stacey, D. W., Requirement for c-ras proteins during viral oncogene transformation. *Nature* **1986,** *320* (6062), 540-543.

14. Vojtek, A. B.; Hollenberg, S. M.; Cooper, J. A., Mammalian Ras interacts directly with the serine/threonine kinase Raf. *Cell* **1993,** *74* (1), 205-214.

15. Sjölander, A.; Yamamoto, K.; Huber, B. E.; Lapetina, E. G., Association of p21ras with phosphatidylinositol 3-kinase. *Proceedings of the National Academy of Sciences* **1991,** *88* (18), 7908-7912.

16. Sundaram, M. V., RTK/Ras/MAPK signaling. *WormBook* **2006**, 1-19.

17. Castellano, E.; Downward, J., RAS interaction with PI3K: more than just another effector pathway. *Genes & cancer* **2011,** *2* (3), 261-274.

18. Mendoza, M. C.; Er, E. E.; Blenis, J., The Ras-ERK and PI3K-mTOR pathways: cross-talk and compensation. *Trends in biochemical sciences* **2011,** *36* (6), 320-328.

19. Willumsen, B. M.; Christensen, A.; Hubbert, N. L.; Papageorge, A. G.; Lowy, D. R., The p21 ras C-terminus is required for transformation and membrane association. *Nature* **1984,** *310* (5978), 583-586.

20. Willingham, M. C.; Pastan, I.; Shih, T. Y.; Scolnick, E. M., Localization of the src gene product of the Harvey strain of MSV to plasma membrane of transformed cells by electron microscopic immunocytochemistry. *Cell* **1980,** *19* (4), 1005-1014.

21. Cox, A. D.; Der, C. J.; Philips, M. R., Targeting RAS Membrane Association: Back to the Future for Anti-RAS Drug Discovery? *Clinical Cancer Research* **2015,** *21* (8), 1819-1827.

22. Kattan, W. E.; Hancock, J. F., RAS Function in cancer cells: translating membrane biology and biochemistry into new therapeutics. *Biochemical Journal* **2020,** *477* (15), 2893-2919.

23. Court, H.; Hahne, K.; Philips, M. R.; Hrycyna, C. A., Biochemical and Biological Functions of Isoprenylcysteine Carboxyl Methyltransferase. *The Enzymes* **2011,** *30*, 71-90.

24. Diver, M. M.; Pedi, L.; Koide, A.; Koide, S.; Long, S. B., Atomic structure of the eukaryotic intramembrane RAS methyltransferase ICMT. *Nature* **2018,** *553* (7689), 526-529.

25. Hancock, J. F.; Cadwallader, K.; Marshall, C. J., Methylation and proteolysis are essential for efficient membrane binding of prenylated p21K-ras (B). *The EMBO journal* **1991,** *10* (3), 641-646.

26. Casey, P. J.; Seabra, M. C., Protein prenyltransferases. *J Biol Chem* **1996,** *271* (10), 5289-92.

27. Henis, Y. I.; Hancock, J. F.; Prior, I. A., Ras acylation, compartmentalization and signaling nanoclusters. *Molecular membrane biology* **2009,** *26* (1-2), 80-92.

28. Wright, L. P.; Philips, M. R., Thematic review series: lipid posttranslational modifications CAAX modification and membrane targeting of Ras. *Journal of lipid research* **2006,** *47* (5), 883-891.

29. Wang, M.; Casey, P. J., Protein prenylation: unique fats make their mark on biology. *Nature reviews Molecular cell biology* **2016,** *17* (2), 110.

30. Berg, T. J.; Gastonguay, A. J.; Lorimer, E. L.; Kuhnmuench, J. R.; Li, R.; Fields, A. P.; Williams, C. L., Splice variants of SmgGDS control small GTPase prenylation and membrane localization. *Journal of Biological Chemistry* **2010,** *285* (46), 35255-35266.

31. Azoulay-Alfaguter, I.; Strazza, M.; Mor, A., Chaperone-mediated specificity in Ras and Rap signaling. *Critical Reviews in Biochemistry and Molecular Biology* **2015,** *50* (3), 194-202.

32. Zimmermann, G.; Papke, B.; Ismail, S.; Vartak, N.; Chandra, A.; Hoffmann, M.; Hahn, S. A.; Triola, G.; Wittinghofer, A.; Bastiaens, P. I., Small molecule inhibition of the KRAS–PDEδ interaction impairs oncogenic KRAS signalling. *Nature* **2013,** *497* (7451), 638-642.

33. Dharmaiah, S.; Bindu, L.; Tran, T. H.; Gillette, W. K.; Frank, P. H.; Ghirlando, R.; Nissley, D. V.; Esposito, D.; McCormick, F.; Stephen, A. G., Structural basis of recognition of farnesylated and methylated KRAS4b by PDEδ. *Proceedings of the National Academy of Sciences* **2016,** *113* (44), E6766-E6775.

34. Prior, I. A.; Lewis, P. D.; Mattos, C., A comprehensive survey of Ras mutations in cancer. *Cancer research* **2012,** *72* (10), 2457-2467.

35. Smith, M. J.; Neel, B. G.; Ikura, M., NMR-based functional profiling of RASopathies and oncogenic RAS mutations. *Proceedings of the National Academy of Sciences* **2013,** *110* (12), 4574-4579.

36. Hunter, J. C.; Manandhar, A.; Carrasco, M. A.; Gurbani, D.; Gondi, S.; Westover, K. D., Biochemical and structural analysis of common cancer-associated KRAS mutations. *Molecular cancer research* **2015,** *13* (9), 1325-1335.

37. Wang, W.; Fang, G.; Rudolph, J., Ras inhibition via direct Ras binding—is there a path forward? *Bioorganic & medicinal chemistry letters* **2012,** *22* (18), 5766-5776.

38. Cox, A. D.; Fesik, S. W.; Kimmelman, A. C.; Luo, J.; Der, C. J., Drugging the undruggable RAS: mission possible? *Nature reviews Drug discovery* **2014,** *13* (11), 828-851.

39. Drosten, M.; Dhawahir, A.; Sum, E. Y.; Urosevic, J.; Lechuga, C. G.; Esteban, L. M.; Castellano, E.; Guerra, C.; Santos, E.; Barbacid, M., Genetic analysis of Ras signalling pathways in cell proliferation, migration and survival. *The EMBO journal* **2010,** *29* (6), 1091-1104.

40. Moore, A. R.; Rosenberg, S. C.; McCormick, F.; Malek, S., RAS-targeted therapies: is the undruggable drugged? *Nature Reviews Drug Discovery* **2020,** *19* (8), 533-552.

41. Heidorn, S. J.; Milagre, C.; Whittaker, S.; Nourry, A.; Niculescu-Duvas, I.; Dhomen, N.; Hussain, J.; Reis-Filho, J. S.; Springer, C. J.; Pritchard, C.; Marais, R., Kinase-Dead BRAF and Oncogenic RAS Cooperate to Drive Tumor Progression through CRAF. *Cell* **2010,** *140* (2), 209-221.

42. Keating, G. M.; Santoro, A., Sorafenib. *Drugs* **2009,** *69* (2), 223-240.

43. Uprety, D.; Adjei, A. A., KRAS: From undruggable to a druggable Cancer Target. *Cancer Treatment Reviews* **2020,** *89*, 102070.

44. Ahmed, T. A.; Adamopoulos, C.; Karoulia, Z.; Wu, X.; Sachidanandam, R.; Aaronson, S. A.; Poulikakos, P. I., SHP2 drives adaptive resistance to ERK signaling inhibition in molecularly defined subsets of ERK-dependent tumors. *Cell reports* **2019,** *26* (1), 65-78. e5.

45. Mainardi, S.; Mulero-Sánchez, A.; Prahallad, A.; Germano, G.; Bosma, A.; Krimpenfort, P.; Lieftink, C.; Steinberg, J. D.; De Wit, N.; Gonçalves-Ribeiro, S., SHP2 is required for growth of KRAS-mutant non-small-cell lung cancer in vivo. *Nature medicine* **2018,** *24* (7), 961-967.

46. Baltanás, F. C.; Zarich, N.; Rojas-Cabañeros, J. M.; Santos, E., SOS GEFs in health and disease. *Biochimica et Biophysica Acta (BBA) - Reviews on Cancer* **2020,** *1874* (2), 188445.

47. Chen, K.; Zhang, Y.; Qian, L.; Wang, P., Emerging strategies to target RAS signaling in human cancer therapy. *Journal of Hematology & Oncology* **2021,** *14* (1), 1-23.

48. Berndt, N.; Hamilton, A. D.; Sebti, S. M., Targeting protein prenylation for cancer therapy. *Nature Reviews Cancer* **2011,** *11* (11), 775-791.

49. Rowell, C. A.; Kowalczyk, J. J.; Lewis, M. D.; Garcia, A. M., Direct demonstration of geranylgeranylation and farnesylation of Ki-Ras in vivo. *Journal of Biological Chemistry* **1997,** *272* (22), 14093-14097.

50. Zhang, F. L.; Kirschmeier, P.; Carr, D.; James, L.; Bond, R. W.; Wang, L.; Patton, R.; Windsor, W. T.; Syto, R.; Zhang, R., Characterization of Ha-ras, N-ras, Ki-Ras4A, and Ki-Ras4B as in vitro substrates for farnesyl protein transferase and geranylgeranyl protein transferase type I. *Journal of Biological Chemistry* **1997,** *272* (15), 10232-10239.

51. Whyte, D. B.; Kirschmeier, P.; Hockenberry, T. N.; Nunez-Oliva, I.; James, L.; Catino, J. J.; Bishop, W. R.; Pai, J.-K., K-and N-Ras are geranylgeranylated in cells treated with farnesyl protein transferase inhibitors. *Journal of Biological Chemistry* **1997,** *272* (22), 14459-14464.

52. Kazi, A.; Xiang, S.; Yang, H.; Chen, L.; Kennedy, P.; Ayaz, M.; Fletcher, S.; Cummings, C.; Lawrence, H. R.; Beato, F., Dual farnesyl and geranylgeranyl transferase inhibitor thwarts mutant KRAS-driven patient-derived pancreatic tumors. *Clinical Cancer Research* **2019,** *25* (19), 5984-5996.

53. Yu, R.; Longo, J.; van Leeuwen, J. E.; Mullen, P. J.; Ba-Alawi, W.; Haibe-Kains, B.; Penn, L. Z., Statin-induced cancer cell death can be mechanistically uncoupled from prenylation of RAS family proteins. *Cancer research* **2018,** *78* (5), 1347-1357.

54. Wang, W.-h.; Yuan, T.; Qian, M.-j.; Yan, F.-j.; Yang, L.; He, Q.-j.; Yang, B.; Lu, J.-j.; Zhu, H., Post-translational modification of KRAS: potential targets for cancer therapy. *Acta Pharmacologica Sinica* **2020**, 1-11.

55. Manandhar, S. P.; Hildebrandt, E. R.; Jacobsen, W. H.; Santangelo, G. M.; Schmidt, W. K., Chemical inhibition of CaaX protease activity disrupts yeast Ras localization. *Yeast* **2010,** *27* (6), 327-343.

56. Mohammed, I.; Hampton, S. E.; Ashall, L.; Hildebrandt, E. R.; Kutlik, R. A.; Manandhar, S. P.; Floyd, B. J.; Smith, H. E.; Dozier, J. K.; Distefano, M. D.; Schmidt, W. K.; Dore, T. M., 8-Hydroxyquinoline-based inhibitors of the Rce1 protease disrupt Ras membrane localization in human cells. *Bioorganic & Medicinal Chemistry* **2016,** *24* (2), 160-178.

57. Hampton, S. E.; Dore, T. M.; Schmidt, W. K., Rce1: mechanism and inhibition. *Critical reviews in biochemistry and molecular biology* **2018,** *53* (2), 157-174.

58. Bergo, M. O.; Lieu, H. D.; Gavino, B. J.; Ambroziak, P.; Otto, J. C.; Casey, P. J.; Walker, Q. M.; Young, S. G., On the physiological importance of endoproteolysis of CAAX proteins: heart-specific RCE1 knockout mice develop a lethal cardiomyopathy. *Journal of Biological Chemistry* **2004,** *279* (6), 4729-4736.

59. Bracha, K.; Lavy, M.; Yalovsky, S., The Arabidopsis AtSTE24 is a CaaXprotease with broad substrate specificity. *Journal of Biological Chemistry* **2002,** *277* (33), 29856-29864.

60. Boyartchuk, V. L.; Ashby, M. N.; Rine, J., Modulation of Ras and a-factor function by carboxyl-terminal proteolysis. *Science* **1997,** *275* (5307), 1796-1800.

61. Fujimura-Kamada, K.; Nouvet, F. J.; Michaelis, S., A novel membrane-associated metalloprotease, Ste24p, is required for the first step of NH2-terminal processing of the yeast a-factor precursor. *The Journal of cell biology* **1997,** *136* (2), 271-285.

62. Tam, A.; Nouvet, F. J.; Fujimura-Kamada, K.; Slunt, H.; Sisodia, S. S.; Michaelis, S., Dual roles for Ste24p in yeast a-factor maturation: NH2-terminal proteolysis and COOH-terminal CAAX processing. *The Journal of cell biology* **1998,** *142* (3), 635-649.

63. Schmidt, W. K.; Tam, A.; Michaelis, S., Reconstitution of the Ste24p-dependent N-terminal proteolytic step in yeast a-factor biogenesis. *Journal of Biological Chemistry* **2000,** *275* (9), 6227-6233.

64. Kim, E.; Ambroziak, P.; Otto, J. C.; Taylor, B.; Ashby, M.; Shannon, K.; Casey, P. J.; Young, S. G., Disruption of the mouse Rce1 gene results in defective Ras processing and mislocalization of Ras within cells. *Journal of Biological Chemistry* **1999,** *274* (13), 8383-8390.

65. Boyartchuk, V. L.; Rine, J., Roles of prenyl protein proteases in maturation of Saccharomyces cerevisiae a-factor. *Genetics* **1998,** *150* (1), 95-101.

66. Trueblood, C. E.; Boyartchuk, V. L.; Picologlou, E. A.; Rozema, D.; Poulter, C. D.; Rine, J., The CaaX proteases, Afc1p and Rce1p, have overlapping but distinct substrate specificities. *Molecular and cellular biology* **2000,** *20* (12), 4381-4392.

67. Hrycyna, C. A.; Clarke, S., Farnesyl cysteine C-terminal methyltransferase activity is dependent upon the STE14 gene product in Saccharomyces cerevisiae. *Molecular and Cellular Biology* **1990,** *10* (10), 5071-5076.

68. Hrycyna, C. A.; Sapperstein, S. K.; Clarke, S.; Michaelis, S., The Saccharomyces cerevisiae STE14 gene encodes a methyltransferase that mediates C-terminal methylation of a-factor and RAS proteins. *EMBO J* **1991,** *10* (7), 1699-709.

69. Cantoni, G. L., Biological methylation: selected aspects. *Annual review of biochemistry* **1975,** *44* (1), 435-451.

70. Davis, T. D.; Kunakom, S.; Burkart, M. D.; Eustaquio, A. S., Preparation, Assay, and Application of Chlorinase SalL for the Chemoenzymatic Synthesis of S-Adenosyl-l-Methionine and Analogs. *Methods in enzymology* **2018,** *604*, 367-388.

71. Wnuk, S. F.; Yuan, C.-S.; Borchardt, R. T.; Balzarini, J.; De Clercq, E.; Robins, M. J., Anticancer and antiviral effects and inactivation of S-adenosyl-l-homocysteine hydrolase with 5 ‘-carboxaldehydes and oximes synthesized from adenosine and sugar-modified analogues. *Journal of medicinal chemistry* **1997,** *40* (11), 1608-1618.

72. Winter-Vann, A. M.; Kamen, B. A.; Bergo, M. O.; Young, S. G.; Melnyk, S.; James, S. J.; Casey, P. J., Targeting Ras signaling through inhibition of carboxyl methylation: an unexpected property of methotrexate. *Proceedings of the National Academy of Sciences* **2003,** *100* (11), 6529-6534.

73. Winter-Vann, A. M.; Baron, R. A.; Wong, W.; dela Cruz, J.; York, J. D.; Gooden, D. M.; Bergo, M. O.; Young, S. G.; Toone, E. J.; Casey, P. J., A small-molecule inhibitor of isoprenylcysteine carboxyl methyltransferase with antitumor activity in cancer cells. *Proc Natl Acad Sci U S A* **2005,** *102* (12), 4336-41.

74. Marcos-Ramiro, B.; Gil-Ordóñez, A.; Marín-Ramos, N. I.; Ortega-Nogales, F. J.; Balabasquer, M.; Gonzalo, P.; Khiar-Fernández, N.; Rolas, L.; Barkaway, A.; Nourshargh, S.; Andrés, V.; Martín-Fontecha, M.; López-Rodríguez, M. L.; Ortega-Gutiérrez, S., Isoprenylcysteine Carboxylmethyltransferase-Based Therapy for Hutchinson–Gilford Progeria Syndrome. *ACS Central Science* **2021,** *7* (8), 1300-1310.

75. Marin-Ramos, N. I.; Balabasquer, M.; Ortega-Nogales, F. J.; Torrecillas, I. R.; Gil-Ordonez, A.; Marcos-Ramiro, B.; Aguilar-Garrido, P.; Cushman, I.; Romero, A.; Medrano, F. J.; Gajate, C.; Mollinedo, F.; Philips, M. R.; Campillo, M.; Gallardo, M.; Martin-Fontecha, M.; Lopez-Rodriguez, M. L.; Ortega-Gutierrez, S., A Potent Isoprenylcysteine Carboxylmethyltransferase (ICMT) Inhibitor Improves Survival in Ras-Driven Acute Myeloid Leukemia. *J Med Chem* **2019,** *62* (13), 6035-6046.

76. Bergman, J. A.; Hahne, K.; Song, J.; Hrycyna, C. A.; Gibbs, R. A., S-Farnesyl-thiopropionic acid triazoles as potent inhibitors of isoprenylcysteine carboxyl methyltransferase. *ACS medicinal chemistry letters* **2012,** *3* (1), 15-19.

77. Majmudar, J. D.; Hodges-Loaiza, H. B.; Hahne, K.; Donelson, J. L.; Song, J.; Shrestha, L.; Harrison, M. L.; Hrycyna, C. A.; Gibbs, R. A., Amide-modified prenylcysteine based Icmt inhibitors: structure–activity relationships, kinetic analysis and cellular characterization. *Bioorganic & medicinal chemistry* **2012,** *20* (1), 283-295.

78. Bergman, J. A.; Hahne, K.; Hrycyna, C. A.; Gibbs, R. A., Lipid and sulfur substituted prenylcysteine analogs as human Icmt inhibitors. *Bioorganic & medicinal chemistry letters* **2011,** *21* (18), 5616-5619.

79. Majmudar, J. D.; Hahne, K.; Hrycyna, C. A.; Gibbs, R. A., Probing the isoprenylcysteine carboxyl methyltransferase (Icmt) binding pocket: sulfonamide modified farnesyl cysteine (SMFC) analogs as Icmt inhibitors. *Bioorganic & medicinal chemistry letters* **2011,** *21* (9), 2616-2620.

80. Zhao, F.; Darling, J. E.; Gibbs, R. A.; Hougland, J. L., A new class of ghrelin O-acyltransferase inhibitors incorporating triazole-linked lipid mimetic groups. *Bioorganic & Medicinal Chemistry Letters* **2015,** *25* (14), 2800-2803.

81. Lau, H. Y.; Wang, M., Small change, big effect: taking RAS by the tail through suppression of post-prenylation carboxylmethylation. *Small GTPases* **2020,** *11* (4), 271-279.

82. Canon, J.; Rex, K.; Saiki, A. Y.; Mohr, C.; Cooke, K.; Bagal, D.; Gaida, K.; Holt, T.; Knutson, C. G.; Koppada, N.; Lanman, B. A.; Werner, J.; Rapaport, A. S.; San Miguel, T.; Ortiz, R.; Osgood, T.; Sun, J.-R.; Zhu, X.; McCarter, J. D.; Volak, L. P.; Houk, B. E.; Fakih, M. G.; O'Neil, B. H.; Price, T. J.; Falchook, G. S.; Desai, J.; Kuo, J.; Govindan, R.; Hong, D. S.; Ouyang, W.; Henary, H.; Arvedson, T.; Cee, V. J.; Lipford, J. R., The clinical KRAS(G12C) inhibitor AMG 510 drives anti-tumour immunity. *Nature* **2019,** *575* (7781), 217-223.

83. Hong, D. S.; Fakih, M. G.; Strickler, J. H.; Desai, J.; Durm, G. A.; Shapiro, G. I.; Falchook, G. S.; Price, T. J.; Sacher, A.; Denlinger, C. S., KRASG12C inhibition with sotorasib in advanced solid tumors. *New England Journal of Medicine* **2020,** *383* (13), 1207-1217.

84. Skoulidis, F.; Li, B. T.; Dy, G. K.; Price, T. J.; Falchook, G. S.; Wolf, J.; Italiano, A.; Schuler, M.; Borghaei, H.; Barlesi, F., Sotorasib for Lung Cancers with KRAS p. G12C Mutation. *New England Journal of Medicine* **2021**.

85. Siegel, R. L.; Miller, K. D.; Fuchs, H. E.; Jemal, A., Cancer statistics, 2022. *CA: A Cancer Journal for Clinicians* **2022,** *72* (1), 7-33.

86. Courtois-Cox, S.; Genther Williams, S. M.; Reczek, E. E.; Johnson, B. W.; McGillicuddy, L. T.; Johannessen, C. M.; Hollstein, P. E.; MacCollin, M.; Cichowski, K., A negative feedback signaling network underlies oncogene-induced senescence. *Cancer Cell* **2006,** *10* (6), 459-472.

87. Simanshu, D. K.; Nissley, D. V.; McCormick, F., RAS proteins and their regulators in human disease. *Cell* **2017,** *170* (1), 17-33.

88. Perez-Sala, D.; Tan, E. W.; Canada, F. J.; Rando, R. R., Methylation and demethylation reactions of guanine nucleotide-binding proteins of retinal rod outer segments. *Proc Natl Acad Sci U S A* **1991,** *88* (8), 3043-6.

89. Philips, M. R.; Pillinger, M. H.; Staud, R.; Volker, C.; Rosenfeld, M. G.; Weissmann, G.; Stock, J. B., Carboxyl methylation of Ras-related proteins during signal transduction in neutrophils. *Science* **1993,** *259* (5097), 977-80.

90. Huizinga, D. H.; Omosegbon, O.; Omery, B.; Crowell, D. N., Isoprenylcysteine methylation and demethylation regulate abscisic acid signaling in Arabidopsis. *The Plant Cell* **2008,** *20* (10), 2714-2728.

91. Deem, A. K.; Bultema, R. L.; Crowell, D. N., Prenylcysteine methylesterase in Arabidopsis thaliana. *Gene* **2006,** *380* (2), 159-166.

92. Oboh, O. T.; Lamango, N. S., Liver prenylated methylated protein methyl esterase is the same enzyme as Sus scrofa carboxylesterase. *J Biochem Mol Toxicol* **2008,** *22* (1), 51-62.

93. Lamango, N. S., Liver prenylated methylated protein methyl esterase is an organophosphate-sensitive enzyme. *J Biochem Mol Toxicol* **2005,** *19* (5), 347-57.

94. Brüsehaber, E.; Böttcher, D.; Bornscheuer, U. T., Insights into the physiological role of pig liver esterase: Isoenzymes show differences in the demethylation of prenylated proteins. *Bioorganic & medicinal chemistry* **2009,** *17* (23), 7878-7883.

95. Morton, C. L.; Potter, P. M., Comparison of Escherichia coli, Saccharomyces cerevisiae, Pichia pastoris, Spodoptera frugiperda, and COS7 cells for recombinant gene expression. *Molecular biotechnology* **2000,** *16* (3), 193-202.

96. Tan, E. W.; Rando, R. R., Identification of an isoprenylated cysteine methyl ester hydrolase activity in bovine rod outer segment membranes. *Biochemistry* **1992,** *31* (24), 5572-5578.

97. Bencharit, S.; Edwards, C. C.; Morton, C. L.; Howard-Williams, E. L.; Kuhn, P.; Potter, P. M.; Redinbo, M. R., Multisite Promiscuity in the Processing of Endogenous Substrates by Human Carboxylesterase 1. *Journal of Molecular Biology* **2006,** *363* (1), 201-214.

98. Bencharit, S.; Morton, C. L.; Hyatt, J. L.; Kuhn, P.; Danks, M. K.; Potter, P. M.; Redinbo, M. R., Crystal structure of human carboxylesterase 1 complexed with the Alzheimer's drug tacrine: from binding promiscuity to selective inhibition. *Chemistry & biology* **2003,** *10* (4), 341-349.

99. Duverna, R.; Ablordeppey, S. Y.; Lamango, N. S., Biochemical and docking analysis of substrate interactions with polyisoprenylated methylated protein methyl esterase. *Curr Cancer Drug Targets* **2010,** *10* (6), 634-48.

100. Cushman, I.; Cushman, S. M.; Potter, P. M.; Casey, P. J., Control of RhoA methylation by carboxylesterase I. *Journal of Biological Chemistry* **2013,** *288* (26), 19177-19183.

101. Amissah, F.; Duverna, R.; Aguilar, B. J.; Poku, R. A.; Kiros, G. E.; Lamango, N. S., Polyisoprenylated methylated protein methyl esterase overexpression and hyperactivity promotes lung cancer progression. *Am J Cancer Res* **2014,** *4* (2), 116-34.

102. Amissah, F.; Duverna, R.; Aguilar, B. J.; Poku, R. A.; Lamango, N. S., Polyisoprenylated methylated protein methyl esterase is both sensitive to curcumin and overexpressed in colorectal cancer: implications for chemoprevention and treatment. *Biomed Res Int* **2013,** *2013*, 416534.

103. Poku, R. A.; Amissah, F.; Duverna, R.; Aguilar, B. J.; Kiros, G. E.; Lamango, N. S., Polyisoprenylated methylated protein methyl esterase as a putative drug target for androgen-insensitive prostate cancer. *Ecancermedicalscience* **2014,** *8*, 459.

104. Aguilar, B. J.; Nkembo, A. T.; Duverna, R.; Poku, R. A.; Amissah, F.; Ablordeppey, S. Y.; Lamango, N. S., Polyisoprenylated methylated protein methyl esterase: a putative biomarker and therapeutic target for pancreatic cancer. *Eur J Med Chem* **2014,** *81*, 323-33.

105. Cushman, I.; Casey, P. J., Role of isoprenylcysteine carboxylmethyltransferase-catalyzed methylation in Rho function and migration. *Journal of Biological Chemistry* **2009,** *284* (41), 27964-27973.

106. Cushman, I.; Casey, P. J., RHO methylation matters: a role for isoprenylcysteine carboxylmethyltransferase in cell migration and adhesion. *Cell Adhesion & Migration* **2011,** *5* (1), 11-15.

107. Harrington, E. O.; Newton, J.; Morin, N.; Rounds, S., Barrier dysfunction and RhoA activation are blunted by homocysteine and adenosine in pulmonary endothelium. *American Journal of Physiology-Lung Cellular and Molecular Physiology* **2004,** *287* (6), L1091-L1097.

108. Ntai, I.; Fornelli, L.; DeHart, C. J.; Hutton, J. E.; Doubleday, P. F.; LeDuc, R. D.; van Nispen, A. J.; Fellers, R. T.; Whiteley, G.; Boja, E. S., Precise characterization of KRAS4b proteoforms in human colorectal cells and tumors reveals mutation/modification cross-talk. *Proceedings of the National Academy of Sciences* **2018,** *115* (16), 4140-4145.

109. Lombardini, J. B.; Talalay, P., Formation, functions and regulatory importance of S-adenosyl-l-methionine. *Advances in Enzyme Regulation* **1971,** *9*, 349-384.

110. Shi, Y.-Q.; Rando, R. R., Kinetic mechanism of isoprenylated protein methyltransferase. *Journal of Biological Chemistry* **1992,** *267* (14), 9547-9551.

111. Ishibashi, Y.; Sakagami, Y.; Isogai, A.; Suzuki, A., Structures of tremerogens A-9291-I and A-9291-VIII: peptidal sex hormones of Tremella brasiliensis. *Biochemistry* **1984,** *23* (7), 1399-1404.

112. Sakagami, Y.; Yoshida, M.; Isogai, A.; Suzuki, A., Peptidal sex hormones inducing conjugation tube formation in compatible mating-type cells of Tremella mesenterica. *Science* **1981,** *212* (4502), 1525-1527.

113. Anderegg, R.; Betz, R.; Carr, S. A.; Crabb, J. W.; Duntze, W., Structure of Saccharomyces cerevisiae mating hormone a-factor. Identification of S-farnesyl cysteine as a structural component. *Journal of Biological Chemistry* **1988,** *263* (34), 18236-18240.

114. Clarke, S.; Vogel, J. P.; Deschenes, R. J.; Stock, J., Posttranslational modification of the Ha-ras oncogene protein: evidence for a third class of protein carboxyl methyltransferases. *Proc Natl Acad Sci U S A* **1988,** *85* (13), 4643-7.

115. Fung, B. K.; Yamane, H. K.; Ota, I. M.; Clarke, S., The gamma subunit of brain G-proteins is methyl esterified at a C-terminal cysteine. *FEBS Lett* **1990,** *260* (2), 313-7.

116. Swanson, R. J.; Applebury, M. L., Methylation of proteins in photoreceptor rod outer segments. *Journal of Biological Chemistry* **1983,** *258* (17), 10599-10605.

117. Chelsky, D.; Ruskin, B.; Koshland Jr, D., Methyl-esterified proteins in a mammalian cell line. *Biochemistry* **1985,** *24* (23), 6651-6658.

118. Stephenson, R. C.; Clarke, S., Identification of a C-terminal protein carboxyl methyltransferase in rat liver membranes utilizing a synthetic farnesyl cysteine-containing peptide substrate. *J Biol Chem* **1990,** *265* (27), 16248-54.

119. Pillinger, M. H.; Volker, C.; Stock, J. B.; Weissmann, G.; Philips, M. R., Characterization of a plasma membrane-associated prenylcysteine-directed alpha carboxyl methyltransferase in human neutrophils. *Journal of Biological Chemistry* **1994,** *269* (2), 1486-1492.

120. Dai, Q.; Choy, E.; Chiu, V.; Romano, J.; Slivka, S. R.; Steitz, S. A.; Michaelis, S.; Philips, M. R., Mammalian prenylcysteine carboxyl methyltransferase is in the endoplasmic reticulum. *Journal of Biological Chemistry* **1998,** *273* (24), 15030-15034.

121. Hrycyna, C. A.; Sapperstein, S. K.; Clarke, S.; Michaelis, S., The Saccharomyces cerevisiae STE14 gene encodes a methyltransferase that mediates C-terminal methylation of a-factor and RAS proteins. *The EMBO journal* **1991,** *10* (7), 1699-1709.

122. Marr, R.; Blair, L.; Thorner, J., Saccharomyces cerevisiae STE14 gene is required for COOH-terminal methylation of a-factor mating pheromone. *Journal of Biological Chemistry* **1990,** *265* (33), 20057-20060.

123. Sapperstein, S.; Berkower, C.; Michaelis, S., Nucleotide sequence of the yeast STE14 gene, which encodes farnesylcysteine carboxyl methyltransferase, and demonstration of its essential role in a-factor export. *Molecular and cellular biology* **1994,** *14* (2), 1438-1449.

124. Marcus, S.; Caldwell, G.; Miller, D.; Xue, C.; Naider, F.; Becker, J., Significance of C-terminal cysteine modifications to the biological activity of the Saccharomyces cerevisiae a-factor mating pheromone. *Molecular and Cellular Biology* **1991,** *11* (7), 3603-3612.

125. Nijbroek, G. L.; Michaelis, S., Functional assays for analysis of yeast ste6 mutants. In *Methods in enzymology*, Elsevier: 1998; Vol. 292, pp 193-212.

126. Diaz-Rodriguez, V.; Distefano, M. D., a-Factor: a chemical biology tool for the study of protein prenylation. *Current topics in peptide & protein research* **2017,** *18*, 133.

127. Romano, J. D.; Schmidt, W. K.; Michaelis, S., The Saccharomyces cerevisiae prenylcysteine carboxyl methyltransferase Ste14p is in the endoplasmic reticulum membrane. *Mol Biol Cell* **1998,** *9* (8), 2231-47.

128. Yang, J.; Kulkarni, K.; Manolaridis, I.; Zhang, Z.; Dodd, R. B.; Mas-Droux, C.; Barford, D., Mechanism of isoprenylcysteine carboxyl methylation from the crystal structure of the integral membrane methyltransferase ICMT. *Mol Cell* **2011,** *44* (6), 997-1004.

129. Schubert, H. L.; Blumenthal, R. M.; Cheng, X., Many paths to methyltransfer: a chronicle of convergence. *Trends in biochemical sciences* **2003,** *28* (6), 329-335.

130. Schubert, H. L.; Blumenthal, R. M.; Cheng, X., 1 Protein methyltransferases: their distribution among the five structural classes of AdoMet-dependent methyltransferases. In *The Enzymes*, Elsevier: 2006; Vol. 24, pp 3-28.

131. Anderson, J. L.; Frase, H.; Michaelis, S.; Hrycyna, C. A., Purification, Functional Reconstitution, and Characterization of the Saccharomyces cerevisiae Isoprenylcysteine Carboxylmethyltransferase Ste14p*♦. *Journal of Biological Chemistry* **2005,** *280* (8), 7336-7345.

132. Wright, L. P.; Court, H.; Mor, A.; Ahearn, I. M.; Casey, P. J.; Philips, M. R., Topology of mammalian isoprenylcysteine carboxyl methyltransferase determined in live cells with a fluorescent probe. *Mol Cell Biol* **2009,** *29* (7), 1826-33.

133. Romano, J. D.; Michaelis, S., Topological and mutational analysis of Saccharomyces cerevisiae Ste14p, founding member of the isoprenylcysteine carboxyl methyltransferase family. *Mol Biol Cell* **2001,** *12* (7), 1957-71.

134. Russ, W. P.; Engelman, D. M., The GxxxG motif: a framework for transmembrane helix-helix association. *Journal of molecular biology* **2000,** *296* (3), 911-919.

135. Ratliff, A. C. STRUCTURAL ANALYSIS AND CONFORMATIONAL DYNAMICS OF THE YEAST ISOPRENYLCYSTEINE CARBOXYL METHYLTRANSFERASE, STE14. Purdue University Graduate School, 2019.

136. Desrosiers, R. R.; Nguyen, Q.-T.; Béliveau, R., The carboxyl methyltransferase modifying G proteins is a metalloenzyme. *Biochemical and biophysical research communications* **1999,** *261* (3), 790-797.

137. Hodges, H. B.; Zhou, M.; Haldar, S.; Anderson, J. L.; Thompson, D. H.; Hrycyna, C. A., Inhibition of membrane-associated methyltransferases by a cholesterol-based metal chelator. *Bioconjugate chemistry* **2005,** *16* (3), 490-493.

138. Bheemanaik, S.; Reddy, Y. V.; Rao, D. N., Structure, function and mechanism of exocyclic DNA methyltransferases. *Biochemical Journal* **2006,** *399* (2), 177-190.

139. Baron, R. A.; Casey, P. J., Analysis of the kinetic mechanism of recombinant human isoprenylcysteine carboxylmethyltransferase (Icmt). *BMC biochemistry* **2004,** *5* (1), 1-12.

140. Diver, M. M.; Long, S. B., Mutational analysis of the integral membrane methyltransferase isoprenylcysteine carboxyl methyltransferase (ICMT) reveals potential substrate binding sites. *J Biol Chem* **2014,** *289* (38), 26007-20.

141. Funk, A. L. Biochemical Elucidation of the Isoprenoid Binding Site of the Yeast Isoprenylcysteine Carboxyl Methyltransferase, Ste14p. Purdue University, 2017.

142. Anderson, J. L.; Henriksen, B. S.; Gibbs, R. A.; Hrycyna, C. A., The isoprenoid substrate specificity of isoprenylcysteine carboxylmethyltransferase: development of novel inhibitors. *Journal of Biological Chemistry* **2005,** *280* (33), 29454-29461.

143. Bergo, M. O.; Leung, G. K.; Ambroziak, P.; Otto, J. C.; Casey, P. J.; Young, S. G., Targeted inactivation of the isoprenylcysteine carboxyl methyltransferase gene causes mislocalization of K-Ras in mammalian cells. *Journal of Biological Chemistry* **2000,** *275* (23), 17605-17610.

144. Ahearn, I. M.; Siddiqui, F.; Abankwa, D.; Philips, M. R., NRAS is unique among RAS proteins in requiring ICMT for trafficking to the plasma membrane. *Life science alliance* **2021,** *4* (5).

145. Davies, B. S.; Fong, L. G.; Yang, S. H.; Coffinier, C.; Young, S. G., The posttranslational processing of prelamin A and disease. *Annual review of genomics and human genetics* **2009,** *10*, 153-174.

146. Markman, B.; Dienstmann, R.; Tabernero, J., Targeting the PI3K/Akt/mTOR pathway--beyond rapalogs. *Oncotarget* **2010,** *1* (7), 530-543.

147. Lau, H. Y.; Ramanujulu, P. M.; Guo, D.; Yang, T.; Wirawan, M.; Casey, P. J.; Go, M.-L.; Wang, M., An improved isoprenylcysteine carboxylmethyltransferase inhibitor induces cancer cell death and attenuates tumor growth in vivo. *Cancer biology & therapy* **2014,** *15* (9), 1280-1291.

148. Skylaki, S.; Hilsenbeck, O.; Schroeder, T., Challenges in long-term imaging and quantification of single-cell dynamics. *Nature Biotechnology* **2016,** *34* (11), 1137-1144.

149. Tellez-Gabriel, M.; Ory, B.; Lamoureux, F.; Heymann, M.-F.; Heymann, D., Tumour heterogeneity: the key advantages of single-cell analysis. *International journal of molecular sciences* **2016,** *17* (12), 2142.

150. Stender, A. S.; Marchuk, K.; Liu, C.; Sander, S.; Meyer, M. W.; Smith, E. A.; Neupane, B.; Wang, G.; Li, J.; Cheng, J.-X.; Huang, B.; Fang, N., Single Cell Optical Imaging and Spectroscopy. *Chemical Reviews* **2013,** *113* (4), 2469-2527.

151. Albeck, J. G.; Mills, G. B.; Brugge, J. S., Frequency-modulated pulses of ERK activity transmit quantitative proliferation signals. *Molecular cell* **2013,** *49* (2), 249-261.

152. Bolognesi, B.; Lehner, B., Reaching the limit. *eLife* **2018,** *7*, e39804.

153. Waters, A. M.; Ozkan-Dagliyan, I.; Vaseva, A. V.; Fer, N.; Strathern, L. A.; Hobbs, G. A.; Tessier-Cloutier, B.; Gillette, W. K.; Bagni, R.; Whiteley, G. R., Evaluation of the selectivity and sensitivity of isoform-and mutation-specific RAS antibodies. *Science signaling* **2017,** *10* (498), eaao3332.

CHAPTER 2. DEVELOPMENTS IN INSTRUMENTATION AND METHODOLOGIES FOR THE STUDY OF STE14-MEDIATED METHYLATION

2.1 Introduction

This chapter summarizes the protocols the author has extensively optimized for the projects included in this dissertation as well as for non-dissertation related projects. Projects related to this dissertation will be covered in more detail in the following chapters.

2.2 Isolation and visualization of substrate-labeled transmembrane helix 2 of Ste14

2.2.1 Summary

We employed a combination of methods and techniques to identify the residues of isoprenylcysteine carboxyl methyltransferase (Icmt) involved in substrate binding. In this section, the protocols from Chapter 3 are described in greater detail including: 1) photolabeling of Ste14 with a photoreactive substrate analog, 2) cleavage of photolabeled Ste14 at specific cysteine residues, 3) isolation of the photolabeled fragment of transmembrane helix 2 (TM2), and 4) visualization of the photolabeled TM2 fragment.

2.2.2 Background

It is proposed that transmembrane helix 2 (TM2) of Ste14 contains key residues that interact with substrate for proper enzymatic function. The crystal structure of *Tribolium castaneum* Icmt (*Tc*-Icmt) along with mutational analyses of *Homo sapiens* (*Hs*-Icmt) and *Anopheles gambiae* (*Ag*-Icmt) Icmts have determined the homologous N-terminal residues that line a hydrophobic, substrate tunnel.[1-4] These residues could be implicated in enzyme structure, substrate binding or orientation, and/or catalytic activity. Mutational analyses of Ste14 and subsequent activity studies, revealed that alanine-mutated residue Leu56 (L56A) preferred the geranylgeranylated form of substrate over the farnesylated from (see Chapter 3).[5] Taken together, these data suggest that the conserved residues along TM2 of Ste14, including Leu56 are important for enzymatic activity. These analyses do not determine if the decrease in activity was due to the disruption of substrate binding. To determine which residues of TM2 were important specifically for binding of substrate,

we leveraged techniques including mutagenesis, photolabeling, chemical cleavage, immunoblotting, fluorescence detection, and mass spectrometry, to name a few. Herein are the protocols for photolabeling, chemical cleavage, isolation of TM2, and visualization of photolabeled TM2. The number of steps required and the low yields of photolabeled TM2 fragment presented significant challenges.

2.2.3 Optimization

Photolabeling

Substrate mimetic, photoreactive probes were synthesized by the Distefano Lab (University of Minnesota) to aid in determining where the substrate interacts with the amino acid sequence of Ste14. These probes are based on a minimal substrate, *N*-acetyl-*S*-farnesyl-L-cysteine (AFC), modified with tunable moieties capable of binding and characterizing Ste14 in the substrate-bound state (Figure 2.1A). The isoprenoid group allows the probe to localize to the proper site within Ste14, and thus Ste14 retains activity with this probe when compared to the wild-type (WT) minimal substrate (AFC). A photoreactive diazirine moiety was introduced into the isoprenoid terminus to covalently bind to Ste14 upon exposure to ultraviolet (UV) irradiation, producing an irreversible-covalent bond between photoreactive-substrate and enzyme. The mechanism by which this bond is made can be seen in Figure 2.1C. The biotin group aids in visualization of photolabeled enzyme via western blotting with NeutrAvidin-HRP antibodies. It can also be useful in enriching the photolabeled enzyme by way of pulldown with NeutrAvidin-agarose resin. Lastly, a fluorescein (5-Fam or FITC) group aided in fluorescent visualization of photolabeled enzyme via Typhoon imager or by probing with fluorescein-HRP antibodies through western blotting.

In an effort to decrease protein degradation throughout the multi-step process of isolating and visualizing photolabeled TM2 of Ste14, probe:enzyme and irradiation times were optimized. Since the overall goal of decreasing protein degradation is to further enhance the signal of photolabeled enzyme fragments, we tested the photolabeling capacity on the purified, NTCB cleaved Ste14 mutant, TA-S77C (Figure 2.1B). This mutant is characterized and described in Chapter 3. Probe to enzyme ratios of 15:1, 10:1 and 3:1 were tested. Though there was no decrease in degradation across ratio conditions, it was evident in the NeutrAvidin-HRP blot that the 15:1 ratio produced the strongest signal in labeling the N-terminal fragment of TA-S77C (Figure 2.1D).

This finding aligned with the previous assays performed by Dr. Amy L. Funk (2017) that utilized probe to enzyme ratios of 15:1 and UV irradiation times of 30 minutes. Thus the 15:1 ratio was selected for all future photolabeling experiments. To further increase signal of photolabeled fragments by decreasing protein degradation, 10 min. and 30 min. UV irradiation times were tested (Figure 2.1E). No differences in degradation between irradiation times or were observed from the photolabeled C-terminal fragment of TA-S77C within the NeutrAvidin-HRP blot. Future photolabeling experiments should utilize a 15:1 ratio of probe:enzyme with 30 min. UV irradiation times. The Distefano Lab has unofficially reported 1% photolabeling of protein by their probes. The main hurdle of these experiments is visualization of photolabeled protein at maximal intensities, which becomes further exacerbated as other steps in the workflow of TM2 isolation further reduce concentrations of photolabeled TM2.

NTCB cleavage

To better isolate TM2 for substrate binding analysis, we can introduce two specific cysteine residues flanking the helix and selectively cleave them using a cysteine specific chemical cleavage reagent. Once photolabeled under native conditions, Ste14 can be cleaved at specific cysteine residues by 2-nitro-5-thiocyanobenzoic acid (NTCB). Generation of a cysteine-less, triple-alanine construct of Ste14 (TA-Ste14) served as a control. We introduced two cysteine residues within TA-Ste14 that flank each end of TM2 to isolate TM2 of Ste14. These mutations at Ile44 and Ser-77 created the double mutant TA-I44C-S77C. Each single mutant was tested separately for activity, photolabeling and NTCB cleavage before proceeding with examination of the double mutant (Chapter 3). Single cysteine mutant, TA-S77C, previously showed the highest cleavage efficiency of any mutant tested, and therefore was used for all NTCB cleavage optimization experiments.

Initial NTCB cleavage experiments of TA-S77C as well as those performed by Dr. Kalub J. Hahne and Dr. Amy L. Funk have shown the majority of the treated protein to be uncleaved and also showed high levels of protein degredation.[5, 6] To decrease protein degradation, initial cleavage incubation times of 16 hours were decreased to 4 hours. Though there was no decrease in degradation, there was also no change in cleavage efficiency, allowing no detriment to the samples and use of the shorter incubation period going forward (data not shown). Next, ratios of NTCB to enzyme were optimized. NTCB reagent concentrations were previously recommended to be

anywhere between 10- to 40-times in excess of protein.[7-9] Dr. Amy L. Funk previously utilized NTCB:enzyme ratios of 462:1, therefore NTCB:enzyme ratios of 10:1, 40:1, 100:1, 462:1 and 800:1 were tested (Figure 2.2).[5] By visualizing both the N- and C-terminal fragments of TA-S77C through α-myc and α-Ste14 immunoblotting, respectively (described in Chapter 3), it was determined that that NTCB:enzyme ratio of 462:1 was optimal. Under these conditions, there was no change in protein degradation. This experiment was performed once for TA-S77C and was repeated for the mutant TA-Q43C (data not shown). TA-Q43C overall showed much lower cleavage levels than the TA-S77C mutant confirming that the 462:1 NTCB:enzyme ratio was optimal for highest cleavage efficiency.

In the optimization of incubation time and NTCB:enzyme ratio, the majority of protein remained uncleaved. Thus, the reaction conditions were further optimized to promote cleavage by changing the denaturing agents and nucleophiles of the experiments. 6 M Guanidine was recommended to increase cleavage efficiency by replacing urea as the denaturing agent.[8, 9] While Efficiency under addition of guanidine remains inconclusive, as samples could not be properly loaded onto sodium dodecyl sulfate-polyacrylamide gel electrophoresis (SDS-PAGE) gels (data not shown). The SDS of the loading buffer started to precipitate in the presence of guanidine during sample preparation SDS-PAGE analysis. Ammonia-catalyzed cleavage was also recommended to increase cleavage efficiency and reduce denaturation with a smaller cleavage incubation time of 1 hour, however these conditions required guanidine as the denaturing agent and thus also produced inconclusive western blotting results (data not shown).[8, 9] Dialysis has been shown to remove the guanidine from NTCB reactions, however the low yields of pure protein and 100 µL reaction volumes of our experiments, made it not a feasible addition to our workflow of isolating TM2.[8-10] Expression systems in organisms other than yeast may overcome some of these difficulties; there is 1% pure protein yield of Ste14 from isolated crude membrane preparations of yeast.[11]

In addition to uncleaved protein, there is a propensity for NTCB to differ in cleavage efficiency for cysteine residues along the Ste14 sequence. As evidenced by the cleavage testing of TA-Q43C, which showed significantly lower NTCB cleavage compared to TA-S77C (data not shown), it is possible that certain areas of Ste14 are inaccessible to the chemical reagent. Ste14 and the areas of interest around TM2 are extremely hydrophobic, therefore reduced cleavage efficiency is not surprising. Diminished cleavage capacity was shown to be true in the

visualization of more than three fragments within the double mutant TA-I44C-S77C sample, indicating missed cleavages at both cysteine residues (Chapter 3).

Enrichment of photolabeled TM2

Residues within TM2 of Ste14 are proposed interact with isoprenylated substrate. Dr. Amy L. Funk previously determined that photoreactive substrate covalently binds to Ste14 between residues Phe46 (F46) and Ser77.[5] Upon mutation, expression and initial testing of Ste14 double-cysteine mutant TA-F46C-S77C, this mutant showed a profound reduction in methyltransferase activity (< 25%, data not shown) compared to the control, TA-Ste14. New N-terminal residues within Loop 1 of Ste14 were mutated to cysteine and studied for activity, photolabeling and cleavage efficiency, resulting in TA-I44C as the leading candidate (data not shown). The double mutant TA-I44C-S77C was successfully expressed and tested for activity, cleavage and photolabeling (Chapter 3).

As stated in the optimization sections for photolabeling and NTCB cleavage, increased efficiencies of these experiments are necessary to increase concentrations of photolabeled and properly cleaved protein, most significantly, photolabeled and cleaved TM2. Given the extensive optimization already performed in these previous steps, methods to enrich and isolate photolabeled TM2 following cleavage are required. The three expected fragments of TA-I44C-S77C, given both 100% photolabeling and cleavage efficiencies, were expected to be 5.4, 13.8 and 20.0 kDa for the TM2, N-terminal and C-terminal fragments respectively (Figure 2.3A). However, with inefficient cleavage and photolabeling capacities, other fragment sizes were also present. These additional fragments were all greater than 10 kDa in molecular weight except for those of TM2 (4.1 and 5.4 kDa) (see Chapter 3).

When previously assessing the less-active double mutant, TA-F46C-S77C, for cleavage and photolabeling of TM2, we identified the presence of the TM2 fragment via matrix-assisted laser desorption/ionization - time of flight/time of flight (MALDI-TOF/TOF) mass spectrometry (Figure 2.3B & C). The samples analyzed through this method were photolabeled and NTCB-treated, however, only non-photolabeled fragments, including that of TM2, were detected. Though initially promising, the lack of photolabeled fragment detection was not surprising given the low efficiency of photolabeling. Nonetheless, the detection of unphotolabeled TM2 is notable, since

to this point, we had been unsuccessful in visualizing the small fragment (photolabeled or not) within SDS-PAGE analyses. Further, the unphotolabeled TM2 fragment displayed maximal signal of the MALDI-TOF/TOF detector, providing the argument that, if isolated, the photolabeled TM2 fragment would have distinguishable signal as well.

Unfortunately, as the newer, more active double mutant, TA-I44C-S77C was being mutated and initially tested, the MALDI mass spectrometer in the Purdue Proteomics Facility (Bindley) was taken out of service and is still awaiting repair. Samples of photolabeled and cleaved TA-I44C-S77C were submitted to the Analytical Mass Spectrometry Core (DRUG) for analyses on their MALDI-TOF/TOF instrument, however there was no signal of any fragments or full-length protein in any of the samples submitted. It is possible that there is no signal because not enough protein was loaded to the sample plate, as previous samples run in the Proteomics Facility contained about 20-times recommended values of protein. It is important to note that upon initial consultation with the Proteomics Facility, it was suggested that anywhere from 0.5 pmol to 10 pmol of protein should be spotted onto sample plate with at least a 1:1 ratio of matrix.[12, 13] In initial analyses where ~25 pmol of sample was spotted, only full length protein was detected (data not shown). For the experiment in which the TM2 fragment was detected, over 200 pmol of protein was spotted onto the sample plate at a 1:2, protein to matrix ratio – 20 times the recommended protein spotting amount. We decided to use the matrix sinapinic acid, which helps to entrap and co-crystalize protein molecules them as it dries.[14, 15] Unfortunately, the MALDI instrument within the DRUG core is currently not in use for further attempts with the new double mutant and will not be until a new scientist if hired to run the facility or current graduate students implement a training and service schedule.

With the lack of availability of a usable MALDI instrument, we shifted our focus to the detection of the TM2 fragment using SDS-PAGE. Optimization of gel conditions necessary to resolve lower molecular weight proteins is summarized below in the next section. We have seen the most success with a 20% acrylamide gel in a 3-morpholinopropane-1-sulfonic acid-Tris-SDS (MOPS-Tris-SDS) running buffer. Without any enrichment steps, the larger molecular weight fragments (> 10 kDa) have maximized band signal intensity (Figure 2.4A), while detection of the lower concentrated TM2 fragment was unsuccessful. To combat diminished detection of the lower concentrated TM2 fragment, we used 10,000 molecular weight (MW) cut-off concentrators (a gift from the Low-Nam Lab, Purdue University, IN) following photolabeling and NTCB cleavage to

separate out the larger fragments. The TM2 fragment was expected to be in the flow-through of the concentrated sample. However, the large volume of the flow-through decreases the concentration of the TM2 fragment when preparing samples for SDS-PAGE analysis. Thus, the flow-through and samples retained in the concentrators were lyophilized (in the Chmielewski Lab) and subsequently reconstituted in minimal amounts of SDS-loading buffer to maximize concentrations for sample loading. As shown in Figure 2.4 using Sypro™ Ruby staining, the concentrator was successful in retaining the larger fragments while the TM2 fragment was collected in the flow-through. This was the first visualization of the TM2 fragment by SDS-PAGE and the first detection of the TM2 fragment in the newer TA-I44C-S77C mutant (Figure 2.4B). It is important to note that the TM2 fragment is resolved alongside the small molecular weight control of epidermal growth factor protein (EGF) which is about 6.4 kDa. Future efforts should continue to isolate the larger molecular weight fragments from the TM2 fragment. This is exemplified by the difficulty in detecting the EGF control, at a loaded mass of 100 ng, in the presence of the larger, more abundant, background fragments (Figure 2.4).

Since the gels detecting the TM2 fragment were visualized by Sypro™ staining, it cannot be confirmed that the TM2 fragment detected was photolabeled by our substrate-mimetic probe. To prove that TM2 was photolabeled, the samples from this experiment were analyzed by NeutrAvidin-HRP western blotting. Although the same amount of protein was loaded into the western blot as in the Sypro™ staining gels, no bands were detected (data not shown). The lack of resolved bands is due to the extremely low levels of photolabeled TM2 fragment present in the sample. In the Sypro™ gels, the EGF control and TM2 fragment bands had similar intensity. Therefore, since 100 ng of the EGF control was loaded, we can assume close to 100 ng of TM2 fragment was present as well. If it is true that 1% of protein is photolabeled (Distefano Lab), then out of the 100 ng of TM2 fragment visualized, 1 ng of TM2 in the gel should have been photolabeled. Detection limits of western blot analysis have been reported to be as low at 100 ng but recommended to be around 2 μg.[16, 17] Our lab can visualize 100 ng of pure protein via α-myc antibodies to analyze pure Ste14 preparations, but it is not recommended to go below this limit. Therefore, it is not surprising that we were not able to visualize photolabeled TM2 fragment in this gel sample as it is well below the 100 ng limit of detection.

To determine TM2 fragment yields within this workflow, we can compare the previously visualized TM2 fragment and the 100 ng of EGF control. This experiment utilized 30 μg of pure

Ste14 protein to be photolabeled, NTCB cleaved and concentrated. After lyophilization 100 µL of SDS-loading buffer was added to prepare samples for SDS-PAGE analysis. Of that 100 µL, 40 µL was loaded into the gel and visualized via Sypro™ staining. Because the bands of the TM2 fragment and the 100ng EGF control were similar in intensity, we can assume that approximately 100 ng of TM2 fragment was loaded into the gel in a 40 µL volume (Figure 2.4B). This gives 250 ng of TM2 fragment produced from the initial 30 µg of protein. Therefore, in this current reaction workflow to isolate the TM2 fragment, without attempting to separate photolabeled from unphotolabeled fragment, 0.8% of resulting protein is TM2 fragment. Of those 250 µg of protein, 2.5 ng is assumed to be photolabeled. Given the 1% photolabeling efficiency suggestion, 2.5 ng is photolabeled of the 250 µg of TM2 fragment. Thus the overall percentage of photolabeled TM2 fragment was reduced to $8x10^{-3}$% of the initial 30 µg of protein. If we are to visualize photolabeled TM2 fragment via NeutrAvidin-HRP western blotting analysis, at which the recommended minimum sensitivity of detection is 100 ng, we would need to start with a minimum of 1204 µg (1.2 mg) of pure protein. Given that there is also a 1% yield of pure protein from crude membrane preparations of yeast, 120 mg of crude membranes must be purified to perform one iteration of this current workflow to detect the photolabeled form of the TM2 fragment via SDS-PAGE analysis.[11] Thus, utilizing other expression systems, such as insect cells with baculovirus, will be useful in increasing protein yields for these experiments.

SDS-PAGE gel conditions

Optimization of the acrylamide composition of the SDS-PAGE gel and running buffer was required to visualize the small molecular weight TM2 fragment, whether photolabeled or not. When optimizing NTCB cleavage efficiencies with mutant TA-S77C, TruPAGE™ 4-20% precast gradient gels were run in a TEA-Tricine-SDS buffer. This preparation allowed for separation and identification of cleavage fragments between 10 and 75 kDa in size (Figure 2.5A). However, for TM2 fragments less than 10 kDa, these gel conditions were not appropriate since the dye front of the gel ran at 10 kDa.

The TruPAGE™ 4-20% gradient gels were run in a MOPS-Tris-SDS buffer with the running buffer of the inner chamber containing sodium bisulfite to better resolve the smaller molecular weight fragments of the TA-I44C-S77C double mutants (Figure 2.5B left). The antioxidant

properties of the sodium bisulfite is known to prevent potential sample reoxidation of reduced protein samples.[18] The dye front of these gels runs with the 10 kDa molecular weight marker of the protein standard (Figure 2.5B right). Interestingly, the lower molecular weights of the protein standard (2 and 5 kDa) ran faster than the dye front (Figure 2.5B right). The bands at 10 kDa that are visible in each lane of the western blot were caused by the lower molecular weights of the dye front (Figure 2.5B left). Under these conditions it was not possible to visualize the small molecular weight control of EGF by Sypro™ staining. It is possible that the protein was somehow running at the dye front and not at the same speed at the protein standard. To circumvent the possible difference in running speeds, we next tried running a 20% acrylamide gel in the same MOPS-Tris-SDS buffer with sodium bisulfite spiked into in the inner chamber (Figure 2.5C). These new conditions allowed separation and resolution of proteins between 37 and 2 kDa. When the dye front was run off the gel, the 2 kDa molecular weight marker of the protein standard remained about one-third of the distance to the bottom of the gel - well away from any possible interaction with the dye front. We were also able to resolve the EGF control under these new conditions and thus these conditions were used for future attempts to resolve the TM2 fragments.

When performing photolabeling and NTCB cleavage reactions of mutants without the need to resolve lower molecular weight fragments (<10 kDa), three different gel conditions could be used: 1) TruPAGE™ 4-20% precast acrylamide gels with TEA-Tricine-SDS buffer, 2) 12% acrylamide gels in a Tris-Glycine-SDS (TGS) buffer or 3) 12% acrylamide gels with 4-(2-hydroxyethyl)-1-piperazineethanesulfonic acid (HEPES) buffer (Figure 2.5A, D & E respectively). While bands were resolved well under gel conditions 1 and 3 (above), they displayed high background fluorescence when attempting to image the photolabeled fragments with the Typhoon imager. Condition 2 reduced the background fluorescence significantly, and thus was used for all future gels that required fluorescence analysis (data not shown). It was also observed that the fragment bands were not resolved with their predicted molecular weight standard. For example, in Figure 2.1D and E, the 17.9 kDa fragment ran slower than that 20.0 kDa fragment. This is elaborated on further in section 2.2.6.

2.2.4 Materials

1. 138 mM 3-morpholinopropane-1-sulfonic acid (MOPS), 1 mM dithiothreitol (DTT) buffer, pH 7.5

2. Biotin-PEG4-K(5-Fam)-AFC(Diazirine) (AFC-FamDiaz, Distefano Lab, University of Minnesota)
3. Pure Ste14 at a concentration of 0.25 µg/µL in photolabeling reaction
4. 96 well plate
5. Digestion Buffer (DigBuffer):
    a. Mastermix of buffer (made fresh in diH_2O):
        i. 233.3 mM glycine, pH 10
        ii. 6 M Urea
    b. In reaction:
        i. 105.9 mM glycine, pH 10
        ii. 2.72 M Urea
6. 40 mM NTCB stock (made fresh in DigBuffer):
    a. On analytical balance, mass small amount from tip of spatula into Eppendorf tube (~0.4-1.0 mg) per experiment
7. Vivaspin® 500 Centrifugal Concentrator (Sartorius VS0101, Göttingen, Germany), (Gift from Low-Nam Lab, Purdue University, IN)
8. Reducing, denaturing loading buffer (SDS-loading buffer):
    a. 5X stock: 25% β-Mercaptoethanol, 0.1% Bromophenol blue, 30% sucrose, 10% sodium dodecyl sulfate, 500mM Tris-HCl pH 6.8
    b. Further dilute to 2X in diH_2O
9. 20% SDS-PAGE gel
10. MOPS-Tris-SDS running buffer
    a. 20X stock: 0.6M MOPS, 1.2M Tris Base, 2% SDS (w/v)
    b. 1X when running buffer (dilute with diH_2O)
11. Sodium bisulfite:
    a. 800X stock: 4M sodium bisulfite
    b. 1X when running (dilute 800X stock into 1X MOPS-Tris-SDS running buffer)
12. Cytiva Amersham™ Protran™ NC Nitrocellulose Membranes (Fisher Scientific, Waltham, MA)
13. Tris-Glycine (TG) running buffer
    a. 10X: 250mM Tris, 1.92M Glycine

b. 1X when running with 20% (v/v) methanol

14. 1X Phosphate-buffered saline (PBS) buffer with 0.05% Tween (PBST)
15. Antibodies:
    a. Pierce™ High Sensitivity NeutrAvidin™ HRP conjugate (Fisher Scientific, Waltham, MA)
16. Sypro™ Ruby Protein Gel Stain (Fisher Scientific, Waltham, MA) (Gift from Low-Nam Lab, Purdue University, IN)
17. Sypro™ Ruby Fixing Solution: 50% (v/v) methanol, 7% (v/v) acetic acid
18. Sypro™ Ruby Washing Solution: 10% (v/v) methanol, 7% (v/v) acetic acid
19. Recombinant Human Epidermal Growth Factor (EGF) (Fisher Scientific, Waltham, MA) (Gift from Low-Nam Lab, Purdue University, IN).
20. Condensed milk (dissolved in PBST)
21. Supersignal™ West Pico PLUS Chemiluminescent Substrate (Fisher Scientific, Waltham, MA)

2.2.5 Protocol

1. Make Digestion Buffer (DigBuffer) Mastermix
    a. Mastermix concentrations: 233.3 mM glycine (pH 10), 6M Urea
2. Make 40 mM stock of NTCB in DigBuffer
    a. Mass NTCB on analytical balance
    b. Dissolve in calculated amount of DigBuffer to create 40 mM stock
3. On ice: Add pure protein, MOPS + DTT buffer, and photolabel to respective COLD reaction tube
    a. Pure protein concentration: 0.25 µg/µL
    b. Photolabel to protein ratio: 15:1
    c. Dilute to reaction volume with MOPS + DTT buffer
4. Incubate on ice, in dark for 10 minutes
5. On ice: transfer samples to pre-chilled 96-well plate (also on ice).
6. Irradiate samples with UV lamp for 30 minutes.
7. Transfer samples to clean, labeled Eppendorf tubes
8. Add NTCB and DigBuffer to each respective tube

a. NTCB to protein ratio: 462:1
    i. Usually have final concentration of 1.75 mM NTCB for each reaction
b. Final reaction concentration DigBuffer: 105.9 mM glycine (pH 10), 2.72 M Urea

9. Digest for 4 hours in 37ºC water bath
10. While digesting, rinse concentrators with diH_2O (x3)
    a. Sartorius Vivaspin ® 500 Centrifugal Concentrator (Low-Nam Lab)
        i. 10,000 MWCO PES
    b. Centrifuge at 12,000 x g at 4ºC for 2-5 min. increments
    c. Label concentrators
11. Concentrate samples at 2-5 min. increments until ~25 µL remains in column
12. Transfer solutions to new, labeled Eppendorf tubes
    a. Separate column and flow-through of samples
13. Lyophilize in Chmielewski lab – O/N at 4ºC
14. Add 100 µL 2X SDS to each sample, vortex to dissolve solid, spin down, heat at 65ºC for 15 min.
15. Vortex and spin down samples before loading into gel
16. Run 20% acrylamide gel
    a. Running buffer: 1x MOPS-Tris-SDS
        i. Spike cathode with 1X $NaHSO_3$
    b. Run at 100 V
17. Transfer gels to nitrocellulose or stain gels
    a. Transfer:
        i. To nitrocellulose paper
        ii. Running buffer: 1x TGS, cold
        iii. Run at 100V for 90 min., in ice bucket
    b. Stain:
        i. Sypro™ Ruby Red using manufacturers protocol (Fisher Scientific)
18. Imaging gels:
    a. Transferred gels

i. NeutrAvidin-HRP at ratio of 1:2000 in 1% BSA/PBST
    1. Incubate in 20% milk/PBST overnight at 4ºC
    2. Incubate with antibody for 3 hours at room temperature
    3. Incubate in West Pico Plus solutions following manufacturers protocol
    4. Image on GeneGnome imager in the Research Instrumentation Facility (Brown)

b. Stain:
    i. Image on Typhoon imager (Biochemistry, Golden Lab)

2.2.6 Conclusions and future work

These protocols have undergone continual optimization to isolate and detect the TM2 fragment and confirm that it is bound to the photoreactive-substrate mimetic. The concentration of photolabeled and cleaved TM2 fragment decreases with each additional step of this process, making it harder to detect. Currently, we have confirmed the presence of cleaved, unphotolabeled TM2 of the TA-F46C-S77C mutant through mass spectrometry analysis. Due to the current state of multiple, nonfunctioning mass spectrometers on campus, we were unable to perform the same analysis on the newer TA-I44C-S77C mutant. We then pivoted our efforts towards visualizing cleaved and photolabeled TM2 fragment through SDS-PAGE analyses. Very recently, we have been able to visualize the cleaved TM2 fragment using Sypro™ stain. The initial visualization of TM2 fragment could not differentiate between photolabeled and unphotolabeled fragment. When similar protein amounts of the same sample were analyzed via NeutrAvidin-HRP western blotting, no detectable levels of photolabeled TM2 fragment were observed. Thus, the concentrations of photolabeled TM2 fragment are too low in our current workflow to be detected. While significant progress has been made thus far, the current workflow will require continued optimization as new steps are added to further concentrate the photolabeled TM2 fragment for detection.

Thus far, we can provide specific conditions for the photolabeling and cleavage protocols. Photolabeling experiments should utilize UV irradiation times between 10 – 30 minutes and contain a 15:1 ratio of probe to enzyme. NTCB cleavage experiments should utilize 4-hour incubation times with NTCB reagent at a ratio of 462:1 with protein. Although there are ways to further optimize these protocols, with the recent visualization of TM2 fragment through SDS-

PAGE analyses, it may be more effective to focus efforts on the procedures that precede cleavage and photolabeling, to better concentrate the cleaved and photolabeled fragment. Nonetheless, one possible way to increase NTCB chemical cleavage is to perform the cleavage reaction within a barocycler. The continual cycling between different pressure conditions may help to integrate the chemical cleavage molecules into more inaccessible regions of the protein. This approach has shown great success in proteomics workflows to better digest proteins with trypsin.[19] Implementation of different reaction components such as guanidine and ammonia have also been proven to increase cleavage in other reports.[8-10] This would require the use of dialysis to remove the guanidine, which would increase the risk of sample loss due to small reaction volume sizes. Overall, increasing the amount of cleaved protein would increase the amount of isolated TM2 for better visualization signal.

TM2 fragment detection via SDS-PAGE analysis was a major step in our workflow progress. Future efforts should focus on visualizing photolabeled TM2 fragment. As previously stated, the levels of photolabeled TM2 fragment relative to its unphotolabeled counterpart are too low for detection. To increase these levels, our current experimental workflow can be expanded to include pulldown of the photolabel after the sample is processed with the 10,000 kDa MW concentrators. The flow-through of the concentrators would be introduced to agarose beads conjugated to NeutrAvidin. The NeutrAvidin would then bind to the biotin moiety of our photolabel. Once bound, the beads would be pelleted and separated from the supernatant that contains unphotolabeled TM2 fragment. SDS-PAGE analysis via Sypro™ staining can be used to confirm that photolabeled fragment was pulled out of the flow through by the beads. SDS-loading buffer can be added to the beads at minimal volumes to keep concentrations of desired protein as high as possible. For Sypro™ analysis, a 20% acrylamide SDS-PAGE gel should be utilized in a MOPS-Tris-SDS buffer containing sodium bisulfite within the inner chamber. If visible via Sypro™ staining, we can confirm that TM2 is labeled with our substrate-mimetic, photoreactive probe. Secondary methods to confirm photolabeling of TM2 are to run the same amount of sample with the same amount of protein in another SDS-PAGE gel, to then be analyzed via NeutrAvidin-HRP western blotting or by fluorescence detection. MALDI can also be utilized to confirm masses of photolabeled TM2 fragment.

It is extremely important when performing any iteration of this workflow with the goal of visualizing the photolabeled TM2 fragment via SDS-PAGE, to note that the amount of

photolabeled TM2 fragment needed to reach a minimum detection limit is 100 ng. This is true for both Sypro™ staining and NeutrAvidin-HRP western blotting. Though the Sypro™ stain is recorded to have detection limits as low as 1 ng, the minimal amount of EGF detected was 100 ng in a test of EGF detection at different concentrations (data not shown). This finding may suggest that the detector of the Typhoon instrument itself is not sensitive enough to detect Sypro™ levels at 1 ng. Therefore, iterations of this experiment should aim to produce well over 100 ng of the photolabeled TM2 fragment. Based on calculations described previously, to produce a minimum of 100 ng of photolabeled TM2 fragment, 1.2 mg of purified TA-I44C-S77C mutant Ste14 protein will be required in an experiment of this nature. With the low yields of Ste14 protein in crude membranes, each iteration of this workflow is extremely costly. To alleviate the cost associated with this workflow, efforts are currently underway to express TA-I44C-S77C mutant Ste14 in Sf9 insect cells via a baculovirus infection system, as this expression system has been shown to increase WT-Ste14 expression 5-fold compared to the current yeast expression system.[20]

There are other potential methods that would require larger rearrangements of the current workflow of experiments. One such method is to include size exclusion chromatography (SEC) via fast protein liquid chromatography (FPLC) to separate out cleaved TM2 fragments. If the FPLC instrument contains fluorescence detectors, one may be able to distinguish between photolabeled and unphotolabeled fragments. One disadvantage to this approach is that this process necessitates much higher starting concentrations of protein than the current workflow as FPLC analysis inherently utilizing and producing larger sample volumes. Another disadvantage to FPLC usage would be the required mass difference to be able to distinguish and properly separate two fragments of different sizes. Other methods to identify the photolabeled TM2 fragment include utilizing different types of mass spectrometry. In collaboration with the McLuckey Lab (Purdue University), initial experiments were performed using a Sciex Triple TOF instrument. Initial results seemed promising with future optimization needed to decrease background signal from the photolabeling and NTCB reaction components. Tandem mass spectrometry (MS/MS) analyses were also attempted in collaboration with the Purdue Proteomics Facility (Purdue University). While high cleavage coverage by a combination of trypsin and chymotrypsin was obtained prior to photolabeling (>90%), upon the addition of photolabeling to samples, detection of any portion of digested protein was low (protocol in section 2.3).

2.3 Tandem mass spectrometry analysis of photolabeled Ste14

2.3.1 Summary

To identify the exact residues of Ste14 covalently bound to a photoreactive substrate-mimetic, we employed a modified, bottom-up, proteomics approach. In this section protocols are described to 1) digest purified Ste14 with proteases and 2) prepare samples for tandem mass spectrometry (MS/MS) analysis.

2.3.2 Background

As described more extensively in Section 2.2 above and Chapter 3, it is proposed that substrate interacts within the N-terminal helices of isoprenylcysteine carboxyl methyltransferase (Icmt), and specifically transmembrane helix 2 (TM2) of Ste14. To validate this, we utilized the previously described photoreactive substrate-mimetic probes synthesized by the Distefano Lab (University of Minnesota) in combination with tandem mass spectrometry (MS/MS).

Bottom-up proteomics incorporates proteolytic digestion of purified protein or more complex protein mixtures for analysis by mass spectrometry.[21] This method is often used to identify proteins that have previously been sequestered from more complex matrices by a predetermined factor. For example, proteins containing the post-translational modification phosphorylation were isolated from plasma membrane samples and analyzed via MS/MS. The sequences experimentally identified were compared to an *in silico* library and the identities of proteins that make up the phosphoproteome of cells within the brain were determined.[22] Since we know the identity of our protein, we can use this method to compare photolabeled peptide sequences of Ste14 to unphotolabeled peptide sequences. The unphotolabeled peptide sequences will serve as our "library" to help identify the sequence within the photolabeled sample that is covalently bound to the photoreactive substrate. The sequences that contain the covalently bound probe are expected to have a mass shift of 1342.6 kDa relative to the identical, unphotolabeled sequence in the unphotolabeled library.

Herein are the protocols for protease digestion and MS/MS analysis of pure, photolabeled Ste14. These protocols will require further optimization as these results are preliminary. These experiments were performed in collaboration with the Purdue Proteomics Facility (Bindley).

2.3.3 Optimization

Proteolytic digestion of pure Ste14

These protocols were first optimized with Ste24 by Dr. Chelsea C. St. Germain.[23] Ste24 is an integral membrane protein that should have similar behavior to Ste14 under these same experimental conditions. Initially, pure Ste14 was treated solely with a trypsin/Lys-C mixture and analyzed via MS/MS to determine the sequence coverage of identified peptides. MS/MS analysis identified 77.0% of the Ste14 sequence (data not shown). The unidentified portions of protein are within loop 4, transmembrane helix 5 and 6 and the C-terminal cytosolic tail.

To further increase the coverage, we decided to perform side-by-side proteolysis reactions with chymotrypsin and a the trypsin/Lys-C mixture. Under the chymotrypsin conditions, there was 56.1% coverage, with some portions of peptides not identified within loops 2 and 4, transmembrane helix 3, and the C-terminal cytosolic tail (Figure 2.6B). The trypsin/Lys-C proteolysis conditions did not reproduce the coverage of the first experiment, only showing identification of 45.5% of the protein (Figure 2.6A). Portions of transmembrane helices 2, 5 and 6, loop 4 and the C-terminal cytosolic tail were incompletely covered. However, the combined coverage of these two conditions produced 90.8% sequence identification, with only portions of loop 4 and the C-terminal cytosolic tail not identified (Figure 2.6C & Figure 2.7). Since the substrate is proposed to bind to N-terminal portions of Ste14, these conditions provided enough sequence coverage to be implemented on photolabeled Ste14.

First, we tested to see if we could retain the same coverage percentages with photolabeled Ste14 protein under the two separate digestion conditions of chymotrypsin and trypsin/Lys-C. Whereas previous experiments were performed by the author using the instrumentation within the Proteomics Facility, these samples had to be processed by the researchers within the facility due to COVID-19 university restrictions. The coverage percentages between the two proteolysis conditions of the photolabeled protein was below 10%. The coverage of the control, unlabeled protein, was also below 10% (data not shown).

2.3.4 Materials

1. 8M Urea (make fresh)
2. 10 mM DTT in 8 M Urea (make fresh)

3. Alkylating mixture: 97.5% acetonitrile, 0.5% triethylphosphine (TEP), 2% 2-iodoethanol (IEtOH) (make fresh)
4. Equilibrium buffer: 0.1% formic acid in diH_2O (make fresh)
5. 25mM ammonium bicarbonate (ABC) (make fresh)
6. Elution buffer #1: 0.1% formic acid, 80% ACN (make fresh)
7. Elution buffer #2: 0.1% formic acid, 99.9% ACN (make fresh)
8. UltraMicroSpin c18 column (gift from Purdue Proteomics Facility)

2.3.5 Protocol

This protocol is adapted from the proteomics protocol by Dr. Chelsea C. St. Germain.[23]

1. Prepare solutions listed above
2. Resuspend protein pellet of previously photolabeled protein (20 µg) in 10 µL of 10 mM DTT in 8M Urea
3. Vortex and spin down sample
4. Let reduce: in dark, on rotating hot plate at 37ºC at 700 rpm for 1 hr.
5. Add 10 µL of alkylating solution. Incubate in dark, at 700 rpm, 37ºC for 1 hr.
6. Split each sample into two tubes of 10µL each (one for trypsin/Lys-C and one for chymotrypsin)
    a. Each tube now has 10 µg of protein
7. Dry the samples in vacuum centrifuge (~1.5-2 hrs.)
8. Add 40 µL of 0.05 µg/µL solution of specific digestion protease in ABC (~2µg protease). Mix at 700 rpm, 37ºC, 30 sec.
9. Load tubes into barocycler and run for 60 cycles (~1 hr)
    a. Each cycle: 20 kpsi, 50sec. atm pressure for 10 sec.
10. Wash UltraMicroSpin C18 columns with ACN (x3)
11. Clean proteolyzed samples with UltraMicroSpin C18 columns following instructions from manufacturer
12. Dry sample in vacuum centrifuge (1.5-2 hrs)
13. Store dried sample in -80ºC or -20ºC freezer in Proteomics Facility freezer for future submission.

2.3.6 Conclusions and future work

The last iteration of the tandem mass spectrometry experiments contained less than optimal coverage in both the photolabeled and unphotolabeled (control) samples (<10% coverage). Since there was previously 90% overall sequence coverage of the control samples, it suggests that the experiment containing the photolabeled samples should be repeated without any changes. It is expected that the photolabeled protein should show similar sequence coverage to the unphotolabeled control. However, the hydrophobic nature of the substrate-mimetic probe may cause the peptide sequence, to which it is bound, to not be identified by the mass spectrometer due to lack of ionization.

Electrospray ionization (ESI) was the ionization method used by the Q-Exactive Orbitrap HF MS used by researchers in the Proteomics Facility to analyze our samples. In previous studies, mass spectrometry analysis of membrane proteins utilizing ESI showed enhanced background signal, which is predominated by the detergents used to purify and stabilize the proteins.[24] ESI is typically suggested for analysis of intact proteins, most likely because full proteins have a higher percentage of amino acids and therefore the improved ionization needed for effective MS analysis.[25] Therefore, future attempts should evaluate methods that utilize intact protein without digestion treatments and methods that reduce the amount of detergents present in the sample to lower background signal.

To enrich the photolabeled portion of the protein for subsequent MS/MS analyses, the same steps used to isolate photolabeled TM2 fragment for SDS-PAGE analysis can be used. It would be best to start with samples enriched after treatment with the 10,000 MW cut-off concentrators and see if a signal of either state of TM2 fragment, photolabeled or unphotolabeled, can be detected. Another enrichment step following concentration would be the pulldown by the agarose beads conjugated to NeutrAvidin. However, as Dr. Chelsea C. St. Germain has reported, the buffers used for pulldown experiments (RIPA) and the attachment of the photolabeled fragment to the agarose beads are unsuitable for analysis on LC-MS/MS (liquid chromatography-MS/MS) instrumentation, as it will destroy the columns being used.[23] Buffer exchanges can be performed to aid with the removal of the detrimental detergents in the RIPA buffer or the pulldown can be performed in a PBS-based buffer that has been shown to have similar success.[23] Since the interaction between biotin and streptavidin is one of the strongest binding interactions recorded in nature, that of NeutraAvidin and biotin is also very strong.[26, 27] The strength of this interaction

presents challenges when trying to remove the beads from the biotin moiety of the probe, while still maintaining sample solutions that are feasible for LC-MS/MS analysis. One alternative is the use of Raney nickel, which hydrogenates thioether bonds. A thioether bond is present in the biotin moiety of the probe. Disadvantages of this method are the material itself being explosive, protein loss and, thus, low signal in subsequent LC-MS/MS analyses. Protein loss may be exacerbated by the interaction of the His-tags engineered into Ste14 for purification means with the nickel of the Raney nickel. Another method to release the photolabeled-substrate from the agarose beads, is to outcompete the NeutrAvidin-agarose with monomeric avidin conjugated to agarose. Another method would be to use the Pierce Monomeric Avidin Agarose (Thermo Scientific) which is marketed for its reversible affinity for biotinylated proteins. Although Thermo Scientific does note that published methods suffer from "low sample recovery, low biotinylated-protein binding, high nonspecific binding, and poor regeneration characteristics."

In addition to the minimal substrate *N*-acetyl-*S*-farnesyl-L-cysteine (AFC) based probes previously discussed, future studies should include performing MS/MS analyses with the geranylgeranylated form (AGGC) of photoreactive substrate. This analysis will show if there are differing interactions of amino acids between the farnesyl and geranylgeranyl isoprenoid groups. The photoreactive, diazirine moiety of the current class of probes is located at the end of the isoprenoid chain (Distefano Lab). It would be interesting to see where the other parts of the isoprenoid chain interact with Ste14 by moving the diazirine moiety closer to the reactive sulfur of the cysteine residue. This has previously been performed with photoreactive analogs in immunoblot analysis (Chapter 3).[5] However, the analysis showed no difference in substrate binding location when the photoreactive group was in the amide or farnesyl group of the substrate.

2.4 Fast protein liquid chromatography (FPLC) purification of Ste14

2.4.1 Summary

This section will describe the determination of optimal pH conditions for purification schemes that included gravity purification followed by fast protein liquid chromatography (FPLC) with a size exclusion chromatography (SEC) column.

2.4.2 Background

Ste14 is proposed to act as a homodimer for optimal stability and enzymatic activity.[20, 28] Recently, Dr. Anna C. Ratliff was able to confirm this via size-exclusion chromatography (SEC), multi-angle exclusion chromatography (MALS) and small angle X-Ray scattering (SAXS). In order to optimize the conditions of SEC-MALS-SAXS, she first set out to understand the SEC purification profile of Ste14 utilizing fast protein liquid chromatography (FPLC).

Because Ste14 is an integral membrane protein, normal molecular weight standards for SEC cannot be used because the detergents that Ste14 is purified in can alter elution volumes compared to the soluble protein standards.[20] This is also stated in the manufacturer's document from GE Healthcare for Superdex High-Performance Columns (2007). In her optimization efforts, Dr. Ratliff also determined that purification at a pH of 6 dramatically changes the SEC chromatograph of Ste14 by pushing the elution peaks further away from the void volume.[20] This could be due to a decrease in the amount of aggregation of Ste14, as it is suggested that membrane proteins be purified at a pH slightly lower than the biological pH to decrease their aggregation.[20] Therefore, all of Dr. Ratliff's subsequent SEC purifications and SEC-MALS-SAXS experiments were performed entirely at the pH of 6.0.

Within the sample preparation preceding SEC purification and SEC-MALS-SAXS experiments, Ste14 undergoes gravity purification with metal affinity resin. Based on the user manual for the resin (Thermo Scientific), all binding and wash conditions are suggested to be at a pH closest to 7. Whereas buffers for elution and regeneration of resin are suggested to range from below 7 in pH and closer to 5 (Thermo Scientific). Therefore, it is possible that the conditions at a pH of 6 for purification fallowed by SEC or SEC-MALS-SAXS, alter the binding ability of the resin to the protein.

2.4.3 Optimization

To better understand if pure protein yields are decreasing due to the use of a lower pH during the purification and analysis scheme used by Dr. Ratliff, three different reaction conditions were tested: A) gravity purification at pH of 7.2 followed by SEC purification at pH 7.2, B) gravity purification at pH 7.2 followed by SEC purification at pH 6.0, C) gravity purification at pH of 6.0 followed by FPLC purification at pH of 6.0 (Figure 2.8).

2.4.4 Materials

1. Cold, 1xEQ buffer stock at respective pH for reaction (7.2 or 6.0): 0.3 M NaCl, 50 mM Na_2HPO_4
2. 10 % *N*-dodecyl-β-D-maltopyranoside (DDM) stock (make fresh in ddH_2O)
3. Lysis buffer (LB) stock, cold (make fresh in 1xEQ buffer): 10% glycerol, 2 mM 4-(2-aminoethyl)benzenesulfonyl fluoride hydrochloride (AEBSF), 1% aprotinin, 0.3 M NaCl, 50 mM Na_2HPO_4
4. FPLC Buffer stock at respective pH for reaction (7.2 or 6.0), cold (make fresh in 1xEQ): 2 mM DTT, 0.05% DDM, 50 mM Na_2HPO_4, 0.3 M NaCl
    a. Must be in an autoclaved bottle
5. TALON® Metal Affinity Resin (Clontech, San Jose, CA)
6. Solubilization Buffer, cold (make fresh in LB): 1% DDM, 20 mM Imidazole, 0.3 M NaCl, 10% glycerol, 2 mM AEBSF, 1% aprotinin, 50 mM Na_2HPO_4
7. Wash Buffer, cold (make fresh in LB): 40 mM Imidazole, 1% DDM, 0.3 M NaCl, 2 mM AEBSF, 1% aprotinin, 50 mM Na_2HPO_4
8. KCl #1 Buffer, cold (make fresh in LB): 40 mM Imidazole, 1% DDM, 500 mM KCl, 0.3 M NaCl, 2 mM AEBSF, 1% aprotinin, 50 mM Na_2HPO_4
9. KCl #2 Buffer, cold (make fresh in LB): 40 mM Imidazole, 0.1% DDM, 500 mM KCl, 0.3 M NaCl, 2 mM AEBSF, 1% aprotinin, 50 mM Na_2HPO_4
10. Elution buffer, cold (make fresh in LB): 1 M Imidazole, 0.1% DDM, 0.3 M NaCl, 2 mM AEBSF, 1% aprotinin, 50 mM Na_2HPO_4
11. MilliporeSigma™ Amicon™ Ultra-15 Centrifugal Filter Unit 30 MWCO (Fisher Scientific, Waltham, MA)
12. GV Durapore ® (0.22 µm) centrifugal filter (Billerica, MA)

2.4.5 Protocol

*Note: this protocol is for a minimum of 100 mg of Sf9 crude membranes. All samples should stay on ice throughout the whole procedure.

1. Prepare 10% DDM and LB solutions

2. Add crude membranes to solubilization buffer (5 mg/mL protein). Rock for 1 hour at 4ºC
    a. Prepare FPLC buffer (0.22 mm, gift from Lyon Lab, Purdue University) by filtering it into autoclaved bottle. Place buffer into fridge.
    b. Prepare FPLC and column (FPLC: "SPICE," column: "Lizzie," Lyon Lab)
        i. Switch column to single column
        ii. Use 1 mL injection loop to reduce aggregation
            1. Wash injection loop with FPLC buffer (x10 total)
        iii. Empty FPLC waste
        iv. Load correct FPLC protocol onto computer
            1. Methods > Hrycyna > Anna > 1 mL loop
        v. Equilibrate column and tubing twice with diH_2O. Make sure retaining correct pressure
        vi. Equilibrate column and tubing at least once with FPLC buffer. Make sure retaining correct pressure
3. Centrifuge solubilization buffer + protein at 100,000 x g for 45 min.
    a. Collect 50 µL of pre-spin for future gel analysis
    b. Complete steps in 2b if not completed
    c. Prepare TALON® Resin and keep on ice
        i. Aliquot 2 mL of suspended resin / 50 mg of crude membrane protein into 15 mL falcon tube
            1. 2 mL of resin per 15 mL falcon tube
        ii. Centrifuge for 2 min. at 1,000 rpm at 4ºC, aspirate supernatant
        iii. Wash with 3 mL of LB
        iv. Repeat steps 3c i – iii (x3 total). Be careful not to dry out resin
4. Split supernatant equally between resin. Rock for 1 hr at 4ºC
    a. Collect 50 µL of post-spin to future gel analysis
    b. Rinse ultra pellet with 3 mL LB and resuspend in 500 µL LB using 20 gauge needle. Save for future gel analysis.
5. Centrifuge down resin + protein at 1,200 rpm. Aspirate supernatant
    a. Save 50 µL of column unbound for future gel analysis

6. Wash the resin + protein by adding 5 mL Wash Buffer to each tube. Rock for 10 min. at 4ºC
7. Centrifuge down resin at 1,200 rpm. Aspirate supernatant.
8. Repeat steps 6-7
9. Add 5 mL KCl#1 Buffer to each tube of resin + protein. Rock for 10 min. at 4ºC
10. Centrifuge down resin at 1,200 rpm. Aspirate supernatant
11. Add 5 mL of KCl#2 Buffer to each tube of resin + protein. Rock for 10 min at 4ºC.
12. Centrifuge down resin at 1,200 rpm. DO NOT aspirate supernatant
13. Add resin + protein + KCl#2 Buffer to columns for gravity filtration at 4ºC. Collect flow through
    a. Combine flow through into one falcon tube and record volume
    b. Save 250 µL (x2) of flow through for gel analysis for a possible activity assay if needed.
14. Elute protein off resin by adding 4 mL of Elution Buffer to the column once the previous buffer has gone through. Do not dry out resin in between buffers.
15. Combine all elution into single, cold 30 kDa molecular weight cut off concentrator.
    a. Save 50 µL of unconcentrated elution for future gel analysis
16. Concentrate protein by spinning at 5,000 x g at 4ºC until the volume is at or below 1.0 mL
    a. Finish preparing FPLC:
        i. Make sure fraction collector is aligned and fill with tubes
        ii. Empty FPLC waste bottle
    b. Save 2, 10 µL aliquots of concentrated sample
17. Filter protein before loading onto FPLC
    a. 500 mL per GV Durapore® filter
    b. Wash filter with 500 µL buffer by spinning at 12,000 x g for 2 min at 4ºC
    c. Filter sample by spinning at 12,000 x g for 2 min. at 4ºC
18. Recombine filtered protein, and load into FPLC through syringe port
    a. Make sure there are no bubbles in the syringe sample before injecting into FPLC
    b. Make sure correct protocol is loaded, and click run

c. If pressure or flow rate are too high, pause the run

19. Collect fractions with protein (~10-15 min. elution time). Save in -80ºC for gel and activity analysis if needed.
20. Clean FPLC
    a. Wash column: equilibrate with autoclaved diH_2O (x2)
        i. If high UV spectrum, re-run again
    b. Rinse FPLC injection tube with 1 mL diH_2O (x10)
    c. Put columns back in tandem set up
    d. Clean out fraction collector

2.4.6 Conclusions and future work

Each condition resolved multiple peaks within the FPLC chromatograph. The shoulder (S) and first two peaks (1 & 2), contain Ste14. It was believed that peak 1 contained aggregated Ste14, as it showed diminished methyltransferase activity compared to peak 2.[20] Peaks 3 through 5 may contain some Ste14, however their fractions from the FPLC were more yellow in color, relative to the first peaks, indicating that it may be Ste14 trapped in excess DDM detergent.[20]

Condition C was able to almost completely condense the shoulder (S) and the first peak (1), which is believed to be dimerized Ste14.[20] This condition allows for easier isolation of dimerized Ste14. However, condition B, lead to the highest yield of pure Ste14 following gravity filtration, (quantification not shown). Although not completely detrimental to purification schemes, this agrees with the theory that pHs lower than 7 could disrupt protein binding to the metal affinity resin. Going forward, condition B should be utilized for purification methods including SEC via FPLC.

2.5 Microscale thermophoresis (MST) of Ste14 and minimal substrates AFC and AGGC

2.5.1 Summary

This section summarizes the protocol and optimization of microscale thermophoresis (MST) to quantify dissociation constants (K_D) of minimal substrates *N*-acetyl-*S*-farnesyl-L-cysteine (AFC) and *N*-acetyl-*S*-geranylgeranyl-L-cysteine (AGGC). Herein are descriptions of 1) overall MST experiment protocols that ultimately required the 2) labeling of Ste14 with fluorescent groups and

the determination of 3) AGGC concentrations and 4) types of lipids suitable for proper MST analysis.

2.5.2 Background

Dr. Christine A. Hrycyna has designed and implemented a robust and replicable *in vitro,* vapor diffusion methyltransferase activity assay that is the basis of her lab's quantification of methylation capacity of species of isoprenylcysteine carboxyl methyltransferase (Icmt), mutations within Icmt, and substrates and inhibitors of Icmt.[11, 29] only apparent K_m (Michaelis-Menten constant) and V_{max} (maximal velocity) values of enzyme-substrate or enzyme-inhibitor pairs can be quantified using this assay. The concentration of the substrate available to the enzyme is not accurately determined due to the nature of this assay containing crude membrane samples or pure Ste14 with added lipids for protein stabilization. For mutational analyses, this assay also cannot determine if changes in activity are due to changes in protein structure and stability, substrate binding and orientation, or alterations to catalytic activity.

To crudely determine structural changes, trypsin digestion patterns of different mutants can be compared to that of wild-type (WT) Ste14. If the cleavage pattern is different, further structural studies like determining melting temperature can be performed on the mutants. The melting temperature will better determine if the mutant has differing stability from the WT protein.

To date, no quantitative and replicable binding assay for Icmt exists. An assay of this capacity would be useful in quantifying binding constants for enzyme-substrate or enzyme-inhibitor pairs. Specifically for Icmt, this would be useful in understanding the differences in how this enzyme accommodates and equally favors substrates with differing isoprenoid modifications; a 15-carbon farnesyl addition or a 20-carbon geranylgeranyl addition. As described in Chapter 3, previously performed mutational analyses of Ste14 and subsequent activity studies of substrates differing in their isoprenoid groups, revealed that alanine-mutated residue Leu56 (L56A) preferred the geranylgeranylated form of substrate over the farnesylated from. It is proposed that the difference in activity between the two substrates for this mutant is due to a difference in binding affinity, making this mutant a perfect candidate for a binding assay study. Residue Leu56 also sits inside of TM2, which is proposed to be the site of substrate-binding (Section 2.1 & Chapter 3).

Efforts in our lab have been made to determine binding constants of prenylated CAAX proteins with the protease Ste24 utilizing the method MST.[23] This method can quantify K_D

(dissociation constant) values by measuring, through fluorescence detection, the differences in the rates of movement of enzyme bound to substrate versus free enzyme away from an infrared (IR)-induced temperature gradient.[30] This method is advantageous due to the low amounts of sample required, the short experiment duration, and the ability to analyze samples with complex matrices, including membrane proteins that require detergents.[30] Other binding quantification methods like fluorescence polarization, are not as tenable for our experiments, due to the flexibility of the PEG4 linker of the fluorescent substrate-probe.

2.5.3 Optimization

MST buffer conditions

Initially when Ste14 was tested by MST analysis, we used pure Ste14 and the AFC-FamDiaz probe as substrate (Figure 2.1A). Because the probe contains a fluoresceine isothiocyanate group (FITC or 5-Fam), it served as the fluorescent portion of the enzyme-substrate pair. The concentration of probe therefore needed to stay constant, so that the change in fluorescence detected was only due to the movement of the protein-substrate pair out of the area of the temperature-gradient (IR laser). Therefore, the pure protein needed to be serially diluted at a range 10-fold above and below the expected K_M value. The K_M values could be assumed from the *in vitro* methyltransferase activity assay described above; for Ste14 and its minimal farnesylated substrate, AFC, the K_M value is about 13 μM.[5, 11] Initial testing of Ste14 by MST revealed variation in background fluorescence amongst all dilution samples. This variation was also shown when Ste24 was tested.[23] We observed that the initial samples containing high protein concentration had the highest background fluorescence. The decrease in fluorescence with protein concentration indicated that a component of the protein or purification buffer may be the cause of the observed fluorescence variation. With the help of the Low-Nam lab, we analyzed all components of the purification buffers and determined that the protease inhibitors AEBSF and aprotinin were fluorescing. Since both inhibitors are small molecules, they should be able to flow through the 30 kDa molecular weight cut off concentrator used during purifications. However, in attempts to reduce the amount of these inhibitors in pure protein samples, the inhibitors seemed to be getting caught in the concentrator, most likely due to the presence of detergent and glycerol. Instead of trying to remove the fluorescent molecules after or during purification, we attempted to keep the

background fluorescence constant. To do this, we performed the serial dilutions for the assay with concentrated purification buffer. Therefore, the same volume of purification buffer was expected in all MST samples. While this approach seemed to level out the fluorescence, there was no way to deduct the background fluorescence that was recommended by either from the Monolith company or other professors who have performed MST. Other methods of performing MST were then searched for in the literature.

In our attempts to circumvent the high levels of background fluorescence, we tried another form of MST which quantifies the of changes in intrinsic fluorescence of protein. Unfortunately, both Ste24 and Ste14 did not show intrinsic fluorescence levels high enough for detection and subsequent K_D quantification. Another viable method is to keep the current MST conditions but redesign the substrate to contain a different fluorophore that is considered a red dye. This method would allow the MST instrument to be changed from the blue wavelength filter to the red wavelength filter. The blue filter had to be used for the 5-Fam-conjugated substrate, under which the protease inhibitors showed fluorescence detection. The purification buffer did not show any fluorescence when tested under the red filter, negating the need for background fluorescence subtraction. The red filter route was taken to analyze Ste24 for subsequent MST analysis.

Labeling Ste14 with Alexa Fluor™ 647 NHS ester

The minimal-**a**-factor substrate for Ste24 will precipitate and at concentrations higher than 40 μM, causing "aggregation" readings by the MST instrument.[23] For *in vitro* vapor diffusion assays, Ste24 activity shows a significant decrease for minimal-**a**-factor substrate at concentrations above 40 μM, due to the substrate's precipitation.[23] Due to substrate precipitation, the substrate of Ste24 has to be photolabeled to keep constant at concentrations below its precipitation limit. The minimal substrate of Ste14, AFC, although hydrophobic, does not have the same properties of the **a**-factor mimetic substrate. AFC is normally tested at 200 μM concentrations in the *in vitro* methyltransferase activity assay with Ste14. This information is important for MST optimization, as it allows Ste14 to be the partner that is fluorescently labeled.

As previously described, the purification buffers did not show detectable background fluorescence with the MST instrument set with the red filters. We therefore decided to label pure WT-Ste14 via the Alexa Fluor™ 647 NHS ester (Invitrogen, gift from Low-Nam Lab, Purdue

University), which labels lysine residues with Alexa 647. Utilizing protocols found to be successful by the Low-Nam lab, our first labeling attempt produced completely inactive but labeled Ste14 protein with a dye to protein ratio of 0.15:1. The next attempt to label protein included a higher concentration of dye and a longer label and protein incubation time. We included not only WT-Ste14, but also L56A mutant Ste14 and F80A mutant Ste14. Unlike L56A, which shows a preference for AGGC vs AFC substrate, F80A is completely inactive with both substrates and is speculated to serve as a negative control for MST analysis. Labeling produced higher than a 1:1 ratio of dye to protein for all Ste14 mutants. WT protein that was about 30% active relative to unlabeled protein (data not shown). Ratios of dye to protein higher than 1 can cause inconsistent fluorescence readings (MST Starting Guide – Monolith NT.115) and thus create another obstacle. With newly labeled WT-Ste14 having increased activity and the lowest dye to protein ratio of all the mutants labeled (1.22:1), using this protein in optimizing the MST protocol was a welcomed improvement.

First, the concentration of labeled protein was determined by testing the fluorescence intensity of varying concentrations of labeled protein. 20 nM labeled WT protein had about 1700 fluorescence counts, well within the workable range of 500 to 2500 counts (MST Starting Guide – Monolith NT.115). Second, binding tests were performed to see if a there was a baseline difference in fluorescence detection between maximally bound and completely unbound protein. Labeled WT protein was tested with (200 μM AFC) and without any substrate. 200 μM AFC was chosen since that is the concentration used in the *in vitro* methyltransferase activity assay for saturating conditions. This showed a detectable difference in the normalized fluorescence for the bound versus unbound state of protein (Figure 2.9A). These values for the bound versus unbound states were averaged between four different samples. The values for each of the four samples varied greatly within both bound and unbound states. This variation contributed to the complete MST experiment (20 nM labeled WT Ste14 with a serial dilution of AFC starting at 200 μM), having no discernable binding curve. It is possible that very minimal amount of substrate was binding to protein resulting in the high amount of unbound substrate and protein, causing this high variation in fluorescent signal between samples. Minimal substrate binding may be due to the lack of lipids within the MST experiment conditions.

Lipid conditions

It is known that lipids are required for purified Ste14 to retain enzymatic activity.[11] Without lipids, there is not only a decrease in enzymatic activity, Ste14 is rendered inactive (Figure 2.9B). Thus, for any assay where native Ste14 is required, lipids should be included. Our *in vitro* vapor diffusion activity assay includes *E. coli* polar extract phospholipids consisting of 67% (wt/wt) phosphatidylethanolamine (PE), 23.2% (wt/wt) phosphatidylglycerol (PG) and 9.8% (wt/wt) CA.

To determine if these *E. coli* lipid extracts were suitable with MST analysis, we first tested background fluorescence levels of these lipids. Unfortunately, working concentrations of these lipids between 10 and 0.7 mg/mL showed fluorescence detection under the red filter method of the MST instrument (Figure 2.9C). Although low, <50 fluorescence counts, the fluorescence levels were similar to those of the purification buffer and also displayed detectable movement when a temperature gradient was induced. Thus, finding different lipids that do not fluoresce was the next step.

We tested 1,2-dioleoyl-sn-glycero-3-phosphocholine (DOPC), DOPC + phosphatidylinositol 4,5-bisphosphate (PIP_2), and 1,2-dioleoyl-sn-glycero-3-[(N-(5-amino-1-carboxypentyl)iminodiacetic acid)succinyl] (nickel salt) (DGS-NTA(Ni)) (Gift from Low-Nam Lab, Purdue University). These lipids showed almost indetectable levels of fluorescence (<10 fluorescence counts) and no change in fluorescence when tested with a temperature gradient, making these great candidates for combination with Ste14. Upon testing Ste14 activity with these lipids compared to the *E. coli* lipid extract mixture, DOPC combined Ste14 has ~22% activity and DOPC+PIP_2 mixture and DGS-NTA(Ni) were inactive (<10%) (Figure 2.9D). This could be due to the lipid samples from the Low-Nam Lab being older stocks and not necessarily due to incompatibility with Ste14, as it has been shown that most lipid and lipid mixtures are capable of supporting pure Ste14 activity.[11]

AGGC concentrations

In addition to testing the farnesylated-minimal substrate, AFC, we wanted to quantify the binding of its geranylgeranylated counterpart. WT-Ste14 does not have a preference for farnesylated versus geranylgeranylated substrate (Chapter 3).[11] Ste14 mutant L56A shows a marked preference for AGGC over AFC in activity making it of specific interest in binding

experiments. It is proposed that the mutated alanine residue provides more room within the hydrophobic substrate pocket to accommodate the larger isoprenoid group (Chapter 3).

Initial *in vitro* methyltransferase activity assay testing of WT-Ste14 with AGGC at normal substrate conditions (200 μM) reduced WT-Ste14 to <50% of that with 200 μM AFC (Figure 2.10A). Previously, studies comparing the preference of AFC versus AGGC for Ste14 mutants utilized AGGC concentrations of 100 μM (Chapter 3).[5] Comparison of WT-Ste14 activity with varying concentrations of AFC and AGGC, showed that 100 μM concentrations of both substrates had maximal and most similar activities between the two substrates (Figure 2.10B). Therefore, 100 μM AGGC is the maximal concentration that should be used in any future activity or binding assays.

2.5.4 Materials

MST

1. Monolith NT.115 capillaries (Nanotemper, San Francisco, CA)
2. Concentrated 1xEQ elution buffer: 1 M Imidazole, 0.1% DDM, 0.3 M NaCl, 2 mM AEBSF, 1% aprotinin, 50 mM Na_2HPO_4
3. Alexa 647 labeled pure Ste14 protein
4. AFC and AGGC 1 mM stocks

Labeling Ste14 with Alexa Fluor™ 647 NHS ester

1. Bovine serum albumin (BSA)
2. Large amounts of purified protein (>100 μg)
3. Alexa Fluor™ 647 NHS ester (Invitrogen, gift from Low-Nam Lab, Purdue University)
4. 1 M $NaHCO_3$ (make fresh in diH_2O)
5. Zeba spin desalting columns (Fisher Scientific, Waltham, MA)

2.5.5 Protocol

MST

*Protocols are followed on the Monolith NT.115 instrument located in Chemical Genomics Facility of DRUG

1. Set instrument to 20 nM labeled protein
    a. If newly labeled protein, must establish concentration that gives fluorescent signal between 500 and 2500 fluorescence counts
2. Set instrument to 30 ºC
3. Add
4. Prepare serial dilutions in the dark
    a. Highest concentration should be 200 µM for AFC and 100 µM for AGGC and diluted by half for each dilution
    b. Each dilution should have a minimum final volume of 20 µL
    c. Add concentrated elution buffer to each tube first
    d. Add substrate to first tube and serial dilute
    e. Add labeled Ste14 protein last
5. Load samples into capillary tubes
6. Wipe tubes with Kimwipes and load onto rack so that sample volume is in the middle of the capillary
7. Set instrument to 80% excitation power and medium MST laser power, and red LED filters.
8. Run expert mode to manually input concentrations
9. Save and export all possible files to external drive

Labeling Ste14 with Alexa Fluor™ 647 NHS ester

*Based off of protocol from South Dakota State University department of Chemistry and Biochemistry (Dr. Shalini T. Low-Nam and Dr. Adam Hoppe

1. Determine concentration of BSA using A_{280} ($A = \varepsilon cl$)
    a. $\varepsilon_{BSA} = 43{,}824\ M^{-1}cm^{-1}$; $MW_{BSA} = 66{,}463$ Da

2. Calculate dilution needed for 50 ug of BSA in 130 µL reaction volume
    a. Dilute in 0.1% DDM solution (that is what is in elution buffer)
3. Calculate dilution of stock dye needed for 5:1 dye to protein in reaction volume; also ensure less than 1% DMSO in reaction
4. . Calculate remaining volume of 1X PBS to use as diluent (remember 1/10 volume of 1M $NaHCO_3$)
5. To begin reaction, dilute protein into PBS and then add 13 µL 10 mM $NaHCO_3$ (you can check the pH at this point; pH should be > 8)
6. Begin timing reaction as soon as dye to added to reaction (a typical timing of 20 minutes at room temperature should suffice). Cover reaction tube with foil and leave constantly agitating (also a good idea to flick reaction periodically, careful not to generate bubbles).
7. All at 4ºC. When 8-10 minutes remain in the incubation, prepare the spin columns for the final purification step:
    a. Twist the lid of the tube a half turn and spin at 800xg for 2 minutes
    b. Dispose of flow through and add 300 µL of 1X PBS to wash
    c. Rinse resin by spinning at 800xg for 1 minute
    d. Repeat rinse step for a total of 5 washes
8. Elute conjugate by applying 130 ¨L reaction to resin and spin at 800xg for 4 minutes
9. Re-run flow through over column at 800xg for 4 minutes; save product in labeled tube, covered with foil (column resin should be colored as the result of binding free dye)
10. Determine dye to protein using spectrophotometry (Nanodrop)
    a. Measure A_{280} and A_{max} of fluorescent conjugate (account for dilution)
        i. Alexa 647
    b. Protein concentration (M) = $[A_{280} – (A_{max} \times CF)]/\varepsilon$
    c. Degree of labeling (ratio) = $(A_{max} \times MW)/(\varepsilon_{dye} \times$ protein concentration)
        i. Correction factor: 0.03
        ii. ε_{dye}: 270,000
        iii. ε_{Ste14}: 239,000

2.5.6 Conclusions and future work

For functional MST experiments that produce a binding curve for Ste14, there three issues were identified that require further optimization: lipids, degree of labeling, and dimerization. First, the experiments should include lipids. Since the current *E. coli* lipid extracts used in the *in vitro* methyltransferase activity assays have components that fluoresce, new lipid extracts should be used. We started testing background fluorescence and Ste14 activity in the presence of DOPC, DOPC + PIP_2, and DGS-NTA(Ni) (gifts from Low-Nam Lab, Purdue University) because Ste14 has been shown to tolerate various lipids and lipid mixtures. Though all showed minimal fluorescence, we observed a significant decrease in Ste14 activity compared to the normally used *E. coli* lipid mixtures. These lipid preparations from the Low-Nam Lab were older stocks than those normally used which could account for the lowered activity of Ste14. Retrying the experiment with newer stocks of these lipids would be useful. Since our *E. coli* lipids contain predominantly PE, we should also test pure PE extracts should be tested next for fluorescence and Ste14 activity.

The second issue is the degree of labeling of the Alexa Fluor™ 647 NHS ester. In the most recent labeling experiment, WT protein had the lowest degree of labeling at a ratio of about 2:1 (dye to protein). It is best for this ratio to be, at a maximum 1:1. If the ratio of dye is higher than protein, this could distort fluorescence readings and thus the binding curve outputs of MST. The NHS ester binds dye to lysine residues of Ste14. There are 17 lysine residues in Ste14 (including in the three engineered myc tags). Of those 17, 15 are solvent exposed (either on the cytosolic or endoplasmic reticulum lumen facing loops), increasing their likelihood of being labeled by the dye. To drive down the degree of labeling we can use a dye that links to residues other than lysine. Ste14 only has three native cysteine residues (99, 121, and 126). Our lab has engineered a cysteine-less Ste14 construct where all three cysteine residues are mutants to alanine (Triple A or TA). This TA variant retains WT-Ste14 activity. Within this cysteine-less construct, we have created an extensive library of single cysteine mutant Ste14 variants to aid many projects. We can use one of those mutants to perform labeling with a cysteine reacting dye. The mutant TA-S77C is a suitable candidate, as it retains WT-Ste14 and TA-Ste14 activity and the residue at position 77 seems to be accessible by other chemical agents such as NTCB cleavage (see section 2.1). This would allow only one residue for the dye to label and should produce at most a 1:1 dye to protein ratio.

Thirdly, Ste14 is known to form functional homodimers.[20, 28] This could present problems for substrate binding quantification through MST. MST binding values become inconclusive when there are more than one binding partner in equilibrium with the protein of interest - in this case homodimer of Ste14 or Ste14 bound to substrate. MST can however determine K_D values of dimerization (< μM) and has successfully determined K_D values for Grb2 dimerization.[31] However, if the majority of the protein in the sample is present as dimers, then the MST instrument most likely will not be able to determine a K_D value for dimerization.

Other areas of optimization for MST include utilizing the substrate-mimetic probes (Distefano Lab) as the fluorescent pair and using the blue light detector of the MST instrument. This approach would require removal of the fluorescent components of the purification buffer. Therefore, optimization of removing AEBSF and aprotinin removal from the elution buffer of purification would be the next logical step. Since the current MST conditions require 20 nM labeled Ste14 protein, it may be useful to perform an *in vitro* methyltransferase activity assay containing 20 nM WT-Ste14 protein and a concentration curve of AFC substrate. This assay will help to decrease the large concentration range of substrate in the current MST workflow which starts at 200 μM and ends at 6 nM AFC.

Methods other than MST have been explored including fluorescence polarization. The substrate-mimetic as the fluorescent partner produces flexibility of the PEG4 linker causing large variability in the fluorescent readings. The protein could be used as the fluorescent pair, but this raises inherent problems with the mass change when protein is bound to substrate as the substrate is too small. This mass change presents the same problem with isothermal titration calorimetry. Since KRas4B is a known substrate of Ste14, we could use the fully processed, yet unmethylated form as the substrate which would cause a significant mass shift when bound to Ste14.

In terms of substrate and cofactor binding, all residues that were found to be inactive with both AFC and AGGC in the studies performed by Dr. Amy L. Funk (2017) should be studied (see Chapter 3). This will help support their role in catalysis or structural properties of the enzyme. In addition to these residues, the residues that were found to have homology between the four species of Icmt most studied (see Chapter 1) but within in the 15-species alignment, should be studied.

2.6 Yeast growth arrest halo assay

2.6.1 Summary

In collaboration with the Distefano Lab (University of Minnesota) and the Trauner Lab (New York University), modified forms of **a**-factor peptide were tested for recognition and subsequent growth arrest in yeast *MAT*α cells. This section describes the optimization of such assays.

2.6.2 Background

The Trauner Lab is well versed in photoswitchable lipids that change conformation of lipid moieties upon UV irradiation and thus can alter lipid bioactivity, metabolism, and biophysical properties. In collaboration with the Distefano Lab, the first photoswitchable isoprenoids were developed with the goal of optically controlling peptide prenylation processing. More information on the scope of this project is in the Appendix.

The Hrycyna Lab set out to test the biological activity of these photoswitchable probes. This is possible by the engineering of the photoswitchable isoprenoid group onto an **a**-factor mimetic peptide. **a**-factor is a mating pheromone secreted by yeast (*Saccharomyces cerevisiae) MAT***a** haploid cells. It is recognized by their haploid counterpart *MAT*α cells. Upon **a**-factor recognition and binding by G-protein-coupled receptor (GPCR) Ste3 of *MAT*α cells, signaling cascades are initiated that terminate in cell fusion of the *MAT*α and *MAT***a** cells to reproduce.[32, 33] Part of this process is G_1 growth arrest of the mating cell.

The mating pathway of these haploid yeast cells is utilized in a mating assay to determine if synthetic **a**-factor mimetic peptides can be properly recognized by *MAT*α cells. Typical mating assays are also called halo assays, where *MAT*α and *MAT***a** cells are plated on top of each other in a specific area. Each haploid cell will secrete their respective mating pheromone (**a**-factor or α-factor) that in turn will be recognized by its counterpart cell). In the areas where both cells are plated, they will undergo reproduction. The mating pheromones can still diffuse through the cell lawn to areas where only one type of cell has been plated. Pheromone diffusion and subsequent recognition causes those cells to undergo cellular arrest, awaiting mating with the other cell type. However, since their counterpart is not present, these cells will die, thus producing a ring or "halo" of no cells.

To test **a**-factor mimetic peptides, the peptides can be directly spotted onto a lawn of *MAT*α cells. The cells will initiate the reproduction pathway and continue to cellular arrest. Because the haploid counterpart *MAT***a** cells were not spotted, a spot will appear on the agar where the *MAT*α cells are no longer present because they could not replicate. These assays will include serial dilutions of the **a**-factor mimetic spotted onto separate areas of the *MAT*α lawn. End-point growth activity can be reported as the lowest concentration of the **a**-factor mimetic that produces a clear area on the agar where cells are no longer present. As the **a**-factor dilutions get lower in concentration, they will become less or in-effective in producing full arrest of all the *MAT*α cells in the area of study. Thus, some *MAT*α cells will continue to grow in the area of study while some undergo cellular arrest.

2.6.3 Optimization

First, dispersal of the **a**-factor mimetic onto the *MAT*α lawn was adjusted. Previously, **a**-factor had been diluted in a yeast peptone dextrose (YPD) based mixture with methanol. Methanol should improve the solubility of the very hydrophobic **a**-factor peptide so that it does not stick to the walls of the glass, polystyrene or polypropylene tubes.[33] Unfortunately, the percent methanol in the YPD mixture was too high, and the spots seen on the agar were not due to cellular arrest, but due to the methanol negatively interacting with the *MAT*α cells. Too address this issue, BSA was then substituted for the methanol.[33] The BSA helped to produce a visible gradient of cellular arrest spots produced by a serial dilution of WT **a**-factor. The BSA overall seemed to improve uniform loading of the **a**-factor sampled onto the plate, producing well rounded spots whereas without the BSA, the spots were not as circular with more jagged edges. Thus, 0.5% BSA was used in the YPD mixture of **a**-factor for all future experiments. In addition to BSA, Triton X 100 was suggested to help form distinct cellular arrest spots.[33] The Triton is incorporated into the YPD plate agar at 0.04%. The presence of Triton increased the size of each spot to make it more pronounced, which would be useful when using very small concentrations of **a**-factor.

Photoswitchable **a**-factor required the use of a specific UV irradiation source engineered by the Trauner Lab (New York University) called the DISCO.[34, 35] It was designed so that each well of a 24-well plate would have its own light source to reduce variations in irradiation between samples. Whereas growth arrest and halo assays are performed on petri dishes, the use of a 24-

well plate would involve its own optimizations. When tested with and without Triton in the agar, the cellular arrest spots became too large and spanned the entire diameter of the well (no cells grew within the well after the treatment of **a**-factor). Therefore, Triton was not incorporated into the agar for future experiments. We also had to optimize the density of *MATα* cells and method of plating within each well. Based on suggestions from Dr. Isaac J. Fisher, assays in petri dishes are plated with $3x10^6$ cells.[36] After plating a variation of *MATα* cell densities and methods, the best lawn density was $25x10^3$ cells plated. The best plating method, also suggested by Dr. Fisher, was to add the cell suspension to a warm, YPD/BSA mixture containing 1% bacto-agar. When the cells were added atop the existing solidified agar of the 24-well plate, the *MATα*-agar mixture solidified, and the cells could grow.

Lastly, the **a**-factor concentration range for the serial dilutions and incubation times were decided. The concentrations chosen had to produce growth arrest spots with radii smaller than that of the plate well, so as it could be distinguished. The concentrations also had to be low enough to surpass the end point of cellular arrest as described above. The incubation time had to be conducive to cell lawn growth but not allow overgrowth of the cells to the point where they start to grow on top of a previously established growth arrest spot. The gradient of 3.0, 0.3, 0.03, 0.015, 0.0075, and 0.0038 ng **a**-factor analog were spotted onto a *MATα* lawn of cells and incubated for 24 hours at 30ºC (Figure 2.11).

2.6.4 Materials

1. *MATα* cells (SM2375[37])
2. Sterile YPD
3. Sterile YPD + 0.5% BSA
4. Bacto agar (Fisher Scientific, Waltham, MA)

2.6.5 Protocol

1. Prepare overnight cultures of *MATα* cells
    a. Place YPD plates (24-well) in incubator to dry O/N to dry (2 total)
2. Grow at 30ºC until saturating – O/N
3. Heat 500 mL beaker of water to 48 ºC with stir bar

4. Check OD_{600} of cells
5. Prep cells for agar plating (x2):
    a. Pellet $1x10^6$ cells (2000 x g for 2 min.)
    b. Rinse with ddH_2O (x2)
    c. Resuspend pellet in 1 mL ddH_2O
6. Prep agar for plating:
    a. Dissolve 33 mg of bacto agar into 3 mL of YPD media (~1.1% agar in solution)
    b. Heat in microwave until boiling
    c. Place in 45ºC water bath for ~15 minutes to equilibrate temperate of agar to 45ºC
    d. Add 1 mL of resuspended cell pellet to 3 mL of agar and plate cells immediately
7. Spread 100 µL of agar-cell mixture onto plate media (~25,000 cells)
    a. *Use P200, cut pipet tip, avoid bubbles
8. Let plate dry for 15 min.

***Perform the following steps without any light exposure, only using Red-light lamp*

9. Make 0.074mM WT **a**-factor dilution from 3.8 mM stock in YPD/0.5% BSA
10. Make the following WT **a**-factor serial dilutions on parafilm. -> under red light
    a. Split dilutions, and place 20 µL on separate piece of parafilm for hand-LED irradiation
    b. Irradiate all dilutions for 2-minutes with hand-LED (370 nm) at the same time (light 3.75 inches from sample)
    c. Spot 2.5 µL of irradiated or non-irradiated onto lawn on respective YPD plates
    d. WT **a**-factor dilution
        i. 7.4×10^{-4} mM: 2 µL of 0.074 mM stock + 198 µL YPD/BSA (3 ng)
        ii. 7.4×10^{-5} mM: 6.0 µL 7.4×10^{-4} mM stock + 54 µL YPD/BSA (0.3ng)
        iii. 7.4×10^{-6} mM: 12.0 µL 7.4×10^{-5} mM stock + 108.0 µL YPD/BSA (0.03ng)
        iv. 3.7×10^{-6} mM: 40.0 µL 7.4×10^{-6} mM stock + 40.0 µL YPD/BSA (0.015 ng)
        v. 1.85×10^{-6} mM: 40.0 µL 3.7×10^{-6} stock + 40.0 µL YPD/BSA (0.0075 ng)
        vi. 9.25×10^{-7} mM: 40.0 µL 1.85×10^{-6} mM stock + 40.0 µL YPD/BSA (0.0038 ng)
11. Make 0.074mM photoswitch **a**-factor dilution from 3.8 mM stock in YPD/0.5% BSA
12. Make the following photoswitch **a**-factor serial dilutions on parafilm. -> under red light (x2)
    a. Split dilution, and place 20 µL on separate parafilm for hand-LED irradiation

b. Irradiate all dilutions for 2-minutes with hand-LED (370 nm) at the same time (light 3.75 inches from sample)
c. Spot 2.5 µL of irradiated or non-irradiated onto lawn on respective YPD plates
d. Photoswitch **a**-factor
    i. 7.4 x 10^{-4} mM: 2 µL of 0.074 mM stock + 198 µL YPD/BSA (3 ng)
    ii. 7.4 x 10^{-5} mM: 6.0 µL 7.4 x 10^{-4} mM stock + 54 µL YPD/BSA (0.3ng)
    iii. 7.4 x 10^{-6} mM: 12.0 µL 7.4 x 10^{-5} mM stock + 108.0 µL YPD/BSA (0.03ng)
    iv. 3.7 x 10^{-6} mM: 40.0 µL 7.4 x 10^{-6} mM stock + 40.0 µL YPD/BSA (0.015 ng)
    v. 1.85 x 10^{-6} mM: 40.0 µL 3.7 x 10^{-6} stock + 40.0 µL YPD/BSA (0.0075 ng)
    vi. 9.25 x 10^{-7} mM: 40.0 µL 1.85 x 10^{-6} mM stock + 40.0 µL YPD/BSA (0.0038 ng)

13. Spot each sample in specific location on plate according to diagram below
    j. Spot 2.5 µL of ddH_2O, YPD & YPD/BSA
        a. Irradiate control samples for 2 min with hand-LED before plating on irradiated plate
14. Let plates dry for 15 min. in dark or under red light
15. Grow cells at 30 ºC for 24 hours and take images
    a. Dark plate: wrapped with aluminum foil
    b. UV plate: with DISCO
        i. Cut 1000 µL pipet tip to 750 µL mark on tip and plate in rubber gaskets to keep 24-well plate level and equidistant from light bulbs
        ii. Place open 24-well plate on top of pipet tips with open face, facing bulbs
            1. Place each well centered on own light bulb
        iii. Place foiled autoclave bin over DISCO apparatus + plate
        iv. Turn on DISCO

2.6.6 Conclusions and future work

Through our optimization efforts, we found that BSA/YPD mixture best helps to solubilize extremely hydrophobic **a**-factor analogs and produces smooth edged, circular spots of growth arrest. When spotting on 24-well plates, densities 24,000 cells should be plated in each well to produce robust yet not overpopulated lawns.

Testing of the photoswitchable **a**-factor analogs showed no significant differences in end-points compared to WT. Significant differences were not found between UV and non-UN irradiated samples. Our collaborative findings in conjunction with contributions by the Hrycyna Lab can be found in the Appendix.

2.7 Figures

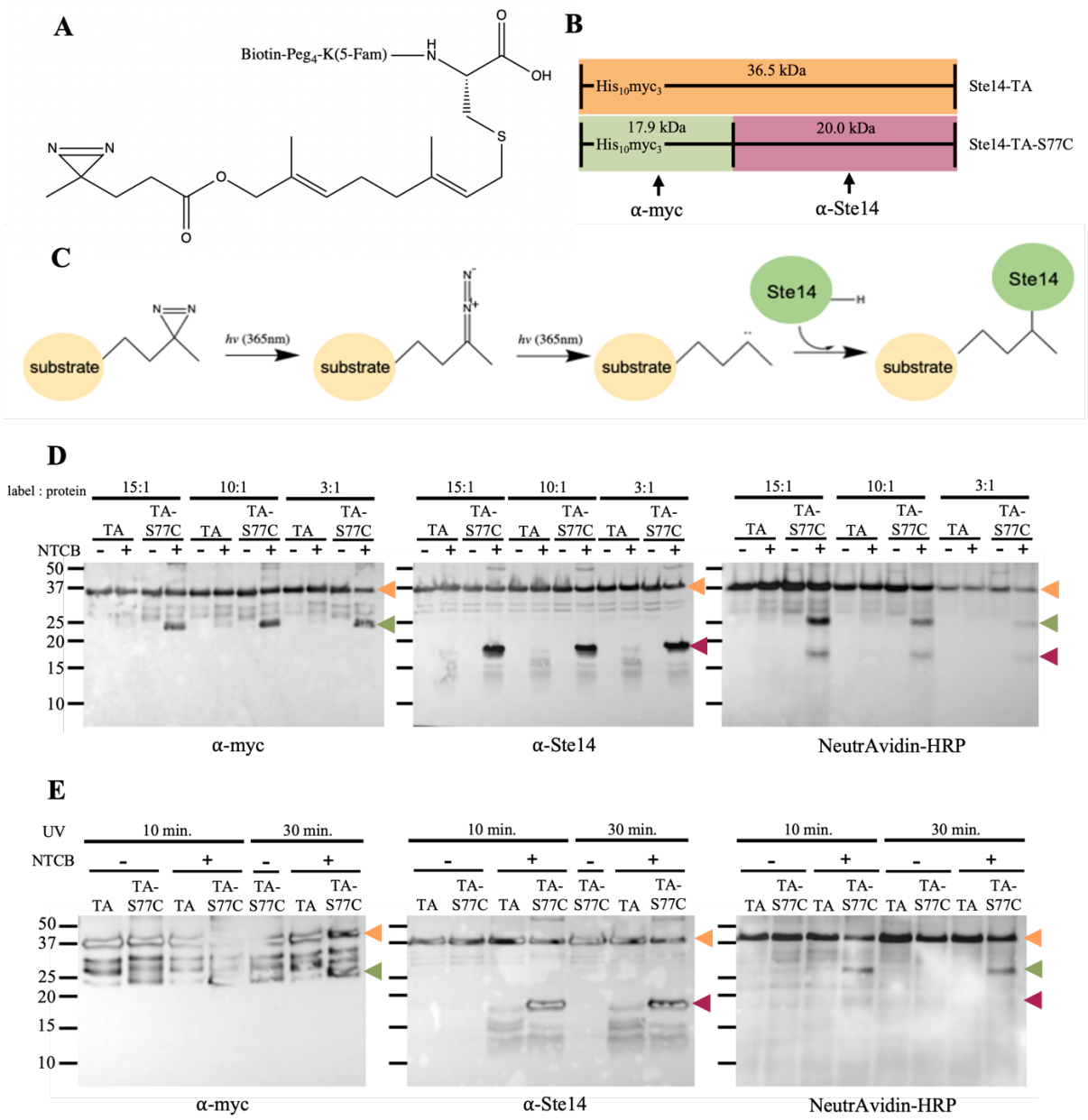

Figure 2.1 Optimization of photolabeling Ste14 with photoreactive substrate, AFC-FamDiaz.

For more detailed method information, see section 2.2. (A) Chemical structure of the photoreactive-substrate mimetic, Biotin-Peg4-K(5-Fam)C(Diazirine)-OH (AFC-FamDiaz) also known as AFC-FamDiaz (Distefano Lab, University of Minnesota). (B) NTCB cleavage patterns (with added mass of photolabel) of the TA-Ste14 construct and the single cysteine mutant, TA-S77C. Antibodies that recognize their respective fragments are listed below the cleavage diagram. (C) Reaction mechanism of photolabeling Ste14 with photoreactive substrate. Figure modified from Kumar, A.B., 2012.[38] (D) & (E) NTCB cleaved fragments were resolved on a 12% acrylamide gel in HEPES running buffer followed by immunoblotting with fragment respective antibodies. N-terminal fragments are recognized by α-myc and C-terminal fragments by α-Ste14. Photolabeled fragments are recognized by the NeutrAvidin-HRP antibody. Colored arrows represent fragments coded in (B). (D) Photolabel to Ste14 protein ratios and (E) UV irradiation times were tested to determine optimal conditions for photolabeling assays.

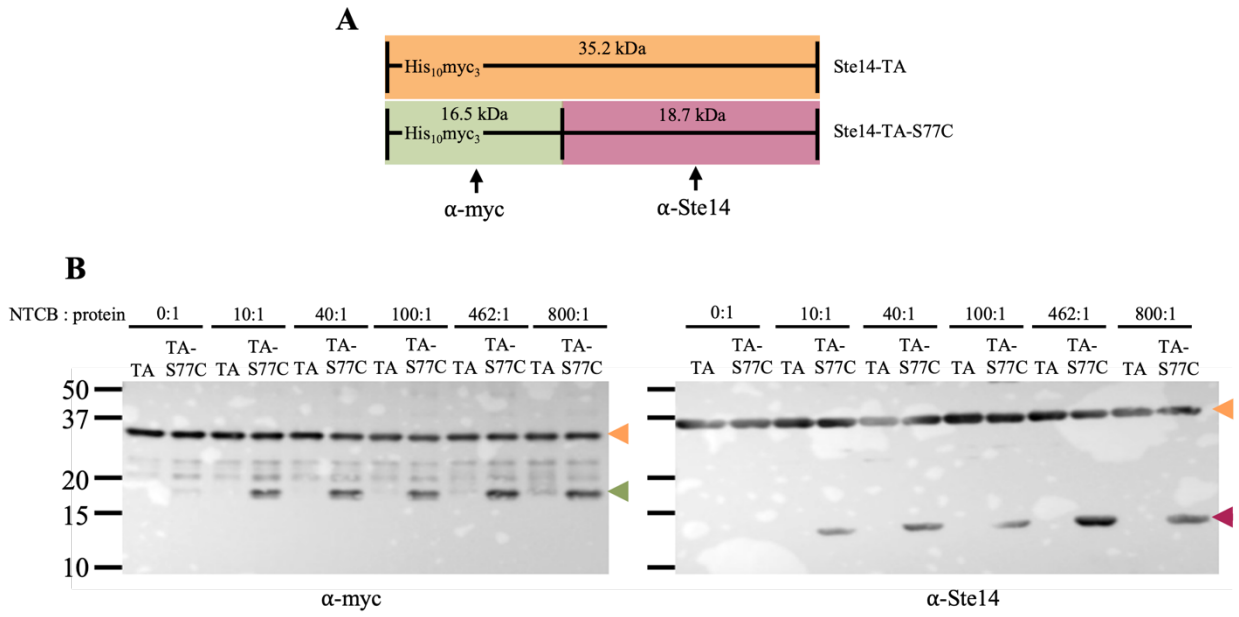

Figure 2.2 Optimization of NTCB cleavage of Ste14.

For more detailed method information, see section 2.2. (A) NTCB cleavage patterns of the TA-Ste14 construct and the single cysteine mutant, TA-S77C. Antibodies that recognize their respective fragments are listed below the cleavage diagram. (B) NTCB to protein ratios were tested to optimize conditions for NTCB cleavage assays. NTCB cleaved fragments were resolved on a 12% acrylamide gel in TGS running buffer followed by immunoblotting with fragment respective antibodies. N-terminal fragments are recognized by α-myc and C-terminal fragments by α-Ste14. Colored arrows represent fragments coded in (A).

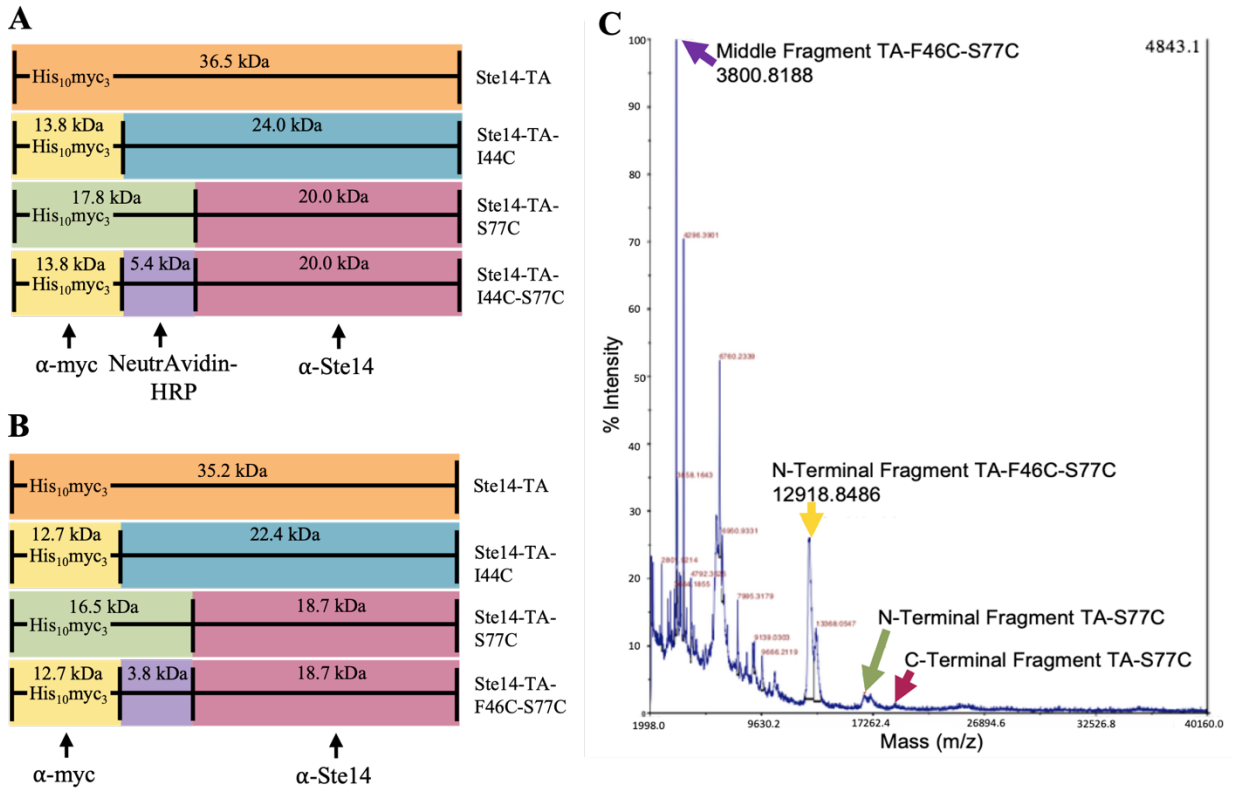

Figure 2.3 Detection of TM2 fragment by mass spectrometry.

For more detailed method information, see section 2.2. (A) NTCB cleavage pattern (with mass addition of probe) of the more active, double cysteine mutant, TA-I44C-S77C. Antibodies that recognize their respective fragments are listed below the cleavage diagram. (B) NTCB cleavage pattern (without mass addition of probe) of the less active, double cysteine mutant, TA-F46C-S77C. Antibodies that recognize their respective fragments are listed below the cleavage diagram. (C) MALDI-TOF/TOF spectra of TA-F46C-S77C when photolabeled and cleaved with NTCB. 7.5 µg of protein was spotted onto plate with sinapinic acid and the experiment was run in the Purdue Proteomics Facility at Purdue University.

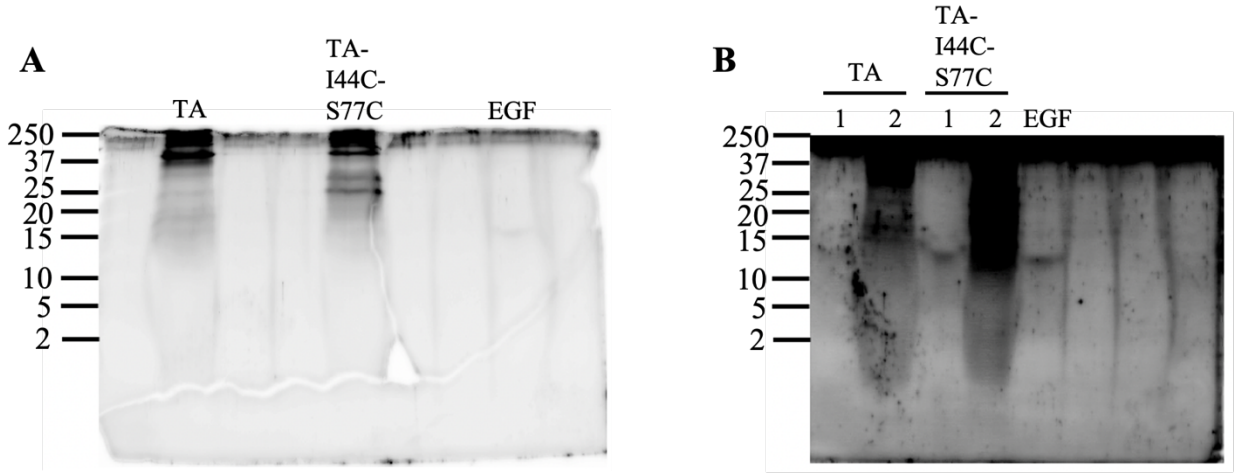

Figure 2.4 SDS-PAGE visualization of TM2 fragment.

For more detailed method information, see section 2.2. 20% acrylamide gels were run in a MOPS-Tris-SDS buffer with $NaHSO_3$ spiked in the cathode. Maximal volumes of each sample (~ 40 µL) were loaded into each well. Sypro™ Ruby staining was used to visualize the peptides via the Typhoon imager. Both TA and TA-I44C-S77C were subject to photolabeling and NTCB cleavage prior to concentration in the 10,000 molecular weight cut off concentrator. 100 ng of EGF was loaded in each gel as a small molecular weight control peptide. (A) Samples retained in the concentrator were run alongside EGF to confirm that the larger molecular weight (>10 kDa) fragments were sequestered from the flow through. (B) 1: samples that were in the flow through of the concentrator. 2: SDS-loading buffer was added to the inner parts of the concentrator to check if the hydrophobic TM2 peptide was stuck there.

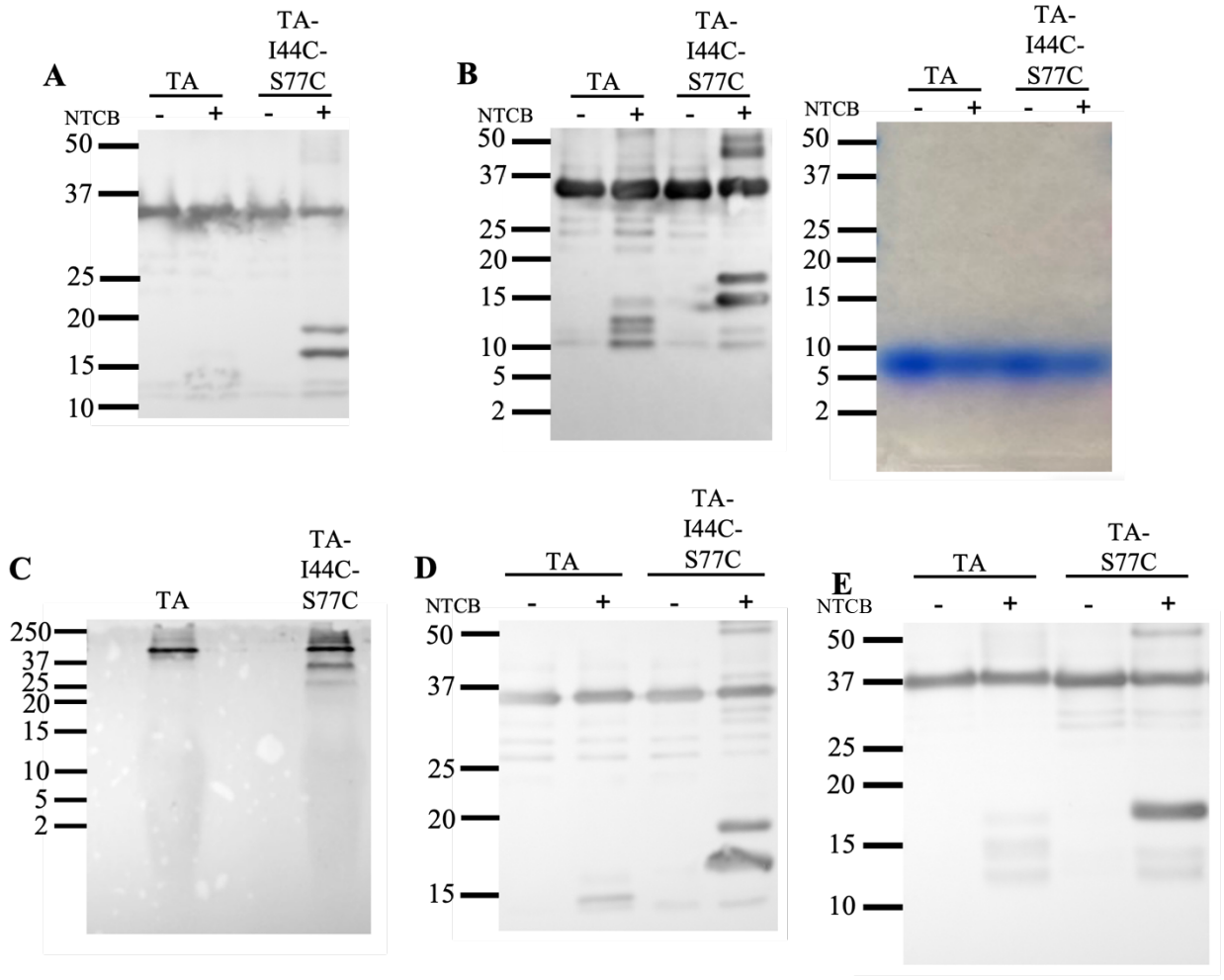

Figure 2.5 SDS-PAGE conditions suitable for specific reaction outcomes.

For more detailed method information, see section 2.2. All samples had been photolabeled prior to NTCB cleavage. (A) TruPAGE™ 4-20% precast acrylamide gel run in TEA-Tricine-SDS buffer. Western blotting was performed with α-Ste14 and α-rabbit antibodies. (B) TruPAGE™ 4-20% precast acrylamide gel run in MOPS-Tris-SDS buffer. The inner chamber contained sodium bisulfite. Left: western blot with α-Ste14 and α-rabbit antibodies. Right: photo of the dye front (blue) on the acrylamide gel before transfer. (C) 20% acrylamide gel run in MOPS-Tris-SDS buffer. The inner chamber contained sodium bisulfite. Western blotting was performed with NeutrAvidin-HRP antibodies. All samples were photolabeled, NTCB cleaved and concentrated. (D) 12% acrylamide gel run in TGS buffer. Western blotting was performed with α-Ste14 and α-rabbit antibodies. (E) 12% acrylamide gel run in HEPES buffer. Western blotting was performed with α-Ste14 and α-rabbit antibodies.

A

MHHHHHHHHHHGPGDPASRGEQKLISEEDLNGEQKLISEEDLNGE
QKLISEEDLNEDPLVLERP**MHQDFQEDEHEYPDIRR**NPLHEVTM
TSYILGILLGIFVGLFPQIRFK**NFNLFIIALSLFHFLEYYITAK**YNP
LK**VHSESFLLNNGK**SYMAAHSFAILECLVESFLFPDLKIFSYSLATK
L**CTVLGCLLVILGQYTRTIAMHTAGHSFSHIVK**TKKESDHVLVK
**TGVYSWSRHPSYLGFFWWAIGTQLLLLNPLSLVIFIFVLWKFFS
DR**IRVEEK**YLIEFFSAEYIEYKNKVGVGIPFI**

B

MHHHHHHHHHHGPGDPASRGEQKLISEEDLNGEQKLISEEDLNGE
QKLISEEDLNEDPLVLERP**MHQDFQEDEHEYPDIRRNPLHEVTM
TSY**ILGILL**GIFVGLFPQIRF**KNFNLFIIALSLFHFLEY**YITAKYNPL
KVHSESFLLNNGKSYMAAHSFAILECLVESFLFPDLKIFSYSLAT
KLCTVLGCL**LVILGQYTRTIAMHTAGHSF**SHIVKTKKESDHVLV
KTGVYSWSRHPSYLGF**FWWAIGTQLLLLNPLSLVIFIFVLWKFFSD
RIRVEEKYLIEFF**SAEYIEYKNKVGVGIPFI**

C

MHHHHHHHHHHGPGDPASRGEQKLISEEDLNGEQKLISEEDLNGE
QKLISEEDLNEDPLVLERP**MHQDFQEDEHEYPDIRRNPLHEVTM
TSYILGILLGIFVGLFPQIRF**K**NFNLFIIALSLFHFLEYYITAKYNP
LKVHSESFLLNNGKSYMAAHSFAILECLVESFLFPDLKIFSYSLA
TKLCTVLGCLLVILGQYTRTIAMHTAGHSFSHIVK**TKKESDHVL
VK**TGVYSWSRHPSYLGFFWWAIGTQLLLLNPLSLVIFIFVLWKF
FSDR**IRVEEK**YLIEFFSAEYIEYKNKVGVGIPFI**

Figure 2.6 Peptide identification of Ste14 through MS/MS analysis.

For more detailed method information, see section 2.3. Blue indicates stretches of identified residues through MS/MS while black indicates residues that were not identified. (A) Ste14 residues identified after trypsin/Lys-C digestion. (B) Ste14 residues identified after chymotrypsin digestion. (C) Combined Ste14 residues identified in (A) & (B)

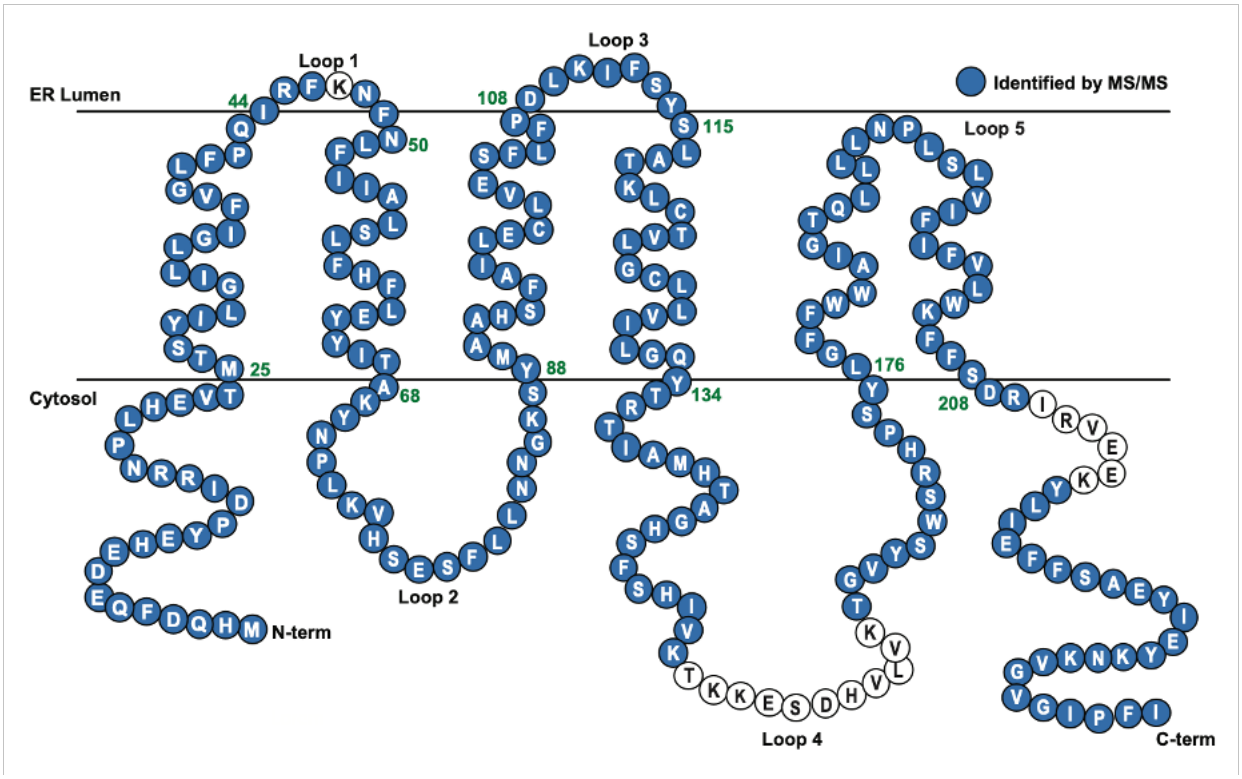

Figure 2.7 Ste14 topology map of residues identified through MS/MS analysis.

For more detailed method information, see section 2.3. Topology map representation of Ste14 residues identified after either trypsin/Lys-C digestion or chymotrypsin digestion.

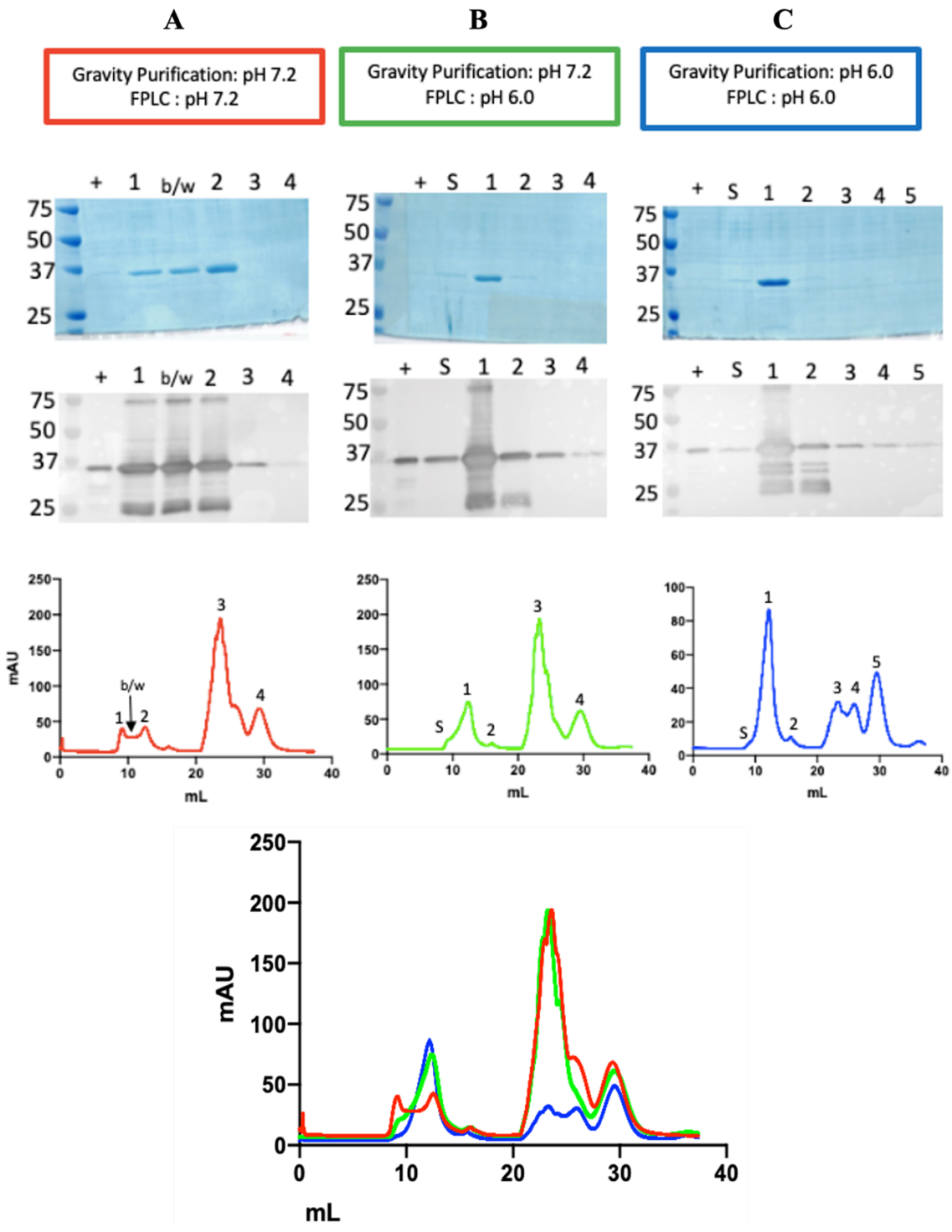

Figure 2.8 Combined gravity and SEC purification condition optimization.

For more detailed method information, see section 2.4. Three different reaction conditions were tested: (A) both gravity and SEC purification at pH 7.2 (red), (B) gravity purification at pH 7.2 followed by SEC purification at pH 6.0 (green), (C) both gravity and SEC purification at pH 6.0 (blue). All conditions include analysis by Coomassie staining (first row of gels), western blotting utilizing α-myc and α-mouse antibodies (second row of gels), FPLC chromatographs (first row of graphs). The final graph is an overall the individual chromatographs for each purification condition.

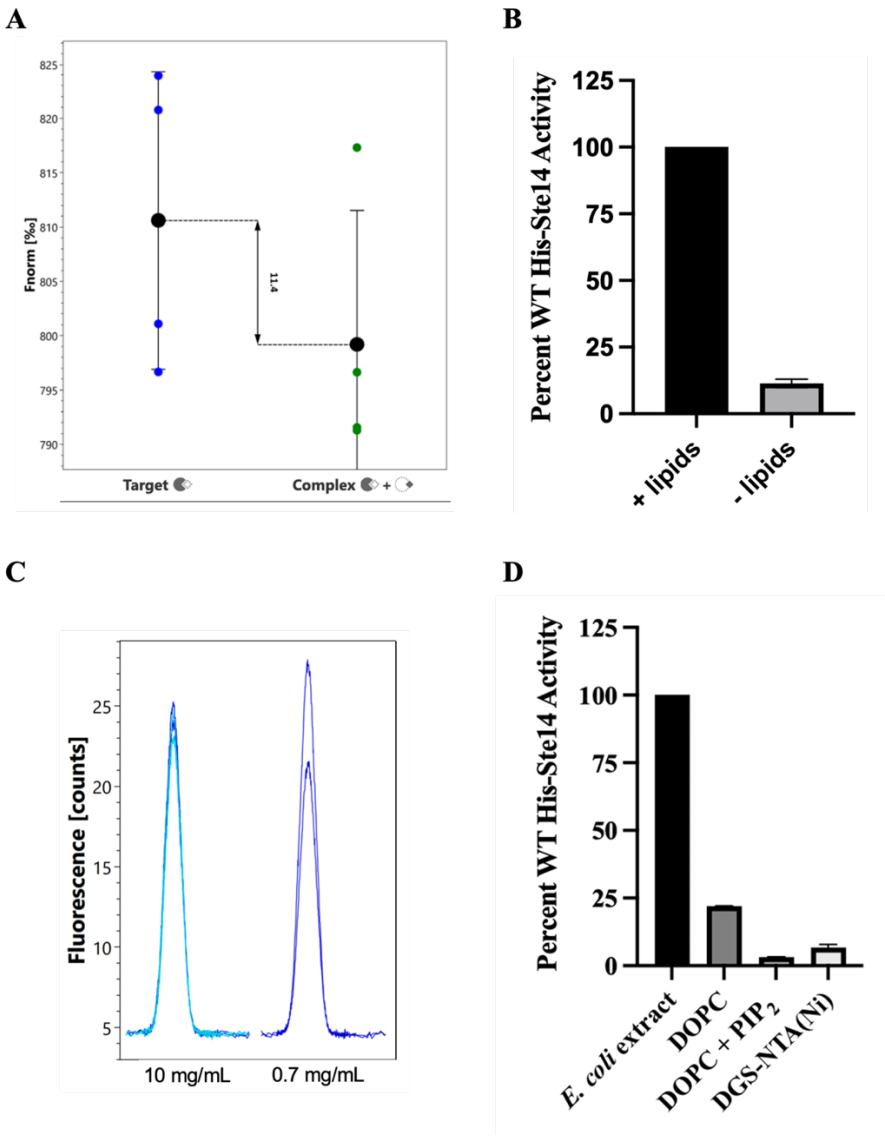

Figure 2.9 Requirement and subsequent problems of including lipids in MST analysis.

For more detailed method information, see section 2.5. (A) MST binding test of purified and fluorescently labeled WT-Ste14 with (complex) and without (target) 200 µM AFC substrate. (B) Methyltransferase activity assay of pure WT-Ste14 with and without 0.7 mg/mL *E. coli* lipid extracts. The activity is normalized to the WT-Ste14 protein in the presence of lipids. (C) Fluorescence levels of *E. coli* lipid extracts used in part (B) in the absence of Ste14 protein. (D) Methyltransferase activity assay of pure WT-Ste14 with *E. coli* lipid extracts, DOPC, DOPC and PIP_2 mixture, and DGS-NTA(Ni) lipids. The activity is normalized to the WT-Ste14 protein in the presence of *E. coli* lipid extracts.

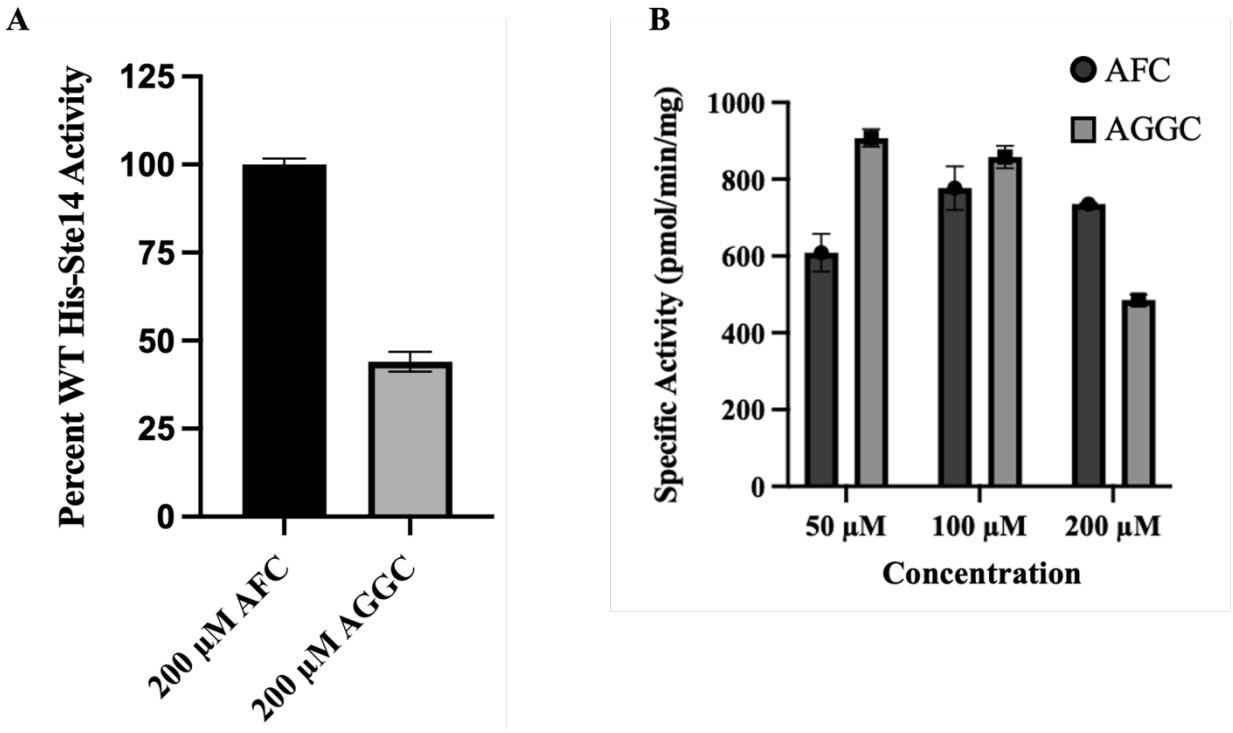

Figure 2.10 Determining working concentrations for AGGC substrate.

For more detailed method information, see section 2.5. Methyltransferase activity assays were performed with crude membrane preparations of WT-Ste14 and the data was normalized to WT-Ste14 with 200 µM AFC substrate. (A) Testing activity of Ste14 with 200 µM AGGC compared to 200 µM AFC. (B) Testing activity of Ste14 with 50, 100 or 200 µM AFC and AGGC.

A

	H_2O	YPD	YPD+ BSA			
a-factor(**Farn**)-OMe	3000	300	30	15	7.5	3.8
a-factor(**Azo**)-OMe	3000	300	30	15	7.5	3.8

B

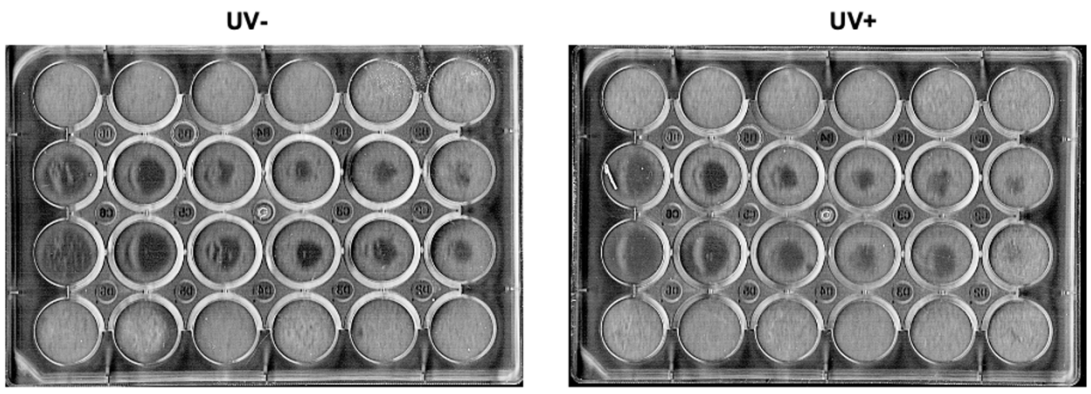

Figure 2.11 Growth arrest assays of *MATα* cells treated with WT or photoswitchable **a**-factor analogs.

For more detailed method information, see section 2.6. (A) Template indicating the amount and identity of compound spotted onto a lawn of *MATα* cells. Amounts are reported in pico grams (pg). Controls of H_2O, YPD and YPD+BSA solutions were also spotted to confirm no contamination. (B) 24-well plates containing YPD agar on top of which *MATα* cells were able to grow. Serial dilutions of each respective analog were spotted onto the lawn and cells were allowed to grow for 24 hours with or without UV exposure.

2.8 References

1. Diver, M. M.; Long, S. B., Mutational analysis of the integral membrane methyltransferase isoprenylcysteine carboxyl methyltransferase (ICMT) reveals potential substrate binding sites. *J Biol Chem* **2014,** *289* (38), 26007-20.

2. Diver, M. M.; Pedi, L.; Koide, A.; Koide, S.; Long, S. B., Atomic structure of the eukaryotic intramembrane RAS methyltransferase ICMT. *Nature* **2018,** *553* (7689), 526-529.

3. Romano, J. D.; Michaelis, S., Topological and mutational analysis of Saccharomyces cerevisiae Ste14p, founding member of the isoprenylcysteine carboxyl methyltransferase family. *Mol Biol Cell* **2001,** *12* (7), 1957-71.

4. Wright, L. P.; Court, H.; Mor, A.; Ahearn, I. M.; Casey, P. J.; Philips, M. R., Topology of mammalian isoprenylcysteine carboxyl methyltransferase determined in live cells with a fluorescent probe. *Mol Cell Biol* **2009,** *29* (7), 1826-33.

5. Funk, A. L. Biochemical Elucidation of the Isoprenoid Binding Site of the Yeast Isoprenylcysteine Carboxyl Methyltransferase, Ste14p. Purdue University, 2017.

6. Hahne, K. J., Characterization of the hydrophobic binding site of isoprenylcysteine carboxyl methyltransferase. **2012**.

7. Lu, H. S.; Gracy, R. W., Specific cleavage of glucosephosphate isomerases at cysteinyl residues using 2-nitro-5-thiocyanobenzoic acid: analyses of peptides eluted from polyacrylamide gels and localization of active site histidyl and lysyl residues. *Arch Biochem Biophys* **1981,** *212* (2), 347-59.

8. Tang, H.-Y.; Speicher, D. W., Identification of alternative products and optimization of 2-nitro-5-thiocyanatobenzoic acid cyanylation and cleavage at cysteine residues. *Analytical biochemistry* **2004,** *334* (1), 48-61.

9. Tang, H. Y.; Speicher, D. W., In vivo phosphorylation of human erythrocyte spectrin occurs in a sequential manner. *Biochemistry* **2004,** *43* (14), 4251-62.

10. Hou, Z.; Stapels, S. E.; Haska, C. L.; Matherly, L. H., Localization of a substrate binding domain of the human reduced folate carrier to transmembrane domain 11 by radioaffinity labeling and cysteine-substituted accessibility methods. *J Biol Chem* **2005,** *280* (43), 36206-13.

11. Anderson, J. L.; Frase, H.; Michaelis, S.; Hrycyna, C. A., Purification, Functional Reconstitution, and Characterization of the Saccharomyces cerevisiae Isoprenylcysteine Carboxylmethyltransferase Ste14p*♦. *Journal of Biological Chemistry* **2005,** *280* (8), 7336-7345.

12. Signor, L.; Erba, E. B., Matrix-assisted laser desorption/ionization time of flight (MALDI-TOF) mass spectrometric analysis of intact proteins larger than 100 kDa. *JoVE (Journal of Visualized Experiments)* **2013,** (79), e50635.

13. Liu, Z.; Schey, K. L., Optimization of a MALDI TOF-TOF mass spectrometer for intact protein analysis. *Journal of the American Society for Mass Spectrometry* **2005,** *16* (4), 482-490.

14. Singhal, N.; Kumar, M.; Kanaujia, P. K.; Virdi, J. S., MALDI-TOF mass spectrometry: an emerging technology for microbial identification and diagnosis. *Frontiers in Microbiology* **2015,** *6*.

15. Fukuyama, Y., MALDI matrix research for biopolymers. *Mass Spectrometry* **2015,** *4* (1), A0037-A0037.

16. Koch, R. J.; Barrette, A. M.; Stern, A. D.; Hu, B.; Bouhaddou, M.; Azeloglu, E. U.; Iyengar, R.; Birtwistle, M. R., Validating Antibodies for Quantitative Western Blot Measurements with Microwestern Array. *Scientific Reports* **2018,** *8* (1), 11329.

17. Nooij, F. J.; Van der Sluijs-Gelling, A. J.; Jol-Van der Zijde, C. M.; Van Tol, M. J.; Haas, H.; Radl, J., Immunoblotting techniques for the detection of low level homogeneous immunoglobulin components in serum. *J Immunol Methods* **1990,** *134* (2), 273-81.

18. Nagy, Z.; Comer, S.; Smolenski, A., Analysis of protein phosphorylation using Phos-Tag gels. *Current Protocols in Protein Science* **2018,** *93* (1), e64.

19. Alvarado, R.; Tran, D.; Ching, B.; Phinney, B. S., A comparative study of in-gel digestions using microwave and pressure-accelerated technologies. *Journal of biomolecular techniques: JBT* **2010,** *21* (3), 148.

20. Ratliff, A. C. STRUCTURAL ANALYSIS AND CONFORMATIONAL DYNAMICS OF THE YEAST ISOPRENYLCYSTEINE CARBOXYL METHYLTRANSFERASE, STE14. Purdue University Graduate School, 2019.

21. Zhang, Y.; Fonslow, B. R.; Shan, B.; Baek, M.-C.; Yates III, J. R., Protein analysis by shotgun/bottom-up proteomics. *Chemical reviews* **2013,** *113* (4), 2343-2394.

22. Wiśniewski, J. R.; Nagaraj, N.; Zougman, A.; Gnad, F.; Mann, M., Brain phosphoproteome obtained by a FASP-based method reveals plasma membrane protein topology. *Journal of proteome research* **2010,** *9* (6), 3280-3289.

23. Theisen, C. CHARACTERIZATION OF THE BINDING SITE OF STE24 DURING THE -AAXING CLEAVAGE. Purdue University Graduate School, 2021.

24. Bagag, A.; Jault, J.-M.; Sidahmed-Adrar, N.; Réfrégiers, M.; Giuliani, A.; Le Naour, F., Characterization of hydrophobic peptides in the presence of detergent by photoionization mass spectrometry. *PLoS One* **2013,** *8* (11), e79033.

25. Whitelegge, J.; Le Coutre, J.; Lee, J.; Engel, C.; Prive, G.; Faull, K.; Kaback, H., Toward the bilayer proteome, electrospray ionization-mass spectrometry of large, intact transmembrane proteins. *Proceedings of the National Academy of Sciences* **1999,** *96* (19), 10695-10698.

26. Green, N., Thermodynamics of the binding of biotin and some analogues by avidin. *Biochemical Journal* **1966,** *101* (3), 774-780.

27. Green, N., Avidin. 1. The use of [14C] biotin for kinetic studies and for assay. *Biochemical Journal* **1963,** *89* (3), 585.

28. Griggs, A. M.; Hahne, K.; Hrycyna, C. A., Functional oligomerization of the Saccharomyces cerevisiae isoprenylcysteine carboxyl methyltransferase, Ste14p. *Journal of Biological Chemistry* **2010,** *285* (18), 13380-13387.

29. Hrycyna, C. A.; Clarke, S., Farnesyl cysteine C-terminal methyltransferase activity is dependent upon the STE14 gene product in Saccharomyces cerevisiae. *Molecular and Cellular Biology* **1990,** *10* (10), 5071-5076.

30. Jerabek-Willemsen, M.; André, T.; Wanner, R.; Roth, H. M.; Duhr, S.; Baaske, P.; Breitsprecher, D., MicroScale Thermophoresis: Interaction analysis and beyond. *Journal of Molecular Structure* **2014,** *1077*, 101-113.

31. Seidel, S. A.; Dijkman, P. M.; Lea, W. A.; van den Bogaart, G.; Jerabek-Willemsen, M.; Lazic, A.; Joseph, J. S.; Srinivasan, P.; Baaske, P.; Simeonov, A., Microscale thermophoresis quantifies biomolecular interactions under previously challenging conditions. *Methods* **2013,** *59* (3), 301-315.

32. Xie, H.; Becker, J.; Gibbs, R.; Naider, F., Structure, biological activity and membrane partitioning of analogs of the isoprenylated a-factor mating peptide of Saccharomyces cerevisiae. *The Journal of Peptide Research* **2000,** *55* (5), 372-383.

33. Nijbroek, G. L.; Michaelis, S., Functional assays for analysis of yeast ste6 mutants. In *Methods in enzymology*, Elsevier: 1998; Vol. 292, pp 193-212.

34. Borowiak, M.; Nahaboo, W.; Reynders, M.; Nekolla, K.; Jalinot, P.; Hasserodt, J.; Rehberg, M.; Delattre, M.; Zahler, S.; Vollmar, A., Photoswitchable inhibitors of microtubule dynamics optically control mitosis and cell death. *Cell* **2015,** *162* (2), 403-411.

35. Morstein, J.; Trauner, D., Photopharmacological control of lipid function. In *Methods in Enzymology*, Elsevier: 2020; Vol. 638, pp 219-232.

36. Fisher, I. J. Understanding Molecular Mechanisms of G-protein subunit βγ Activation of Downstream Effectors. University of Rochester, 2020.

37. Huyer, G.; Kistler, A.; Nouvet, F. J.; George, C. M.; Boyle, M. L.; Michaelis, S., Saccharomyces cerevisiae a-factor mutants reveal residues critical for processing, activity, and export. *Eukaryotic Cell* **2006,** *5* (9), 1560-1570.

38. Kumar, A. B., Design, synthesis and evaluation of novel diazirine photolabels with improved ambient light stability and fluorous-based enrichment capacity. **2012**.

CHAPTER 3. ELUCIDATION OF THE PRENYLATED CAAX PROTEIN BINDING SITE IN THE ICMT FROM S. CEREVISIAE, STE14

3.1 Note

This manuscript/chapter includes contributions from Amy L. Funk, Kalub J. Hahne, Jeffrey S. Vervacke, Mark D. Distefano and Christine A. Hrycyna. It is in preparation to be submitted for publishing.

The author of this dissertation, Ariana L. Cardillo, contributed to every section of this chapter with contributions in the following sections: Amy L. Funk contributed to the abstract, results, experimental procedures, and discussion sections and Jeffrey S. Vervacke contributed to the experimental procedures and supplemental data (Figure 3.S.6) related to the synthesis and chemical characterization of the substrate-mimetic probes. Jeffrey S. Vervacke synthesized the benzophenone and diazirine-based substrate analogs used in this study. Kalub J. Hahne performed the mutagenesis of the Ste14 alanine mutants and TA-S77C. Amy L. Funk performed the *in vitro* methyltransferase activity studies with the AFC and AGGC substrates on the alanine mutants (Figures 3.1C, 3.2, & 3.S.2). Amy L. Funk also performed the experiments comparing the benzophenone-based probes (Figure 3.S.5 C & D). The author of this dissertation, Ariana L. Cardillo, cloned the TA-I44C and TA-I44C-S77C mutants and performed the subsequent expression, activity, and trypsin digestion studies on all mutants (Figures 3.4A, 3.S.3 & 3.S.4). She also performed the NTCB and AFC-FamDiaz studies (Figures 3.3 & 3.4). In addition, she designed all figures (except Figure 3.S.2 & 6) by using GraphPad Prism, Adobe Illustrator, ChemDraw, and PyMOL and performed all statistical analyses on activity data.

3.2 Abstract

Isoprenylcysteine carboxyl methyltransferase (Icmt) is an integral membrane protein that performs the only reversible step of three primary C-terminal post-translational modifications (PTM) on the CAAX family of proteins which includes many Ras superfamily proteins. The modifications add significant hydrophobicity to the C-terminus of the protein that aids in their proper localization to lipid membranes for cell signaling and protein trafficking. Further,

methylation may serve as a point of regulation. Ras proteins are implicated in many diseases but are difficult to target directly due to the lack of suitable binding pockets on the protein's surface. Recently, research has shifted to targeting the PTM enzymes, especially methylation through Icmt due to its specificity as the sole methyltransferase that acts on these proteins. Using biochemical tools, we aim to understand in mechanistic detail how the yeast Icmt, Ste14, mediates catalysis at the membrane/cytosol interface, accommodating both the hydrophilic cofactor, *S*-adenosyl-L-methionine (SAM), and a lipophilic isoprenylated substrate, with the ultimate goal of designing better substrate-mimetic inhibitors. Through alanine-scanning mutagenesis of conserved residues and substrate specificity assays with two known substrates of Ste14 containing different isoprenoid groups, we identified several residues in the N-terminal region of Ste14, notably Leu56, that appear to significantly decrease recognition of *N*-acetyl-*S*-farnesyl-L-cysteine (AFC) while retaining that of *N*-acetyl-*S*-geranylgeranyl-L-cysteine (AGGC). These results suggested that these residues may comprise part of the substrate binding site of Icmt. Based on the crystal structure of a eukaryotic Icmt and subsequent activity studies of Ste14 and other eukaryotic Icmt homologs, the SAM binding site has been localized to the C-terminus with a hydrophobic cavity suitable for the lipidated substrate within the N-terminus. Complementary to this, our data suggested the TM2 region of Ste14 specifically, contributes most prominently to the isoprenylated substrate binding site of Icmt. To test this hypothesis, we used photoreactive substrate analogs based on AFC, the cysteine-specific cleavage reagent 2-nitro-5-thiocyanobenzoic acid (NTCB), and a library of purified Ste14 cysteine mutants. We determined that the majority of labeling occurs between amino acids 44-77 of Ste14.

3.3 Introduction

Cancer is the second leading cause of death in the United States with 1.9 million new diagnoses projected for 2022 (ACS – Cancer Facts & Figures, 2022). *RAS* genes are the most frequently mutated gene family that contribute to cancer resulting in their extensive study for the direct regulation of Ras proteins.[1] These small GTPases are docked to the plasma membrane and regulate the relay of extracellular, mitogenic signals to downstream signal propagation, cell growth and differentiation. After years of unsuccessfully targeting Ras proteins and garnering the term "undruggable", the first direct inhibitor of G12C mutated KRas4B, sotorasib, was fast tracked for approval by the FDA this past year.[2-4] Up to this point the approach to inhibiting Ras activity in

cancer cells was through indirect inhibition via the well characterized downstream effector signaling pathways or perturbation of Ras association to the plasma membrane.[2, 4] With many unsuccessful attempts, researchers have pivoted to targeting the post-translational modifications (PTMs) of Ras proteins, which are necessary for the proper cellular trafficking to the plasma membrane and downstream signaling of these proteins.

All isoforms of Ras protein are classified as CAAX proteins, where their most C-terminal residues consist of a cysteine ("C"), two aliphatic residues ("AA") and one of several residues ("X"). CAAX proteins must undergo three sequential post-translational modifications for proper functioning and cellular translocation: first, isoprenylation of the terminal cysteine residue by either farnesyltransferase (FTase) or geranylgeranyltransferase (GGTase) depending on the identity of the X residue, followed by proteolysis of the -AAX residues by Ras converting enzyme 1 (Rce1), and terminated with methylation of the free carboxylate on the isoprenylated cysteine by isoprenylcysteine carboxyl methyltransferase (Icmt). Although prenylation and proteolysis have been studied as indirect targets for oncogenic signaling pathways, small molecules targeting these enzymes have not been suitable enough to advance to clinical trials or have failed once tested on humans due to their low solubility and cell permeability.[5-9]

Icmt is the founding and sole member of a unique class of integral membrane methyltransferases. Compared to the other proteins targeting in the Ras signaling pathway, its uniqueness and singular role produces an ideal candidate for specific drug targeting.[10, 11] Interestingly of these three modifications, methylation is the only reversible process, indicating a possible point of regulation for these proteins.[12-14] Although only a small modification, loss of methylation has been shown to significantly decrease KRas4B localization to the plasma membrane and concomitantly reduce downstream Ras signaling.[15-19] To develop the most potent inhibitors of Icmt it is important to understand how Icmt binds its substrate and cofactor. Icmt accommodates both a diverse set of protein substrates containing larger hydrophobic isoprenoid groups with charged carboxylate ions, and the amphipathic methyl donor *S*-adenosyl-L-Methionine (SAM). SAM is a well characterized cofactor that serves as the methyl donor for many SAM-dependent methyltransferases and is the second-most utilized cellular cofactor, after ATP.[20, 21] Although Icmt is best characterized for the residues that interact with SAM within a specific SAM-binding domain of the enzyme, SAM-mimetic inhibitors of Icmt may have off targets in the many methyltransferases the cofactor serves. This could include off target effects in processes

such as epigenetic regulation, cellular signaling, and metabolite degradation.[22] More recent inhibitors of SAM-dependent methyltransferases have found success in outcompeting the substrate while relying on bound SAM to either allosterically stabilize the substrate binding site or aid in direct SAM-inhibitor interactions.[23] To develop potent, substrate competing inhibitors for Icmt, elucidation of the residues involved in the mechanism of the enzyme is of great importance.

The two solved 3D structures of Icmt give some insights into substrate binding, but leave much of the mechanistic detail to be inferred. The first structure, *Methanosarcina acetivorans* methyltransferase (*Ma*-MTase) was originally classified as a prokaryotic Icmt due to its co-crystallization with SAM and its identity as integral membrane protein.[13] However, it has no known biological substrates since there are no known prenylated proteins in prokaryotes and also shows little sequence homology with the eukaryotic homologs of Icmt.[14] Its 14% homology with other eukaryotic Icmts is retained within the SAM-binding domains, but provides little information about the isoprenylated substrate binding sites, which would be most useful for current Icmt inhibitor design.[13, 14] A more recent structure of a eukaryotic Icmt from *Tribolium castaneum* (*Tc*-Icmt) provides more structural insights on isoprenylated substrate interactions with Icmt, however the geranylgeranylated substrate present during crystallization could not be confirmed as the density present within the proposed substrate binding cavity.[14]

Comprehensive mutational analyses of the activities of specific residues of Icmt have been performed on multiple species of Icmt including *Anopheles gambiae* (*Ag*-Icmt) and *Saccharomyces cerevisiae (Sc*-Icmt or Ste14).[24-26] Although useful in understanding which residues reduce enzyme activity when mutated, these mutational activity studies do not determine if these changes in activity are due to changes in protein structure and/or stability, substrate binding and/or orientation, or alterations to the enzyme's catalytic mechanism. They also do not comprehensively study which residues allow for the incorporation of the differing isoprenoid groups of the substrate, whether farnesylated or geranylgeranylated.

To better understand which residues of Icmt help the enzyme to accommodate the bulkier geranylgeranyl isoprenoid group versus the smaller farnesyl group of a substrate, we employed an extensive alanine-scanning mutagenesis study of the conserved residues and tested their activities with minimal substrates containing either isoprenoid group. We found that although the conserved residues remain mostly in C-terminal half of the protein (Figure 3.1A), the residues that showed variation in activity between farnesylated and geranylgeranylated substrates were in the N-terminal

half. Specifically, residue Leu56 showed the most dramatic preference for the geranylgeranylated substrate over the farnesylated form. This allowed us to better characterize substrate interactions of transmembrane helix 2 (TM2) of Ste14, of which Leu56 resides. Based on previous success of our lab with determining substrate features required for binding and enzymatic activity utilizing photoreactive substrate analogs,[27] we employed a newly designed photoreactive substrate that will help characterize the region(s) of Icmt involved in substrate binding, with Ste14 as our Icmt model. This method confirmed that TM2 is the predominant region of Ste14 involved in isoprenylated substrate binding.

3.4 Results

3.4.1 Alanine-scanning mutagenesis reveals catalytic important conserved residues of Ste14

Previously, a sequence alignment of fifteen unique eukaryotic Icmt protein sequences was performed to identify conserved residues that may be important for structure and function. The alignment revealed 42 identical and 35 similar residues.[28] Considering the extensive research done on four specific species of Icmt *Hs*-, *Tc*-, *Ag*-, and *Sc*-, Clustal Omega was used to determine the similarity between their sequences. Depicted on the predicted topology map of Ste14, 60 similar (red) and 66 identical residues (blue) were identified (Figure 3.1A & Figure 3.S.1). Additionally several previously determined Ste14 loss-of-function mutants (G13E, L81F, G132R, P173L, E213D, E213Q, E214D and L217S) aligned with the conserved residues further validating their importance for catalytic activity.[25] As a result, characterization of conserved residues was completed by performing alanine-scanning mutagenesis. A Ste14 construct containing 10 histidine residues followed by three myc tags engineered at the N-terminus of the protein sequence ($His_{10}myc_3$N-Ste14 or His-Ste14), was used as a template to prepare these mutants. The 76 conserved residues from the 15 species alignment performed by Court *et al.* were mutated to alanine and the native alanine residues were mutated to glycine using site-directed mutagenesis. Residue Asn191 was not mutated as this residue has been previously shown to be critical for the hairpin turn between TM regions 5 and 6. Romano *et al.* showed that upon Asn191 mutation to leucine, a non-turn-inducing residue, the C-terminal tail translocated from the cytosol to the ER lumen.[25]

Wild-type (WT) His-Ste14 and mutants were overexpressed in a Δ*STE14* yeast strain (SM1188). Crude membranes of each were isolated as established by Anderson *et al.*[29] Expression of each mutant was analyzed by immunoblot analysis using an α-Ste14 polyclonal antibody that recognizes the last 42 amino acids of the protein.[30] Expression patterns of all mutants were similar to WT His-Ste14 (data not shown). Each mutant was then tested with two well-characterized minimal substrates, AFC and AGGC. With various published mutagenesis studies already completed using Ste14 and other orthologs, we decided to use those two molecules to differentiate between residues involved primarily with lipophilic substrate binding versus cofactor binding. The structures of these compounds only differ in the isoprenoid moiety, where AFC contains a 15-carbon farnesyl group and AGGC has a 20-carbon geranylgeranyl group (Figure 3.1B). Previous research has shown that Icmts including WT His-Ste14 do not exhibit a preference for AFC or AGGC as a substrate[31, 32] and these data were corroborated by our data as well (Figure 3.1C). Thus, we performed an *in vitro* methyltransferase activity assay with crude membranes of each alanine or glycine mutant (5 μg), AFC or AGGC (200 μM) and [^{14}C]-SAM (20 μM) as the methyl donor, using WT His-Ste14 as a positive control. Not surprisingly, the results showed that mutations within Loop 4 and the C-terminal tail of the protein produced enzymes that were inactive with both substrates. Past work revealed two highly conserved SAM binding motifs, M1 (RHPxY) and M2 (R[x]$_3$EE), to be located in this area.[25] Methyltransferase assay results of the residues spanning these areas (Arg136 – Pro237) revealed 27 mutants with >10% WT activity with AFC while 14 of these mutants were completely inactive and speculated to be involved in SAM binding. To analyze the prenylated substrate binding characteristics of the 76 conserved residues, we constructed a topology map of Ste14 color coded for the ratio of AGGC to AFC activities (0.01-2.20, 2.21-4.20, 4.21-6.20, > 6.21) to highlight residues that had a significant fold change in substrate specificity of the alanine mutants (Figure 3.2A). Mutants that revealed activities <15% of WT Ste14 with both AFC and AGGC substrates were classified as inactive. Interestingly, N-terminal His-Ste14 mutants showed a preference for one substrate over the other, unlike the WT enzyme. Mutations in the N-terminal and TM1 regions (V23A, M25A, S27A, I29A and L30A) all resulted in preference for the longer substrate, AGGC, as shown by an increase of at least more than 10% WT activity. The most notable variation of substrate specificity from WT was with the His-Ste14 mutant L56A in TM2. The L56A variant was almost completely devoid of activity with AFC (14% WT) while retaining activity with the AGGC substrate (130% WT) (Figure 3.2B). In addition to

the hydrophobic amino acids in the predicted TM domains, Loop 2 cytosolic mutants (N71A, V75A, E78A and S79A) showed noteworthy alterations from WT specificity (Figure 3.2A). Furthermore, a few His-Ste14 mutants located in the projected cytosol-membrane interface manifested a preference for AGGC (Y88A, A91G, G177A and I183A) (Figure 3.2A). Finally, we observed several loss-of-function N-terminal mutants (<5% WT activity with AFC) that included G31A, H60A, E63A, Y64A, F80A, L81A, L82A.

3.4.2 Mutational analysis reveals importance of Leu56 for substrate recognition by Ste14

To further characterize the results obtained with the L56A mutant, we mutated this amino acid to alternative lipophilic residues. Isoleucine was used to mimic the leucine side chain while phenylalanine was employed to introduce a hydrophobic, but also aromatic group. These mutants were tested using the *in vitro* methyltransferase activity assay with both AFC and AGGC (Figure 3.2C). L56F and L56I regained specific activity with the AFC substrate with 77% and 66% WT, respectively. Also, both mutants were active (>100% WT) with AGGC. Additionally, double mutants with L56A, N71A and V75A were constructed to see if L56A further reduced an already lowered AFC preference. Not surprisingly, the presence of L56A within mutants L56A-N71A and L56A-V75A abrogated AFC activity (1% WT for both) (Figure 3.2D). Their activity with AGGC was slightly reduced compared to their single mutant counterparts. The His-Ste14 double alanine mutant N71A-V75A was inactive with both AFC and AGGC (Figure 3.2D).

3.4.3 Purified and functional single cysteine-substituted His-Ste14 mutants

Next, single cysteine mutants were created using the cysteine-less His-Ste14 template where the three native cysteine residues were mutated to alanine (His-Ste14-Triple Alanine or TA). Mutant proteins TA-S77C, TA-I44C, and double mutant TA-I44C-S77C were overexpressed in a Δ*STE14* strain and crude membranes were isolated.[29] Activity and expression of the crude membranes of each mutant were assayed using an *in vitro* methyltransferase activity assay and immunoblot analysis with the α-myc monoclonal antibody. All mutants were active (>75% WT activity with AFC) and had expression levels comparable to WT (Figure 3.4A & Figure 3.S.3). Additionally, we analyzed any substantial tertiary structural changes of the His-Ste14-TA single cysteine mutants by performing limited protease sensitivity assays with trypsin (Figure 3.S.4).

Crude membranes of WT-, TA- and each cysteine mutant Ste14 variant were incubated with or without trypsin and subjected to immunoblot analysis probing with an α-myc antibody. From these data, all mutants showed comparable digestion patterns to WT in the presence of trypsin suggesting that no significant structural changes occurred due to these mutations. The cysteine mutants were subsequently purified using metal affinity resin as described previously by Anderson and Frase *et al.*(2005). Purity and expression levels of the pure protein for each mutant was analyzed by Coomassie stained SDS-PAGE and immunoblot with the α-myc antibody, respectively (Figure 3.S.3). All the cysteine mutant proteins were expressed at levels similar to WT His-Ste14 and the cysteine-less mutant (TA). Additionally, the activity of each purified mutant was tested using an *in vitro* methyltransferase activity assay with pure protein (~0.3 μg), AFC (200 μM) and reconstitution into lipid vesicles before incubation with [^{14}C]-SAM (20 μM). All mutants maintained WT activity and were used for the following photolabeling and NTCB cleavage assays (data not shown).

3.4.4 NTCB cleavage narrows labeled peptide fragment between N-terminal residues 44-77 of Ste14

Based on results from the AFC and AGGC preference studies, our next goal was to narrow down the region of Ste14 that the substrate has directly contacts. We developed a workflow to help identify regions of Ste14 that a photoreactive substrate analog has contact with. Substrate-mimetic photoreactive analogs were developed that would covalently bind to Ste14 upon UV irradiation. Our single-cysteine residues, cloned within the cysteine-less construct of Ste14, were used to separate the N- and C-terminal portions of Ste14 using a cysteine specific chemical cleavage reagent NTCB. NTCB causes the spontaneous hydrolysis of an amide bond through the cyclization of a cysteine side chain when exposed to basic conditions.[34, 35] As a result, the photoreactive analogs in combination with NTCB could be used to label and cleave the protein at specified locations on the N-terminal half to narrow the residues involved in the substrate binding site of Ste14. This would leave either the N- or C-terminal fragments of Ste14 bound to and detectable by the engineered moieties of the photoreactive substrate.

Localizing our points of interest to the N-terminal half of Ste14, we sought out a hydrophilically exposed residue just downstream of TM2 that would be amenable to chemical cleavage and was not implicated in the activity or structure of Ste14. TA-S77C retained WT and

TA His-Ste14 activity, had expression levels consistent with the two controls, and maintained cleavage patterns of WT His-Ste14 upon trypsin digestion (Figure 3.4A & Figures 3.S.3-4). The purified single cysteine mutant, using TA His-Ste14 as a control, was photolabeled with a newly designed substrate analog AFC-FamDiaz. This photoreactive substrate contains biotin, diazirine, and fluorescein moieties (Figure 3.3A). Previous research from our laboratory showed that the diazirine moiety was more effective at labeling and a better substrate presumably due to the linear diazirine structure better mimicking the native farnesyl group compared to the previously used benzophenone-based substrate probes.[36] This substrate analog labeled His-Ste14 efficiently and was confirmed to be a substrate (Figure 3.3B). TA and TA77C were treated with AFC-FamDiaz and irradiated with UV light on ice to form a covalent bond between the substrate and the enzyme. Following irradiation, the enzyme-substrate complex was subjected to cleavage with NTCB for 4 hours at 37ºC resulting in peptide fragments with predicted molecular weights due to the placement of the single cysteine residues. The expected peptide fragments for the TA and TA-S77C mutants are shown in Figure 3.3C. Samples were fractionated using a 12% SDS-PAGE and immunoblot analysis with termini specific antibodies - α-myc recognizes the three N-terminal myc tags and the α-Ste14 antibody recognized the C-terminal 42 residues of the protein. NeutrAvidin-HRP was used to detect the substrate biotin tag or the labeled peptide fragment (Figure 3.3C). As expected, the molecular weight of each of the cleaved peptides on the α-myc and α-Ste14 probed blots corresponding to the calculated fragment sizes seen in Figure 3.4C. His-Ste14-TA showed no cleavage bands which was expected due to the lack of cysteine residues present. Interestingly, these results showed that AFC-FamDiaz bound to the N-terminal peptide fragments of the TA-S77C mutant as seen in the alignment of cleaved peptides on the α-myc and NeutrAvidin-HRP blots (Figure 3.3D). Together, these data suggest that diazirine moiety is labeling specifically the N-terminal 77 amino acids of His-Ste14.

Our next goal was to further narrow down the transmembrane region of Ste14 that may have contact with the photoreactive substrate. A single cysteine mutant, TA-I44C, was designed in the predicted Loop 1 region of His-Ste14 to be used for the photolabeling and chemical cleavage assay. The TA-I44C mutant was also evaluated for significant structural alterations using the trypsin digestion assay noted above; its specific activity, expression level and purity were similar to the previous mutants (Figure 3.4A and Figures 3.S.2-4). As observed with the C-terminal cysteine mutants, the results with photolabeling and NTCB cleavage of TA-I44C revealed that the peptide

fragments on the α-Ste14 and NeutrAvidin-HRP blots aligned (Figure 3.4B & C). This result suggested that the substrate analog labeled Ste14 C-terminally to residue 44.

As a result, we cloned the double mutant TA-I44C-S77C, with the two cysteine mutants flanking TM2 of Ste14. This mutant retained WT expression and activity levels and did not show any significant structural alterations using trypsin digestion (Figure 3.4A and Figures 3.S.3-4). Upon photolabeling and subsequent NTCB cleavage of the double-mutant, peptide fragments matched those of the single mutants suggesting that the substrate analog labeled Ste14 within its N-terminus, specifically between residues 44-77 (Figure 3.4B & C). However, multiple fragments were visible, insinuating missed cleavages of the NTCB cleavage reagent.

We then sought to further test if different portions of substrate have contact with different areas of Ste14. We utilized two previously characterized photoreactive substrates of Ste14 with their photoreactive benzophenone groups located in either the amide or farnesyl portion of the protein (Figure 3.S.5 A).[33] TA-S77C underwent photolabeling and NTCB cleavage with both analogs and revealed identical substrate labeling N-terminal to residue 77 (Figure 3.S.5 B&C).

3.5 Discussion

Isoprenylcysteine carboxyl methyltransferase is the only enzyme identified to date that functions as a methyltransferase of CAAX proteins. Given the vast number of cellular pathways influenced by CAAX processing, most studied for Ras proteins, it is essential to elucidate the structure and function of Icmt. Previously a 3.4Å crystal structure of a prokaryotic Icmt ortholog, *Ma*-Icmt, revealed a well-conserved C-terminal region important for the binding of the co-substrate, SAM.[13] The crystal structure indicates two previously determined conserved motifs: M1 (RHPxY) and M2 (R[x]$_3$EE) that contain essential residues for SAM binding.[25] Additionally, the crystal structure indicated a hydrophobic substrate access tunnel involving both the N- and C-termini that may be involved in substrate binding and aid in its interaction with SAM. However, the N-terminal domain of *Ma*-Icmt has poor sequence conservation and has very limited activity toward minimal substrates of eukaryotic Icmts, such as AFC, most likely because there are no known prenylated proteins in prokaryotes. It has since been termed *Ma*-MTase. As a result, this crystal structure is useful for studying the SAM interaction but is not a great model for substrate binding.

Recently, the first eukaryotic Icmt ortholog, *Tc*-Icmt, was crystallized at 2.3Å.[14] It revealed an enclosed and defined SAM binding cavity with access to the substrate through a slender hydrophobic 'tunnel'. Combined with previous mutational analysis data from another eukaryotic Icmt species (*Ag*-Icmt), Diver *et al.* suggested and reiterated many residues with important contacts between substrate and cofactor. However, the substrate co-crystalized with Icmt was not resolved, leaving the density within the substrate binding tunnel to be inferred. With the goal of designing future inhibitors of Icmt as a means of halting CAAX protein signaling, including most notably the oncogenic signaling of Ras proteins, structural information about substrate-enzyme binding is of most importance to design the most selective inhibitors. The most powerful, competitive inhibitors most likely will resemble both substrate and cofactor, however cofactor-mimetic inhibitors alone will most likely have alternative targets, as SAM is the second most ubiquitously used cofactor in a cell.[20, 21] Therefore, alternative methods are needed to locate and characterize the substrate binding site. Here, we utilized site-directed mutagenesis, photoaffinity probes based on Icmt substrates and biochemical techniques to characterize the substrate binding site of Icmt.

Using alanine-scanning mutagenesis, we have identified numerous conserved residues that are essential for Ste14 activity. Consistent with insights from crystal structure of the eukaryotic ortholog, *Tc*-Icmt, mutations of residues in the proposed C-terminal conserved SAM binding motifs (M1 and M2) had very low activity with both substrates which may result from the inability to bind the cofactor rather than the substrate. Interestingly, since most of the sequence identity is retained C-terminally between Icmt isoforms (Figure 3.1A), we identified numerous N-terminal Ste14 mutants in TM1, TM2, and loop 2 that manifested a difference in catalytic activity from WT with either AFC or AGGC (Figure 3.2A). Many of these Ste14 mutants are located in the predicted hydrophobic TM regions and predicted hydrophobic substrate tunnel and may play a role in interacting with the isoprenoid moiety of the CAAX protein substrate.[14, 26]

The L56A mutation in TM2 resulted in the most significant change in substrate specificity. When leucine was substituted for alanine, the activity with AFC was severely decreased, which may be due to lost interaction between the lipid portion of the substrate and the residue. Thus, Leu56 appears to be essential for interacting with the 15-carbon group. In contrast, L56A retains WT activity with AGGC. This 5-carbon longer isoprenoid group may be able to form this necessary hydrophobic interaction with additional lipophilic residues in TM2 allowing for activity, since residue 56 is located centrally to the proposed hydrophobic substrate core of Icmt (Figure

3.5). We propose that this residue interacts directly with the isoprenoid group of the substrate. To test this hypothesis, we mutated Leu56 to alternative hydrophobic residues and observed a rescue of the activity with the AFC substrate for phenylalanine and isoleucine substitutions. We propose that the hydrophobic character of this residue help to configure or stabilize the shorter farnesylated group.

In addition to the TM segments, several mutations were identified in proposed Loop 2 of Icmt that also showed preference for the longer substrate, AGGC, or were inactive with either substrate. Double alanine mutants with L56A and two alanine mutants from Loop 2 (N71A and V75A) further showed that this cytosolic region of the protein is also important for substrate binding. These data suggest that TM1 and 2, and Loop 2 may be forming and amphipathic substrate tunnel to provide access to the methyl donor SAM. This is in agreement with the eukaryotic, *Tc*-Icmt crystal structure, which proposes a 22Å long 6Å wide substrate tunnel and cavity that is lined primarily with aromatic amino acids correspond to Ste14 residues Phe52, Leu56, Phe59, Leu81, Asn83, and Tyr88 of the N-terminus, as well as more C-terminal residues, Phe178, Trp181, Phe198, Phe205 and Phe206.[14] N-terminal residues Leu81, Asn83 and Tyr88 are proposed to create a depression in the bilayer and anchor the enzyme to better accommodate the larger peptide portion of the substrates upstream of the C-terminal, modified cysteine residue. The C-terminal residues, Phe178, Phe205 and Phe206 within in TM5 and TM6 that are proposed to line the substrate cavity were also previously not proposed to be involved in SAM binding motifs.

In our study, these residues were shown to be inactive or have lowered activity with both substrates, further enhancing their proposed role in positioning the substrate within the lipid tunnel, and specifically the carboxylate to interact with SAM and become methylated. Although the crystal structure provides insight into potential contacts with substrate, our data provide the first evidence that the N-terminus of the protein participates to varying degrees in the interaction with the two different isoprenoid groups of Icmt substrates.

In addition to site-directed mutagenesis and substrate specificity testing, we utilized previously characterized biotinylated photoaffinity substrates of His-Ste14 reported by Hahne *et al.* and the chemical cleavage reagent NTCB to further define the substrate binding site. NTCB has proved useful to identify active site peptides in a number of cases. It has been particularly useful for characterizing transmembrane domains involved in substrate binding including the human reduced folate carrier as well as to decipher the location of post translational modifications

of the human erythrocyte spectrin.[37, 38] This procedure was optimized by Tang *et al*. and results in the spontaneous hydrolysis of an amide by cyclization of the cysteine side chain. As a result, we employed these techniques to validate that the N-terminal residues contribute to the substrate binding site of His-Ste14.

By designing single cysteine His-Ste14 mutants at exposed positions in concert with photoreactive substrate analogs and chemical cleavage, we were able to identify peptide fragments involved in the substrate binding site. We used a newly synthesized photoreactive substrate analog containing a more favorable photoreactive diazirine group and retaining higher Ste14 activity than the previously characterized benzophenone analogs (Figure 3.3A). Labeling was found to be within the N-terminal fragment preceding residue 77 of His-Ste14. The identified area includes TM1, TM2 and parts of Loop 2 of His-Ste14 and encompasses the noteworthy Leu56 residue. The catalytic mechanism of Icmt catalyzes methyl transfer via a ordered bi bi reaction mechanism where SAM binds first followed by the isoprenylated substrate followed by the respective release of the methylated substrate and SAH product.[39, 40] As a result, photolabeling and chemical cleavage experiments were performed with the addition of the cofactor SAM, resulting in immunoblot results similar to those performed here without SAM (data not shown). Additionally, high levels of unlabeled Ste14 are seen in the photolabeling and cleavage immunoblots (Figure 3.3 and 3.4). To help increase photolabeling efficiency, substate analogs and purified cysteine mutants were reconstituted into lipids before labeling and cleavage since Icmt is a known integral membrane protein. We did not see any increase in photolabeling efficiency (data not shown). Finally, we tested whether the amide and farnesyl portions of the substrate have different contact areas of Ste14 using substrate analogs with benzophenone groups positioned in each area. Both probes labeled Ste14 N-terminally to residue 77 (Figure 3.S.6).

To isolate TM2 containing residue Leu56, and further narrow the area of Ste14 interacting with substrate, we designed a second cysteine mutant in concert with the S77C mutant within Loop 1, TA-I44C-S77C. We further speculated that TM2 is involved in substrate binding as the residues in TM1, specifically Gly31 within the GxxxGxxxG motif, are involved in homodimerization of Ste14 (Ratliff *et al*., *unpublished).* Photolabeling and NTCB cleavage of this mutant in combination with the new substrate analog AFC-FamDiaz**,** revealed substrate binding to Ste14 primarily within TM2 (Figure 3.4C). Remarkably, we were able to observe changes in peptide fragment size within a few amino acids with this protocol using immunoblot analysis (data not

shown). The region of TM2 and Loop 2 studied (residues 44 to 77) of His-Ste14 are highly conserved with 7 similar and 7 identical residues. 5 of those conserved residues appear to be essential for catalytic activity by demonstrating specific activities under 15% with both substrates.

In conclusion, the novel research reported here elucidates residues and TM regions within Icmt, Ste14, which are critical for the recognition of the lapidated substrate. As noted above, using alanine-scanning mutagenesis and activity testing with AFC and AGGC, it was possible to identify residues in TM1, TM2, and Loop 2 that are essential for Ste14 activity due to substrate – residues that were previously not well characterized due to sequence homology being retained mostly in the C-terminus for cofactor binding. Furthermore, residue Leu56 was intriguing with a different substrate specificity profile than WT, drastically favoring AGGC. Finally, using photolabeling and chemical cleavage, we were able to corroborate our activity assay results with the substrate analogs labeling a fragment containing TM2 (residues 44 to 77) of His-Ste14. This knowledge will be indispensable to understand the structure and function of Icmt, an essential PTM enzyme of CAAX proteins including many members of the Ras superfamily.

3.6 Experimental Procedures

3.6.1 Biochemical materials

All oligonucleotides were obtained from Integrated DNA Technologies, Inc. (Coralville, IA). All restriction enzymes and the Q5® Site-Directed Mutagenesis Kit were obtained from New England Biolabs (Ipswich, MA). GoTaq® Green Mater Mix and LigaFast™ Rapid DNA ligation system were purchased from Promega (Madison, WI). QIAquick PCR Purification and DNA Gel Extraction kit were purchased from Qiagen (Germantown, MD). GeneJET plasmid miniprep kit, EcoRI NeutrAvidin-HRP conjugate, SuperSignal West Pico chemiluminescence (ECL), Amicon Ultra 30,000 MWCO concentrators, Amersham nitrocellulose membrane (0.22 μm) and DTT were purchased from Thermo Fisher Scientific, Inc. (Waltham, MA). BigDye® Terminator v3.1 was purchased from Applied Biosystems (Foster City, CA). AEBSF was purchased from Gold Biotechnology (Olivette, MO). Aprotinin was purchased from Research Products International (Mount Prospect, IL). *N*-acetyl-*S*-farnesyl-L-cysteine (AFC) and *N*-acetyl-*S*-geranylgeranyl-L-cysteine (AGGC) was purchased from Enzo Life Sciences (Farmingdale, NY) and Cayman Chemical (Ann Arbor, MI). The detergent *N*-Dodecyl-β-D-maltopyranoside (DDM) was

purchased from Anatrace, Inc. (Maumee, OH). TALON® metal affinity resin was purchased from Takara Bio USA, Inc. (San Jose, CA). All lipids were purchased from Avanti Polar Lipids, Inc. (Alabaster, AL). 2-nitro-5-thiocyanobenzoate (NTCB), trypsin (porcine pancreas), and 4-20% TruPAGE™ precast protein gels were purchased from Sigma-Aldrich (St. Louis, MO). *S*-adenosyl-L-[*methyl*-^{14}C]methionine was purchased from Perkin Elmer (Waltham, MA). The α-myc monoclonal antibody (9E10), the goat α-mouse IgG-HRP, the goat α-rabbit IgG-HRP and the subcloning efficiency *Escherichia coli* DH5α competent cells were purchased from Invitrogen (Carlsbad, CA). The SM1058 and SM1188 yeast strains and the α-Ste14 polyclonal antibody were gifts from Dr. S. Michaelis (The Johns Hopkins University School of Medicine). The photoreactive substrate analogs were synthesized by the Distefano Laboratory (The University of Minnesota-Twin Cities). Biosafe II scintillation fluid was purchased from Research Products International (Mount Prospect, IL). All other materials were purchased from Fisher Scientific (Waltham, MA).

3.6.2 Chemical synthesis materials

All solvents and reagents used for the synthesis of the diazirine isoprenoid analog (**AFC-FamDiaz**) and solid-phase peptide synthesis of the photoactivatable peptides were of analytical grade and purchased from Peptides International (Louisville, KY), NovaBioChem® (Nohenbrunn, Germany) or Sigma-Aldrich (St. Louis, MO). NHS-PEG$_4$-Biotin was obtained from Thermo Scientific (Waltham, MA). HR-ESI-MS analysis was performed using a Bio-TOF-II (Bruker) mass spectrometer.

3.6.3 Synthesis of Biotin-Peg$_4$-K(5-Fam)C(Diazirine)-OH (AFC-FamDiaz)

This modified dipeptide was prepared via a modification of a previously describe procedure.[36] Synthesis began on preloaded Fmoc-Cys(Trt)-Wang resin (50 μmol) and the chain was elongated using HCTU/N-Methylmorpholine in a single coupling step with 4 equivalents of both Fmoc-Lys(Dde)-OH and HTCU for 30 min. Following coupling, the N-terminal amine was deprotected with 10% piperidine in DMF (5 mL, v/v) and the presence of the resulting free amine was confirmed by ninhydrin analysis.[41] The resin was washed with CH_2Cl_2 (2 x 5 mL) and dried *in vacuo* overnight. The free amino terminus was biotinylated in DMF (5 mL) with NHS-PEG$_4$-Biotin (0.35 mg, 60 μmol, 1.2 eq) in the presence of DIEA (10.4 μL, 5.0 μmol, 0.1 eq) for 16 h.

After acylation, the resin-bound peptide was washed thoroughly with CH_2Cl_2 (3 x 5 mL) and dried *in vacuo*. The peptide was then reacted with 5% hydrazine in DMF (5 mL, v/v) to orthogonally remove they Dde protected side chain of lysine. After verifying the deprotection was complete by ninhydrin analysis, the peptide was washed with CH_2Cl_2 (3 x 5 mL), dried *in vacuo* for 1 hour, and then reacted with 5-Fam NHS ester (33 mg, 60 µmol, 1.2 eq) in the presence of DIEA (10.4 µL, 5.0 µmol, 0.1 eq) overnight. The resin was filtered, washed with CH_2Cl_2 (3 x 5 mL), dried *in vacuo* for 1 hour, and analyzed via ninhydrin analysis to confirm acylation of the side chain. The dipeptide was cleaved from the resin and simultaneously deprotected by treatment with Reagent B containing TFA (5 mL), triisopropylsilane (0.25 mL) and H_2O (0.25 mL) for 2 hours at rt. The product was precipitated out in cold H_2O (50 mL) divided into two vials, frozen, and lyophilized overnight to yield a total crude mass of 36 mg (69% yield). The was dissolved in minimal DMF (2 x 1 mL) and then diluted into a mixture of DMF/n-Butanol/H_20 (0.10% TFA) (3:1:1 v/v/v, 5 mL total volume). Diazirine-Br [114 mg, 332 µmol, 10 eq, (*2E,6E)-8-bromo-2,6-dimethylocta-2,6-dien-1-yl 3-(3-methyl-3H-diazirin-3-yl) propanoate]* was added to the crude dipeptide solution and the alkylation reaction was initiated by the addition of $Zn(OAc)_2 \cdot 2H_2O$ (35 mg, 166 µmol, 5 eq).[36] After 6 hours, the reaction was analyzed by analytical RP-HPLC, purified by semipreparative C_{18} RP-HPLC, and identified via ESI-TOF MS. This reaction yielded 4.6 mg (11% yield) of the desired alkylated dimer with a purity of 98%. HR-ESI-MS: calcd for $C_{66}H_{87}N_8O_{18}S_2$ $[M + H]^+$ 1343.556 found 1343.548. Characterization in Figure 3.S.6

3.6.4 Cloning

For the alanine-scanning mutagenesis mutants, cysteine-less His-Ste14 (TA) construct and the TA-S77C mutants, overlap extension PCR site-directed mutagenesis was performed to create the His-Ste14 mutants according to previous protocols.[24, 29, 42] Briefly, each PCR product containing the specific mutations was digested with XmaI and SacII and ligated into the His-Ste14 expression plasmid pCHH10m3N containing *URA3* gene and a phosphoglycerate kinase promoter (P_{PGK}) for protein expression.[29] PCR products underwent EcoRI test cuts to confirm the Ste14 DNA insert was ligated into template vector. DNA products were transformed into *E.* coli DH5α competent cells for further amplification and purified with the DNA Gel Extraction kit (Qiagen). All constructs were verified using bi-directional dye-terminator sequencing (BigDye® Terminator v3.1) by Purdue University Genomics Facility (genotype: 2µ URA3 P_{PGK}-His_{10}-myc_3N-STE14-

mutant). Plasmids were transformed into SM1188 cells and grown at 30ºC on synthetic complete medium in the absence of uracil (SC-URA).[42]

TA-I44C and TA-I44C-S77 mutants were cloned using the NEB Q5® Site-Directed Mutagenesis Kit. Briefly, end-to-end (nonoverlapping) primers were designed in combination with the Q5 Hot Start High-Fidelity DNA Polymerase to ensure robust and exponential amplification of mutations. TA and TA-S77C DNA were used respectively as templates for the TA-I44C and TA-I44C-S77C mutants. The PCR product then underwent rapid phosphorylation and ligation by a proprietary KLD mixture containing a kinase, ligase and Dpnl. EcoRI test cuts were performed on the resulting DNA to confirm the Ste14 DNA insert was ligated into template vector. DNA products were transformed into *E.* coli DH5α competent cells for further amplification and purified with the DNA Gel Extraction kit (Qiagen). Constructs were verified by Genewiz (South Plainfield, NJ) using Sanger sequencing methods (genotype: 2μ URA3 P_{PGK}-His_{10}-myc_3N-STE14-mutant). Plasmids were transformed into SM1188 cells and grown at 30ºC on synthetic complete medium in the absence of uracil (SC-URA).[42]

3.6.5 Yeast strains and crude membrane preparations from yeast cells

$His_{10}myc_3$N-Ste14p (His-Ste14) and mutants were overexpressed in SM1188, a *ΔSTE14* deletion strain, as previously described with minor modifications.[29] DTT reagent was added to increase transformation efficiency. Crude membrane preparations from the yeast strains overexpressing His-Ste14 and mutants were prepared as previously described, with the following modifications.[29] Following centrifugation at 100,000 x g for 1 h, the membrane pellet was resuspended in 10 mM Tris-HCl, pH 7.5, aliquoted, flash frozen in liquid N_2 and stored at -80ºC. Total protein concentration was determined using the Bradford protein assay using Coomassie Plus protein assay reagent.

3.6.6 Purification of His-Ste14 strains from crude membranes

His-Ste14 and mutants were purified as previously described.[29] Briefly, crude membrane protein (5 mg/mL) was solubilized in a phosphate-based buffer (0.3M NaCl, 50 mM Na_2HPO_4, 10% glycerol, 1% aprotinin, and 2 mM AEBSF) containing 20 mM imidazole and 1% DDM before centrifugation to remove the insoluble fraction. Supernatant was incubated with TALON® metal

affinity before washing and the purified protein was eluted from the column by the addition of 1M imidazole buffer. All purification buffers were at a pH of 7.2. The fraction was concentrated in 30 kDa molecular weight cut off (MWCO) and protein concentration was determined by an Amido Black protein assay.[43]

3.6.7 SDS-PAGE Coomassie stain and immunoblot analysis of pure protein

Purified protein (1 μg) in 2X SDS-loading buffer (0.5 M Tris-HCl, pH 6.8, 30% sucrose (w/v), 10% sodium dodecylsulfate (w/v), 3.5 M 2-mercaptoethanol and 0.1% bromophenol blue (w/v)) was heated at 65°C for 15 min and then resolved on a 10% SDS-PAGE in 1xTris-glycine-SDS (TGS) buffer. The gels were either stained with Coomassie (0.25% (w/v) Coomassie Brilliant Blue R-250, 80% methanol and 20% acetic acid) or transferred to a nitrocellulose membrane (0.22 μm) in 1X-TG buffer for 90 min. The membrane was blocked at 4°C overnight in 20% (w/v) non-fat dry milk in phosphate-buffered saline with Tween-20 (137 mM NaCl, 2.7 mM KCl, 4 mM Na_2HPO_4, 1.8 mM KH_2PO_4 and 0.05% (v/v) Tween-20, pH 7.4) (PBST). The blocked membrane was incubated for 2 hours at room temperature with α-myc (1:10,000) monoclonal antibody in 5% (w/v) non-fat dry milk in PBST. The membrane was washed in PBST three times and incubated for 1 hour at room temperature with goat α-mouse IgG-HRP (1:6,000) in 5% (w/v) dry milk in PBST. The membranes were washed three times with PBST and the protein bands were visualized using ECL.

3.6.8 *In vitro* methyltransferase vapor diffusion assay

Reactions were performed as described previously.[10, 29] Crude membrane extracts (5 μg) in Tris-HCl buffer (100 mM, pH 7.4) was incubated with AFC, AGGC or AFC-FamDiaz (200 μM). Then [^{14}C]-SAM (20 μM) was added and the solution was incubated for 30 minutes at 30°C. After, the reaction is stopped with 50 μL of 1 M NaOH/1% SDS, spotted on filter paper and lodged in the neck of a scintillation tube filled with 10 mL of scintillation fluid and capped. After incubation at room temperature for 3 hours, the filter paper was removed, and radioactivity of the scintillation fluid was measured using a Packard Tri-Carb 1600CA Liquid Scintillation Analyzer. Background counts from the empty vector control were subtracted from the total overall counts of all samples. For purified protein (~0.3 μg) and AFC (200 μM) were reconstituted in *E. coli* lipid vesicles (50

μg) by rapid dilution in 3-(N-morpholino) propanesulfonic acid (MOPS) buffer (125 mM, pH 7.4), vortexed and incubated on ice for 10 min. Pure protein is treated in the same way as crude membranes after the addition of 20 μM [^{14}C]-SAM (20 μM). Specific activity is calculated by pmol of methyl groups transferred to substrate per mg of protein per minute. Each experiment contained duplicates of each reaction sample and scintillation counting is reported as the average of three scans. Assays were repeated in triplicate.

3.6.9 Trypsin digest of crude His-Ste14 strain membranes

Crude membrane protein (20 μg) was incubated with trypsin (0.25 mg/mL) in Tris-HCl (10 mM, pH 7.5) for 15 min at 37°C. Negative control samples were performed with phosphate saline buffer (PBS) instead of trypsin. The reaction was stopped with the addition of AEBSF (1 mM). The protein was then precipitated by the addition of trichloroacetic acid (TCA, 10%), incubated at 4°C for 15 min and pelleted by centrifugation for 15 min at 4°C at 13,000 x g. Pellet was resuspended in 2X SDS loading buffer followed by heating at 65°C for 15 min. Samples were then resolved with a 12% SDS-PAGE and transferred to nitrocellulose (0.22 μm). The membrane was blocked overnight at 4°C in 20% (w/v) non-fat dry milk in PBST. The blocked membrane was incubated for 2 h at room temperature with α-myc (1:10,000) monoclonal primary antibodies in 5% (w/v) non-fat dry milk in PBST. The membrane was washed in PBST three times and incubated for 1 h at room temperature with goat α-mouse IgG-HRP (1:4,000) in 5% (w/v) dry milk in PBST, respectively. The membrane was washed three times with PBST and the protein bands were visualized using ECL.

3.6.10 Photocrosslinking and NTCB cleavage of purified His-Ste14 cys-less and single-cysteine mutants

Purified His-Ste14p-TA and mutants (30 μg) were incubated with AFC-FamDiaz (100 μM) in 138 mM MOPS buffer (pH 7.4) plus 1 mM DTT for 10 min on ice. The samples were UV irradiated (365 nm) in 96-well plates for 30 min on ice. The labeled protein samples were then cleaved with 25 μL of 4 mM NTCB (2-nitro-5-thiocyanobenzoic acid) in digest buffer (105.9 mM glycine, pH 10, and 2.72 M urea) and incubated at 37°C for 4 hours. After digestion, 50 μL of 5X SDS loading buffer was added and samples were heated for 30 min at 65ºC. Then samples were

subjected to either 12% SDS-PAGE run in HEPES buffer or precast 4-20% gradient SDS-PAGE run in MOPS-Tris-SDS buffer. The MOPS running buffer conditions required the inner chamber of the gel box to be spiked with a final concentration of 1X sodium bisulfite to prevent potential sample reoxidation. The gels were then either stained with silver staining procedures or transferred to nitrocellulose membranes (0.22 μm) in a 1X-TG buffer for 90 minutes.[44] The membranes were blocked at 4°C overnight in 20% (w/v) non-fat dry milk in PBST. The blocked membranes were incubated for 2 hours at room temperature with the respective primary antibodies: α-myc (1:10,000) or α-Ste14 (1:10,000) in 5% (w/v) non-fat dry milk in PBST. The membranes were washed in PBST three times and incubated for 1 hour at room temperature with goat α-mouse IgG-HRP (1:6,000) or goat α-rabbit IgG-HRP (1:10,000) in 5% (w/v) dry milk in PBST, respectively. Additionally, a separate nitrocellulose was probed with NeutrAvidin-HRP (1:2,000) in 1% BSA in PBST for 3 hours at room temperature to detect the biotin tag of the substrate analog. Finally, all membranes were washed three times with PBST and the protein bands were visualized using ECL.

3.7 Figures

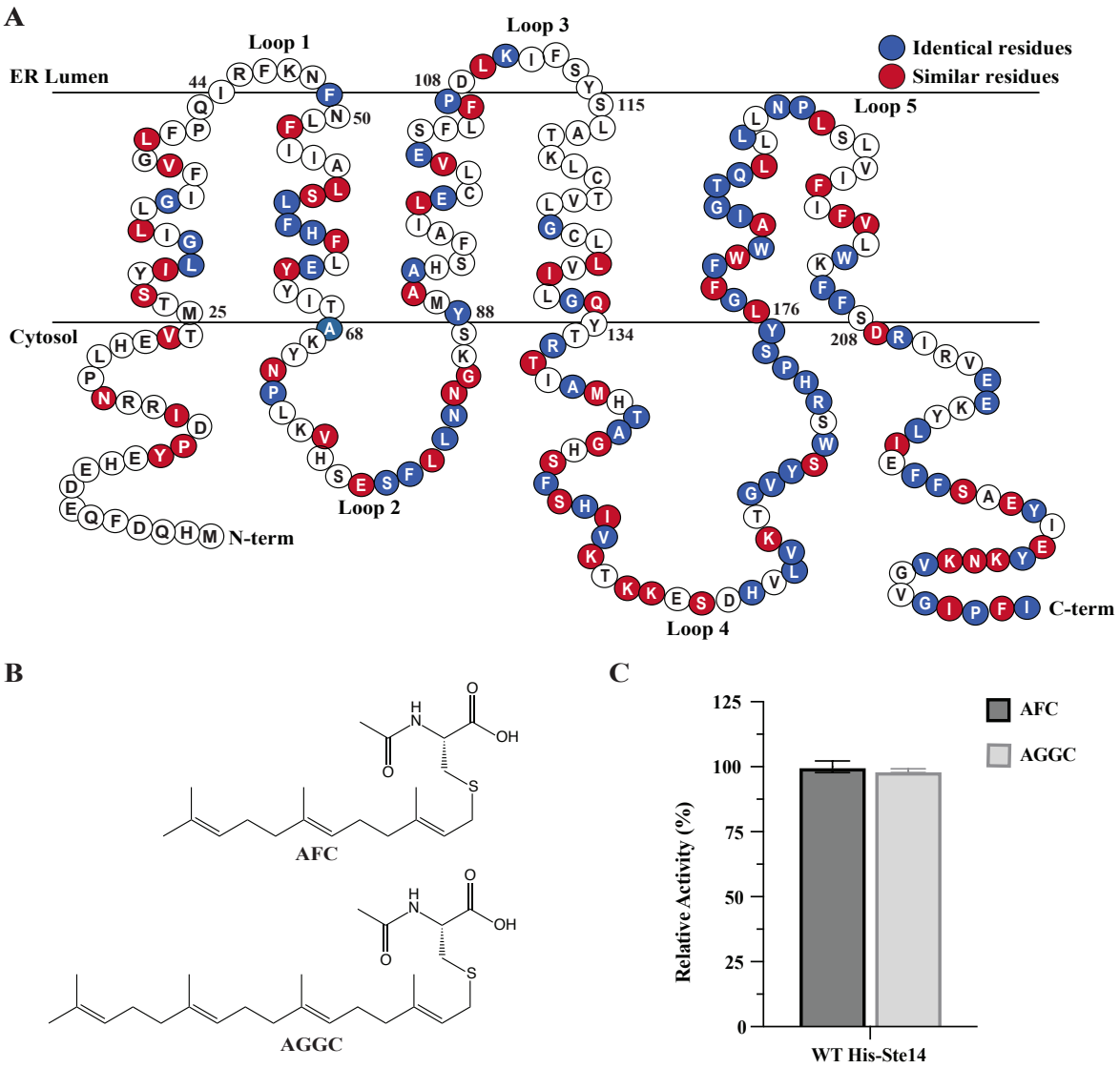

Figure 3.1 Important homologous residues of Icmt species and lack of substrate specificity between two isoprenoid groups.

(A) Sequences alignment of four most studied species of Icmt (*Hs, Tc, Ag,* and *Sc*) represented on predicted 2D topology map of Ste14. Red indicates similar residues and blue indicates identical residues between the four species. (B) Structures of minimal prenylated protein substrates containing a 15-carbon farnesyl chain, *N*-acetyl-*S*-farnesyl-L-cysteine (AFC), or a 20-carbon geranylgeranyl chain, *N*-acetyl-*S*-geranylgeranyl-L-cysteine (AGGC). (C) Wild-type His-Ste14 activity from an *in vitro* methyltransferase activity assay tested with AFC (dark grey) or AGGC substrate (light grey). Data was normalized to AFC conditions. Error bars represent S.D. No statistical significance was observed.

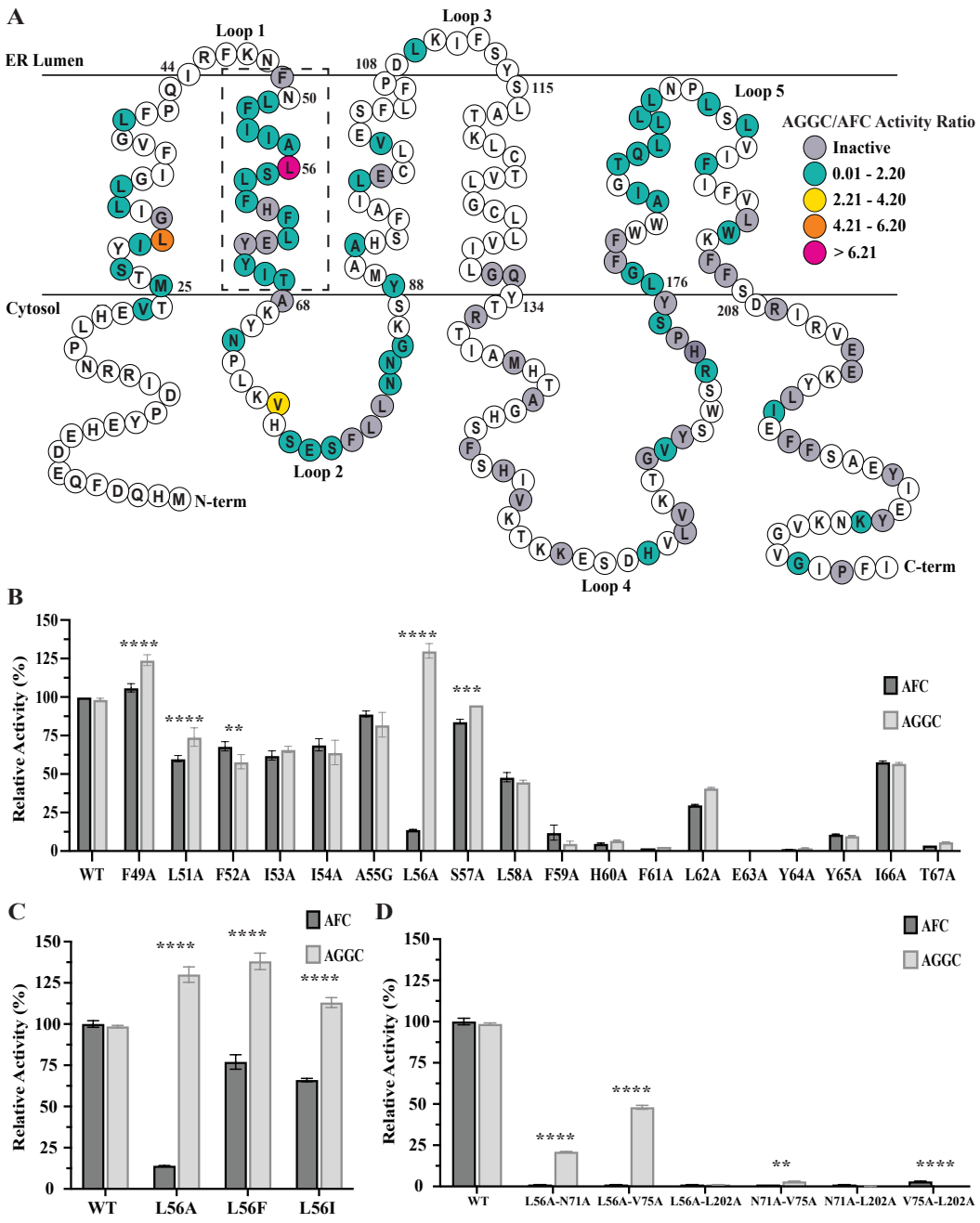

Figure 3.2 Alanine scanning mutagenesis and substrate specificity testing of the highly conserved residues within Ste14 indicate regions of proposed substrate recognition within the N-terminus of protein.

Conserved residues were mutated to alanine (or glycine in the case of an original alanine mutants) and tested with AFC or AGGC in *in vitro* methyltransferase activity assays. The ratio of AGGC to AFC for each residue is color coded on the predicted topology map of Ste14. (B) Specific values from part (A) of *in vitro* methyltransferase activity assay for each mutant within TM2 of Ste14. Statistical analyses performed comparing each mutants AFC and AGGC activities. **: p = 0.0012, ***: p = 0.0002, ****: p < 0.0001, (C) *In vitro* methyltransferase activity assay activity of Leu56 mutated to alanine and more natively similar phenylalanine and isoleucine. ****: p= <0.0001 (D) *In vitro* methyltransferase activity assay activity of double mutants consisting of a combination of L56A, N71A, V75A and L202A. In all graphs: normalized to WT-Ste14 with AFC and error bars represent S.D., **: p=0.0064, ****: p=<0.0001.

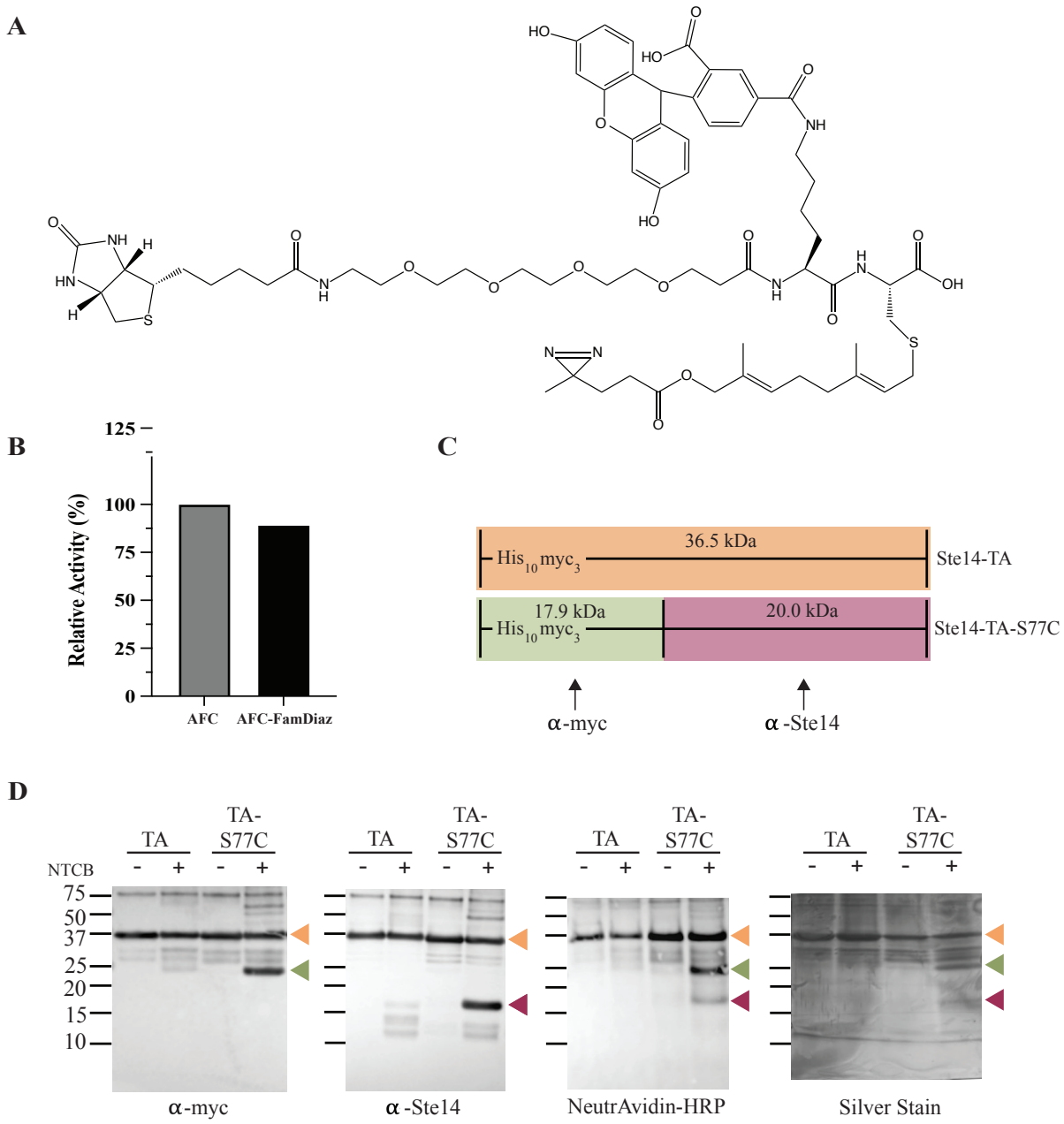

Figure 3.3 Diazirine containing photoreactive probe labels Ste14 N-terminally to residue 77

(A) Structure of substrate mimetic photoreactive probe containing diazirine (AFC-FamDiaz), fluorescein and biotin moieties for better characterization of binding to enzyme. (B) *in vitro* methyltransferase activity assay of AFC-FamDiaz with wild-type His-Ste14 compared and normalized to minimal substrate, AFC. Error bars represent S.D. (C) Predicted peptide fragments of His-Ste14-TA and TA-S77C after undergoing photolabeling with AFC-FamDiaz followed by chemical cleavage by NTCB. All masses include addition of photoreactive substrate analog. (D) Immunoblot analysis of photolabeled and NTCB cleaved His-Ste14 single cysteine mutants. Digested peptides were resolved in 12% SDS-PAGE in HEPES running buffer followed by immunoblot analysis using termini-specific antibodies. The N-terminal peptide fragments were recognized by α-myc, the C-terminal fragments by α-Ste14, and the photolabeled fragments by Neutravidin-HRP.

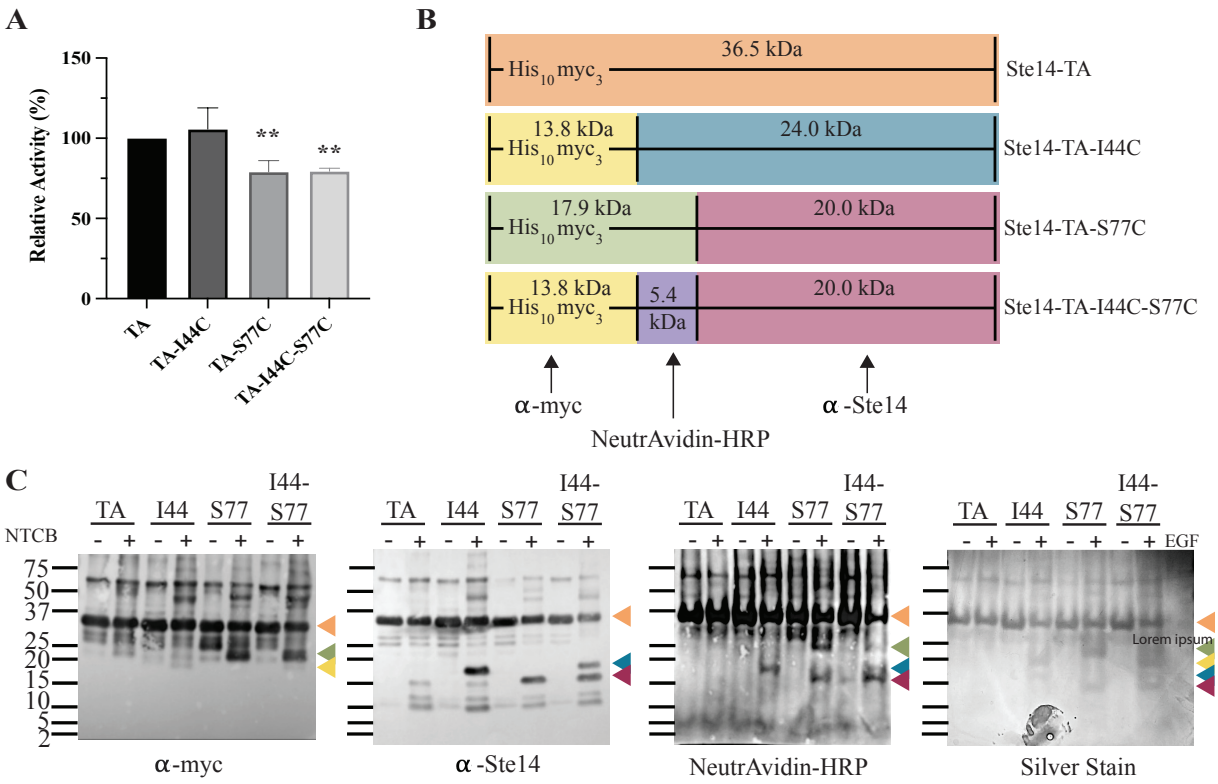

Figure 3.4 Photolabeling and chemical cleavage of purified His-Ste14 double cysteine mutant reveals TM2 primarily involved in substrate binding.

(A) *In vitro* methyltransferase activity assay activities of single and double cysteine mutants with AFC. Each mutant is normalized to TA His-Ste14. Error bars represent S.D. Statistical analyses performed comparing each mutant to TA **: $0.0258 > p > 0.0235$ (B) Predicted peptide fragments of His-Ste14-TA, TA-I44C, TA-S77C and TA-I44C-S77C after undergoing photolabeling with compound AFC-FamDiaz followed by chemical cleavage by NTCB. All fragment masses include the addition of the photoreactive substrate analog. (C) Immunoblot analysis of photolabeled and NTCB cleaved His-Ste14 cysteine mutants. Digested peptides were resolved in 4-20% SDS-PAGE in MOPS-Tris-SDS running buffer followed by immunoblot analysis using termini-specific antibodies. The N-terminal peptide fragments were recognized by α-myc, the C-terminal fragments by α-Ste14, and the photolabeled fragments by Neutravidin-HRP.

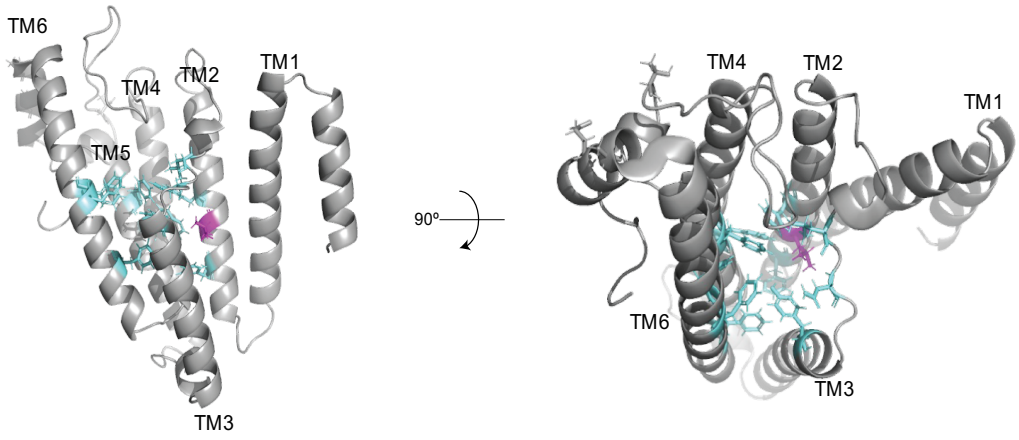

Figure 3.5 Proposed 3D structure of Ste14 shows Leu56 residue central to substrate binding pocket.

PyMOL structures of Ste14 mapped on to the known *Tc*-Icmt structure (PDB: 5V7P). Cyan colored residues are those proposed to line the substrate binding pocket and the Leu56 residue is in magenta. (Left) shows side view of protein. (Right) 90º rotation down to look into the substrate binding tunnel.

3.8 Supplemental Information

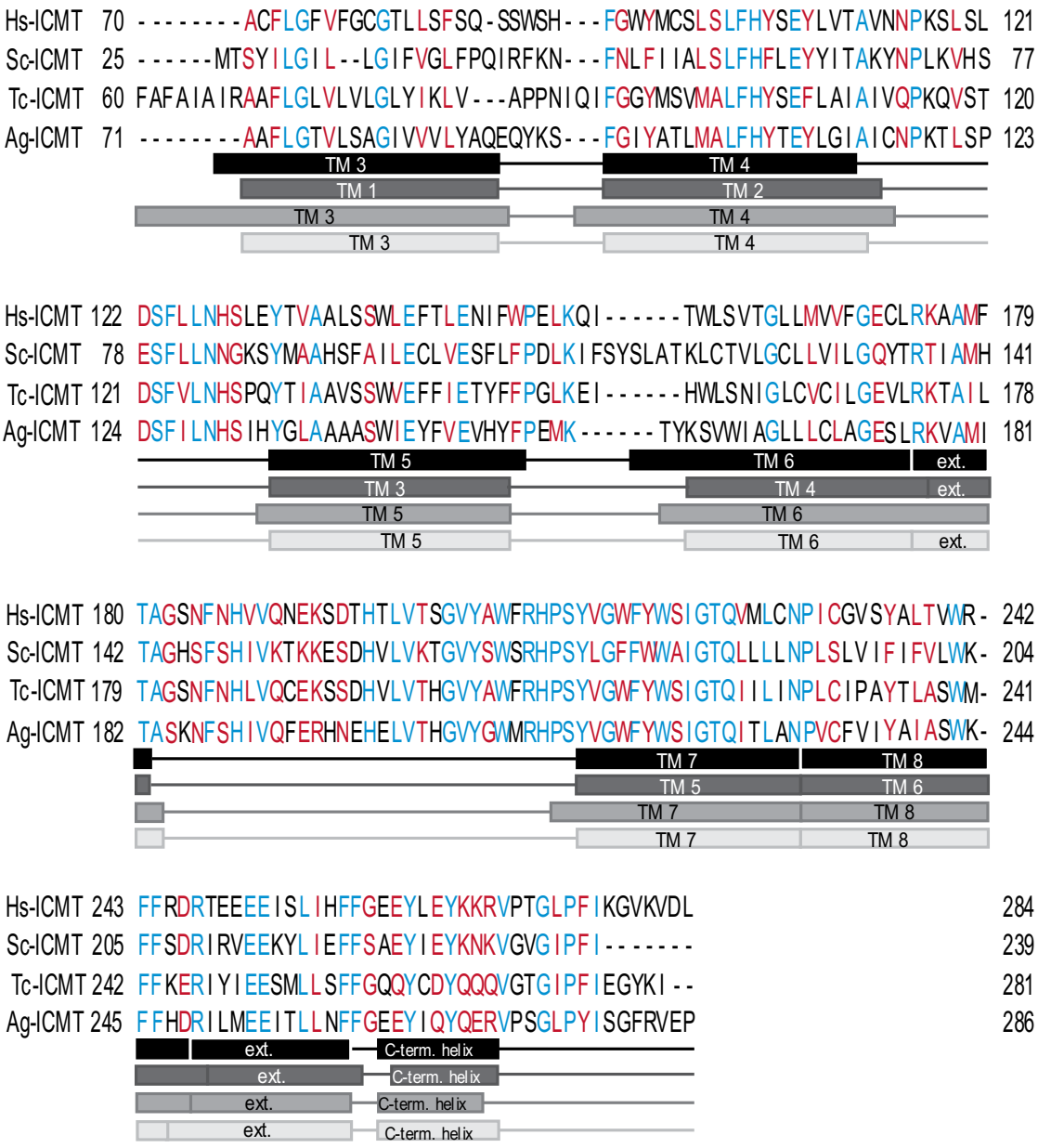

Figure 3.S.1 Sequence alignment of four most studied Icmt homologs.

Clustal Omega was utilized to align the sequences of *Hs-, Sc-, Tc-* and *Ag*-Icmt. Red are similar residues and blue are identical residues. The structural features are represented below the amino acid residues in the same order as the sequences. Rectangles represent transmembrane (TM) regions of protein.

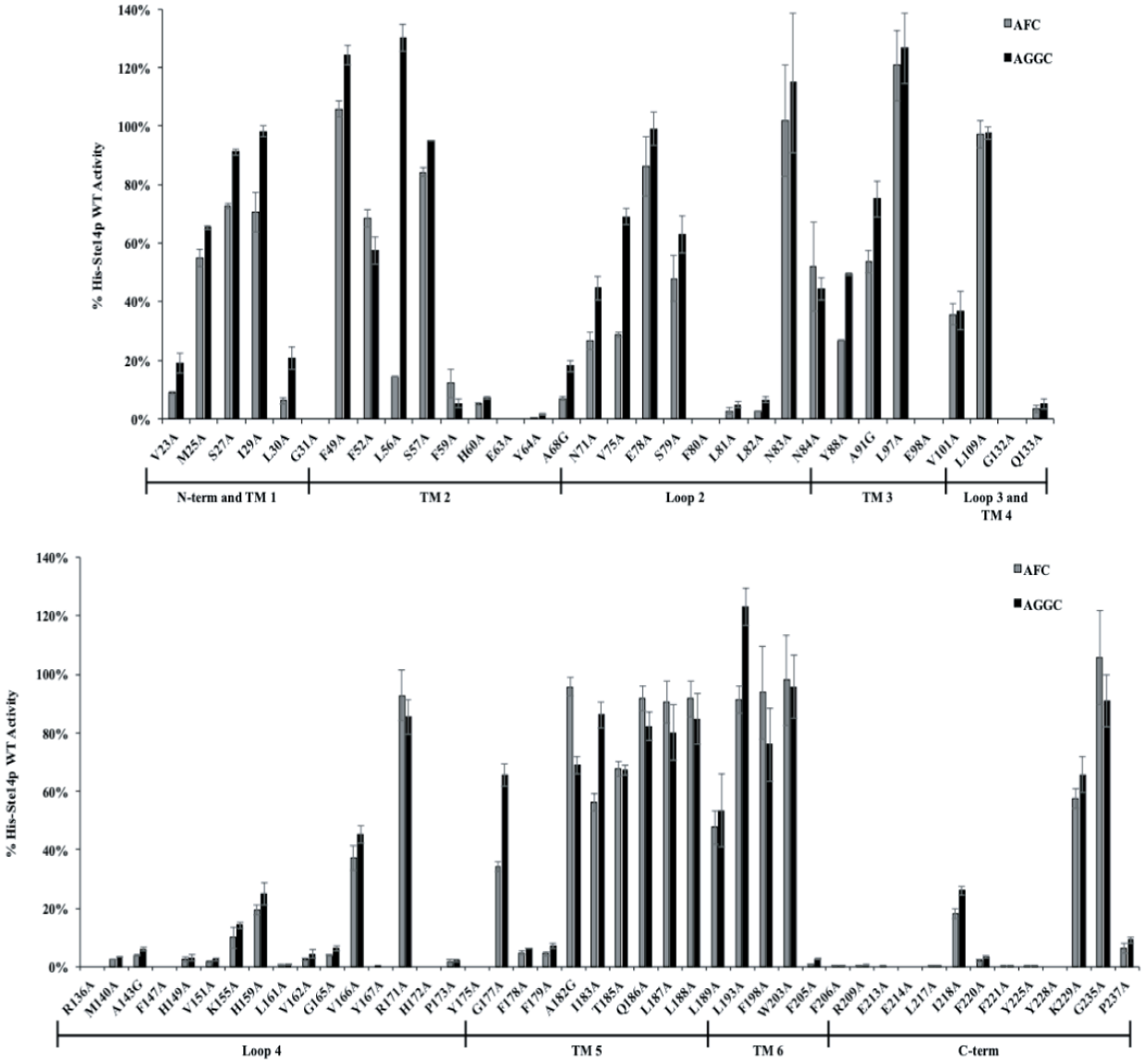

Figure 3.S.2 Quantitative data of alanine-scanning mutagenesis and substrate specificity testing of the highly-conserved residues within Ste14p indicate regions of proposed substrate recognition in the N-terminus of the protein..

Specific activities of mutants were determined using an *in vitro* methyltransferase activity assay. Percent activity was compared to WT His-Ste14 and AFC. The error bars represent ± S.D.

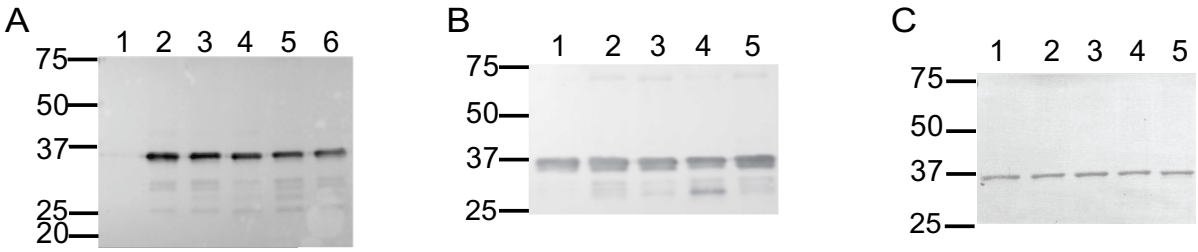

Figure 3.S.3 Ste14 cysteine mutants have same expression in crude membrane and pure forms of protein.

(A) Immunoblot of 0.1 µg of crude membranes probed with α-myc. Lanes 1: Δ*STE14*, 2: WT, 3: TA, 4: TA-I44C, 5: TA-S77C, 6: TA-I44C-S77C. (B) Immunoblot of 0.1 µg of pure protein probed with α-myc and α-mouse. Lanes 1: WT, 2: TA, 3: TA-I44C, 4:TA-S77C, 5: TA-I44C-S77C. (C) Silver stain of 1 µg pure protein. Lanes 1: WT, 2: TA, 3: TA-I44C, 4: TA-S77C, 5: TA-I44C-S77C.

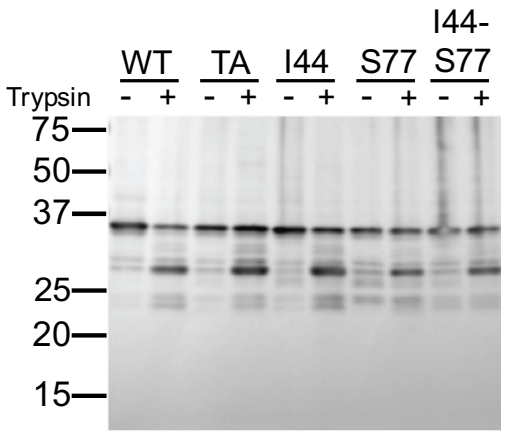

Figure 3.S.4 Trypsin digestion of cysteine mutants show similar cleavage patterns to WT-Ste24 protein.

Immunoblot of 0.1 µg of crude membranes after treatment with trypsin protease. Western blot probed with α-myc and α-mouse.

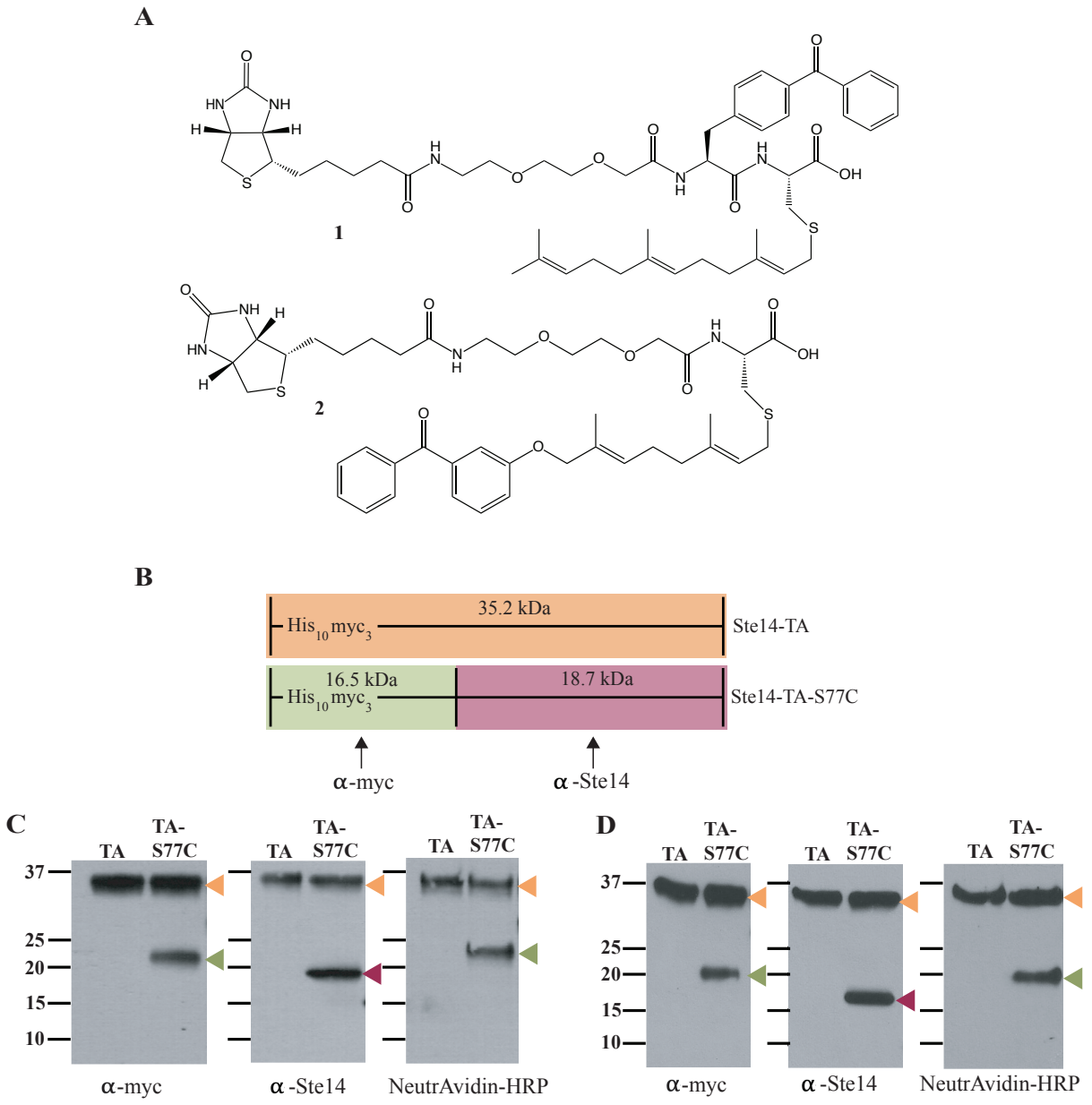

Figure 3.S.5 Photoreactive groups of substrate analogs located in amide and farnesyl portion of substrate label Ste14 N-terminally to residue 77.

(A) Structures of substrate mimetic photoreactive probes based on the structure of AFC. Structure **1** contains the photoreactive benzophenone group within the amide portion of the substate and **2** within the lipid group. (B) Predicted peptide fragments of His-Ste14-TA and TA-S77C after undergoing chemical cleavage by NTCB. Masses do not include the addition of the photoreactive substrate analog. (C-D) Immunoblot analysis of photolabeled and NTCB cleaved His-Ste14 single cysteine mutants. Pure His-Ste14 mutated protein were photolabeled with (C) analog **1** or (D) analog **2** and then incubated with NTCB for 24 hours. Digested peptides were resolved in 4-20% SDS-PAGE in TruPAGE™ TEA-Tricine-SDS running buffer followed by immunoblot analysis using termini-specific antibodies. The N-terminal peptide fragments were recognized by α-myc, the C-terminal fragments by α-Ste14, and the photolabeled fragments by Neutravidin-HRP.

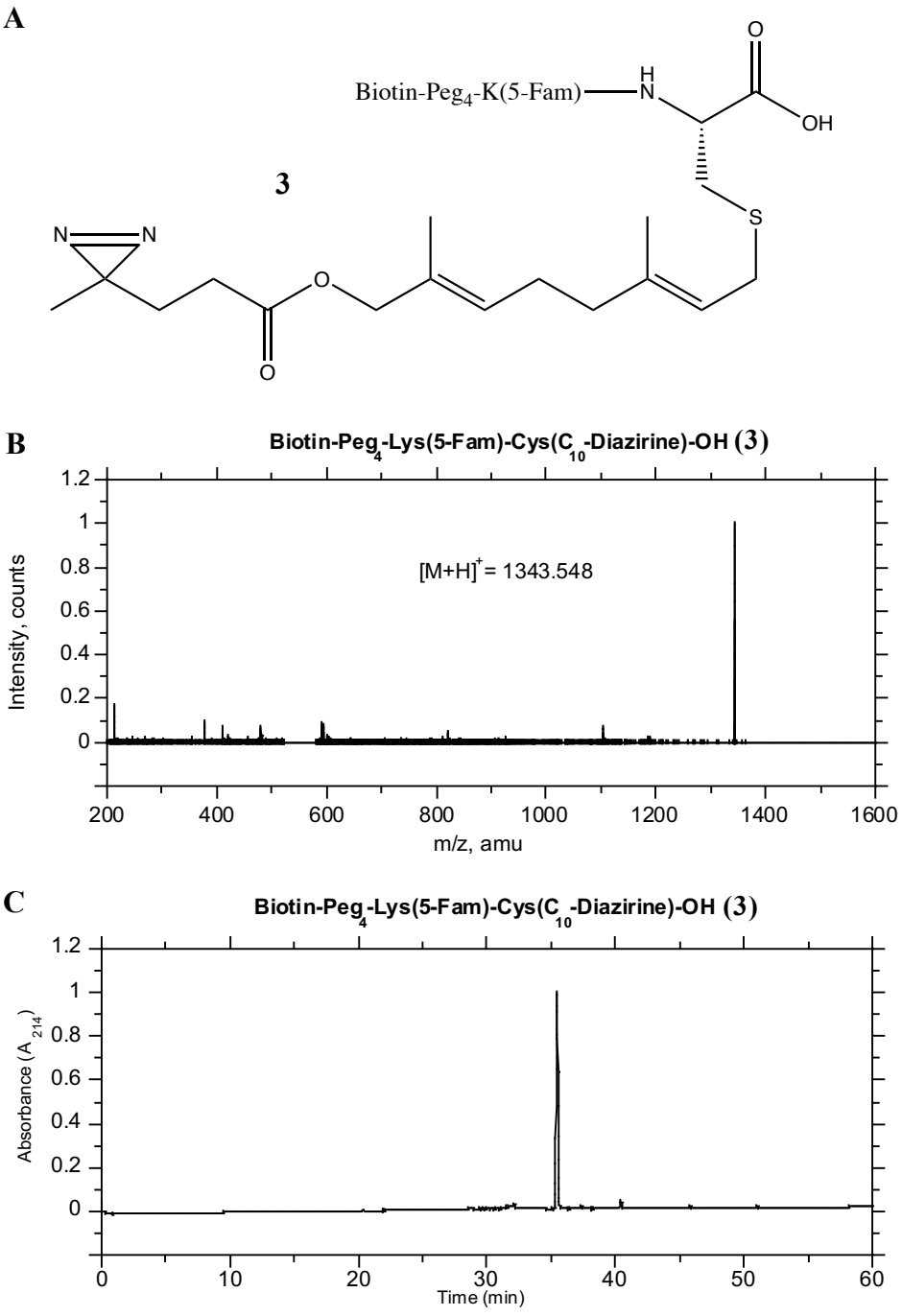

Figure 3.S.6 Synthesis of AFC based photoreactive substrate with diazirine utilized for optimal identification of Ste14p labeled peptide fragment.

(A*)* Structure of substrate analog, **3**, containing a biotin tag, fluorescein moiety and diazirine photoreactive group. Previous research from Vervacke *et al.* revealed that the diazirine photoactive group was an improved substrate and labeled His-Ste14p more efficiently. (B-C), Mass spectrum and analytical RP-HPLC chromatogram for Biotin-Peg$_4$-Lys(5-Fam)-Cys(C$_{10}$-Diazirine)-OH (**3**)**.** Linear gradient 0-100% CH_3CN (0.1%TFA) in 60 min, detected at 214

3.9 References

1. Waters, A. M.; Der, C. J., KRAS: the critical driver and therapeutic target for pancreatic cancer. *Cold Spring Harbor perspectives in medicine* **2018,** *8* (9), a031435.

2. Cox, A. D.; Fesik, S. W.; Kimmelman, A. C.; Luo, J.; Der, C. J., Drugging the undruggable RAS: mission possible? *Nature reviews Drug discovery* **2014,** *13* (11), 828-851.

3. Molina-Arcas, M.; Samani, A.; Downward, J., Drugging the Undruggable: Advances on RAS Targeting in Cancer. *Genes* **2021,** *12* (6), 899.

4. Moore, A. R.; Rosenberg, S. C.; McCormick, F.; Malek, S., RAS-targeted therapies: is the undruggable drugged? *Nature Reviews Drug Discovery* **2020,** *19* (8), 533-552.

5. Sun, J.; Qian, Y.; Hamilton, A. D.; Sebti, S. M., Both farnesyltransferase and geranylgeranyltransferase I inhibitors are required for inhibition of oncogenic K-Ras prenylation but each alone is sufficient to suppress human tumor growth in nude mouse xenografts. *Oncogene* **1998,** *16* (11), 1467-1473.

6. Peterson, Y. K.; Kelly, P.; Weinbaum, C. A.; Casey, P. J., A novel protein geranylgeranyltransferase-I inhibitor with high potency, selectivity, and cellular activity. *Journal of Biological Chemistry* **2006,** *281* (18), 12445-12450.

7. deSolms, S. J.; Ciccarone, T. M.; MacTough, S. C.; Shaw, A. W.; Buser, C. A.; Ellis-Hutchings, M.; Fernandes, C.; Hamilton, K. A.; Huber, H. E.; Kohl, N. E., Dual Protein Farnesyltransferase− Geranylgeranyltransferase-I Inhibitors as Potential Cancer Chemotherapeutic Agents. *Journal of medicinal chemistry* **2003,** *46* (14), 2973-2984.

8. Bergo, M. O.; Lieu, H. D.; Gavino, B. J.; Ambroziak, P.; Otto, J. C.; Casey, P. J.; Walker, Q. M.; Young, S. G., On the physiological importance of endoproteolysis of CAAX proteins: heart-specific RCE1 knockout mice develop a lethal cardiomyopathy. *J Biol Chem* **2004,** *279* (6), 4729-36.

9. Wahlstrom, A. M.; Cutts, B. A.; Karlsson, C.; Andersson, K. M.; Liu, M.; Sjogren, A.-K. M.; Swolin, B.; Young, S. G.; Bergo, M. O., Rce1 deficiency accelerates the development of K-RAS–induced myeloproliferative disease. *Blood* **2007,** *109* (2), 763-768.

10. Hrycyna, C. A.; Clarke, S., Farnesyl cysteine C-terminal methyltransferase activity is dependent upon the STE14 gene product in Saccharomyces cerevisiae. *Molecular and Cellular Biology* **1990,** *10* (10), 5071-5076.

11. Hrycyna, C. A.; Sapperstein, S. K.; Clarke, S.; Michaelis, S., The Saccharomyces cerevisiae STE14 gene encodes a methyltransferase that mediates C-terminal methylation of a-factor and RAS proteins. *EMBO J* **1991,** *10* (7), 1699-709.

12. Schubert, H. L.; Blumenthal, R. M.; Cheng, X., 1 Protein methyltransferases: Their distribution among the five structural classes of AdoMet-dependent methyltransferases. In *The Enzymes*, Elsevier: 2006; Vol. 24, pp 3-28.

13. Yang, J.; Kulkarni, K.; Manolaridis, I.; Zhang, Z.; Dodd, R. B.; Mas-Droux, C.; Barford, D., Mechanism of isoprenylcysteine carboxyl methylation from the crystal structure of the integral membrane methyltransferase ICMT. *Mol Cell* **2011,** *44* (6), 997-1004.

14. Diver, M. M.; Pedi, L.; Koide, A.; Koide, S.; Long, S. B., Atomic structure of the eukaryotic intramembrane RAS methyltransferase ICMT. *Nature* **2018,** *553* (7689), 526-529.

15. Bergo, M. O.; Leung, G. K.; Ambroziak, P.; Otto, J. C.; Casey, P. J.; Young, S. G., Targeted inactivation of the isoprenylcysteine carboxyl methyltransferase gene causes mislocalization of K-Ras in mammalian cells. *J Biol Chem* **2000,** *275* (23), 17605-10.

16. Bergo, M. O.; Gavino, B. J.; Hong, C.; Beigneux, A. P.; McMahon, M.; Casey, P. J.; Young, S. G., Inactivation of Icmt inhibits transformation by oncogenic K-Ras and B-Raf. *J Clin Invest* **2004,** *113* (4), 539-50.

17. Marin-Ramos, N. I.; Balabasquer, M.; Ortega-Nogales, F. J.; Torrecillas, I. R.; Gil-Ordonez, A.; Marcos-Ramiro, B.; Aguilar-Garrido, P.; Cushman, I.; Romero, A.; Medrano, F. J.; Gajate, C.; Mollinedo, F.; Philips, M. R.; Campillo, M.; Gallardo, M.; Martin-Fontecha, M.; Lopez-Rodriguez, M. L.; Ortega-Gutierrez, S., A Potent Isoprenylcysteine Carboxylmethyltransferase (ICMT) Inhibitor Improves Survival in Ras-Driven Acute Myeloid Leukemia. *J Med Chem* **2019,** *62* (13), 6035-6046.

18. Ahearn, I. M.; Siddiqui, F.; Abankwa, D.; Philips, M. R., NRAS is unique among RAS proteins in requiring ICMT for trafficking to the plasma membrane. *Life science alliance* **2021,** *4* (5).

19. Winter-Vann, A. M.; Baron, R. A.; Wong, W.; dela Cruz, J.; York, J. D.; Gooden, D. M.; Bergo, M. O.; Young, S. G.; Toone, E. J.; Casey, P. J., A small-molecule inhibitor of isoprenylcysteine carboxyl methyltransferase with antitumor activity in cancer cells. *Proc Natl Acad Sci U S A* **2005,** *102* (12), 4336-41.

20. Cantoni, G. L., Biological methylation: selected aspects. *Annual review of biochemistry* **1975,** *44* (1), 435-451.

21. Davis, T. D.; Kunakom, S.; Burkart, M. D.; Eustaquio, A. S., Preparation, Assay, and Application of Chlorinase SalL for the Chemoenzymatic Synthesis of S-Adenosyl-l-Methionine and Analogs. *Methods in enzymology* **2018,** *604*, 367-388.

22. Zhang, J.; Zheng, Y. G., SAM/SAH analogs as versatile tools for SAM-dependent methyltransferases. *ACS chemical biology* **2016,** *11* (3), 583-597.

23. Ferreira de Freitas, R.; Ivanochko, D.; Schapira, M., Methyltransferase Inhibitors: Competing with, or Exploiting the Bound Cofactor. *Molecules* **2019,** *24* (24), 4492.

24. Griggs, A. M.; Hahne, K.; Hrycyna, C. A., Functional oligomerization of the Saccharomyces cerevisiae isoprenylcysteine carboxyl methyltransferase, Ste14p. *Journal of Biological Chemistry* **2010,** *285* (18), 13380-13387.

25. Romano, J. D.; Michaelis, S., Topological and mutational analysis of Saccharomyces cerevisiae Ste14p, founding member of the isoprenylcysteine carboxyl methyltransferase family. *Mol Biol Cell* **2001,** *12* (7), 1957-71.

26. Diver, M. M.; Long, S. B., Mutational analysis of the integral membrane methyltransferase isoprenylcysteine carboxyl methyltransferase (ICMT) reveals potential substrate binding sites. *J Biol Chem* **2014,** *289* (38), 26007-20.

27. Hahne, K. J., Characterization of the hydrophobic binding site of isoprenylcysteine carboxyl methyltransferase. **2012**.

28. Court, H.; Hahne, K.; Philips, M. R.; Hrycyna, C. A., Biochemical and Biological Functions of Isoprenylcysteine Carboxyl Methyltransferase. *The Enzymes* **2011,** *30*, 71-90.

29. Anderson, J. L.; Frase, H.; Michaelis, S.; Hrycyna, C. A., Purification, Functional Reconstitution, and Characterization of the Saccharomyces cerevisiae Isoprenylcysteine Carboxylmethyltransferase Ste14p*♦. *Journal of Biological Chemistry* **2005,** *280* (8), 7336-7345.

30. Romano, J. D.; Schmidt, W. K.; Michaelis, S., The Saccharomyces cerevisiae prenylcysteine carboxyl methyltransferase Ste14p is in the endoplasmic reticulum membrane. *Mol Biol Cell* **1998,** *9* (8), 2231-47.

31. Anderson, J. L.; Henriksen, B. S.; Gibbs, R. A.; Hrycyna, C. A., The isoprenoid substrate specificity of isoprenylcysteine carboxylmethyltransferase: development of novel inhibitors. *Journal of Biological Chemistry* **2005,** *280* (33), 29454-29461.

32. Perez-Sala, D.; Gilbert, B. A.; Tan, E. W.; Rando, R. R., Prenylated protein methyltransferases do not distinguish between farnesylated and geranylgeranylated substrates. *Biochemical Journal* **1992,** *284* (3), 835-840.

33. Hahne, K.; Vervacke, J. S.; Shrestha, L.; Donelson, J. L.; Gibbs, R. A.; Distefano, M. D.; Hrycyna, C. A., Evaluation of substrate and inhibitor binding to yeast and human isoprenylcysteine carboxyl methyltransferases (Icmts) using biotinylated benzophenone-containing photoaffinity probes. *Biochemical and biophysical research communications* **2012,** *423* (1), 98-103.

34. Tang, H.-Y.; Speicher, D. W., Identification of alternative products and optimization of 2-nitro-5-thiocyanatobenzoic acid cyanylation and cleavage at cysteine residues. *Analytical biochemistry* **2004,** *334* (1), 48-61.

35. Lu, H. S.; Gracy, R. W., Specific cleavage of glucosephosphate isomerases at cysteinyl residues using 2-nitro-5-thiocyanobenzoic acid: analyses of peptides eluted from polyacrylamide gels and localization of active site histidyl and lysyl residues. *Archives of Biochemistry and Biophysics* **1981,** *212* (2), 347-359.

36. Vervacke, J. S.; Funk, A. L.; Wang, Y.-C.; Strom, M.; Hrycyna, C. A.; Distefano, M. D., Diazirine-containing photoactivatable isoprenoid: synthesis and application in studies with isoprenylcysteine carboxyl methyltransferase. *The Journal of organic chemistry* **2014,** *79* (5), 1971-1978.

37. Hou, Z.; Stapels, S. E.; Haska, C. L.; Matherly, L. H., Localization of a substrate binding domain of the human reduced folate carrier to transmembrane domain 11 by radioaffinity labeling and cysteine-substituted accessibility methods. *Journal of Biological Chemistry* **2005,** *280* (43), 36206-36213.

38. Tang, H. Y.; Speicher, D. W., In vivo phosphorylation of human erythrocyte spectrin occurs in a sequential manner. *Biochemistry* **2004,** *43* (14), 4251-62.

39. Baron, R. A.; Casey, P. J., Analysis of the kinetic mechanism of recombinant human isoprenylcysteine carboxylmethyltransferase (Icmt). *BMC biochemistry* **2004,** *5* (1), 1-12.

40. Shi, Y.-Q.; Rando, R. R., Kinetic mechanism of isoprenylated protein methyltransferase. *Journal of Biological Chemistry* **1992,** *267* (14), 9547-9551.

41. Muting, D.; Kaiser, E., Quantitative estimation of α-amino N in biological material by the ninhydrin reaction. *Hoppe-Seyler's Zeitschrift fur physiologische Chemie* **1963,** *332*, 276-281.

42. Elble, R., A simple and efficient procedure for transformation of yeast. *Bio Techniques* **1992,** *13*, 18-20.

43. Schaffner, W.; Weissmann, C., A rapid, sensitive, and specific method for the determination of protein in dilute solution. *Analytical biochemistry* **1973,** *56* (2), 502-514.

44. Swain, M.; Ross, N. W., A silver stain protocol for proteins yielding high resolution and transparent background in sodium dodecyl sulfate-polyacrylamide gels. *Electrophoresis* **1995,** *16* (1), 948-951.

CHAPTER 4. THE ROLE OF METHYLATION IN THE REGULATION OF KRAS4B DISTRIBUTION AND ACTIVITY

4.1 Preface

In the wake of the COVID-19 pandemic in the Spring of 2020 and in accordance with the Indiana State Governor's Stay-at-Home-Order, Purdue University moved to remote work for all personnel except those designated as essential. This halted all in-lab research experiments for about three months. During that time, the Hrycyna Lab pivoted to remote data analysis and exploring new experimental avenues and ventures for the lab. This enabled exploration, review, and discussion of well-characterized research of a main protein of study in the lab, isoprenylcysteine carboxyl methyltransferase (Icmt).

Icmt modifies various proteins that are implicated in many disease pathways. Most notable of these proteins are all Ras protein isoforms. I have always been interested in studying oncogenic pathways, which is one of the reasons I initially joined the Hrycyna Lab. During the period of the Stay-At-Home-Order, I specifically explored how Icmt affects Ras isoform KRas4B. Our lab is rooted in chemistry, allowing for the study of the catalytic mechanism of Icmt at the amino acid level. Previous lab members have extensively and meticulously studied the structure, mechanism, and activity of Icmt, permitting me to consider a broader question of the connection between molecular features of Icmt and global cellular and tissue-level outcomes. It is known that Icmt inhibition causes the mislocalization of KRas4B from the plasma membrane, however the canonical immunofluorescence localization studies performed by Bergo *et al.* (2000) show a significant amount of KRas4B still at the plasma membrane. My ideas were fueled by a curiosity about how to reconcile the partial mislocalization with dramatic signaling defects. To better understand the relationship between molecular fingerprints, localization, and signaling, we sought to provide a comprehensive model for Ras methylation as a regulator of its behaviors. Therefore, a collaboration between the Hrycyna Lab and Low-Nam lab was formed to provide an interdisciplinary perspective on this challenging question.

This chapter will discuss our efforts to leverage our structural insights with a new workflow for mapping KRas4B genotype and post-translational modification to the downstream responses of MAPK activation and cell crawling, called impulse-response functions. The preliminary data we have generated creates the springboard to gain a more holistic understanding of Ras translation,

trafficking, and signaling, as well as nodes for therapeutic targeting. Our primary finding that TM2 and loop 2 bear key residues for substrate recognition and binding suggest a candidate interface for small molecule inhibitor development.

Here, I will discuss new methodology in targeting Icmt and propose assays that can be used to not only assess changes in catalytic activity of Icmt, but also monitor the cellular-level effects on Ras, as a function of clinically relevant mutations. These studies will not only allow for better understanding of Ras signaling as a function of methylation and better design of Icmt inhibitors, but may have large implications on an endogenous regulation pathway of KRas4B that has always been speculated, but never identified.

4.2 Background

KRas4B was first molecularly characterized in the 1970s and has since been extensively studied for its role in oncogenesis.[1] Out of the four total Ras isoforms, it alone contributes to over 80% of all cancer causing Ras missense mutations.[2, 3] Despite the substantial resources invested in studying Ras proteins, no direct inhibitor of KRas4B had been deemed an effective enough treatment for approval by the Food and Drug Administration (FDA) until May of 2021 – thus leading to its classification as "undruggable."[3-7]

Ras proteins are small GTPases that signal from the plasma membrane to regulate many signaling pathways including cell growth, differentiation, proliferation and survival.[4, 7] The pathways downstream of KRas4B activation are well characterized and have served as potential sites for indirectly inhibiting oncogenic KRas4B function. Approaches have focused on both the protein effectors of Ras as well as the upstream protein processing pathway required for proper cellular translocation and signaling of Ras.[7-15] Through this research, they have also found that different mutations of KRas4B are prevalent in different cancer types and also have different modes of action within KRas4B oncogenic signaling.[16-18] Attempts at characterizing the specific mutants aided in the discovery and potency of the newly FDA approved drug, sotorasib (Lumakras™), as it only abates activity in G12C mutated KRas4B.[19-21] Currently, there is a need to further define these mutations, as more individualized treatments are proving to be the most successful within cancer.

In a recent proteomics study, all forms of KRas4B present in human colorectal cells and tumors were profiled.[22] Interestingly, two different patient samples containing amounts of G13D

mutated KRas4B had different amounts of methylated versus unmethylated KRas4B (18% and 79% methylated respectively). In another patient sample also harboring wild-type (WT) and G12V mutated KRas4B, there were differences in methylation of KRas4B between the isoforms; 49% of WT KRas4B was methylated and 9% of KRas4B^{G12V} was methylated. Methylation is the final post-translational modification (PTM) of KRas4B processing and is required for proper plasma membrane localization and subsequent signaling.[23-27] It is also the only reversible step of the PTM processing pathway and is performed by a single known methyltransferase, isoprenylcysteine carboxyl methyltransferase (Icmt).[24, 28-32] For this reason it has been speculated, but never confirmed, that methylation has a regulatory role in Ras and other CAAX proteins. Taken together with the differing methylation states of KRas4B in colorectal cancer samples, there is further indication of a regulatory role of methylation, which may be different between different KRas4B mutants as well.

Methylation is not only known to be important for plasma membrane localization of CAAX proteins but also in their protein-protein interactions. Recently, phosphodiesterase-δ (PDEδ or PDE6δ) interactions with KRas4B have been implicated in the methylation state of KRas4B.[33] PDEδ was initially known as the δ-subunit of photoreceptor diesterase which is involved in the phototransducin pathway.[33] However, more recently it has been known to bind prenylated proteins and in the case of KRas4B, aid in its spatial organization throughout the cell.[34-36] Dharmaiah *et al* (2016) showed that PDEδ not only requires the isoprenoid of CAAX proteins to form an interaction, but the methyl group increased the binding affinity of KRas4B and PDEδ by a factor of 40.[33]

Since the discovery of Icmt and subsequent identification of Ras as a substrate, it has been widely studied for its implications in KRas4B cellular mislocalization experiments. In combination with immunoblot detection of activation of proteins downstream of Ras signaling, this is the main mode of analysis for new Icmt inhibitors that act as indirect inhibitors of KRas4B oncogenic signaling. However, the majority of these studies fail to study KRas4B at endogenous levels of expression.[11, 14, 15, 26, 37-40] Overexpression systems have been utilized to enhance the threshold detection within experiments but without consideration of the cellular exhaustion of resources, overloading of signaling pathways, and cellular regulation disruption that these systems are causing and by default, do not produce results that best represent the natural state of KRas4B.[41]

Thus, our goal is to better understand the role of methylation as a possible regulator in KRas4B signaling within endogenous expression systems of the protein (Figure 4.1).

4.3 Experimental Methodology

To better understand the possible role of methylation as a regulator of CAAX proteins and their signaling pathways, we will first focus on the effects of methylation on KRas4B signaling within endogenous expression systems of the protein. KRas4B serves as our model CAAX protein for methylation studies, as it is the only isoform of Ras that does not get further modified after methylation by the addition of a palmitoyl group.[42, 43]

Within our main goal, we have the following questions (as stated in the Chapter 1):

- What are the effects of methylation on endogenous KRas4B?
- Can KRas4B be at the plasma membrane when unmethylated?
- Are all cells responding uniformly to Icmt inhibition?
- Can unmethylated KRas4B propagate a signal

This section will seek to explain the experiments and methodologies under development that will be employed in the future to answer these questions (Figure 4.2).

4.3.1 Icmt inhibition

Icmt is the sole methyltransferase that acts on KRas4B and will be the point of inhibition to study the effects of KRas4B methylation states on its cellular distribution and signaling. Multiple methods will be taken to inhibit Icmt including small interfering RNA (si-RNA) and known small molecule inhibitors.

Of the published small molecule inhibitors, cysmethynil is the most well characterized and widely used.[14] However, it has very low solubility and bioavailability compared to newer compounds. The newest class of inhibitors revealed a compound (UCM-13207 or compound 21) to have an IC_{50} of 1.4 μM.[44] Although this inhibitor was designed as a therapeutic for progeria disorders, it showed promise for clinical use after sensitivity *in vitro* and *in vivo*. It also showed mislocalization of Ras with well documented experimental parameters that could be modified and implemented within our study. Although not commercially available, this compound requires a two-step synthesis of picolinic acid and a prenylated precursor molecule. The precursor can be

synthesized based on a previous publication using N-pheylacrylamide and octylamine as starting material and in combination with dry acetonitrile and DBU was synthesized in 16 hours.[15] Based on the reaction criteria, it may be a molecule that our lab can synthesize in-house for use in this study.

4.3.2 Plasma membrane localization of endogenous KRas4B

In this research, KRas4B will serve as the model protein for methylation. The vast research on KRas4B localization studies mostly employ the transfection of engineered GFP-KRas4B plasmids into cells to elicit large, detectable levels of KRas4B. However, our research seeks to study the effects of methylation on endogenous levels of KRas4B. To accomplish this within such systems, immunofluorescence is required using fluorescently conjugated antibodies specific to KRas4B. Unfortunately, the identifying feature of each isoform is the small, 25 residue, C-terminal hypervariable regions of Ras.[42, 43] Nonspecific binding of otherwise isoform specific Ras antibodies, has been a concern and roadblock for many researchers since all mammalian cells express all isoforms of Ras.[18, 45] To specifically measure the localization of the KRas4B isoform, our research study will use isogenic cell lines of wild-type and oncogenic mutations specific KRas4B variants.

The mouse embryonic fibroblasts (MEFs) produced by the Barbacid Lab and commercially available through the National Cancer Institute (NCI) are Ras-less with a floxed KRas gene.[46, 47] This allows for the expression of KRas4B specific variants or truly Ras-less cells that contain hyperactive, V600E mutated BRaf for cell survival. With only one isoform of Ras present, we can better determine the effects of methylation on cellular localization of KRas4B as well as other cellular outputs. Therefore, all future experiments will be performed on these isogenic MEF cells.

Confocal microscopy will be useful in differentiating the cellular plasma membrane (PM) from other portions of the cell and has been a common microscopy method for previous Ras localization studies.[14, 15, 44] Differing from other studies, KRas4B PM localization will be quantified. This will require an irreversible, fluorescent PM stain. We will also perform the quantification at the single-cell level to better understand the distribution of methylations effects. It has been shown that populational averages are not always in agreement with single-cell distributions and qualitative dynamics, especially within the pathways we will study here.[48, 49] This

will be in combination with more classical localization methods, including subcellular fractionation and western blotting, which will give population averages of cell lysate samples.

4.3.3 KRas4B activation state at the plasma membrane

Ras is implicated in multiple pathways. Its activity within those pathways can be measured directly by determining its nucleotide-binding state or indirectly by measuring activation of proteins downstream of Ras signaling. Classical analyses of Ras activation include immunoblot visualization of activated proteins downstream of Ras signaling such as MEK, ERK, and Akt. More recent research has utilized a Ras-GTP pull-down assay to determine activity state.[15] This employs the use of the Ras binding domain (RBD) of direct downstream effector protein, cRaf. If KRas4B is in its active (GTP-bound) within cell lysates, upon incubation with cRaf RBD conjugated to agarose beads, GTP-bound Ras will associate with the Raf RBD and can be pulled out of solution through the agarose beads. Immunoblotting visualization within the pull-down samples will determine if Ras was active within these samples. However, these studies and the immunoblot analysis of downstream effector activation, provide global and population averages of thousands of cells from cell lysates. They also cannot state that the activity profiles obtained by these methods are of KRas4B localized to the PM unless they subfractionate the cell lysates prior to experimentation. Cell-to-cell analysis will aid in better understanding if the observed phenotypes are consistent from cell to cell or if some cells have very large populations of active KRas4B and thus produce higher overall averages within western blots.

Our research will use a direct activity measurement of KRas4B which also applies the RBD of Raf. Developed by the Groves Lab, the RBD is conjugated to a fluorophore and can detect single molecule recruitment of each individual RBD to the PM.[50] This will give us very discrete information about the levels of activated Ras at the plasma membrane as well as the duration of their activity. Total internal reflection fluorescence (TIRF) microscopy should be used for this type of analysis. Dr. Shalini T. Low-Nam has already obtained KRas4B activity states for different KRas4B oncogenic variants (Q61L and G12V) within the isogenic MEF line we will be employing (unpublished).

Ras nanoclusters at the plasma membrane

Activated, GTP-bound Ras molecules are known to cluster along the plasma membrane for signal propagation through the MAPK pathway.[51, 52] [53] These clusters contain about 7 individual Ras proteins and are sites of Raf activation and heightened signaling. Interestingly, in the KRas4B proteomics analysis performed by Ntai *et al.* (2018) within colorectal tumor samples that contained both WT and G13D mutated KRas4B, only 11% and 29% of the overall KRas4B protein was mutated for two patient samples respectively. This may suggest that only a small number of mutated KRas4B is required to cause large scale downstream signaling effects.

The Ras RBD, described above, can be implemented to help understand if mutant KRas4B cells contain only a few or a large distribution of KRas4B nanoclusters. It is possible that from the study by Ntai *et al.* (2018) all cells contained similar, low amounts of mutated KRas4B nanoclusters that were able to propagate oncogenic pathways at a large scale collectively, or some cells contained larger amounts of KRas4B nanocluster, while others did not. This information will provide useful in understanding if only a few molecules of KRas4B are required to have considerable downstream signaling effects, which can be monitored using the kinase translocation receptor (KTR) experimentation described below. Preliminary data from Dr. Shalini T. Low-Nam utilizing the Ras RBD technology, suggests that the distribution and dwell time of active KRas4B at the plasma membrane differs between WT and mutated KRas4B (unpublished). Furthermore, the results differ between different KRas4B oncogenic variants. Implementation of an Icmt inhibitor within these studies, will help us to better understand if methylation affects active KRas4B distribution and PM dwell time compared to the previously obtained preliminary data by Dr. Low-Nam.

4.3.4 KRas4B activation of downstream protein effectors

As stated above, classical analyses of Ras activation include immunoblot visualization of activated proteins downstream of Ras signaling. More specific, cell-to-cell analyses can be performed to better understand if unmethylated Ras is still activating downstream proteins in the signaling pathway. Previously established kinase translocation reporters (KTRs) use phosphorylation to initiate a nucleocytoplasmic shuttling event in response to ERK activation for single-cell quantitation .[48] ERK is a downstream effector of Ras signaling. Its translocation into

the nucleus after activation, is one of the last steps of the MAPK pathway. The ERK KTR has five engineered components; the docking site which allows the protein of interest to recognize the KTR; the nuclear export sequence (NES); the nuclear localization sequence (NLS); and the phosphorylation site, which determines the nuclear translocation; and a fluorescent tag for quantitative measurement. KTRs will be phosphorylated by active ERK, which remains in the nucleus when active. In order for KTRs to be available within the nucleus, the NLS must be exposed, and thus the KTR must be dephosphorylated. Once within the nucleus, active ERK can bind the ELK docking site, phosphorylate the KTR, and cause the NES to be exposed. The KTR will then translocate out of the nucleus and the cytosol will contain the fluorescent signal. If ERK is inactive, the KTR cannot be phosphorylated, leaving the NLS exposed and fluorescence signal restricted within the nucleus.

Dr. Shalini T. Low-Nam has obtained preliminary data of KRas4B downstream signaling by way of ERK KTR reports for different KRas4B oncogenic variants (Q61L and G12V) within the isogenic MEF line we will be employing (unpublished). These data suggest that the duration of activation differs between WT and mutated KRas4B cells. It also suggests differences between the different KRas4B oncogenic mutants as well as cell to cell differences. This information, in combination with the preliminary results from the Ras RBD studies (described above), highlight the importance in understanding if KRas4B requires a large distribution or small hotspots of nanoclusters to elicit a large downstream response at the single-cell level. In combination with an Icmt inhibitor, these studies would further define the role of methylation in active KRas4B PM distribution and downstream signal propagation.

4.3.5 Effects of methylation on cell migration

KRas4B is not only implicated in the MAPK pathway, but also the phosphatidylinositol-3-kinase (PI3K) pathway (Figure 4.1). When associated with Ras, PI3K adds a phosphate to phosphatidylinositol (4,5) di-phosphate (PIP_2) to produce secondary messenger phosphatidylinositol (3,4,5) tri-phosphate (PIP_3). This pathway is involved in cell growth, differentiation, proliferation and cellular motility.[54, 55] To measure the impacts of methylation across longer length and time scales, we can monitor MEF crawling behaviors which may provide insights into metastatic transformations in signaling behaviors.

For our study, we will refer to an impulse-response (I-R) function to measure discrete inputs (impulses) detected by living cells and map these to behavioral changes (responses).[56] Borrowing from the signal processing literature, this is a recent development to extrapolate signal integration mechanisms from direct observation of inputs that are detected and processed into a downstream outcome.[56] The strength in the approach is in mapping how single cells undergo decision-making processes and accesses both successful and failed responses without the need to measure all proteins involved. Impulses can include Icmt inhibitors or stimulation of Ras-involved pathway activation by the addition of epidermal growth factor (EGF). In the case of a model for oncogenic spread, the response corresponds to the distance and speed of individual cells crawling across a field of view. This approach enables measurement of how even subtle stimuli/inputs, such as adding a methyl group to a protein, effect macroscopic cellular changes.

Ras activation of PI3K requires Ras to be at the plasma membrane as the interaction between the two proteins is fairly weak (high μM range). Ras being localized to the PM will place it into close proximity with PI3K and thus stabilize their interaction.[55] Methylation has been known to regulate chemotaxis of bacteria and leukocytes but utilizes other soluble methyltransferases.[57, 58] It will be interesting to better understand if methylation of CAAX proteins has a similar regulatory role.

In addition to Ras, other CAAX proteins have a role in cellular chemotaxis. GTPases, RhoA and Rac1 are two such molecules that have direct roles in actin organization and cell migration.[59, 60] Within MDA-MB-231 breast cancer cells, methylation was shown to alter cellular migration, adhesion and spreading through RhoA and Rac1. Upon Icmt inhibition with cysmethynil, the actin cytoskeleton was disrupted as well as the ability of Rho and Rac1 to be activated through thrombin and EGF stimulation. This is thought to be caused by unmethylated Rac1 and Rho proteins increasing their association with RhoGDI, which binds Rho and Rac1 in their inactive, GDP-bound states.[61] GDIs are thought to aid in the dissociation of Rho and Rac1 from cellular membranes and also sequester the proteins away from the activating GEFs.

With this information, it will be important to better characterize the effects of methylation on cellular migration in different cell cancer lines, as well as different KRas4B mutant states, as it is known that different Ras variants have differing metastatic mechanisms (see section below).

4.3.6 Mutant specific profiling

Ras mutations are mostly gain-of-function mutations within three different codon hotspots for residues Gly12, Gly13 and Gln61.[62] However, their mechanisms in increasing Ras signaling are not the same. As previously described in Chapter 1, these mutational hotspots have different implications in the rates of intrinsic and GAP-mediated GTP hydrolysis, nucleotide exchange, and binding affinities for GTP and effector proteins.[17, 63] It will be interesting to study how the methylation state of Ras affects the outputs of these different mutational hotspots.

Interestingly, not only are the mechanisms of these mutations different in their respective activation of Ras oncogenic signaling, but also the oncogenic features of cancers harboring specific mutants are different. Some cancers are more invasive and spread faster, while others have softer or more stiff tumor phenotypes.[64-67] Therefore, it will be important to utilize the I-R function to not only study the role of methylation in KRas4B activation, but more macroscopic analyses of the role of methylation in the invasiveness of each type of cancer or KRas4B variant. Response functions for studies on invasiveness can include cell crawling (as described above) and cellular adhesion. Another thing to consider is the surrounding environment in which tumors grow and metastasize. For oncogenesis, most of these environments are more rigid or stiff, allowing cells to have more contact.[64, 67] We can also simulate different environments in terms of stiffness (impulse) to study the different migration rates and adhesion (responses) with respect to each KRas4B variant.

The isogenic, Ras-less MEFs (described above), not only express only KRas4B but also express the different oncogenic variants of the protein within individual cell lines. We will utilize these cells within our study to comprehensively analyze the effects of methylation on each variant. Therefore, each variant will be studied and compared in each of the experiments described above.

4.4 Methods

4.4.1 Preparation of cell lysates

Previously plated MEF in a 6-well plate were grown to desired confluence or density. They were rinsed with cold, 1X phosphate-buffered saline (PBS). 100 µL of RIPA lysis buffer (50mM Tris-HCl (pH 8.0), 150 mM NaCl, 1% IGEPAL®, 0.1% sodium dodecyl sulfate (SDS), and 0.5% sodium deoxy) was added to each well per $1x10^6$ cells. Adherent cells were removed from dish

with cell scrapers and the suspension was transferred to an Eppendorf tube. Cells were agitated on rotator for 30 min. at 4ºC followed by pelleting at 12,000 rpm for 20 min at 4ºC. Supernatant was used for subsequent Bradford assay or immunoblot analysis.

4.4.2 Bradford

The following method is based on the manufacturer's protocol for the Pierce Coomassie Plus (Bradford) Assay Reagent from Thermo Fisher Scientific with the following modifications. A standard curve of 0, 0.25, 0.50, 1.0, 2.5, 5., 7.5. 10.0, and 2.0 µg BSA were made through serial dilutions with deionized, distilled water (ddH_2O), on a 96-well plate. Cell lysates of about 200,000 cells per sample were prepared as described above. To keep cell lysate protein concentration high and sample volume low, cells were plated in multiple well of a 6-well plate and 200 µL of lysis buffer was added to the first well. Once lysed as described above, the lysate was used to lyse the cells of the next well, thus combining cell lysate into the minimal volume possible. 10 µL of each sample were diluted in half. 200 µL of Pierce Coomassie Plus (Bradford) Assay Reagent (Thermo Fisher Scientific, Waltham, MA) was added to each sample including the BSA standard curve. Absorbances were measured at 595 nm on a Synergy H4 microplate reader (Agilent Biotek, Santa Clara, California). If the lysate samples were above the 2.0 µg BSA absorbance at 595nm, the sample was further dilute by a factor of 5.

4.4.3 Immunoblots of protein expression in cell lysate

Prepared cell lysates (previously described) were added to an SDS-loading buffer (2X SDS-loading buffer final concentration). They were resolved on a 10% SDS-PAGE gel, run at 165V in TGS buffer and transferred to nitrocellulose paper in TG buffer at 100V for 90 min. The nitrocellulose was blocked overnight in 20% (w/v) dry milk in PBST at 4ºC. β-actin rabbit monoclonal antibody was probed at ratio of 1:1000 in 5% (w/v) milk in PBST for 2 hours at room temperature (Cell Signaling Technologies, Danvers, MA). Icmt was probed with a rabbit α-Icmt polyclonal antibody (1:300) in 5% (w/v) dry milk in PBST for 2 hours at room temperature (Bioss, Woburn, MA). Both β-actin and α-Icmt primary antibodies were followed by 3, 10-minute washes with PBST and goat α-rabbit IgG-HRP (1:10,000) in 5% (w/v) dry milk in PBST. A number of

different pan-Ras and KRas4B specific antibodies were tested; information is denoted in the figure legend

4.4.4 Immunoblots of protein expression in cell lysate

MEFs grown in high glucose Dulbecco's modified eagle's media (DMEM) (Gibco, Waltham, MA) supplemented with 10% heat-inactivated fetal bovine serum (FBS), 1% penicillin streptomycin (Gibco), and 100X pyruvate (Gibco) at 37ºC and 5% CO_2. Plated ~ 50,000 cells to each coverslip the night before for desired confluency within 24 or 48 hours. Cells were plated in phenol-free media with the same components as above. Cells were stained with fluorophore-conjugated antibodies in 1X PBS for each respective experiment (details in figure legends). Cells were blocked with 1 mL FBS or fish skin gelatin for 5 min, fixed with 2% paraformaldehyde (PFA) for 5 min., and permeabilized with 0.1% Triton X-100 for 1-2 min and then stained with fluorophore-conjugated antibodies. Specific antibodies and conditions specified in figure legends. The coverslips were rinsed with 1X PBS between every step. Coverslips were mounted with ProLong™-Gold Antifade Mountant with DAPI (Thermo Fisher, Waltham, MA) and stored at 4ºC in the dark. Samples were then imaged through confocal microscopy using the Nikon A1R-MP in the Purdue Imaging Facility (PIF) or the following instrument located in the Low-Nam Lab: Ti2-E Nikon Eclipse inverted fluorescence microscope system that is equipped with TIRF objectives, a Perfect Focus system, and stabilization table. 405, 488, 461, and 640 nm laser lines are couples into a single optical fiber with achievable power densities in the MW range. A quad-color excitation cube is also installed. Widefield imaging is possible by an LED (X-Cite) lamp and excitation filters (405, 488, 561, 640 nm). A reflection interference contrast (RICM) excitation cube is also equipped. A motorized mirror is used rapid switching between laser and lamp excitation. A diascopic lamp provides brightfield capacity. Clean-up filters are positioned in front of the detector for elimination of non-specific emission signals. Data are captured on an EM-CCD (Andor iXon Life). All components are integrated and controlled by Nikon Elements software.

4.4.5 Icmt siRNA treatment of MEFs

MEFs were plated for a final amount of $1x10^6$ cells when lysed in DMEM media with 10% FBS, 1% penicillin streptomycin and 100X pyruvate. 125 pmol of *Icmt* specific siRNA (s204160,

Thermo Fisher, Waltham, MA) was plated per well in a 6-well plate based on the manufacturer's protocol with differing ratios of transfection agent polyethylenimine (PEI) to RNA. Control experiments contained 125 pmol Silencer Select Negative Control No.1 siRNA (Thermo Fisher, Waltham, MA). Opti-MEM™ I Reduced Serum Medium (Gibco, Waltham, MA), PEI and siRNA were first mixed in an Eppendorf tube (in that order) and incubated at room temperature for 10-15 min. Complete sample was added to cells in a dropwise fashion. Cells were incubated for prescribed siRNA treatment time (72 or 96 hours) at 37ºC, 5% CO_2. Cells were then lysed and analyzed through immunoblotting as described above.

4.4.6 Cell migration

MEFs were plated onto glass coverslips for a final maximal confluence of ~50% in phenol-free DMEM with 10% FBS, 1% penicillin streptomycin and 100X pyruvate and incubated at 37ºC and 5% CO_2. If testing under starvation conditions, media was changed after 1-2 hours incubation to phenol-free, FBS-free media and incubated overnight. Coverslips were loaded onto the Ti2-E Nikon Eclipse microscope and configured RICM and brightfield imaging every 15 min. over a period of 24 hours. The microscope additionally contained a stage incubator to keep the cells in an environment of 37ºC and 5% CO_2. Cellular migration was measured for each 15-minute timepoint using home written software in MATLAB.

4.5 Results and discussion

The goal of this research is to better understand the possible regulatory role of methylation in the localization and signaling of KRas4B. Herein, the framework for experiments have been rationalized and described and for some, primarily implemented. MEF containing various KRas4B oncogenic mutations were first analyzed for their endogenous Ras expression. We were able to detect very low levels of WT-KRas4B after trying various combinations of a panel of Ras specific antibodies and also confirmed that the $BRaf^{V600E}$ KRas-null MEFs indeed do not contain Ras. However, detection methods will need to be optimized, as yet they have not been reproduced (Figure 4.3A). Ras antibodies have a reputation of difficulty in immunoblotting and immunofluorescence experiments. It is recommended to load between 20 and 40 μg of cell lysate in order to visualize Ras through western blotting, which is a larger amount for protein detection.[45]

Since we are utilizing KRas4B MEFs with an isogenic background, we can use a combination of Ras antibodies that are specific to KRas4B or can bind all four isoforms. Our initial success was with the KRas4B specific monoclonal antibody from Sigma-Aldrich (WH0003845M1) that was previously recommended.[45] However, we tested over three different Ras antibodies. Icmt expression levels were also visualized (~32 kDa), but contain a lot of background and nonspecific binding and also have not been reproduced (Figure 4.3B). We also could not confirm silencing of *Icmt* with its specific siRNA. We tried to optimize the conditions, however could not visualize the western blots due to optimization efforts with the antibodies.

In addition, immunofluorescence experiments were optimized for antibody combinations. A pan-Ras antibody primarily conjugated to Alexa-Fluor 555 (64520, Cell Signaling Technology, Danvers, MA) showed Ras labeling within WT MEF however, there was very high background labeling (data not shown). Less background was seen with monoclonal pan Ras antibody (MA1-012, Thermo Fisher) in combination with donkey α-mouse-Alexa 555 (A-31570, Thermo Fisher) or goat α-mouse-Alexa 555 (A-21422, Thermo Fisher) when the image contrast was increased to maximal amounts (Figure 4.4A). This is acceptable for single wavelength images, however in combination with other fluorophores, the contrast of those images will have to be increased similarly. Our experiments will combine a plasma membrane stain as well as fluorophores targeting Ras, and therefore the fluorescence intensity of Ras should be increased. To decrease background fluorescence, we switched from blocking the samples with FBS to blocking with fish skin gelatin, since it does not contain IgG or serum proteins (Biotium manufacturer information). We also tested the fluorescently-conjugated secondary antibodies listed above alone with MEF to determine if they were contributing to the non-specific binding, but they did not show any indication of non-specific binding to cells, however they did bind the glass. We then decided to flame the coverslips and store them in ddH_2O and this reduced the background fluorescence slightly.

We also began optimizing the membrane stain MemBrite™ Fix488/515 Dye (30093A, Biotium). We were able to label the cell membranes but were not able to keep the dye from permeabilizing into the endomembrane systems of the cell (Figure 4.4B). Fixing performed by PFA was more suitable than fixing under methanol conditions however we decreased the PFA percentage to 2% PFA incubated for 5 minutes. Permeabilization was also optimized to 01%

Triton X for 1 to 2 minutes to reduce the holes within the cell membrane, and thus the intercalation of the plasma membrane dye.

Preliminary cell migration data was also collected for WT, G12D and G13D mutated KRas4B MEFs. Surprisingly, WT MEFs moved the fastest, followed by G12D, with G13D moving the slowest (Figure 4.5). Finishing the panel of KRas4B mutants (G12V and Q61L), as well as testing them under starved and stimulated conditions will be the next steps before introducing an Icmt inhibitor.

The research proposed here along with previously determined structural insights of Icmt provide a comprehensive methodology to interrogate the possible regulatory role of methylation through Icmt. To date, there are very few comprehensive studies that span orders of magnitude in space and time, from methylation to cellular signaling outputs, particularly at the single-cell level. Methylation has been speculated to have a regulatory role, as it is the only reversible post-translational modification of the CAAX processing pathway.[24, 28, 29, 57] Although other CAAX proteins undergo further PTMs after methylation, it is a wonder why the addition of such a small molecule has implications in plasma membrane localization, protein activity, and protein-protein interactions.[24, 33, 68] Furthermore, the use of SAM as a methyl donor is energetically costly to a cell, as it requires a molecule of ATP to synthesize a molecule of SAM.[69] This research could further be used to design methylation sensors that expand upon existing approaches for nucleic acid-methylation detection. This would allow detection and tracking of various methylated proteins throughout the cell. Methylation may be a small player, but could have an enormous role in not only the endogenous regulation of cell signaling but also as a point of tunability for future research and therapeutics within these pathways. Icmt is the sole methyltransferase known to act on CAAX proteins, and thus presents itself as a very specific target in small molecule drug design. The structural information of Icmt discovered in Chapter 2 combined with the preliminary data of this chapter, have laid a solid foundation for the implementation and success of this project.

4.6 Figures

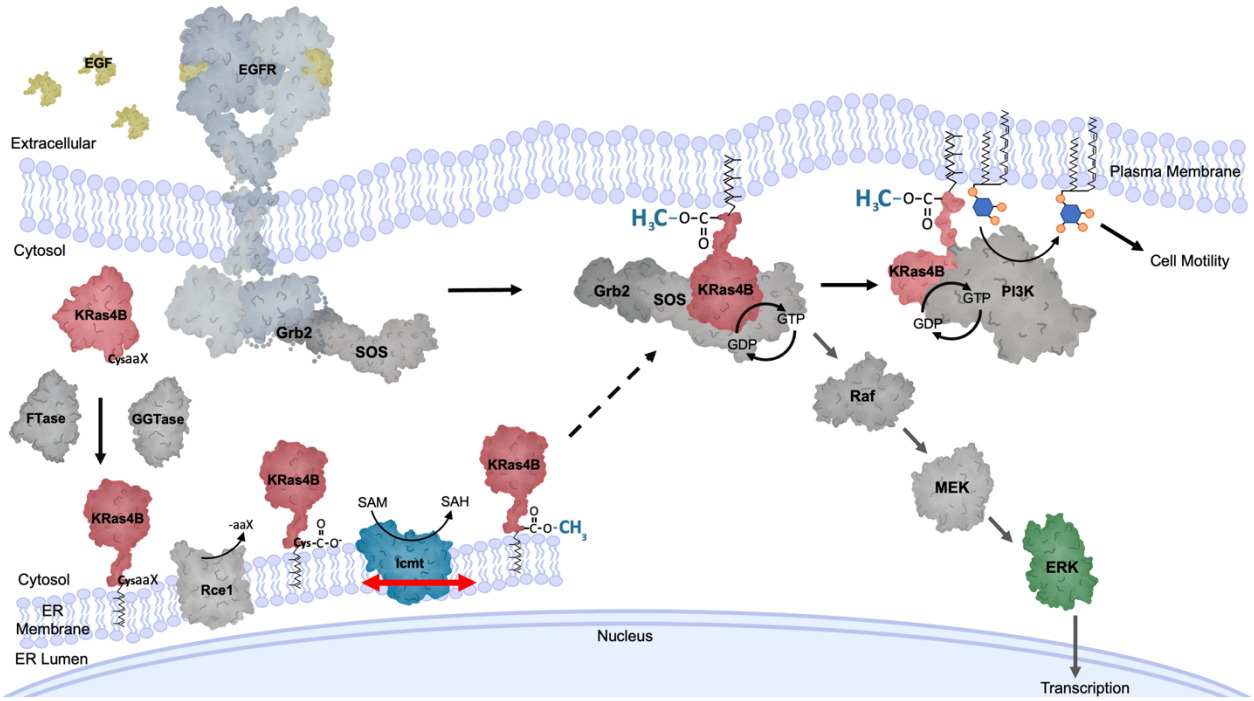

Figure 4.1 KRas4B post-translational modifications and signaling cascade.

Canonical KRas4B signaling begins with extracellular EGF binding EGFR. This causes dimerization and recruits Grb2-SOS to the plasma membrane. Once at the PM, Grb2-SOS can bind fully processed KRas4B. Before its localization to the PM, KRas4B undergoes three required post-translational modifications on its most C-terminal cysteine residue of its CAAX motif: farnesylation, proteolysis, and methylation. Of those three steps, methylation is the only reversible process making it a possible point of regulation for KRas4B and other CAAX proteins. KRas4B then translocates to the PM possibly with the help of PDEδ and other unidentified chaperones. Once at the PM KRas4B can associate and bind SOS which help it to stay in the GTP-bound (active) step. GTP-bound Ras can bind and activate downstream effectors such as Raf of the MAPK pathway or PI3K, which is implicated in many processes including Akt and mTOR. The PDB structures of which each protein is based are, The PDB structures of which each protein is based are, Ras: 4OBE & 4DSO, FTase: 1S63, GGTase-I: 3GFT, Rce1: 4CAD, Icmt: 5VG9, Grb2: 1JYU, SOS: 3KSY, Raf: 3C4C, MEK: 4MNE, ERK: 4GT3, PI3K: 4OVV, EGFR: 1NQL, 1IVO, 2JWA, 1M17 and 2GS6.

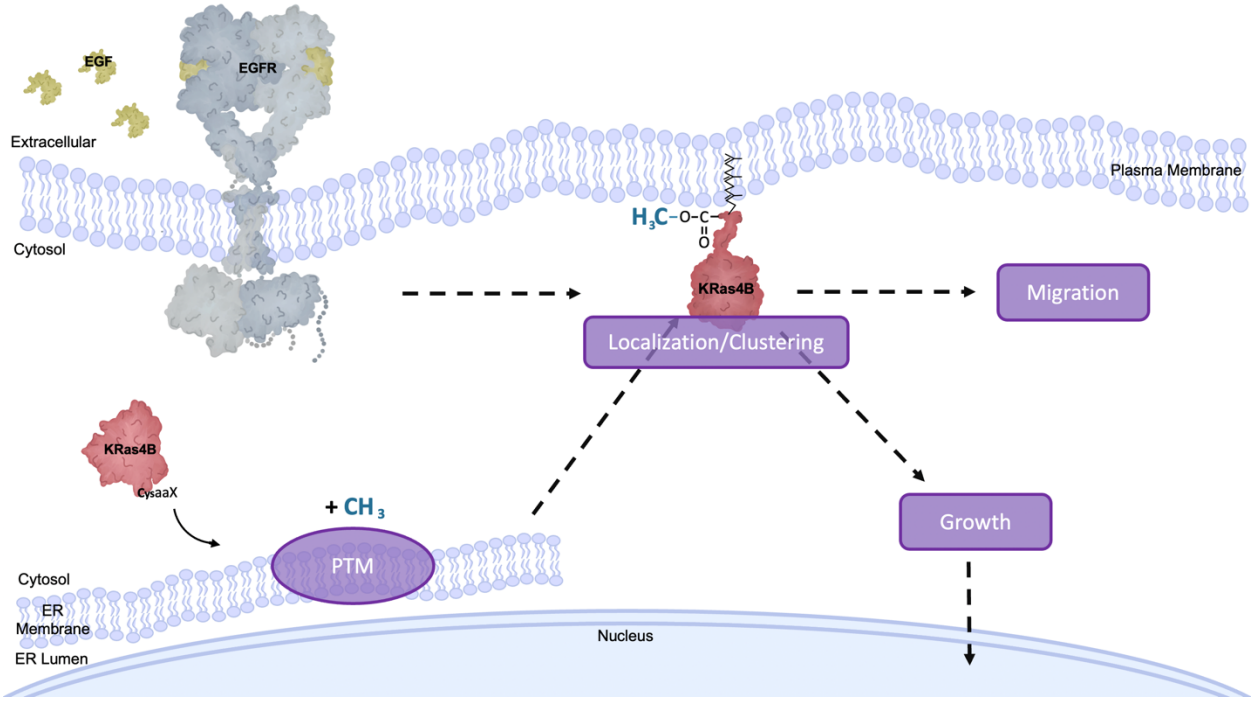

Figure 4.2 Experimental methodology of the impact of methylation on KRas4B.

Based on the pathway described in Figure 4.1 each topic of research is symbolized. We will evaluate the localization/clustering, cellular growth and ERK signaling, and cellular migration in response to the methylation PTM state of KRas4B. PDB: Ras: 4OBE & 4DSO, PI3K: 4OVV, EGFR: 1NQL, 1IVO, 2JWA, 1M17 and 2GS6.

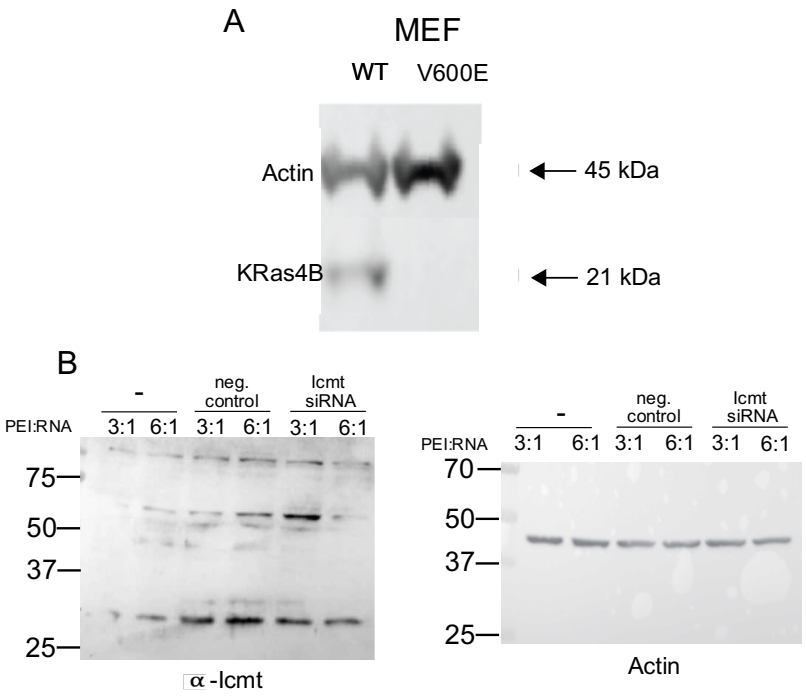

Figure 4.3 Antibody detection of Ras, Icmt and Actin.

(A) Immunoblot of WT-KRas4B and BRaf^{V600E}-Rasless MEFs. Antibody ratios are described in methods. (B) Immunoblot of siRNA treatment of WT-KRas4B MEFs with differing ratios of PEI. Left: Icmt (~32 kDa), Right: Actin (~45 kDa). Antibody conditions are described in methods.

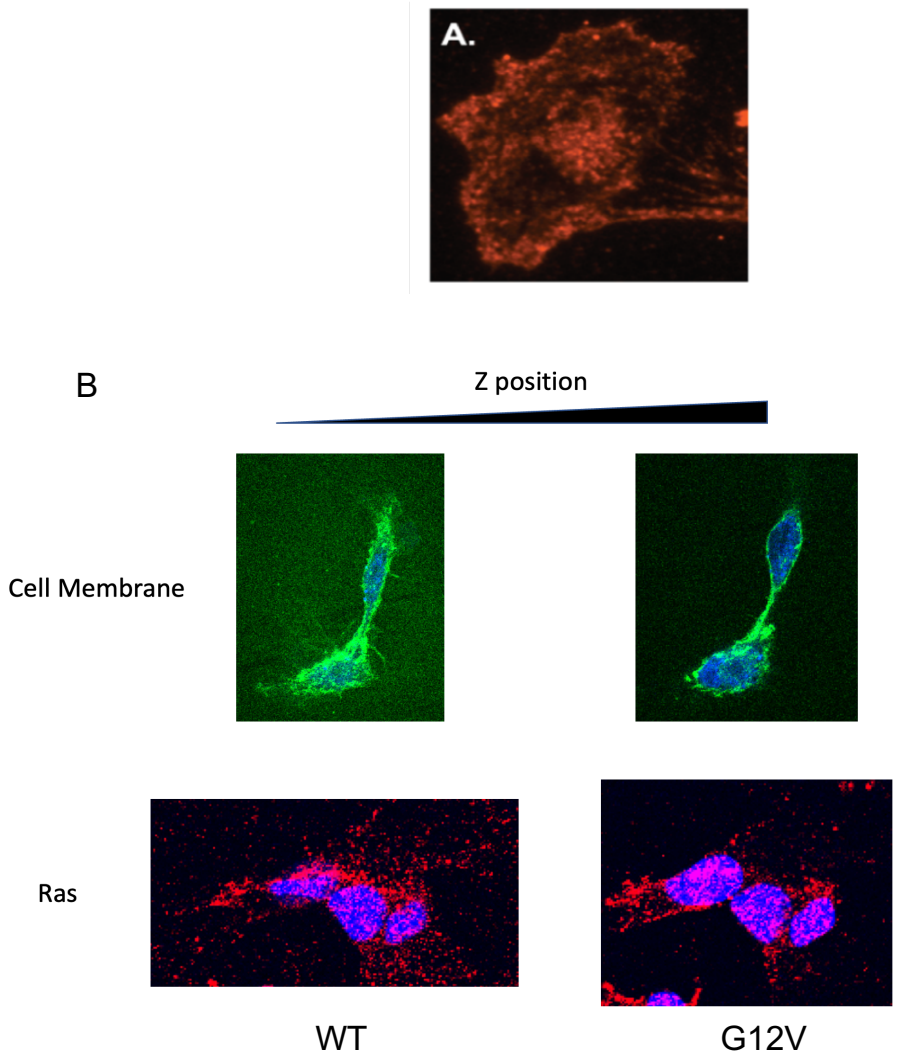

Figure 4.4 Immunofluorescent detection of KRas4B, plasma membrane and nucleus

(A) Immunofluorescent detection of KRas4B in WT MEFs using pan-Ras primary antibody (MA1-012, Thermo Fisher) at (1:200) with donkey α-mouse-Alexa 555 (A-31570, Thermo Fisher) (1:200). Cells were mounted with DAPI and imaged with the Ti2-E Nikon Eclipse modified microscope (Low-Nam Lab). (B) Confocal microscopy analysis with Nikon A1R-MP in the Purdue Imaging Facility (PIF) of WT (left column) and G12V (right column) mutated KRas4B MEFs. MemBrite stained the plasma membrane (1:1000) following manufacturer's protocols (Biotium) and pan Ras-Alexa 555 primary conjugated antibody (1:250). Both conditions were mounted in ProLong Gold with DAPI.

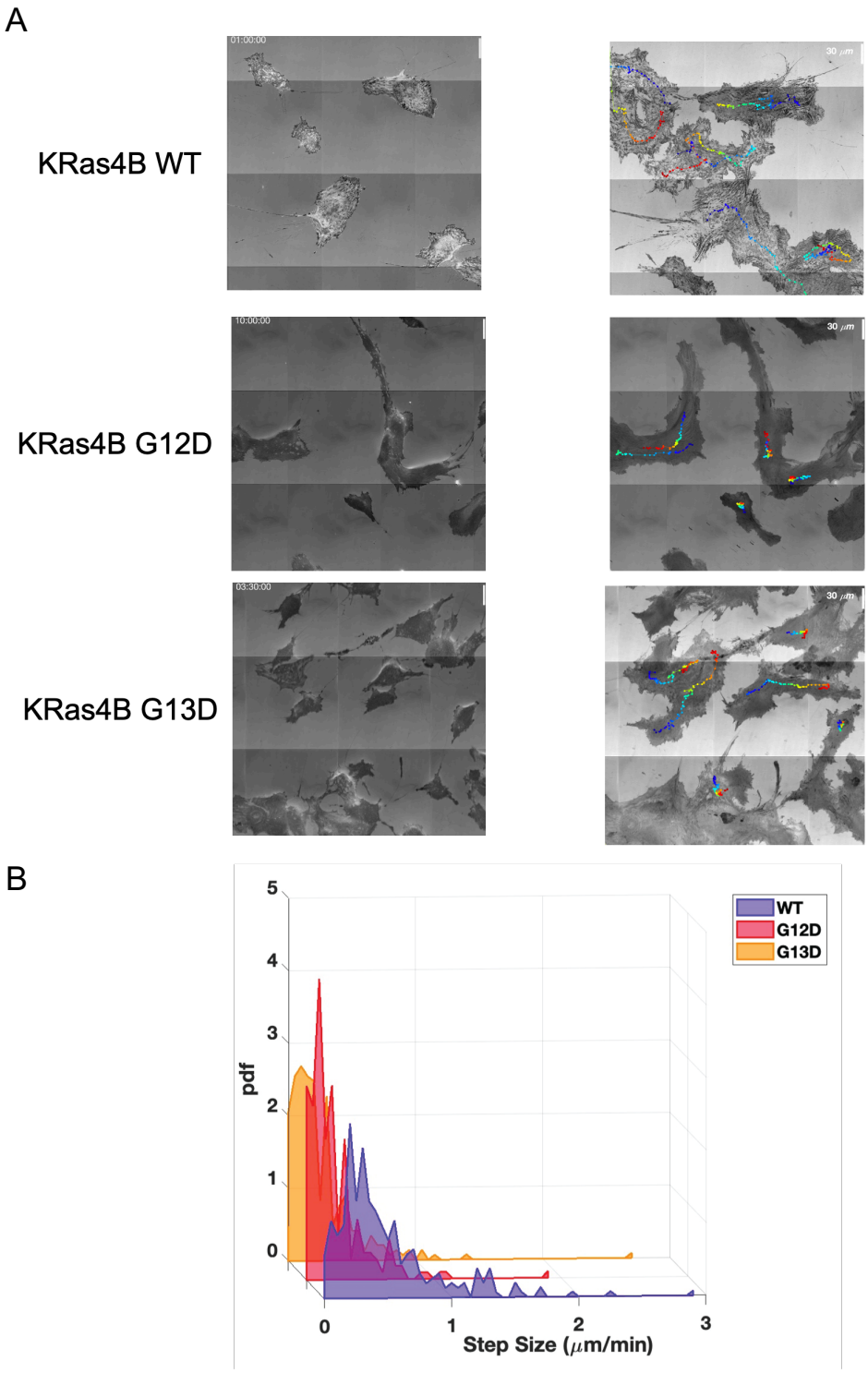

Figure 4.5 Cell crawling rates of MEF KRas4B oncogenic variants.

(A) KRas4B WT, G12D or G13D migration measured over a period of 24 hours. Experimental conditions are in the methods section. Left: primary images of cells at timepoint 0 of experiment. Right: traces of the crawling cells from their points of origin (blue) to their terminating position (red) over the course of the experiment. (B) Histogram displaying the probability that a cell will take each size step based on the crawling experiment in part A.

4.7 References

1. Malumbres, M.; Barbacid, M., RAS oncogenes: the first 30 years. *Nature Reviews Cancer* **2003,** *3* (6), 459-465.

2. Waters, A. M.; Der, C. J., KRAS: the critical driver and therapeutic target for pancreatic cancer. *Cold Spring Harbor perspectives in medicine* **2018,** *8* (9), a031435.

3. Cox, A. D.; Fesik, S. W.; Kimmelman, A. C.; Luo, J.; Der, C. J., Drugging the undruggable RAS: mission possible? *Nature reviews Drug discovery* **2014,** *13* (11), 828-851.

4. Molina-Arcas, M.; Samani, A.; Downward, J., Drugging the Undruggable: Advances on RAS Targeting in Cancer. *Genes* **2021,** *12* (6), 899.

5. Moore, A. R.; Rosenberg, S. C.; McCormick, F.; Malek, S., RAS-targeted therapies: is the undruggable drugged? *Nature Reviews Drug Discovery* **2020,** *19* (8), 533-552.

6. Rudolph, J.; Settleman, J.; Malek, S., Emerging Trends in Cancer Drug Discovery—From Drugging the "Undruggable" to Overcoming Resistance. *Cancer Discovery* **2021,** *11* (4), 815-821.

7. Uprety, D.; Adjei, A. A., KRAS: From undruggable to a druggable Cancer Target. *Cancer Treatment Reviews* **2020,** *89*, 102070.

8. Heidorn, S. J.; Milagre, C.; Whittaker, S.; Nourry, A.; Niculescu-Duvas, I.; Dhomen, N.; Hussain, J.; Reis-Filho, J. S.; Springer, C. J.; Pritchard, C.; Marais, R., Kinase-Dead BRAF and Oncogenic RAS Cooperate to Drive Tumor Progression through CRAF. *Cell* **2010,** *140* (2), 209-221.

9. Baltanás, F. C.; Zarich, N.; Rojas-Cabañeros, J. M.; Santos, E., SOS GEFs in health and disease. *Biochimica et Biophysica Acta (BBA) - Reviews on Cancer* **2020,** *1874* (2), 188445.

10. Berndt, N.; Hamilton, A. D.; Sebti, S. M., Targeting protein prenylation for cancer therapy. *Nature Reviews Cancer* **2011,** *11* (11), 775-791.

11. Kazi, A.; Xiang, S.; Yang, H.; Chen, L.; Kennedy, P.; Ayaz, M.; Fletcher, S.; Cummings, C.; Lawrence, H. R.; Beato, F., Dual farnesyl and geranylgeranyl transferase inhibitor thwarts mutant KRAS-driven patient-derived pancreatic tumors. *Clinical Cancer Research* **2019,** *25* (19), 5984-5996.

12. Mohammed, I.; Hampton, S. E.; Ashall, L.; Hildebrandt, E. R.; Kutlik, R. A.; Manandhar, S. P.; Floyd, B. J.; Smith, H. E.; Dozier, J. K.; Distefano, M. D.; Schmidt, W. K.; Dore, T. M., 8-Hydroxyquinoline-based inhibitors of the Rce1 protease disrupt Ras membrane localization in human cells. *Bioorganic & Medicinal Chemistry* **2016,** *24* (2), 160-178.

13. Davis, T. D.; Kunakom, S.; Burkart, M. D.; Eustaquio, A. S., Preparation, Assay, and Application of Chlorinase SalL for the Chemoenzymatic Synthesis of S-Adenosyl-l-Methionine and Analogs. *Methods in enzymology* **2018,** *604*, 367-388.

14. Winter-Vann, A. M.; Baron, R. A.; Wong, W.; dela Cruz, J.; York, J. D.; Gooden, D. M.; Bergo, M. O.; Young, S. G.; Toone, E. J.; Casey, P. J., A small-molecule inhibitor of isoprenylcysteine carboxyl methyltransferase with antitumor activity in cancer cells. *Proc Natl Acad Sci U S A* **2005,** *102* (12), 4336-41.

15. Marin-Ramos, N. I.; Balabasquer, M.; Ortega-Nogales, F. J.; Torrecillas, I. R.; Gil-Ordonez, A.; Marcos-Ramiro, B.; Aguilar-Garrido, P.; Cushman, I.; Romero, A.; Medrano, F. J.; Gajate, C.; Mollinedo, F.; Philips, M. R.; Campillo, M.; Gallardo, M.; Martin-Fontecha, M.; Lopez-Rodriguez, M. L.; Ortega-Gutierrez, S., A Potent Isoprenylcysteine Carboxylmethyltransferase (ICMT) Inhibitor Improves Survival in Ras-Driven Acute Myeloid Leukemia. *J Med Chem* **2019,** *62* (13), 6035-6046.

16. Prior, I. A.; Hood, F. E.; Hartley, J. L., The frequency of Ras mutations in cancer. *Cancer research* **2020,** *80* (14), 2969-2974.

17. Smith, M. J.; Neel, B. G.; Ikura, M., NMR-based functional profiling of RASopathies and oncogenic RAS mutations. *Proceedings of the National Academy of Sciences* **2013,** *110* (12), 4574-4579.

18. Prior, I. A.; Lewis, P. D.; Mattos, C., A comprehensive survey of Ras mutations in cancer. *Cancer research* **2012,** *72* (10), 2457-2467.

19. Canon, J.; Rex, K.; Saiki, A. Y.; Mohr, C.; Cooke, K.; Bagal, D.; Gaida, K.; Holt, T.; Knutson, C. G.; Koppada, N.; Lanman, B. A.; Werner, J.; Rapaport, A. S.; San Miguel, T.; Ortiz, R.; Osgood, T.; Sun, J.-R.; Zhu, X.; McCarter, J. D.; Volak, L. P.; Houk, B. E.; Fakih, M. G.; O'Neil, B. H.; Price, T. J.; Falchook, G. S.; Desai, J.; Kuo, J.; Govindan, R.; Hong, D. S.; Ouyang, W.; Henary, H.; Arvedson, T.; Cee, V. J.; Lipford, J. R., The clinical KRAS(G12C) inhibitor AMG 510 drives anti-tumour immunity. *Nature* **2019,** *575* (7781), 217-223.

20. Hong, D. S.; Fakih, M. G.; Strickler, J. H.; Desai, J.; Durm, G. A.; Shapiro, G. I.; Falchook, G. S.; Price, T. J.; Sacher, A.; Denlinger, C. S., KRASG12C inhibition with sotorasib in advanced solid tumors. *New England Journal of Medicine* **2020,** *383* (13), 1207-1217.

21. Skoulidis, F.; Li, B. T.; Dy, G. K.; Price, T. J.; Falchook, G. S.; Wolf, J.; Italiano, A.; Schuler, M.; Borghaei, H.; Barlesi, F., Sotorasib for Lung Cancers with KRAS p. G12C Mutation. *New England Journal of Medicine* **2021**.

22. Ntai, I.; Fornelli, L.; DeHart, C. J.; Hutton, J. E.; Doubleday, P. F.; LeDuc, R. D.; van Nispen, A. J.; Fellers, R. T.; Whiteley, G.; Boja, E. S., Precise characterization of KRAS4b proteoforms in human colorectal cells and tumors reveals mutation/modification cross-talk. *Proceedings of the National Academy of Sciences* **2018,** *115* (16), 4140-4145.

23. Silvius, J. R.; l'Heureux, F., Fluorimetric evaluation of the affinities of isoprenylated peptides for lipid bilayers. *Biochemistry* **1994,** *33* (10), 3014-22.

24. Philips, M. R.; Pillinger, M. H.; Staud, R.; Volker, C.; Rosenfeld, M. G.; Weissmann, G.; Stock, J. B., Carboxyl methylation of Ras-related proteins during signal transduction in neutrophils. *Science* **1993,** *259* (5097), 977-80.

25. Hancock, J. F.; Cadwallader, K.; Marshall, C. J., Methylation and proteolysis are essential for efficient membrane binding of prenylated p21K-ras (B). *The EMBO journal* **1991,** *10* (3), 641-646.

26. Bergo, M. O.; Leung, G. K.; Ambroziak, P.; Otto, J. C.; Casey, P. J.; Young, S. G., Targeted inactivation of the isoprenylcysteine carboxyl methyltransferase gene causes mislocalization of K-Ras in mammalian cells. *Journal of Biological Chemistry* **2000,** *275* (23), 17605-17610.

27. Wright, L. P.; Philips, M. R., Thematic review series: lipid posttranslational modifications CAAX modification and membrane targeting of Ras. *Journal of lipid research* **2006,** *47* (5), 883-891.

28. Chelsky, D.; Ruskin, B.; Koshland Jr, D., Methyl-esterified proteins in a mammalian cell line. *Biochemistry* **1985,** *24* (23), 6651-6658.

29. Perez-Sala, D.; Tan, E. W.; Canada, F. J.; Rando, R. R., Methylation and demethylation reactions of guanine nucleotide-binding proteins of retinal rod outer segments. *Proceedings of the National Academy of Sciences* **1991,** *88* (8), 3043-3046.

30. Yang, J.; Kulkarni, K.; Manolaridis, I.; Zhang, Z.; Dodd, R. B.; Mas-Droux, C.; Barford, D., Mechanism of isoprenylcysteine carboxyl methylation from the crystal structure of the integral membrane methyltransferase ICMT. *Mol Cell* **2011,** *44* (6), 997-1004.

31. Diver, M. M.; Pedi, L.; Koide, A.; Koide, S.; Long, S. B., Atomic structure of the eukaryotic intramembrane RAS methyltransferase ICMT. *Nature* **2018,** *553* (7689), 526-529.

32. Hrycyna, C. A.; Clarke, S., Farnesyl cysteine C-terminal methyltransferase activity is dependent upon the STE14 gene product in Saccharomyces cerevisiae. *Molecular and Cellular Biology* **1990,** *10* (10), 5071-5076.

33. Dharmaiah, S.; Bindu, L.; Tran, T. H.; Gillette, W. K.; Frank, P. H.; Ghirlando, R.; Nissley, D. V.; Esposito, D.; McCormick, F.; Stephen, A. G., Structural basis of recognition of farnesylated and methylated KRAS4b by PDEδ. *Proceedings of the National Academy of Sciences* **2016,** *113* (44), E6766-E6775.

34. Zhang, H.; Liu, X.-h.; Zhang, K.; Chen, C.-K.; Frederick, J. M.; Prestwich, G. D.; Baehr, W., Photoreceptor cGMP phosphodiesterase δ subunit (PDEδ) functions as a prenyl-binding protein. *Journal of Biological Chemistry* **2004,** *279* (1), 407-413.

35. Chandra, A.; Grecco, H. E.; Pisupati, V.; Perera, D.; Cassidy, L.; Skoulidis, F.; Ismail, S. A.; Hedberg, C.; Hanzal-Bayer, M.; Venkitaraman, A. R., The GDI-like solubilizing factor PDEδ sustains the spatial organization and signalling of Ras family proteins. *Nature cell biology* **2012,** *14* (2), 148-158.

36. Zimmermann, G.; Papke, B.; Ismail, S.; Vartak, N.; Chandra, A.; Hoffmann, M.; Hahn, S. A.; Triola, G.; Wittinghofer, A.; Bastiaens, P. I., Small molecule inhibition of the KRAS–PDEδ interaction impairs oncogenic KRAS signalling. *Nature* **2013,** *497* (7451), 638-642.

37. Winter-Vann, A. M.; Kamen, B. A.; Bergo, M. O.; Young, S. G.; Melnyk, S.; James, S. J.; Casey, P. J., Targeting Ras signaling through inhibition of carboxyl methylation: an unexpected property of methotrexate. *Proceedings of the National Academy of Sciences* **2003,** *100* (11), 6529-6534.

38. Bergman, J. A.; Hahne, K.; Song, J.; Hrycyna, C. A.; Gibbs, R. A., S-Farnesyl-thiopropionic acid triazoles as potent inhibitors of isoprenylcysteine carboxyl methyltransferase. *ACS medicinal chemistry letters* **2012,** *3* (1), 15-19.

39. Majmudar, J. D.; Hodges-Loaiza, H. B.; Hahne, K.; Donelson, J. L.; Song, J.; Shrestha, L.; Harrison, M. L.; Hrycyna, C. A.; Gibbs, R. A., Amide-modified prenylcysteine based Icmt inhibitors: structure–activity relationships, kinetic analysis and cellular characterization. *Bioorganic & medicinal chemistry* **2012,** *20* (1), 283-295.

40. Lau, H. Y.; Ramanujulu, P. M.; Guo, D.; Yang, T.; Wirawan, M.; Casey, P. J.; Go, M.-L.; Wang, M., An improved isoprenylcysteine carboxylmethyltransferase inhibitor induces cancer cell death and attenuates tumor growth in vivo. *Cancer biology & therapy* **2014,** *15* (9), 1280-1291.

41. Bolognesi, B.; Lehner, B., Reaching the limit. *eLife* **2018,** *7*, e39804.

42. Gorfe, A. A.; Grant, B. J.; McCammon, J. A., Mapping the nucleotide and isoform-dependent structural and dynamical features of Ras proteins. *Structure* **2008,** *16* (6), 885-896.

43. Hancock, J. F., Ras proteins: different signals from different locations. *Nature reviews Molecular cell biology* **2003,** *4* (5), 373-385.

44. Marcos-Ramiro, B.; Gil-Ordóñez, A.; Marín-Ramos, N. I.; Ortega-Nogales, F. J.; Balabasquer, M.; Gonzalo, P.; Khiar-Fernández, N.; Rolas, L.; Barkaway, A.; Nourshargh, S.; Andrés, V.; Martín-Fontecha, M.; López-Rodríguez, M. L.; Ortega-Gutiérrez, S., Isoprenylcysteine Carboxylmethyltransferase-Based Therapy for Hutchinson–Gilford Progeria Syndrome. *ACS Central Science* **2021,** *7* (8), 1300-1310.

45. Waters, A. M.; Ozkan-Dagliyan, I.; Vaseva, A. V.; Fer, N.; Strathern, L. A.; Hobbs, G. A.; Tessier-Cloutier, B.; Gillette, W. K.; Bagni, R.; Whiteley, G. R., Evaluation of the selectivity and sensitivity of isoform-and mutation-specific RAS antibodies. *Science signaling* **2017,** *10* (498), eaao3332.

46. Drosten, M.; Dhawahir, A.; Sum, E. Y.; Urosevic, J.; Lechuga, C. G.; Esteban, L. M.; Castellano, E.; Guerra, C.; Santos, E.; Barbacid, M., Genetic analysis of Ras signalling pathways in cell proliferation, migration and survival. *The EMBO journal* **2010,** *29* (6), 1091-1104.

47. Lechuga, C. G.; Salmón, M.; Paniagua, G.; Guerra, C.; Barbacid, M.; Drosten, M., RASless MEFs as a Tool to Study RAS-Dependent and RAS-Independent Functions. *Methods Mol Biol* **2021,** *2262*, 335-346.

48. Regot, S.; Hughey, J. J.; Bajar, B. T.; Carrasco, S.; Covert, M. W., High-sensitivity measurements of multiple kinase activities in live single cells. *Cell* **2014,** *157* (7), 1724-1734.

49. Albeck, J. G.; Mills, G. B.; Brugge, J. S., Frequency-modulated pulses of ERK activity transmit quantitative proliferation signals. *Molecular cell* **2013,** *49* (2), 249-261.

50. Huang, W. Y.; Alvarez, S.; Kondo, Y.; Lee, Y. K.; Chung, J. K.; Lam, H. Y. M.; Biswas, K. H.; Kuriyan, J.; Groves, J. T., A molecular assembly phase transition and kinetic proofreading modulate Ras activation by SOS. *Science* **2019,** *363* (6431), 1098-1103.

51. Cho, K.-J.; Hancock, J. F., Ras nanoclusters. *Small GTPases* **2013,** *4* (1), 57-60.

52. Van, Q. N.; Prakash, P.; Shrestha, R.; Balius, T. E.; Turbyville, T. J.; Stephen, A. G., RAS nanoclusters: Dynamic signaling platforms amenable to therapeutic intervention. *Biomolecules* **2021,** *11* (3), 377.

53. Henis, Y. I.; Hancock, J. F.; Prior, I. A., Ras acylation, compartmentalization and signaling nanoclusters. *Molecular membrane biology* **2009,** *26* (1-2), 80-92.

54. Vivanco, I.; Sawyers, C. L., The phosphatidylinositol 3-Kinase–AKT pathway in human cancer. *Nature Reviews Cancer* **2002,** *2* (7), 489-501.

55. Nussinov, R.; Tsai, C.-J.; Jang, H., Oncogenic Ras Isoforms Signaling Specificity at the Membrane. *Cancer Research* **2018,** *78* (3), 593-602.

56. Lin, J. J.; Low-Nam, S. T.; Alfieri, K. N.; McAffee, D. B.; Fay, N. C.; Groves, J. T., Mapping the stochastic sequence of individual ligand-receptor binding events to cellular activation: T cells act on the rare events. *Science Signaling* **2019,** *12* (564), eaat8715.

57. Venkatasubramanian, K.; Hirata, F.; Gagnon, C.; Corcoran, B.; O'Dea, R.; Axelrod, J.; Schiffmann, E., Protein methylesterase and leukocyte chemotaxis. *Molecular Immunology* **1980,** *17* (2), 201-207.

58. Clarke, S.; Sparrow, K.; Panasenko, S.; Koshland, D. E., Jr., In vitro methylation of bacterial chemotaxis proteins: characterization of protein methyltransferase activity in crude extracts of Salmonella typhimurium. *J Supramol Struct* **1980,** *13* (3), 315-28.

59. Van Aelst, L.; Joneson, T.; Bar-Sagi, D., Identification of a novel Rac1-interacting protein involved in membrane ruffling. *The EMBO Journal* **1996,** *15* (15), 3778-3786.

60. Matozaki, T.; Nakanishi, H.; Takai, Y., Small G-protein networks:: Their crosstalk and signal cascades. *Cellular Signalling* **2000,** *12* (8), 515-524.

61. Cushman, I.; Casey, P. J., Role of isoprenylcysteine carboxylmethyltransferase-catalyzed methylation in Rho function and migration. *Journal of Biological Chemistry* **2009,** *284* (41), 27964-27973.

62. Hobbs, G. A.; Der, C. J.; Rossman, K. L., RAS isoforms and mutations in cancer at a glance. *J Cell Sci* **2016,** *129* (7), 1287-92.

63. Hunter, J. C.; Manandhar, A.; Carrasco, M. A.; Gurbani, D.; Gondi, S.; Westover, K. D., Biochemical and structural analysis of common cancer-associated KRAS mutations. *Molecular cancer research* **2015,** *13* (9), 1325-1335.

64. Rizki, A.; Weaver, V. M.; Lee, S.-Y.; Rozenberg, G. I.; Chin, K.; Myers, C. A.; Bascom, J. L.; Mott, J. D.; Semeiks, J. R.; Grate, L. R.; Mian, I. S.; Borowsky, A. D.; Jensen, R. A.; Idowu, M. O.; Chen, F.; Chen, D. J.; Petersen, O. W.; Gray, J. W.; Bissell, M. J., A human breast cell model of preinvasive to invasive transition. *Cancer research* **2008,** *68* (5), 1378-1387.

65. Roszkowska, K. A.; Gizinski, S.; Sady, M.; Gajewski, Z.; Olszewski, M. B., Gain-of-Function Mutations in p53 in Cancer Invasiveness and Metastasis. *International Journal of Molecular Sciences* **2020,** *21* (4), 1334.

66. Fujita, M.; Norris, D.; Yagi, H.; Walsh, P.; Morelli, J.; Weston, W.; Terada, N.; Bennion, S.; Robinson, W.; Lemon, M., Overexpression of mutant ras in human melanoma increases invasiveness, proliferation and anchorage-independent growth in vitro and induces tumour formation and cachexia in vivo. *Melanoma research* **1999,** *9* (3), 279-291.

67. Ou, G.; Thakar, D.; Tung, J. C.; Miroshnikova, Y. A.; Dufort, C. C.; Gutierrez, E.; Groisman, A.; Weaver, V. M., Visualizing mechanical modulation of nanoscale organization of cell-matrix adhesions. *Integrative Biology* **2016,** *8* (7), 795-804.

68. Michaelson, D.; Ali, W.; Chiu, V. K.; Bergo, M.; Silletti, J.; Wright, L.; Young, S. G.; Philips, M., Postprenylation CAAX processing is required for proper localization of Ras but not Rho GTPases. *Molecular biology of the cell* **2005,** *16* (4), 1606-1616.

69. Lombardini, J. B.; Talalay, P., Formation, functions and regulatory importance of S-adenosyl-l-methionine. *Advances in Enzyme Regulation* **1971,** *9*, 349-384.

APPENDIX. OPTICAL PROBING OF PRENYLATION PROCESSING WITH PHOTOSWITCHABLE ISOPRENOIDS

Note:

*Supplemental information not included

Manuscript contributed to by:

NYU: Johannes Morstein, Julian Schackmann, Dirk Trauner

Minnesota: Taysir Bader, Mark Distefano

Purdue: Ariana L. Cardillo, Christine A. Hrycyna

Syracuse: Sudhat Ashok, James Hougland

The author of this dissertation, Ariana L. Cardillo, contributed to the writing on this manuscript, especially pertaining to the sections of prenylation processing. She performed all enzymatic activity assays of Ste24, Rce1 and Ste14 as well as the yeast growth arrest assays.

Abstract

Photoswitchable lipids have emerged as attractive tools for the optical control of lipid bioactivity, metabolism, and biophysical properties. While many glycero- and sphingolipids have been successfully rendered photoswitchable, reversible control of most other lipid classes has not been achieved. Herein, we develop the first photoswitchable analogs of an isoprenoid lipid and systematically assess their potential for optical control of various steps along the prenylation processing pathway of CAAX proteins in *Saccharomyces cerevisiae*. One photoswitchable analog of farnesylpyrophosphate (**AzoFPP-1**) is readily attached to peptide substrates by farnesyltransferase in a light-dependent manner. Subsequent steps in prenylation processing, (proteolysis by either Ste24 or RCE1 and carboxymethylation by Ste14) as well as the bioactivity of a fully processed, photoswitchable peptide (**a**-factor) analog are less susceptible to optical control by the photoisomerization of their photoswitchable isoprenoid. Combined, this study presents a new approach for the optical control of protein prenylation. Additionally, optical probing of several enzymatic conversions along the prenylation processing pathway and the bioactivity of photoswitchable **a**-factor analogues revealed a lower dependence of these processes on isoprenoid structure.

Introduction

10 to 20% of all mammalian proteins are thought to undergo protein lipidation.[1] The most common types of this posttranslational modification are fatty acylation and prenylation.[2] Protein prenylation is an irreversible attachment of an isoprenoid lipid with 3 isoprene repeats (farnesylation, 15 carbons) or 4 isoprene repeats (geranylgeranylation, 20 carbons) by either protein farnesyl transferase (FTase), or types 1 or 2 geranylgeranyl transferase (GGTAse I or II). These groups are attached to the cysteine residue of a 4 amino acid CAAX sequence, where a is an aliphatic amino acid, and X is a variable position dictating the type of prenylation. [3] This step is followed by removal of the aaX sequence by either ZMPSTE24 or Ras Converting CAAX Endopeptidase 1 (RCE1) enzymes,[4,5] and finally methylation of the newly exposed carboxycysteine by Protein-S-isoprenylcysteine O-methyltransferase (ICMT).[6] Combined, these modifications determine the functional/activity states of the lipidated protein.[7] Several chemical probes have been developed to study and inhibit protein prenylation as a means to disrupt processing of CAAX proteins implicated in disease pathways.[8] Farnesyltransferase inhibitors (FTIs) have been explored in several trials for cancer therapy[9] and have recently been approved for the treatment of hepatitis D virus infections, progeria, and progeroid laminopathies.[10] To attain improved spatiotemporal control of protein farnesylation, we have previously endowed FTIs with photocleavable protecting groups that enable the light-triggered activation of these molecules.[11] While this approach principally enables precise farnesyltransferase (FTase) inhibition, it does not allow direct control of the structure and function of the isoprenoid lipid. We envisioned, that this could be achieved through incorporation of a reversibly photoswitchable moiety, such as hydrophobic azobenzenes, into an isoprenoid lipid. In recent years, this approach has been extensively explored for photoswitchable sphingolipids and glycerolipids.[12] These photolipids have been used to control biological targets of signaling lipids, including GPCRs,[13–15] ion channels,[16–18] enzymes,[19–22] nuclear hormone receptors,[23,24] and immunoreceptors,[25] and as a means to control membrane biophysics in model membranes[26–28] and cells.[29] However, to date this approach has not been extended to other important classes of lipids, such as steroids or isoprenoids. We proposed that isoprenoid lipids could be mutually amenable to this approach and azobenzenes could be incorporated into farnesylpyrophosphates (FPPs). This was further motivated by previously reported arene-rich analogs that provided for rapid protein attachment catalyzed by FTase (Figure 1A).[30] These included a benzyl phenyl ether which is a structural isostere

('azoster'[31,32]) of azobenzenes. Photoswitchable analogs could in principle allow for the optical control of substrate prenylation, processing, and bioactivity (Figure 1B). Herein we systematically explore the use of photoswitchable FPP analogs, termed **AzoFPP**s for the optical control of protein prenylation, prenylation processing, and bioactivity of a prenylated mature peptide (Figure 1C). Each enzymatic step is explored with a peptide substrate in the *trans*- or *cis*-forms to probe the relative sensitivity of protein prenylation processing steps for lipid structure. Finally, we explore the bioactivity of the mature, fully processed, peptide **a**-factor in a yeast growth arrest assay.

Results and Discussion

Design, Synthesis, and Photophysical Characterization of Photoswitchable FPP Analogs.

We pursued the synthesis of two photoswitchable analogs of FPP (Figure 2A). The first analog, **AzoFPP-1**, was based on direct incorporation of an azobenzene into FPP. The second analog, **AzoFPP-2**, was inspired by a previously reported Aryl-FPP derivative developed by Spielmann et al., which shows better steady-state kinetic parameters for prenylating a H-Ras sequence than the wild-type (WT) FPP.[30] This analog allowed for straight-forward azologization[31,32] to attain a photoswitchable analog. Briefly, 3-hydroxy azobenzene (**2**) was coupled to a prenol-derived alcohol (**1**) via Mitsunobu reaction, followed by deprotection, which was transformed into a chloride under Appel conditions. This allowed the introduction of the pyrophosphate functionality. Ion exchange chromatography and further purification gave **AzoFPP-1** (**5**). The azobenzene precursor **6** for **AzoFPP-2** (**7**) was generated under Bayer-Mills conditions followed by a similar reaction sequence to yield the pyrophosphate (Figure 2A). UV-Vis spectroscopy shows that **AzoFPP-1** behaved similarly to an unsubstituted azobenzene (Figure 2B). Isomerization from the thermodynamically favored *trans*-configuration to the *cis*-form was triggered with UV irradiation (λ = 365 nm). This process was reversible using blue light (λ = 460 nm) over multiple cycles (Figure 2C). Both compounds were bistable and underwent thermal relaxation to the *trans*-isomer with $t_{1/2}$ = 25 h for **Azo-FPP-1** and $t_{1/2}$ = 29 h for **Azo-FPP-2**, measured in PBS buffer at 37 °C.

Optical control of peptide farnesylation

Our design was further supported by molecular docking studies of the photoswitchable FPP analogs into the structure of *Rattus norvegicus* FTase (FTase, PDB 1JCR). Notably, we found that

trans-AzoFPP-1 (Figure 2E) exhibits a similar binding pose relative to the peptide substrate compared to endogenous FPP (Figure 2D), while *cis*-AzoFPP-1 exhibits some visible steric clash with leucin of the substrate peptide CVLS, indicating that this photoisomer could be a less effective substrate for transfer by reducing the binding of the peptide substrate, which is the second step in the kinetic mechanism of the enzyme after farnesyl diphosphate (FPP) binding.[33–35]

Based on our docking results, we decided to biochemically explore the farnesylation of a model peptide (8a) with AzoFPP-1 by *yeast* farnesyltransferase (yFTase) *in vitro* (Figure 3A & B). The peptide contains a Dansyl fluorophore for visualization, an RAG sequence to increase solubility and ionization in mass spectrometry, and a CVIA sequence derived from the prenylated yeast mating pheromone a-Factor. The ratio of 8a to the corresponding farnesylated peptide 8b (with FPP) or 8c/d (with AzoFPP-1) could be monitored by LC-MS. While the substrate 8a exhibited a single peak with the retention time 27.9 min under the chosen conditions (Figure SI ##), incubation with FTase resulted in formation of a second peak with the retention time 58.8 min and the mass of 8b in the presence of FPP and 55.1 min and the mass of 8c in the presence of AzoFPP-1. At saturating substrate concentrations (22 μM FPP, 2.4 uM peptide), 63.2% of 8a were converted to 8b and this conversion was not significantly affected by irradiation with UV-A light (Figure 3C). On the other hand, 51% of 8a were converted to 8c under the same conditions with AzoFPP-1. Upon irradiation with UV-A light, this conversion was markedly reduced to 10%, demonstrating that *trans*-AzoFPP-1 undergoes significantly more effective transfer to the peptide substrate allowing for optical control of substrate farnesylation. It is worth noting that the reaction mixture was allowed to relax for 12 hours after quenching, thus only 8c is observed and not 8d. Substrate AzoFPP-2 did not undergo FTase-catalyzed transfer to a peptide substrate and was therefore not further pursued in this study.

Optical probing of prenylation processing

Following farnesylation, we decided to investigate the other posttranslational modifications of the prenylation processing pathway, proteolysis and carboxymethylation, and the bioactivity of peptides containing the photoswitchable isoprenoid group. To this end, we used the yeast mating pheromone, a-factor, as a bioactive model peptide. a-factor has been extensively studied for its three posttranslational modifications (prenylation, proteolysis and carboxymethylation) which are required for proper mating between two haploid yeast (*S. cerevisiae)* cells.[36–40] a-Factor precursors

9a and 10a exhibiting VIA and COOH C-termini were synthesized by traditional solid phase peptide synthesis. a-Factor precursor 11a with a methyl ester C-terminus was synthesized using side chain anchoring methodology, which was previously developed by us.[41,42] These peptides were then prenylated chemically with a *trans,trans*-Farnesyl bromide (b) or AzoFPP-1 chloride precursor (c) at pH 5.0 in the presence of $Zn(OAc)_2$ and NaI. These conditions were optimized based on previously reported procedures.[41–45] Peptides exhibiting a VIA (9b and 9c), COOH (10b and 10c), or COMe (11b and 11c) terminus were obtained in this manner. Using these model peptides, each prenylation posttranslational modification step was assayed for activity toward its respective a-factor substrates in either the *trans*-form (dark) or *cis*-form (after UV-A irradiation) for light-dependent conversion. Compounds 9b and 9c were used in combination with the proteases Rce1 and Ste24 and 10b and 10c with the carboxyl methyltransferase Ste14 (Figure 4A). To do this we irradiated samples using our Cell DISCO system[46,47] (5 ms irradiation every 15s at 370 nm). Each enzyme only exhibited minimal light-dependent activity differences when treated with saturating amounts of substrate (Figure 4B). These enzymes were further tested with a-factor substrate below K_M values and showed similar results (Figure SI ##).

Subsequently, we evaluated the bioactivity of 11b, 11c, and 11d in a yeast growth arrest halo assay using the DISCO adapted to a 24 well format (Figure 4C).[39,48] All three peptides were found to be bioactive and exhibit very similar potencies, indicating that the bioactivity of a-factor is not sensitive to the structural prenyl-group variations explored. Combined, our optical probing of the prenylation processing pathway suggests, that our photoswitchable analogs permit selective control of peptide lipidation by farnesyltransferase and exhibit little effect on subsequent processing steps.

Concluding Remarks

Here we show that isoprenoid lipids can be functionalized with a molecular photoswitch to function as photoswitchable substrates for peptide prenylation by farnesyltransferase. This presents an important extension of photolipids to a new class of lipids which has not been previously addressed with this approach.[12,49] The development of the photoswitchable FPP analog AzoFPP-1 and its integration into a series of photoswitchable a-factor analogs, allowed us to systematically probe the light-dependence of various steps in protein prenylation, processing, and a-factor bioactivity. Our study revealed that peptide lipidation with AzoFPP-1 occurs in a light-

dependent fashion, while proteolysis, carboxymethylation, and bioactivity are less susceptible to photoisomerization. These findings indicate that the initial lipidation step is more tightly controlled by lipid structure than subsequent processing steps and that our tools enable selective optical control of this initial step. As such, we believe that photoswitchable isoprenoid lipids could be a new class of widely applicable tools for the optical control of processes that sense or are tightly controlled by isoprenoid structure.

To date 2213 isoprenoid lipids have been described (LIPID MAPS[50,51]). Many of these exhibit linear isoprenoid chains that could be functionalized with an azobenzene in an analogous fashion to yield optical control of their function. Linear isoprenoid lipids with interesting bioactivity include the tocotrienols (Vitamin E),[52] cannabinoids (cannabigerol or cannabigerolic acid),[53] the moenomycin antibiotics,[54] or other natural products such as auraptene and umbelliprenin.[55] Isoprenoid lipids have further been used in the design of synthetic pharmacophores, such as the Ras inhibitor Salirasib.[56,57] Future efforts will address the development of photoswitchable isoprenoids based on these and other bioactive metabolites to assess how modular the described approach is for this lipid class.

Figure Legends

Figure 1. Design of photoswitchable FPP analogs and optical probing of prenylation processing. (A) 'Azologization' of FPP and arene-rich analog. (B) Schematic of protein farnesylation and subsequent processing. (C) Schematic of optical probing of peptide prenylation and processing with photoswitchable FPP analogs.

Figure 2. Synthesis, photophysical characterization, and molecular docking of photoswitchable farnesylpyrophosphate analogs. (A) Chemical synthesis of AzoFPP-1 and AzoFPP-2. (B) The UV-Vis spectra of AzoFPP-1 in varying wavelength-adapted photostationary states. 50 μM AzoFPP-1 in PBS. (C) Reversible cycling between photoisomers with alternating illumination at the two distinct wavelengths 365 nm and 460 nm, indicating the fast kinetics of the isomerization. 50 μM AzoFPP-1 in PBS. (D) Crystal structure of FTase (grey) bound to farnesylpyrophosphate (green) and FPP-receiving peptide substrate (grey sticks). Spheres shown for leucin of receiving peptide CVLS sequence. PDB 1JCR (E) Molecular docking of AzoFPP-1 in *trans* (cyan) and *cis* (purple) into FTase. Spheres shown for leucin of substrate peptide CVLS sequence.

Figure 3. Optical control of peptide farnesylation. (A) Schematic of model peptide substrate farnesylation with **AzoFPP-1** in the *trans* and *cis* form. (B) Chemical structure of peptide substrate for FTase (**8**) and **a**-factor variants (**9-11**) with various functionalizations (**a-d**). (C & D) HPLC trace of **8a** to **8b (C) or 8c (D)** conversion upon incubation of **8a** with FPP and FTase in the dark (top) or after UV-A irradiation (bottom). Substrate concentrations were at saturating levels. (E) Quantification of (C) and (D). Error bars represent SEM.

Figure 4. Optical probing of prenylation processing pathway. (A) Schematic of prenylation processing with photoswitchable **a**-factor analogs in the *trans* and *cis* form. (B) Quantification with and without UV-A irradiation of Rce1 and Ste24 activity with compounds **9b** and **9c/d** (15 μM), and Ste14 activity with compounds **10b** and **10c/d** (25 μM). (C) Yeast growth arrest halo assay with and without UV-A irradiation of compounds **11b** and **11c/d**. Amount of substrate spotted is listed in table above with solution controls in the first row. Quantified growth end-point values listed in table below. Error bars represent SEM.

Figures

Figure 1.

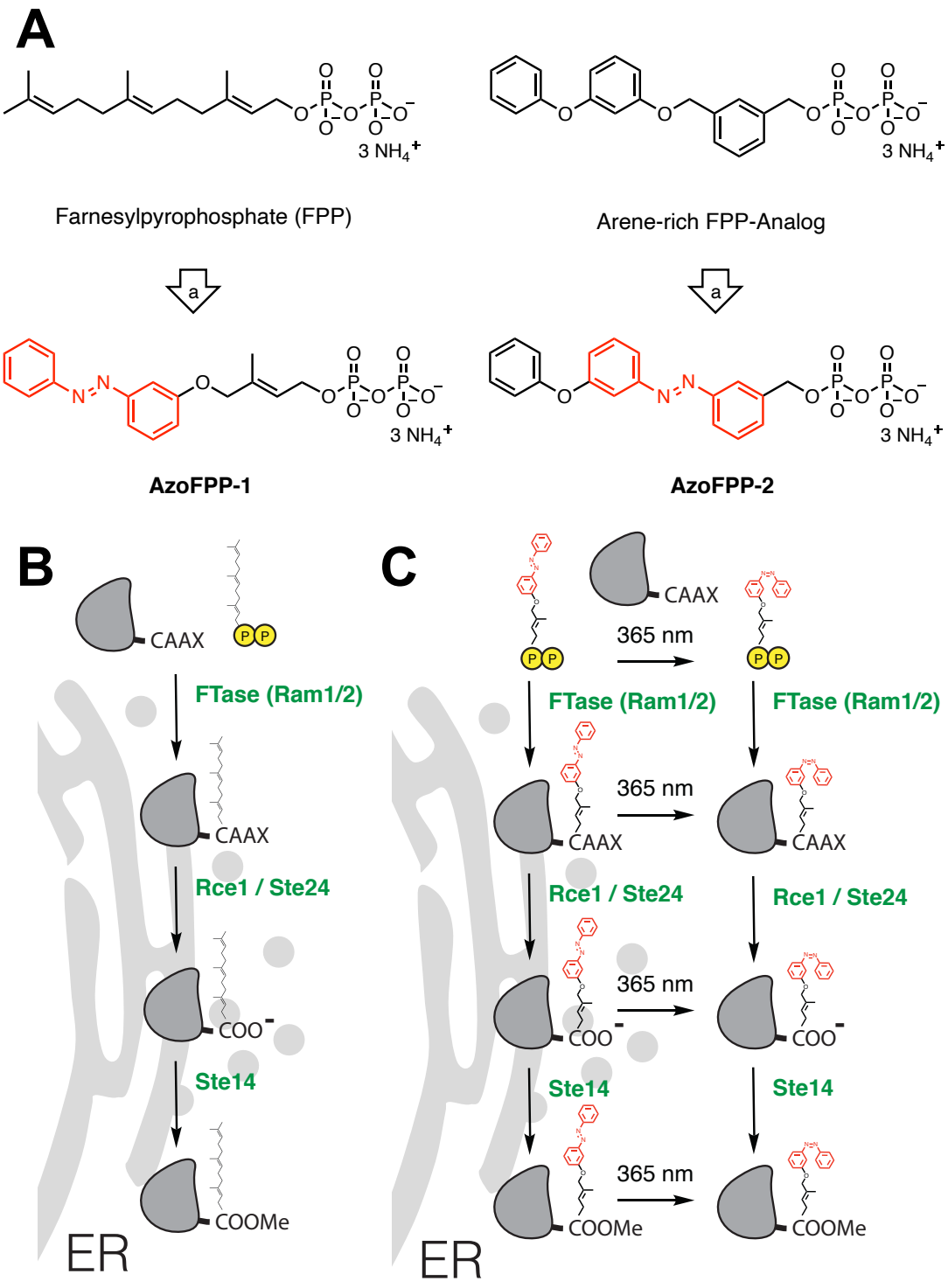

Figure 2.

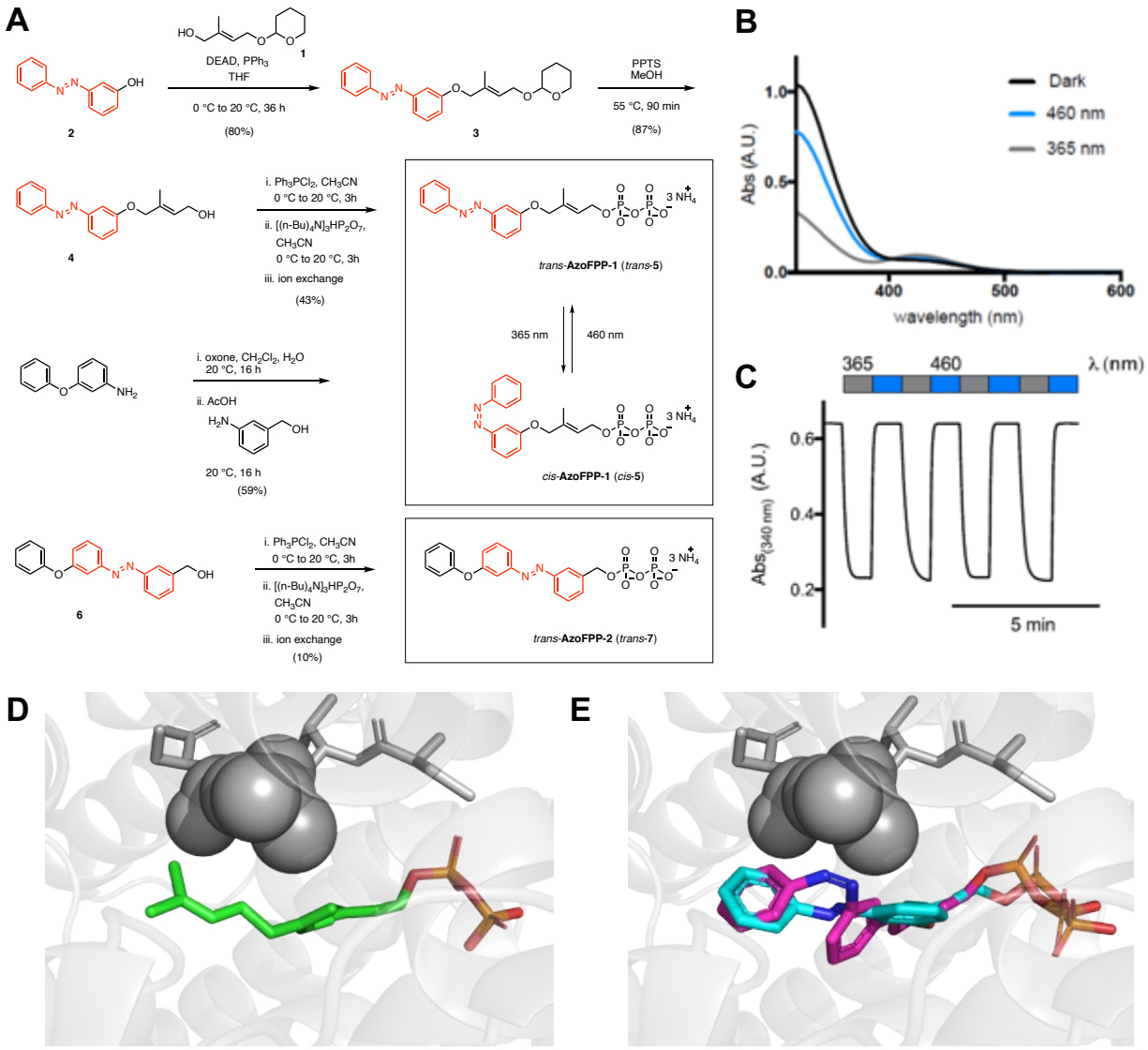
A
DEAD, PPh3
THF
0 °C to 20 °C, 36 h
(80%)
PPTS
MeOH
55 °C, 90 min
(87%)
i. Ph3PCl2, CH3CN
0 °C to 20 °C, 3h
ii. [(n-Bu)4N]3HP2O7,
CH3CN
0 °C to 20 °C, 3h
iii. ion exchange
(43%)
trans-AzoFPP-1 (trans-5)
365 nm
460 nm
cis-AzoFPP-1 (cis-5)
i. oxone, CH2Cl2, H2O
20 °C, 16 h
ii. AcOH
20 °C, 16 h
(59%)
trans-AzoFPP-2 (trans-7)
(10%)
B
Dark
460 nm
365 nm
Abs (A.U.)
wavelength (nm)
C
365
460
λ (nm)
Abs(340 nm) (A.U.)
5 min
D
E

Figure 3.

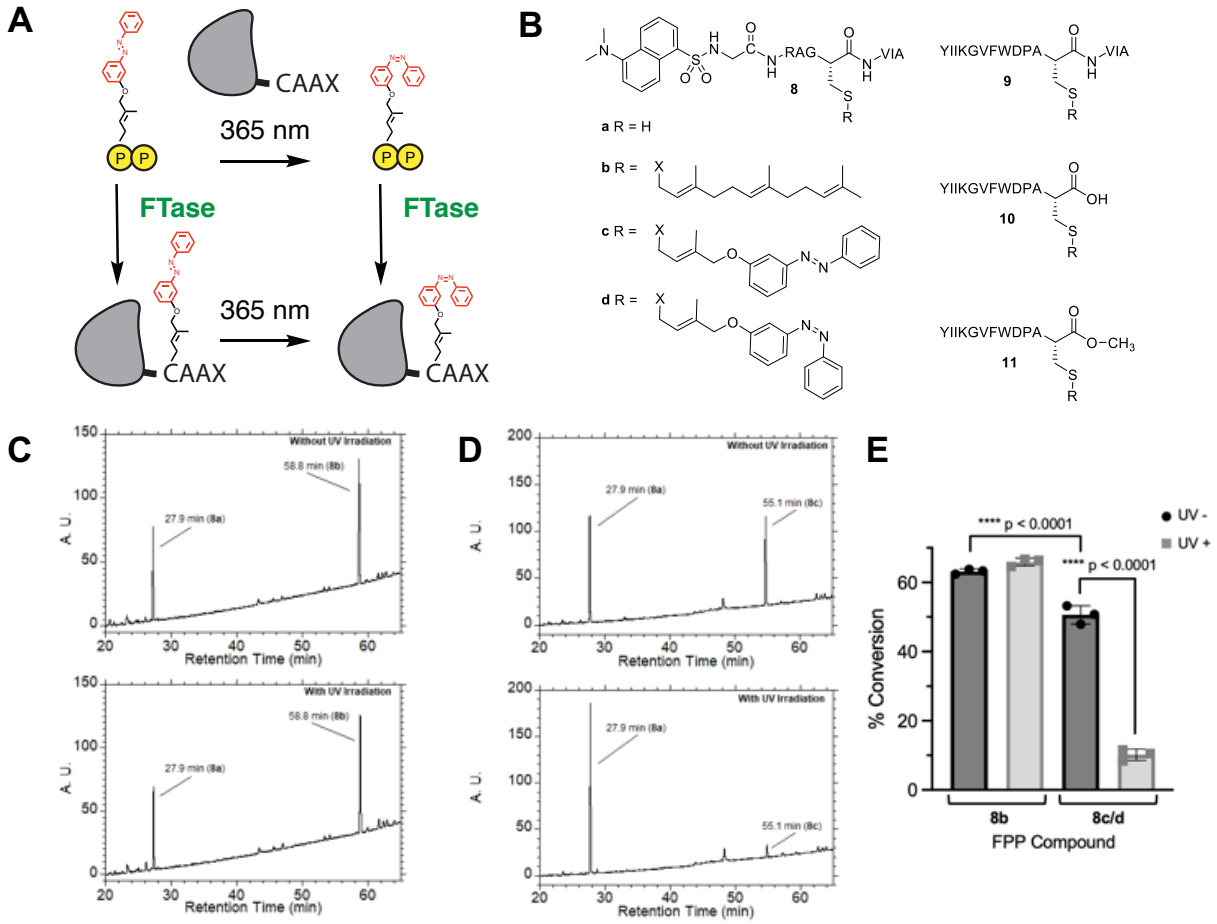
A
CAAX
365 nm
FTase
FTase
365 nm
CAAX
CAAX
B
a R = H
b R =
c R =
d R =
8
9
10
11
YIIKGVFWDPA
VIA
OH
O–CH3
C
Without UV Irradiation
With UV Irradiation
58.8 min (8b)
27.9 min (8a)
A. U.
Retention Time (min)
D
Without UV Irradiation
With UV Irradiation
27.9 min (8a)
55.1 min (8c)
A. U.
Retention Time (min)
E
**** p < 0.0001
**** p < 0.0001
UV -
UV +
% Conversion
8b
8c/d
FPP Compound

Figure 4.

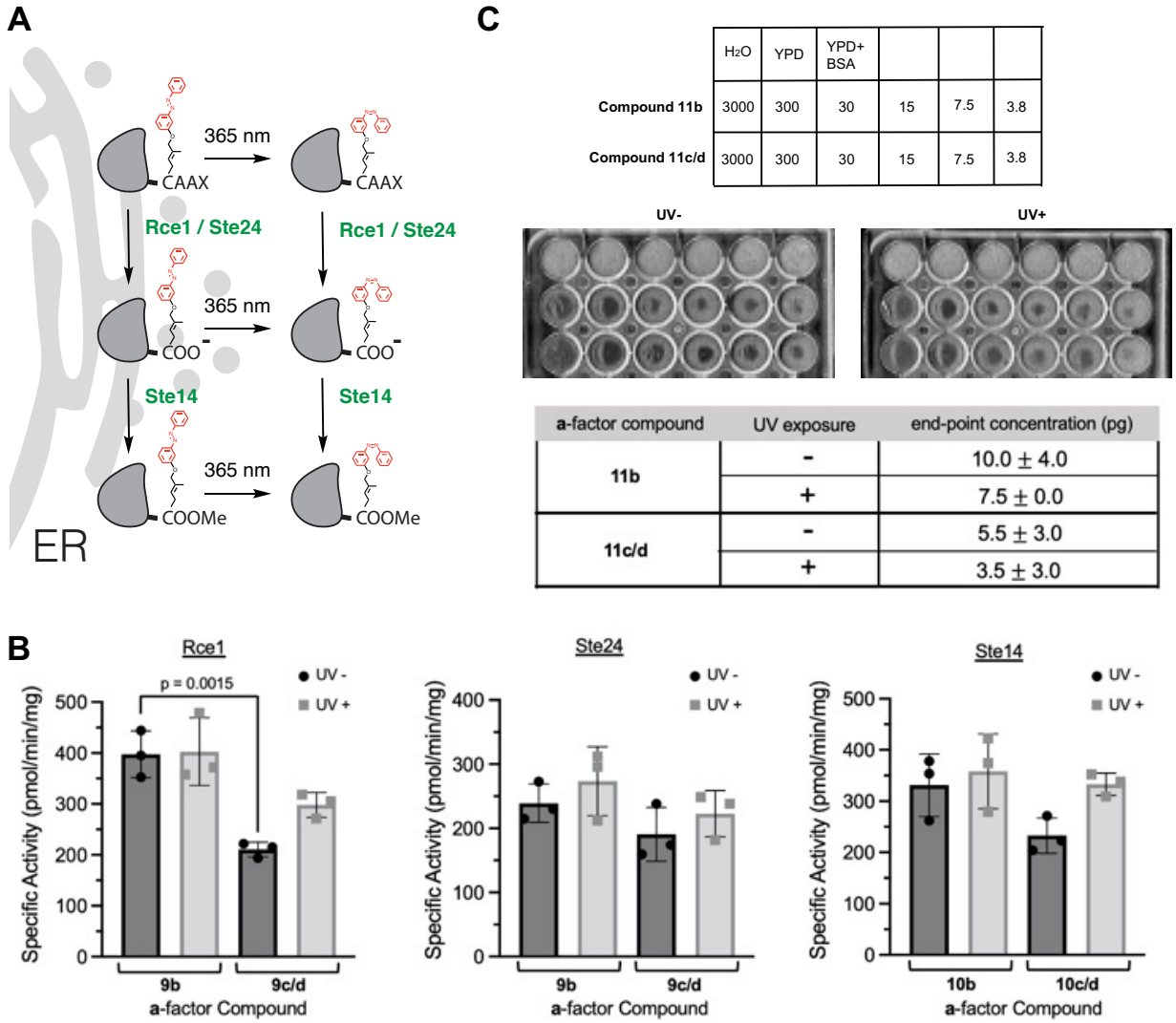

References

1. Khoury, G. A.; Baliban, R. C.; Floudas, C. A. Proteome-Wide Post-Translational Modification Statistics: Frequency Analysis and Curation of the Swiss-Prot Database. *Sci. Rep.* **2011**, *1* (1), 90. https://doi.org/10.1038/srep00090.

2. Jiang, H.; Zhang, X.; Chen, X.; Aramsangtienchai, P.; Tong, Z.; Lin, H. Protein Lipidation: Occurrence, Mechanisms, Biological Functions, and Enabling Technologies. *Chem. Rev.* **2018**, *118* (3), 919–988. https://doi.org/10.1021/acs.chemrev.6b00750.

3. Wang, M.; Casey, P. J. Protein Prenylation: Unique Fats Make Their Mark on Biology. *Nat. Rev. Mol. Cell Biol.* **2016**, *17* (2), 110–122. https://doi.org/10.1038/nrm.2015.11.

4. Ma, Y. T.; Chaudhuri, A.; Rando, R. R. Substrate Specificity of the Isoprenylated Protein Endoprotease. *Biochemistry* **1992**, *31* (47), 11772–11777. https://doi.org/10.1021/bi00162a014.

5. Ashby, M. N.; King, D. S.; Rine, J. Endoproteolytic Processing of a Farnesylated Peptide in Vitro. *Proc. Natl. Acad. Sci. U. S. A.* **1992**, *89* (10), 4613–4617. https://doi.org/10.1073/pnas.89.10.4613.

6. Hrycyna, C. A.; Clarke, S. Farnesyl Cysteine C-Terminal Methyltransferase Activity Is Dependent upon the STE14 Gene Product in Saccharomyces Cerevisiae. *Mol. Cell. Biol.* **1990**, *10* (10), 5071–5076. https://doi.org/10.1128/mcb.10.10.5071-5076.1990.

7. Gelb, M. H.; Brunsveld, L.; Hrycyna, C. A.; Michaelis, S.; Tamanoi, F.; Van Voorhis, W. C.; Waldmann, H. Therapeutic Intervention Based on Protein Prenylation and Associated Modifications. *Nat. Chem. Biol.* **2006**, *2* (10), 518–528. https://doi.org/10.1038/nchembio818.

8. Palsuledesai, C. C.; Distefano, M. D. Protein Prenylation: Enzymes, Therapeutics, and Biotechnology Applications. *ACS Chem. Biol.* **2015**, *10* (1), 51–62. https://doi.org/10.1021/cb500791f.

9. William Pass, D. V. M. FTase Inhibition Holds Promise for RAS Targeting and Beyond. **2018**.

10. Dhillon, S. Lonafarnib: First Approval. *Drugs* **2021**, *81* (2), 283–289. https://doi.org/10.1007/s40265-020-01464-z.

11. Abate-Pella, D.; Zeliadt, N. A.; Ochocki, J. D.; Warmka, J. K.; Dore, T. M.; Blank, D. A.; Wattenberg, E. V.; Distefano, M. D. Photochemical Modulation of Ras-Mediated Signal Transduction Using Caged Farnesyltransferase Inhibitors: Activation by One- and Two-Photon Excitation. *ChemBioChem* **2012**, *13* (7), 1009–1016. https://doi.org/10.1002/cbic.201200063.

12. Trauner, D.; Morstein, J. Optical Control of Glycerolipids and Sphingolipids. *Chimia* **2021**, *75* (12), 1022–1025. https://doi.org/10.2533/chimia.2021.1022.

13. Frank, J. A.; Yushchenko, D. A.; Fine, N. H. F.; Duca, M.; Citir, M.; Broichhagen, J.; Hodson, D. J.; Schultz, C.; Trauner, D. Optical Control of GPR40 Signalling in Pancreatic β-Cells. *Chem. Sci.* **2017**, *8* (11), 7604–7610. https://doi.org/10.1039/C7SC01475A.

14. Morstein, J.; Hill, R. Z.; Novak, A. J. E.; Feng, S.; Norman, D. D.; Donthamsetti, P. C.; Frank, J. A.; Harayama, T.; Williams, B. M.; Parrill, A. L.; Tigyi, G. J.; Riezman, H.; Isacoff, E. Y.; Bautista, D. M.; Trauner, D. Optical Control of Sphingosine-1-Phosphate Formation and Function. *Nat. Chem. Biol.* **2019**, *15* (6), 623. https://doi.org/10.1038/s41589-019-0269-7.

15. Morstein, J.; Dacheux, M. A.; Norman, D. D.; Shemet, A.; Donthamsetti, P. C.; Citir, M.; Frank, J. A.; Schultz, C.; Isacoff, E. Y.; Parrill, A. L.; Tigyi, G. J.; Trauner, D. Optical Control of Lysophosphatidic Acid Signaling. *J. Am. Chem. Soc.* **2020**, *142* (24), 10612–10616. https://doi.org/10.1021/jacs.0c02154.

16. Frank, J. A.; Moroni, M.; Moshourab, R.; Sumser, M.; Lewin, G. R. Photoswitchable Fatty Acids Enable Optical Control of TRPV1. **2015**, *6*, 7118. https://doi.org/10.1038/ncomms8118.

17. Lichtenegger, M.; Tiapko, O.; Svobodova, B.; Stockner, T.; Glasnov, T. N.; Schreibmayer, W.; Platzer, D.; de la Cruz, G. G.; Krenn, S.; Schober, R.; Shrestha, N.; Schindl, R.; Romanin, C.; Groschner, K. An Optically Controlled Probe Identifies Lipid-Gating Fenestrations within the TRPC3 Channel. *Nat. Chem. Biol.* **2018**, *14* (4), 396–404. https://doi.org/10.1038/s41589-018-0015-6.

18. Leinders-Zufall, T.; Storch, U.; Bleymehl, K.; Schnitzler, M. M. y; Frank, J. A.; Konrad, D. B.; Trauner, D.; Gudermann, T.; Zufall, F. PhoDAGs Enable Optical Control of Diacylglycerol-Sensitive Transient Receptor Potential Channels. *Cell Chem. Biol.* **2018**, *25* (2), 215-223.e3. https://doi.org/10.1016/j.chembiol.2017.11.008.

19. Frank, J. A.; Yushchenko, D. A.; Hodson, D. J.; Lipstein, N.; Nagpal, J.; Rutter, G. A.; Rhee, J.-S.; Gottschalk, A.; Brose, N.; Schultz, C.; Trauner, D. Photoswitchable Diacylglycerols Enable Optical Control of Protein Kinase C. *Nat Chem Biol* **2016**, *12* (9), 755–762. https://doi.org/10.1038/nchembio.2141.

20. Kol, M.; Williams, B.; Toombs-Ruane, H.; Franquelim, H. G.; Korneev, S.; Schroeer, C.; Schwille, P.; Trauner, D.; Holthuis, J. C.; Frank, J. A. Optical Manipulation of Sphingolipid Biosynthesis Using Photoswitchable Ceramides. *eLife* **2019**, *8*, e43230. https://doi.org/10.7554/eLife.43230.

21. Morstein, J.; Kol, M.; Novak, A. J. E.; Feng, S.; Khayyo, S.; Hinnah, K.; Li-Purcell, N.; Pan, G.; Williams, B. M.; Riezman, H.; Atilla-Gokcumen, G. E.; Holthuis, J. C. M.; Trauner, D. Short Photoswitchable Ceramides Enable Optical Control of Apoptosis. *ACS Chem. Biol.* **2021**, *16* (3), 452–456. https://doi.org/10.1021/acschembio.0c00823.

22. Tei, R.; Morstein, J.; Shemet, A.; Trauner, D.; Baskin, J. M. Optical Control of Phosphatidic Acid Signaling. *ACS Cent. Sci.* **2021**, *7* (7), 1205–1215. https://doi.org/10.1021/acscentsci.1c00444.

23. Morstein, J.; Trads, J. B.; Hinnah, K.; Willems, S.; Barber, D. M.; Trauner, M.; Merk, D.; Trauner, D. Optical Control of the Nuclear Bile Acid Receptor FXR with a Photohormone. *Chem. Sci.* **2020**, *11* (2), 429–434. https://doi.org/10.1039/C9SC02911G.

24. Hinnah, K.; Willems, S.; Morstein, J.; Heering, J.; Hartrampf, F. W. W.; Broichhagen, J.; Leippe, P.; Merk, D.; Trauner, D. Photohormones Enable Optical Control of the Peroxisome Proliferator-Activated Receptor γ (PPARγ). *J. Med. Chem.* **2020**, *63* (19), 10908–10920. https://doi.org/10.1021/acs.jmedchem.0c00654.

25. Hartrampf, N.; Seki, T.; Baumann, A.; Watson, P.; Vepřek, N. A.; Hetzler, B. E.; Hoffmann-Röder, A.; Tsuji, M.; Trauner, D. Optical Control of Cytokine Production Using Photoswitchable Galactosylceramides. *Chem. – Eur. J.* **2020**, *26* (20), 4476–4479. https://doi.org/10.1002/chem.201905279.

26. Pernpeintner, C.; Frank, J. A.; Urban, P.; Roeske, C. R.; Pritzl, S. D.; Trauner, D.; Lohmüller, T. Light-Controlled Membrane Mechanics and Shape Transitions of Photoswitchable Lipid Vesicles. *Langmuir* **2017**, *33* (16), 4083–4089. https://doi.org/10.1021/acs.langmuir.7b01020.

27. Doroudgar, M.; Morstein, J.; Becker-Baldus, J.; Trauner, D.; Glaubitz, C. How Photoswitchable Lipids Affect the Order and Dynamics of Lipid Bilayers and Embedded Proteins. *J. Am. Chem. Soc.* **2021**, *143* (25), 9515–9528. https://doi.org/10.1021/jacs.1c03524.

28. Chander, N.; Morstein, J.; Bolten, J. S.; Shemet, A.; Cullis, P. R.; Trauner, D.; Witzigmann, D. Optimized Photoactivatable Lipid Nanoparticles Enable Red Light Triggered Drug Release. *Small* **2021**, *17* (21), 2008198. https://doi.org/10.1002/smll.202008198.

29. Jiménez-Rojo, N.; Feng, S.; Morstein, J.; Pritzl, S. D.; Harayama, T.; Asaro, A.; Vepřek, N. A.; Arp, C. J.; Reynders, M.; Novak, A. J. E.; Kanshin, E.; Ueberheide, B.; Lohmüller, T.; Riezman, H.; Trauner, D. Optical Control of Membrane Fluidity Modulates Protein Secretion. bioRxiv February 14, 2022, p 2022.02.14.480333. https://doi.org/10.1101/2022.02.14.480333.

30. Subramanian, T.; Pais, J. E.; Liu, S.; Troutman, J. M.; Suzuki, Y.; Leela Subramanian, K.; Fierke, C. A.; Andres, D. A.; Spielmann, H. P. Farnesyl Diphosphate Analogues with Aryl Moieties Are Efficient Alternate Substrates for Protein Farnesyltransferase. *Biochemistry* **2012**, *51* (41), 8307–8319. https://doi.org/10.1021/bi3011362.

31. Broichhagen, J.; Frank, J. A.; Trauner, D. A Roadmap to Success in Photopharmacology. *Acc. Chem. Res.* **2015**, *48* (7), 1947–1960. https://doi.org/10.1021/acs.accounts.5b00129.

32. Morstein, J.; Awale, M.; Reymond, J.-L.; Trauner, D. Mapping the Azolog Space Enables the Optical Control of New Biological Targets. *ACS Cent. Sci.* **2019**, *5* (4), 607–618. https://doi.org/10.1021/acscentsci.8b00881.

33. Dolence, J. M.; Poulter, C. D. A Mechanism for Posttranslational Modifications of Proteins by Yeast Protein Farnesyltransferase. *Proc. Natl. Acad. Sci.* **1995**, *92* (11), 5008–5011. https://doi.org/10.1073/pnas.92.11.5008.

34. Dolence, J. M.; Cassidy, P. B.; Mathis, J. R.; Poulter, C. D. Yeast Protein Farnesyltransferase: Steady-State Kinetic Studies of Substrate Binding. *Biochemistry* **1995**, *34* (51), 16687–16694. https://doi.org/10.1021/bi00051a017.

35. Pompliano, D. L.; Rands, E.; Schaber, M. D.; Mosser, S. D.; Anthony, N. J.; Gibbs, J. B. Steady-State Kinetic Mechanism of Ras Farnesyl:Protein Transferase. *Biochemistry* **1992**, *31* (15), 3800–3807. https://doi.org/10.1021/bi00130a010.

36. Anderegg, R. J.; Betz, R.; Carr, S. A.; Crabb, J. W.; Duntze, W. Structure of Saccharomyces Cerevisiae Mating Hormone A-Factor. Identification of S-Farnesyl Cysteine as a Structural Component. *J. Biol. Chem.* **1988**, *263* (34), 18236–18240.

37/. Diaz-Rodriguez, V.; Distefano, M. D. A-Factor: A Chemical Biology Tool for the Study of Protein Prenylation. *Curr. Top. Pept. Protein Res.* **2017**, *18*, 133–151.

38. Diaz-Rodriguez, V.; Mullen, D. G.; Ganusova, E.; Becker, J. M.; Distefano, M. D. Synthesis of Peptides Containing C-Terminal Methyl Esters Using Trityl Side-Chain Anchoring: Application to the Synthesis of a-Factor and a-Factor Analogs. *Org. Lett.* **2012**, *14* (22), 5648–5651. https://doi.org/10.1021/ol302592v.

39/ Diaz-Rodriguez, V.; Hsu, E.-T.; Ganusova, E.; Werst, E. R.; Becker, J. M.; Hrycyna, C. A.; Distefano, M. D. A-Factor Analogues Containing Alkyne- and Azide-Functionalized Isoprenoids Are Efficiently Enzymatically Processed and Retain Wild-Type Bioactivity. *Bioconjug. Chem.* **2018**, *29* (2), 316–323. https://doi.org/10.1021/acs.bioconjchem.7b00648.

40/ Marcus, S.; Caldwell, G. A.; Miller, D.; Xue, C. B.; Naider, F.; Becker, J. M. Significance of C-Terminal Cysteine Modifications to the Biological Activity of the Saccharomyces Cerevisiae a-Factor Mating Pheromone. *Mol. Cell. Biol.* **1991**, *11* (7), 3603–3612. https://doi.org/10.1128/MCB.11.7.3603.

41. Bader, T. K.; Rappe, T. M.; Veglia, G.; Distefano, M. D. Chapter Eight - Synthesis and NMR Characterization of the Prenylated Peptide, a-Factor. In *Methods in Enzymology*; Wand, A. J., Ed.; Biological NMR Part A; Academic Press, 2019; Vol. 614, pp 207–238. https://doi.org/10.1016/bs.mie.2018.09.025.

42. Diaz-Rodriguez, V.; Ganusova, E.; Rappe, T. M.; Becker, J. M.; Distefano, M. D. Synthesis of Peptides Containing C-Terminal Esters Using Trityl Side-Chain Anchoring: Applications to the Synthesis of C-Terminal Ester Analogs of the Saccharomyces Cerevisiae Mating Pheromone a-Factor. *J. Org. Chem.* **2015**, *80* (22), 11266–11274. https://doi.org/10.1021/acs.joc.5b01376.

43. Yang, C. C.; Marlowe, C. K.; Kania, R. Efficient Method for Regioselective Isoprenylation of Cysteine Thiols in Unprotected Peptides. *J. Am. Chem. Soc.* **1991**, *113* (8), 3177–3178. https://doi.org/10.1021/ja00008a059.

44. Yang, C. C.; Marlowe, C. K.; Kania, R. Efficient Method for Regioselective Isoprenylation of Cysteine Thiols in Unprotected Peptides. *J. Am. Chem. Soc.* **1991**, *113* (8), 3177–3178. https://doi.org/10.1021/ja00008a059.

45. Wollack, J. W.; Zeliadt, N. A.; Ochocki, J. D.; Mullen, D. G.; Barany, G.; Wattenberg, E. V.; Distefano, M. D. Investigation of the Sequence and Length Dependence for Cell-Penetrating Prenylated Peptides. *Bioorg. Med. Chem. Lett.* **2010**, *20* (1), 161–163. https://doi.org/10.1016/j.bmcl.2009.11.026.

46. Borowiak, M.; Nahaboo, W.; Reynders, M.; Nekolla, K.; Jalinot, P.; Hasserodt, J.; Rehberg, M.; Delattre, M.; Zahler, S.; Vollmar, A.; Trauner, D.; Thorn-Seshold, O. Photoswitchable Inhibitors of Microtubule Dynamics Optically Control Mitosis and Cell Death. *Cell* **2015**, *162* (2), 403–411. https://doi.org/10.1016/j.cell.2015.06.049.

47. Morstein, J.; Trauner, D. Chapter Eleven - Photopharmacological Control of Lipid Function. In *Methods in Enzymology*; Chenoweth, D. M., Ed.; Chemical Tools for Imaging, Manipulating, and Tracking Biological Systems: Diverse Methods for Prokaryotic and Eukaryotic Systems; Academic Press, 2020; Vol. 638, pp 219–232. https://doi.org/10.1016/bs.mie.2020.04.025.

48. Nijbroek, G. L.; Michaelis, S. Functional Assays for Analysis of Yeast Ste6 Mutants. *Methods Enzymol.* **1998**, *292*, 193–212. https://doi.org/10.1016/s0076-6879(98)92016-x.

49. Morstein, J.; Impastato, A. C.; Trauner, D. Photoswitchable Lipids. *ChemBioChem* **2021**, *22* (1), 73–83. https://doi.org/10.1002/cbic.202000449.

50. Mullard, A. Finding the Way with LIPID MAPS. *Nat. Rev. Mol. Cell Biol.* **2008**, *9* (2), 92–92. https://doi.org/10.1038/nrm2342.

51. O'Donnell, V. B.; Dennis, E. A.; Wakelam, M. J. O.; Subramaniam, S. LIPID MAPS: Serving the next Generation of Lipid Researchers with Tools, Resources, Data, and Training. *Sci. Signal.* **2019**, *12* (563), eaaw2964. https://doi.org/10.1126/scisignal.aaw2964.

52. Pearce, B. C.; Parker, R. A.; Deason, M. E.; Qureshi, A. A.; Wright, J. J. Hypocholesterolemic Activity of Synthetic and Natural Tocotrienols. *J. Med. Chem.* **1992**, *35* (20), 3595–3606. https://doi.org/10.1021/jm00098a002.

53. Nachnani, R.; Raup-Konsavage, W. M.; Vrana, K. E. The Pharmacological Case for Cannabigerol. *J. Pharmacol. Exp. Ther.* **2021**, *376* (2), 204–212. https://doi.org/10.1124/jpet.120.000340.

54. Ostash, B.; Walker, S. Moenomycin Family Antibiotics: Chemical Synthesis, Biosynthesis, and Biological Activity. *Nat. Prod. Rep.* **2010**, *27* (11), 1594–1617. https://doi.org/10.1039/C001461N.

55. Fiorito, S.; Preziuso, F.; Sharifi-Rad, M.; Marchetti, L.; Epifano, F.; Genovese, S. Auraptene and Umbelliprenin: A Review on Their Latest Literature Acquisitions. *Phytochem. Rev.* **2020**. https://doi.org/10.1007/s11101-020-09713-5.

56. Furuse, J.; Kurata, T.; Okano, N.; Fujisaka, Y.; Naruge, D.; Shimizu, T.; Kitamura, H.; Iwasa, T.; Nagashima, F.; Nakagawa, K. An Early Clinical Trial of Salirasib, an Oral RAS Inhibitor, in Japanese Patients with Relapsed/Refractory Solid Tumors. *Cancer Chemother. Pharmacol.* **2018**, *82* (3), 511–519. https://doi.org/10.1007/s00280-018-3618-4.

57. Rotblat, B.; Ehrlich, M.; Haklai, R.; Kloog, Y. The Ras Inhibitor Farnesylthiosalicylic Acid (Salirasib) Disrupts The Spatiotemporal Localization Of Active Ras: A Potential Treatment For Cancer. In *Methods in Enzymology*; Small GTPases in Disease, Part B; Academic Press, 2008; Vol. 439, pp 467–489. https://doi.org/10.1016/S0076-6879(07)00432-6.